
Division of Drug Delivery and Tissue Engineering

School of Pharmacy

# *In Vitro* Investigation into Strategies for Mucosal Delivery of Proteins

**Driton Vllasaliu MPharm MRPharmS**

**Thesis submitted to the University of Nottingham for the degree of Doctor of Philosophy**

**February 2010**

# Abstract

Mucosal surfaces offer a potential for non-invasive delivery of proteins. The role of these surfaces, however, is to limit the movement of material from the external environment (mucosal lumen) into systemic circulation. Mucosal absorption of protein therapeutics is constrained through several physiological barriers such as mucus and mucociliary clearance, protease enzymes, epithelial tight junctions (TJs) and cellular membranes. This work explores different strategies with the view to improving the transport of macromolecules (proteins and protein drug models) across polarised epithelial cell layers *in vitro*, which could potentially be a reflection of improved mucosal absorption and bioavailability *in vivo*. The Calu-3 cell line was used in this work to produce such layers, serving as an *in vitro* model of the airway epithelium. Following growth of Calu-3 cells on filters under air-interface culture conditions polarised layers of closely packed cells were formed. The cell layers exhibited a TEER $\geq$500 $\Omega cm^2$ and cells showed structural features similar to the native epithelium, including the TJs, the microvilli and the secretory granules. Cell layers presented a barrier to the permeability of FITC-dextrans (FDs, paracellular markers) and nanoparticles (NPs).

The first class of tested compounds, namely alkylglycoside (AG) surfactants, exhibited severe toxicity at concentrations considerably lower than those used in the literature. Data indicated that the cellular toxicity of AGs possibly results from a membrane effect. Investigation of calcium depletion as a proposed strategy to improve mucosal absorption of protein therapeutics, revealed that calcium depletion on the apical side produced limited TJ opening, as demonstrated by reversible decrease in transepithelial electrical resistance (TEER) and modest enhancement of

permeability of macromolecules. Although combined apical and basolateral calcium exhaustion produced significant effects on TJs, this scenario becomes irrelevant in an *in vivo* situation. Application of chitosan in the form of solution and NPs to Calu-3 layers demonstrated that chitosan NPs formulated by the ionic gelation method, exhibit a similar TJ-opening effect to solution. This was shown by similarities in measurable indicators of TJ opening such as reduction in TEER and enhancement of dextran permeability across the cell layers. Furthermore, chitosan NP and solution exhibited similar effects on the TJ protein, Zonula Occludens-1. These results therefore indicated that chitosan NPs could potentially be used to carry and protect fragile therapeutic proteins to the mucosal surface(s) of interest and at the same time promote their absorption through TJ opening.

TJ opening as a strategy to improve mucosal absorption of macromolecular therapeutics is rather inefficient for larger proteins such as antibodies, or for nano-sized drug carriers following their mucosal administration; this led to investigation of the IgG/neonatal Fc receptor (FcRn) transcytotic pathway. Immunostaining data demonstrated that Calu-3 cells express FcRn. IgG was shown to traverse the Calu-3 layers and studies characterizing this transport indicated FcRn involvement in this process. Confocal microscopy revealed that IgG- or Fc-adsorbed NPs were taken up by Calu-3 cells. Adsorption of Fc on the surface of NPs was seen to promote their cellular uptake and transport across the cell layers. Characterisation of cell uptake and transport of Fc-NPs revealed data that strongly suggested FcRn involvement in these processes.

# Acknowledgements

First and foremost I offer my sincerest gratitude to my principal supervisor, Dr Snow Stolnik, who has supported me throughout my PhD with her wisdom, and kind patience, whilst allowing me the opportunity to explore the work in my own way. One simply could not wish for a supervisor who takes on the role of both mentor and friend.

It is difficult to overstate my gratitude to my other supervisors, Professor Cameron Alexander, Dr Martin Garnett and Professor Mike Eaton. With their enthusiasm, inspiration and great efforts in encouraging me to explore new ideas and to take risks, they helped me to realise my potential and to get the most out of my work. I would like to extend my thanks also to Dr Bryan Smith from UCB, Professor Martyn Davies, my internal assessor, Professor Lisbeth Illum and Dr Cynthia Bosquillon for their expert opinion and advice.

Furthermore, I wish to extend my appreciation to Dr Susan Anderson for her help and training with microscopy and to Dr Elizabeth Pearson, Dr Sanyogita Puri and Dr Ya Tsz Turner for their invaluable coaching and assistance for other essential techniques. On a daily basis, I have been helped (and badgered) by Christine Grainger-Boultby, a fine technician who kept me in check (most of the time) and always managed to bring a smile to my face. I give special thanks to Ruth Exposito-Harris and Luca Casettari, not only for their direct contribution to the work detailed in this thesis, but also for their professional dedication and friendship.

Throughout my PhD, I have been blessed with a friendly, cheerful and funny group of fellow students. In particular I would like to thank Alpesh, Katsu, Gerard, Meera, Vicky, Lizzy, Manali, Paulina, Klara, Jennie, Dimitra and Mathieu. Very special thanks to Emilia Moradi who has been a source of not only encouragement, support and enthusiasm, but also unforgettable friendship, banter and fun.

I want to express my profound appreciation to my girlfriend and fellow colleague Robyn Fowler for her professional guidance, understanding, and kind patience even during hard times of study and particularly during the write-up period when I was forgiven on numerous occasions for being socially inept and most probably, devoid of all romance.

I want to acknowledge the Department of Pharmacy in providing me with the support and equipment I have needed to produce and complete my thesis and also the BBSRC and UCB for funding my studies.

I feel an overwhelming sense of gratitude towards Professor Timothy M. Cox, a truly passionate physician at Addenbrookes Hospital, Cambridge. To this man I ultimately owe my life and so it goes without saying that without his strong dedication, profound skill and faith, I would not be where I am today and I certainly would never have been able to follow my dream in taking on this PhD. His devout commitment and kindness will always be remembered.

And finally my deepest gratitude to my parents, Mr Maliq and Mrs Hava Vllasaliu for their nurture, encouragement and support not only in my academic aspirations, but

throughout my life. In dedicating this thesis to them, I only hope I can repay just a fraction of the debt I owe them. I wish to further thank my sisters, Ermira and Donjeta, my beautiful nieces, Rea and Ena, my charming nephew, Adri and my extended family. Their love and encouragement fuelled my determination to succeed.

# Table of Contents

# List of Figures

## Chapter 1



## Chapter 2



## Chapter 3

# Chapter 4

## Chapter 5

## Chapter 6

## Chapter 7

# List of Tables

# Abbreviations

| | |
|---|---|
| % | Percentage |
| ° | Degree |
| °C | Degree Celsius |
| AB/AM | Antibiotic/Antimycotic |
| AEE | Apical Early Endosome |
| AG | Alkylglycoside |
| AIC | Air-Interfaced Culture |
| ARE | Apical Recycling Endosome |
| ATCC | American Type Culture Collection |
| ATP | Adenosine-5'-triphosphate |
| BEE | Basolateral Early Endosome |
| bIgG | Bovine Immunoglobulin G |
| BSA | Bovine Serum Albumin |
| C-CPE | Clostridium Perfringens Enterotoxin |
| CFHBSS | Calcium-Free Hank's Balanced Salt Solution |
| CFTR | Cystic Fibrosis Transmembrane Conductance Regulator |
| CLIC | Clathrin-Independent Carrier |
| CLSM | Confocal Laser Scanning Microscopy |
| $CO_2$ | Carbon dioxide |
| CRE | Common Recycling Endosome |
| Da | Dalton |
| DABCO | 1,4-Diazabicyclo-octane |
| DAPI | 4'-6-Diamidino-2-phenylindole |
| DDM | Dodecylmaltoside |

| | |
|---|---|
| $dH_2O$ | Distilled Water |
| DLS | Dynamic Light Scattering |
| DMEM | Dulbeco's Modified Eagles Medium |
| DMSO | Dimethylsulphoxide |
| DMβCD | Dimethyl-ß-Cyclodextrin |
| DQ | Degree of Quaternization |
| ECACC | European Collection of Cell Cultures |
| EDTA | Ethylene Diamine Tetraacetic Acid |
| ELISA | Enzyme-Linked Immunosorbent Assay |
| EMEM | Essential Minimum Eagle's Medium |
| Epo | Erythropoietin |
| Fab | Fragment antigen binding (of Immunoglobulin G) |
| FBS | Foetal Bovine Serum |
| Fc | Fragment crystallizable (of Immunoglobulin G) |
| FcRn | Neonatal Fc receptor |
| FD | Fluorescein Isothiocyanate-dextran |
| FD4 | Fluorescein Isothiocyanate-dextran 4 kilodalton |
| FD10 | Fluorescein Isothiocyanate-dextran 10 kilodalton |
| FD20 | Fluorescein Isothiocyanate-dextran 20 kilodalton |
| FD40 | Fluorescein Isothiocyanate-dextran 40 kilodalton |
| FD70 | Fluorescein Isothiocyanate-dextran 70 kilodalton |
| FD150 | Fluorescein Isothiocyanate-dextran 150 kilodalton |
| FDA | Food and Drug Administration |
| FITC | Fluorescein Isothiocyanate |
| FSH | Follicle-Stimulating Hormone |

| | |
|---|---|
| GEEC | GPI-Enriched Endocytic Compartment |
| GLP-1 | Glucagon-Like Peptide-1 |
| HBSS | Hank's Balanced Salt Solution |
| HEPES | 4-(2-hydroxyethyl)-1-piperazineethanesulfonic acid |
| HPLC | High Performance Liquid Chromatography |
| HRP | Horseradish Peroxidase |
| IC50 | Half Maximal Inhibitory Concentration |
| IF | Intrinsic Factor |
| IgG | Immunoglobulin G |
| JAM | Junctional Adhesion Molecules |
| kDa | Kilodalton |
| LCC | Liquid-covered culture |
| LDH | Lactate Dehydrogenase |
| LE | Late Endosome |
| M | molar |
| mM | Millimoles |
| MDCK | Madin-Darby canine kidney |
| MES | 2-(N-Morpholino)ethanesulfonic acid |
| ml | Millilitre |
| MTS | 3-(4,5-dimethylthiazol-2-yl)-5(3-carboxymethonyphenol)-2-(4-sulfophenyl)-2H-tetrazolium |
| Muc-1 | Mucin-1 |
| $M_W$ | Molecular weight |
| NAC | N-acetylcysteine |
| NAD | Nicotinamide adenine dinucleotide (oxidized) |

| | |
|---|---|
| NADH | Nicotinamide adenine dinucleotide (reduced) |
| nm | Nanometer |
| NP | Nanoparticle |
| PAA | Polyacrylic Acid |
| PAMAM | Polyamidoamine |
| $P_{app}$ | Apparent permeability coefficient |
| PBCA | poly(butyl cyanoacrylate) |
| PBS | Phosphate Buffered Saline |
| PC | Polycarbophil |
| PEG | Polyethylene Glycol |
| PES | Phenazine Ethosulfate |
| PIBCA | poly(isobutyl cyanoacrylate) |
| PKC | Protein Kinase C |
| PLA | Polylactic acid |
| PLGA | poly(lactic-co-glycolic acid) |
| RhG-CSF | Recombinant human Granulocyte Colony-Stimulating Factor |
| rHV2 | Recombinant Hirudin-2 |
| rIgG | Rabbit Immunoglobulin G |
| sCT | Salmon Calcitonin |
| SDS-PAGE | Sodium Dodecyl Sulfate Polyacrylamide Gel Electrophoresis |
| SEM | Scanning Electron Microscopy |
| siRNA | Small Interfering RNA |
| TDM | Tetradecylmaltoside |
| TEER | Transepithelial Electrical Resistance |

| | |
|---|---|
| TEM | Transmission Electron Microscopy |
| TJ | Tight Junction |
| TJAP | Tight Junction Associated Protein |
| TL | Tomato Lectin |
| TMB | 3,3,5,5-tetramethylbenzidine |
| TMC | *N*-trimethyl chitosan chloride |
| TNF | Tumor Necrosis Factor |
| TPP | Pentasodium tripolyphosphate |
| Tri-DM | Tridecylmaltoside |
| TRITC | Tetramethyl Rhodamine Iso-Thiocyanate |
| v/v | Volume per unit Volume |
| $VB_{12}$ | Vitamin B12 |
| w/v | Weight per unit Volume |
| YG | Yellow-Green |
| ZO-1 | Zonula occludens-1 |
| µl | Microlitre |
| µm | Micrometer |
| Ω | Ohm (electrical resistance unit) |

# Chapter 1

# Mucosal Delivery of Protein Therapeutics

## 1.1 Why deliver protein therapeutics mucosally?

The development of drugs based on biotechnology products is a rapidly expanding area within the pharmaceutical industry. A recent report by the Pharmaceutical Research and Manufacturers of America (PhRMA) states that in 2008 there were 633 biotechnology medicines ('biologics') in development, for more than 100 diseases (1). A large proportion of these are therapeutics based on different proteins, including monoclonal antibodies and recombinant hormones (Figure 1.1). The United States Food and Drug Administration (FDA) has so far approved more than 130 proteins and peptides for therapeutic purposes (2). The growth in protein drugs (and biologics in general) is unfortunately not matched by developments of effective and convenient delivery systems for this class of therapeutics. Currently, protein drugs are predominantly administered parenterally. This is due to their high molar mass, hydrophilicity and their inability to withstand the environment in the gastrointestinal tract, resulting in an inadequate absorption and hence poor bioavailability following oral administration. However, disadvantages associated with the parenteral route, including patient discomfort and high cost, necessitate research into alternative ways of administering this class of therapeutics.

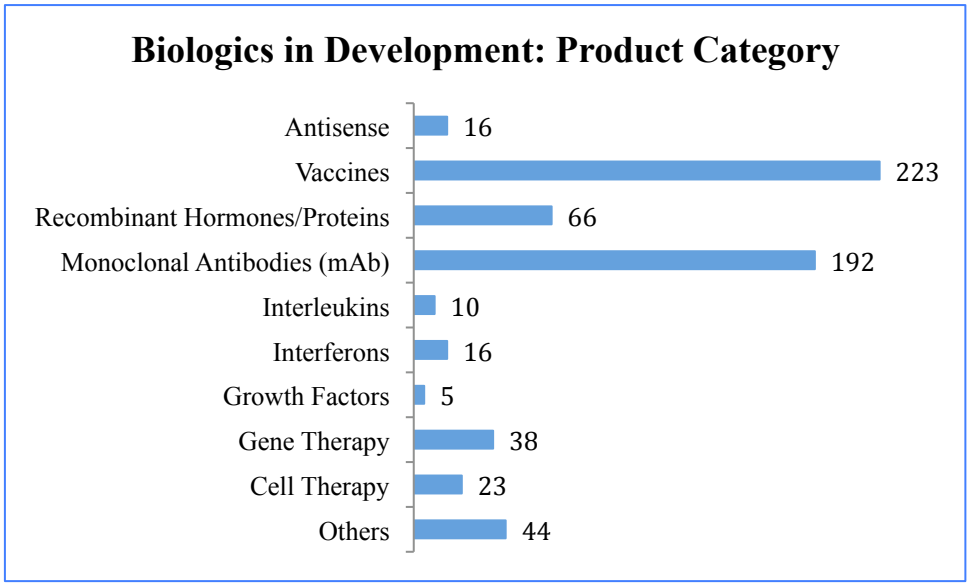


***Figure 1.1. Different classes of biologics in development in 2008. Adopted (and modified) from PhRMA [1].***

Arguably, the withdrawal of the pulmonary-delivered insulin, Exubera®, from the market in 2008 resulted in the shutdown of many research projects on pulmonary delivery of proteins in the pharmaceutical industry (3). However, as will be discussed later, non-parenteral delivery of protein drugs is still being explored by researchers in academia and the pharmaceutical industry and many interesting developments have been made. Examples of technologies, their associated companies and therapeutic proteins/peptides under development are listed in Table 1.1.

| Delivery pathway | Oral | Pulmonary | Nasal | Buccal |
|---|---|---|---|---|
| **Technologies (associated companies)** | Eligen® (Emisphere)<br>LPM™ (DOR Biopharma)<br>Spheromers™<br>PIN™ (Spherics)<br>Polymer/Bioadhesive platform (Coremed Inc.) | Promaxx (Baxter Healthcare Corporation)<br>Technosphere® (MannKind Corporation)<br>MicroDose Electronic dry powder inhaler (MicroDose Therapeutx)<br>Polymer/Bioadhesive platform (Coremed Inc.) | CPE-215® (CPEX Pharmaceuticals)<br>Intravail® (Aegis Therapeutics)<br>Thiomers (ThioMatrix) | Rapidmist™ (Generex)<br>Thiomers (ThioMatrix) |
| **Therapeutic proteins under investigation (associated companies)** | Insulin (Oramed)<br>Salmon calcitonin, heparin, glucagon-like peptide-1 (GLP-1), insulin, human growth hormone (Emisphere)<br>Insulin (Extrawell)<br>Insulin (Diabetology Ltd.)<br>Leuprolide (DOR Biopharma)<br>Nodlin and Nodexen (NOD Pharmaceuticals Inc.) | Insulin, PTH, salmon calcitonin, GLP-1 (MannKind Corporation)<br>Insulin (Microdose Therapeutx)<br>Insulin (Coremed Inc.) | Insulin (CPEX Pharmaceuticals, Inc.)<br>Insulin, GLP-1 (MDRNA)<br>Insulin, salmon calcitonin, PTH, and desmopressin (Unigene)<br>GLP-1 (Amylin) | Insulin (Biodel Inc) |
| **Marketed products (associated companies)** | Minirin® (Ferring)<br>Nocutil® (Gebro Pharma) | None known | Miacalcin® (calcitonin, Novartis)<br>Minirin® (desmopressin, Ferring)<br>Suprecur® (Sanofi-Aventis)<br>Fortical® (Unigene) | Oral-lyn™ (India) (Generex) |

***Table 1.1 Examples of delivery technologies and therapeutic proteins currently being investigated/marketed for mucosal administration by the Pharmaceutical Industry.***

***For more information the reader is referred to companies' websites. Table modified from Moeller et al. (3)***

## 1.2 Crossing the mucosal barriers: possible pathways

While some small, amphipathic molecules have the ability to partition into and out of lipid bilayer membranes (apical and basolateral) allowing them to readily enter and leave the epithelial cells without a specific transport system (Figure 1.2a), the transport of smaller hydrophilic macromolecules is limited to the paracellular route (i.e. between adjacent cells; Figure 1.2b). Larger macromolecules and nano-sized particles can also be transported across the cells *via* transcytosis route through a series of vesicular structures (Figure 1.2c). However, the organization and movement of these vesicles is highly regulated to minimize the non-selective transport of macromolecules into and out of the body (4).

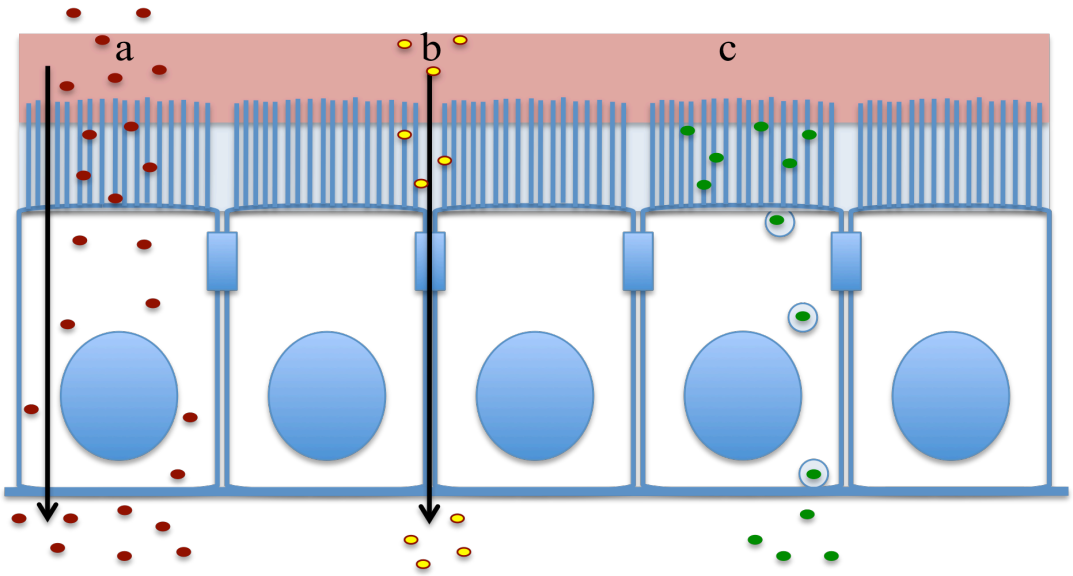


***Figure 1.2. Possible pathways for translocation of molecules and nanoparticles across the mucosal surfaces. a) Trancellular route, applicable to small, lipophilic molecules, b) Paracellular (between cells) route, relevant to relatively small, hydrophilic macromolecules, and c) Transcytosis (which may be receptor mediated), through which large macromolecules and nanoparticles can potentially traverse the mucosal surfaces.***

## 1.3 Barriers to mucosal absorption

Successful delivery and systemic absorption of protein therapeutics following mucosal administration requires several biological barriers to be overcome. Using the airway mucosa as an example, these barriers are presented schematically in Figure 1.3.

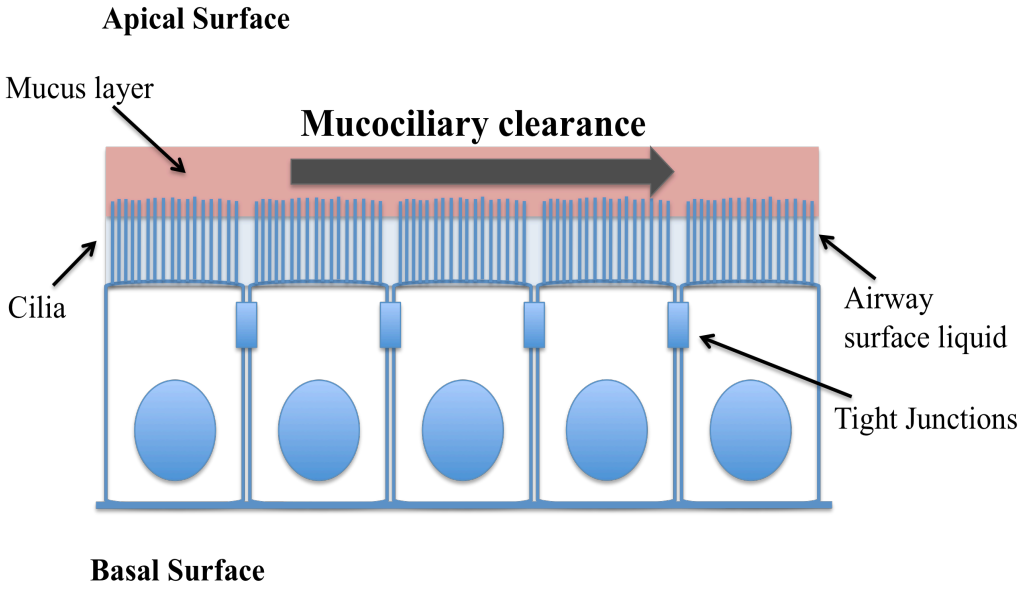


***Figure 1.3. Barriers to mucosal drug absorption. In mucosal surfaces such as nasal and bronchial, columnar ciliated epithelial cells are interconnected by tight junctions. Cells are covered by a layer of mucus, which is normally secreted by goblet cells (not included in the schematic). Cilia beat in a synchronized fashion, resulting in unidirectional movement of mucus (represented by the gray arrow). This mucociliary clearance mechanism clears the mucus-trapped material (which may include administered drugs) from the mucosal surfaces.***

Drug absorption across the mucosal surfaces is in some cases affected by mucus (5) and a functional mucociliary clearance mechanism. For example, in the nasal mucosa the mucociliary mechanism clears 50% of the administered dose (applied as a spray) from its ciliated respiratory mucosa within 15-20 minutes (6). The presence of proteases that may degrade the administered protein drug is also an important barrier limiting the availability of peptides and proteins at the mucosal surface and hence

their absorption (7). Finally, the existence of tight junctions (TJs) between adjacent epithelial cells, limits the permeability of macromolecules larger than approximately 1000 Da (8, 9). Transcellular movement (i.e. through individual epithelial cells) of hydrophilic macromolecules on the other hand is severely limited due to the physico-chemical nature of epithelial cell plasma membranes (5). The restriction of drug movement and mucosal absorption presented by mucus and the TJs is discussed in detail below.

### 1.3.1 The mucus barrier

The mucus barrier is essential in protecting vulnerable surfaces in the respiratory, intestinal, eye and reproductive tissues from invasion by foreign agents including bacteria, viruses, allergens and irritants. Furthermore, mucus also acts as a lubricant, aiding functions such as blinking and movement of food through the digestive system.

The mucus gel is mainly composed of linear, glycosylated mucin fibers entangled into a dense network (10, 11). The combination of mucin fiber composition and its architecture results in strong interactions between mucus and foreign molecules, severely inhibiting or hindering their movement through the gel (12, 13).

Factors affecting the rate of drug diffusion through mucus include the relative size of the drug molecule, the effective mesh size of the mucus gel and interactions between the drug and the components of mucus (14). It was long thought that the mucus barrier prevents the uptake of large molecules primarily by hindering their diffusion, with an inverse relationship between molecular weight and diffusion coefficient of the drug frequently reported (14). However, it is now known that most proteins, including

large antibodies diffuse easily through mucus (15). For example, Saltzman *et al.* (16) found that the diffusion of antibodies through human cervical mucus is relatively unimpeded, with antibodies diffusing through the mucus almost as readily as in water. This is thought to be because the mesh size of mucin fibres within mucus (approximately 1 μm) is much larger than most proteins (16).

In contrast to macromolecules, there is strong evidence that mucus presents a considerable barrier to the movement of nanoparticles (NPs) (17). In an attempt to improve their transport through mucus, Wang *et al*. (18) recently attached PEG on the surface of NPs and measured their diffusion rate in cervicovaginal mucus. The authors coated the surface of negatively charged 220 nm diameter polystyrene particles, which normally exhibit poor diffusion in mucus, with differently sized PEG, at different densities. Coating of the particles with short-length PEG at high density resulted in neutralisation of the particles' negative surface charge, which afforded diffusion in mucus gel at a rate just ten times slower than in water. Reduction of PEG coating density on the surface of particles decreased the rate of particle transport, which was explained by less effective screening of the negative charge of the particle surface resulting in binding of particles to mucin fibres. The results of this study therefore suggested that particle transport in mucus could potentially be improved by a net neutral surface to avoid binding, and a small radius to avoid entanglement with the mucin network.

Lai *et al*. (17) further demonstrated that large NPs, if properly coated, can rapidly penetrate human mucus. In this study the authors used high-speed multiple particle tracking to quantify transport rates of different particles in samples of fresh human

cervicovaginal mucus. PEGylated NPs of 500 nm and 200 nm in diameter were found to diffuse through mucus with an effective diffusion coefficient only 4- and 6-fold lower than that for the same particles in water (the diffusion coefficient of uncoated particles of 100–500 nm diameter was 2,400- to 40,000-fold lower in mucus than in water). Interestingly, the rate of particle diffusion in mucus was enhanced more for larger PEGylated NPs of 200 nm and 500 nm than for smaller, 100 nm particles.

In another study, Cu *et al*. (19) examined the effect of immobilization of PEG with different molecular weight (2, 5 and 10 kDa) onto the surface of poly(lactic-*co*-glycolic)acid (PLGA) NPs (170 nm diameter) at a range of densities from 5-100% on diffusion in cervical mucus. The reported observations indicated that incorporation of PEG onto the surface of particles enhanced the diffusion of particles in cervical mucus (diffusion of PEGylated particles was 3- to 10-fold higher than that of unmodified particles), in addition to improving particle dispersion and neutralizing the surface charge. Particle diffusion in mucus was strongly dependent on the molecular weight of PEG and the coating density.

While the studies discussed above demonstrated that PEGylation improved the transport of NPs through mucus, Huang *et al*. (20) have shown that grafting of PEG increases the mucoadhesiveness of acrylic-based hydrogels, sticking to mucus strands in a way that would inhibit transport. Whether PEGylation facilitates transport through the mucus gel or provides mucoadhesion seems to be an effect of its molecular weight, coating density and the structure to which it is attached (e.g. nanoparticle *versus* polymeric hydrogels).

### 1.3.2 Intercellular Tight Junctions

The intercellular tight junctions (TJ) encircle the epithelial cells in a belt-like manner at the apical cellular borders (21), separating the membrane surfaces of these cells into the apical and basolateral regions. The homotypic contact made by TJs across the intercellular spaces between the adjoining epithelial cells (22, 23) provides a structural barrier against paracellular permeation (24, 25), maintaining the restrictive barrier of the mucosae. The TJs regulate the passage of ions, water and molecules through the paracellular pathway (26). Furthermore the TJs limit the diffusion of proteins and lipids between the apical and basolateral domains of the plasma membrane (27) and recruit cytoskeletal and signaling molecules involved in cell polarity, growth, differentiation and apoptosis (28).

TJs are observed by Electron Microscopy as a series of fusion points (sometimes referred to as 'kissing points') between the outer leaflets of the membrane of the adjacent cells. Structural components of the TJs include the transmembrane proteins such as claudins, occludin and junction adhesion proteins, as well as cytoplasmic plaque proteins including zonula occludens-1/2/3, cingulin and 7H6 (29). Both claudin and occludin are tetra-span (four-pass) proteins consisting of four transmembrane regions and two extracellular domains, which are capable of interactions with complementary molecules on adjacent cells forming adhesion points and through lateral copolymerization forming continuous strands (26). Cytoplasmic plaque proteins are thought to link claudin and occludin to the actin cytoskeleton through PDZ domains and cross-link the transmembrane junction proteins (28). Furthermore the cytoplasmic plaque proteins may have a role in vesicular trafficking to the TJ and cell signaling through their associated kinases and other less

characterized functions such as gene expression (28). A TJ inter-connecting adjacent nasal epithelial cells of excised porcine mucosa (respiratory region), imaged using Electron Microscopy by our group is presented in Figure 1.4.

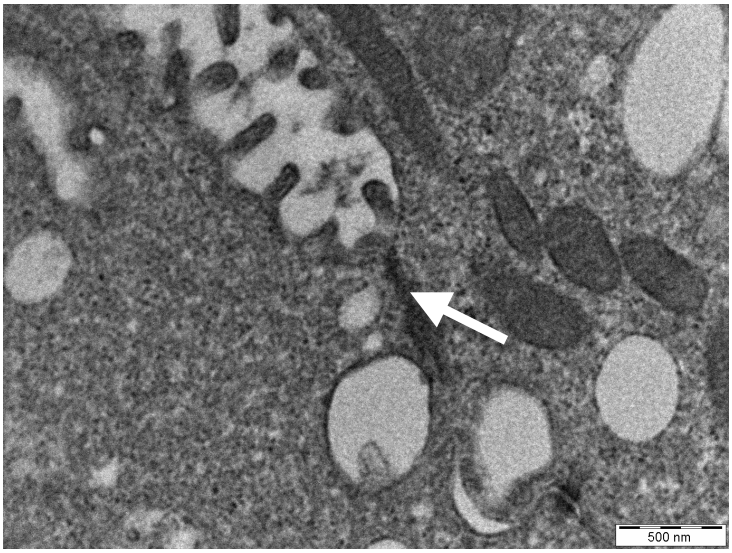


***Figure 1.4. Nasal epithelial cells interconnected by a tight junction. Transmission Electron Microscopy (TEM) micrograph of epithelial cells obtained from tissue samples from excised porcine nasal mucosa (respiratory region). Arrow indicates a tight junction between the cells.***

TJs comprise a major barrier towards the paracellular transport of larger solutes (30). The dimensions of the paracellular space lie between 10 and 30–50 Å, suggesting that solutes having a molecular radius exceeding 15 Å (3.5 kDa) will be excluded from this route (31): this includes most therapeutic proteins.

## 1.4 Mucosal administration of protein drugs: potential routes

### 1.4.1 Oral route

The oral route is the preferred way of drug administration due to the ease of self-administration, convenience and lower costs (32). However, the gastrointestinal tract is a complicated system of organs designed primarily to break down food and absorb nutrient molecules. Following their oral administration, many peptides and proteins

will be destroyed before absorption can take place in the small intestine. This is because of the presence of proteolytic enzymes (2) and an unfavorable acidic environment (33). *In vivo* studies with native insulin in a murine model have shown bioavailabilities of less than 1% following administration *via* the oral route (34). This low level of bioavailability is generally not acceptable, as unlike small chemical entities, with protein pharmaceuticals the cost of goods is generally high. Consequently, a drug product having a relatively low bioavailability requires a high dose to achieve the desired therapeutic effects, which presents problems with regards to its cost effectiveness.

Therapeutic proteins/peptides intended for oral administration under development by the pharmaceutical industry include Glucagon-like peptide-1 (GLP-1, a gut hormone possessing physiological properties, including stimulation of insulin secretion, that make it a potentially useful compound for treatment of diabetes) by Emisphere, which is currently in phase I clinical trials. Oral insulin is also under development by Emisphere, Oramed, Diabetology, Extrawell and most likely by other companies. The oral insulin product by Diabetology, called Capsulin, incorporates absorption enhancers and exhibits a reported bioavailability of 6-10% relative to injected insulin (35).

### 1.4.2 Pulmonary route

The respiratory system can be separated anatomically into the conducting regions, consisting of the air-transmitting passages of the nose, nasopharynx, larynx, trachea, bronchi and bronchioles (36), and respiratory regions (where exchange of gases occurs) comprising of alveolar ducts and saccules. The structure of the conducting

airways changes gradually as the diameter of the respiratory tubes becomes smaller (37), with the pseudostratified, columnar and ciliated epithelium with goblet cells and submucosal glands changing into a flattened squamous organization lacking in goblet cells or glands. The change in structural features of the airways is presented schematically in Figure 1.5.

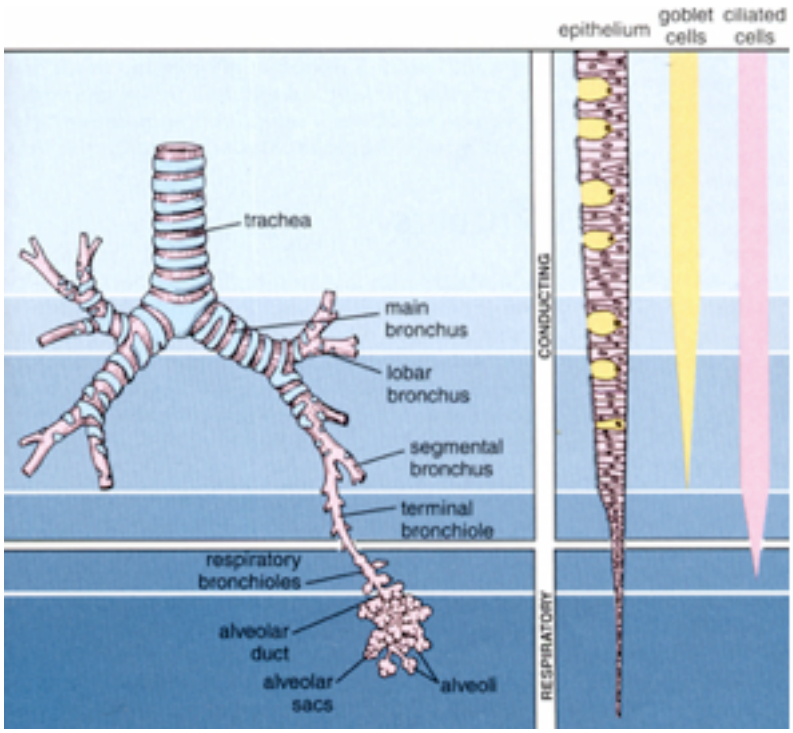


***Figure 1.5. Structural features of the respiratory tube wall throughout the system, starting from trachea to alveoli. Adopted from (38).***

In the upper airways mucus functions to clear entrapped particulates entering the lung. The ciliated epithelial cells move the tracheal mucus sheet (containing inhaled, trapped particles) in an escalator-like fashion to its juncture with the esophagus, following which the trapped material is swallowed and cleared from the airway; this mucocilliary clearance mechanism provides an important host innate defense mechanism against invading organisms and exogenous particulate material.

Pulmonary administration is attractive for non-invasive drug delivery because of the very large surface area (approximately 140 $m^2$) for drug absorption (39), thin alveolar epithelial cells presenting minimal barriers to transport, avoidance of the first-pass metabolism and minimal enzymatic activity within the lungs (2). On the other hand, factors that may limit the use of the pulmonary route for delivery of protein drugs include lung disease, smoking and the necessity to control the breathing rate (39).

In terms of developments in the pharmaceutical industry, MannKind Corp. is actively seeking to market pulmonary insulin (Afrezza), with the company filing for FDA approval in 2009. Furthermore, an unnamed inhaled insulin product by MicroDose Therapeutx has completed its phase I clinical trial, while Alveair™ (produced by Coremed Inc.) and an unnamed product (both insulin formulations designed for inhalation) made by Baxter are both in phase I trials (40).

### 1.4.3 Nasal route

Some of the characteristics of the nasal cavity that make the delivery of therapeutics through the nasal mucosa attractive, include the relatively large surface area available for absorption (approximately 150 $cm^2$), the highly vascularised submucosa, and the avoidance of both gastric and first pass metabolism (8). Furthermore, the nasal mucosa exhibits a lower enzymatic activity when compared to the gastrointestinal tract (41). The nasal epithelial layer is covered by a mucus blanket, synthesized by the goblet cells, nasal and lacrimal glands, and plasma transudate. The mucus blanket, which traps particles larger than 4 μm, consists of two layers: an underlying sol (water) layer close to the epithelium and a superficial gel layer. Mucus is 90-95% water, 1-2% salt, 2-3% mucin and proteins. The pH of nasal secretions in adults is

5.5-6.5 (42).

Of the three different regions of the nose (vestibular, respiratory and olfactory), the respiratory region is important for nasal delivery due to its large surface area and rich vasculature. Nasal mucosal epithelium consists of ciliated, non-ciliated, goblet and basal cells. The respiratory region is lined with pseudostratified columnar epithelium and within this region the ciliated columnar cell is the predominant type. Each ciliated cell contains around 100 cilia each about 5 μm long. The cilia beat in a synchronised fashion to clear the covering mucus layer (mucociliary clearance) at a rate of 6 mm/min (43).

Potential problems associated with the use of the nasal route for drug delivery include filtration of foreign particulates and rapid mucociliary clearance, which may affect the absorption of macromolecules (44). Other factors such as nasal secretions and the pH of the nasal cavity must be considered, as it is important to preserve the physiological functions and conditions of the nasal cavity (45). Nasal mucosa exhibits a low molecular weight ($M_W$) cut-off (approximately 1000 Da) for macromolecular absorption (41) and therefore absorption enhancers have been extensively investigated as a possible solution to this problem.

Marketed nasal formulations are restricted to peptides such as desmopressin (Minirin®, Ferring) and buserelin (Suprecur®, Sanofi-Aventis). These formulations are plain peptide solutions with no absorption enhancers, which explains their relatively modest bioavailabilities of approximately 3–10% (3). An unnamed insulin nasal spray developed by MDRNA and a nasal liquid emulsion spray (Nasulin) by CPEX

Pharmaceuticals are both in phase II clinical studies. Nasal formulations of the GLP-1 analogue exenatide are also in development by Amylin Pharmaceuticals and MDRNA (both in phase II trials) (40).

### 1.4.4 Buccal route

Delivery through the buccal cavity offers avoidance of first pass metabolism as the blood vessels of the oral mucosa drain directly into the jugular vein. Furthermore, the oral cavity is highly vascularized (2) and provides an environment almost free from the acidity and protease activity encountered elsewhere in the mucosa (46). The surface of the buccal mucosa consists of a stratified squamous epithelium composed of 40–50 cell layers (47). While the cells of the intestinal and nasal epithelia are joined by TJs, the presence of these structures is rare in the oral mucosa (48), where the membranes of the epithelial cells are surrounded by a hydrophilic intercellular matrix composed of relatively polar lipids (47). However, the presence and variable flow rate of saliva acts as a barrier to drug transport (2). Furthermore, observed regional variation in drug permeability in the buccal mucosa (49) gives rise to challenges for reproducible delivery and maximal bioavailability. Many buccal delivery systems based on bioadhesion have been described for numerous therapeutics based on peptides or proteins (50). For example, buccal delivery of calcitonin and GLP-1 using an adhesive tablet showed 37% (51) and 41% (52) bioavailabilities, respectively.

A sublingual tablet formulation of Desmopressin (Minirin®) has been developed and marketed by Ferring Pharmaceuticals, but has a low bioavailability of 0.25% (3). Some of the technologies under development contain mucoadhesive excipients like

thiomers developed by ThioMatrix, while others, such as insulin product Oral-lyn™ contain absorption enhancers to help the drug cross the epithelial barrier. With regards to the latter product, relative bioavailabilities of 7–9% have been reported by its manufacturer (Generex). Biodel Inc. is also developing an oral formulation of insulin designed for sublingual administration (VIAtab™), which is currently in phase I studies.

### 1.4.5 Other mucosal routes

Other sites that have been explored for delivery of protein therapeutics include rectal, vaginal and ocular mucosas. Rectal delivery of proteins provides a greater systemic bioavailability compared to the oral route of administration (53) and also avoidance of enzymatic degradation as there may be protein absorption by the lymphatic system (39). However, limitations with this approach include bacterial activity, interference from fecal material, and longer disintegration and dissolution times in the colon environment (54). Furthermore, rectal administration of drugs has poor cultural acceptance in some countries (2).

Ocular absorption occurs predominantly through the nasolacrimal system. In contrast to the intestinal and nasal epithelia, which consist of a single layer of cells joined by TJs, the corneal epithelium is made of several layers of cells, also joined by TJs (47). A number of peptides and proteins, including insulin, thyrotropin-releasing hormone, luteinizing hormone-releasing hormone, encephalin, calcitonin, and glucagon have been administered through the ocular route (55). Although the ocular route potentially provides relatively fast systemic absorption and the absorbed protein avoids first pass metabolism, the presence of peptidases in relatively high concentrations in tear fluid

can affect protein drug stability. Furthermore, the irritation caused by application of the drug to the eye can also trigger tear formation, leading to lower bioavailabilities (56).

Studies investigating the potential use of the vaginal mucosa for protein delivery have found localized adverse reactions and low, variable absorption (39). Moreover, the non-applicability in both sexes limits the use of this route.

## 1.5 Improving mucosal delivery: common investigated strategies

Different strategies have been explored in an effort to improve the absorption and bioavailability of mucosally delivered protein therapeutics, as illustrated in Figure 1.6. These include the use of delivery systems that prolong the contact time of the drug with the mucosal surfaces (mucoadhesive polymers) (57, 58) (Figure 1.6a), agents that increase membrane fluidity or disrupt cell membranes (e.g. surfactants) (59-61) (Figure 1.6b) and compounds that open the epithelial TJs (Figure 1.6c). Receptor-mediated transcytotic pathways (Figure 1.6d) have also been investigated for their potential in transmucosal delivery of protein therapeutics, as will be discussed later. Furthermore, compounds that improve mucosal drug access such as mucolytics (62-65), those that increase the stability of the administered protein drug, e.g. proteolytic enzyme inhibitors (66, 67), and agents which dissociate protein aggregation (e.g. cyclodextrins) (68) have also been employed for the same purpose.

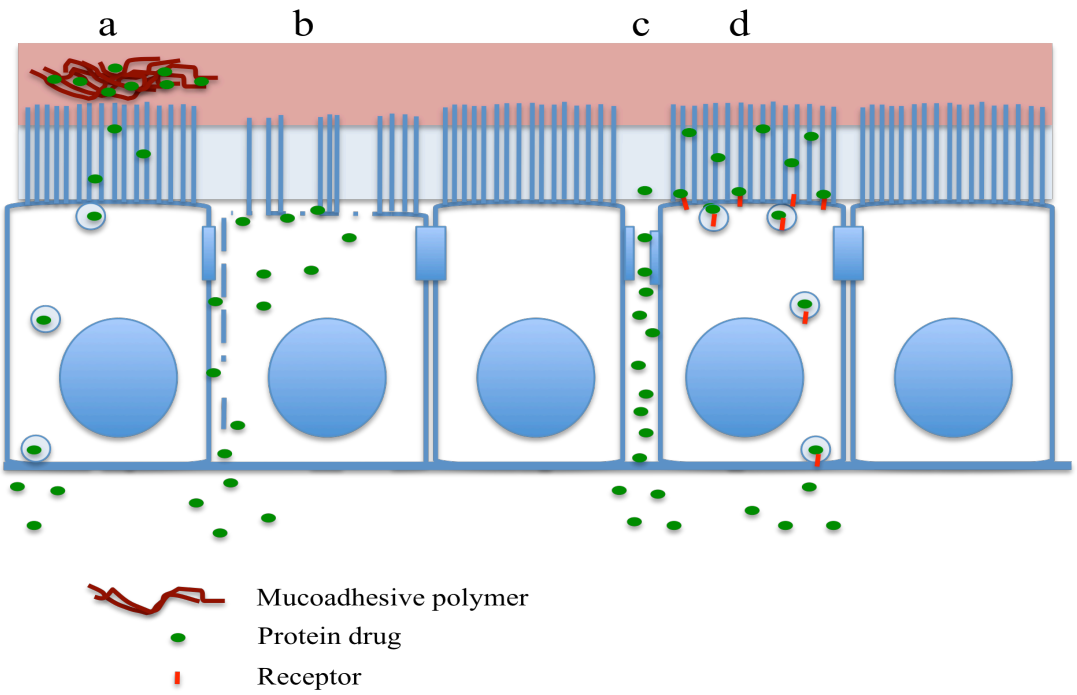


***Figure 1.6. Common strategies investigated for improvement of mucosal absorption of protein therapeutics. a) Mucoadhesive polymers prolonging the residence time of the complexed protein drug at the mucosal surface, b) Surface-active permeability enhancers compromising cell membrane integrity, whereby otherwise membrane-impermeable protein drug crosses the epithelial barrier, c) TJ opening where the paracellular space is increased, improving the paracellular access of protein molecules, and d) Exploiting epithelial transcytotic mechanisms by conjugating the drug (or a drug carrier nanoparticulate system) to a ligand (not shown) that is transported transepithelially via this route.***

### 1.5.1 Absorption enhancers

Absorption (or permeation/permeability) enhancers are compounds that transiently disrupt the epithelial barrier and TJs, thereby increasing the permeability of drugs and potentially improving the drug's bioavailability. An ideal enhancer would be non-toxic and biocompatible, pharmacologically inert, compatible with drugs and exhibit a reversible effect to limit or prevent damage to epithelia. Common absorption enhancers include surfactants, which enhance absorption by improving the transcellular transport (by disrupting the lipid bilayer), calcium chelators and

chitosans, which act on the paracellular transport (through disruption of the TJs) (69).

*1.5.1.1 Surfactants*

Various ionic and non-ionic surfactants have been investigated for their potential use as mucosal absorption enhancers. Their absorption-enhancing property has been demonstrated in many studies (70-72). However, a large number of these studies found that the use of surfactants as permeability enhancers is associated with cell toxicity, frequently observed in the form of cell membrane damage, altered cell morphology (70, 73-75) and mucociliary arrest (76, 77), which limits their application.

Recently, alkylglycosides, a class of nonionic amphipathic surfactant compounds containing alkyl chains of variable lengths, glycosidically attached to either a monosaccharide or disaccharide have been investigated, both *in vitro* and *in vivo*, for their potential to improve the systemic bioavailability of macromolecular peptides and proteins delivered mucosally (59-61, 78-80). Alkylglycosides will be discussed in greater detail in Chapter 4.

*1.5.1.2 Calcium-depleting agents*

The role of extracellular calcium in regulating the epithelial TJs and therefore maintaining the barrier property of the epithelium has been known for a long time. Studies on epithelial cell lines showed that depletion of extracellular calcium prevents the formation of TJs (81), induces opening of (existing) TJs (21, 82) and increases TJ permeability (21, 83-86). As a result, different compounds possessing an ability to bind calcium, reducing its extracellular levels, have been investigated for their

potential to enhance the mucosal absorption of macromolecules through the paracellular route. However, the conditions under which extracellular calcium depletion produces pronounced opening of the TJs and whether this strategy can be used to improve the absorption of macromolecular therapeutics in the *in vivo* settings is somewhat unclear from the literature. Work attempting to address these points was conducted in this thesis and is presented in Chapter 5.

*1.5.1.3 Polymeric enhancers*

**Chitosan,** the deacetylated form of chitin, is one of the most extensively investigated polymeric absorption enhancer. This is probably due to its low production costs, biodegradability, biocompatibility and FDA approval (87). Its property to enhance the absorption of macromolecules across the mucosal surfaces has been demonstrated in many studies. For example, chitosan salts, such as hydrochloride and glutamate increased the transport of buserelin and insulin *in vitro* (88). The capacity of chitosan to enhance the intestinal transport of peptides was also confirmed *in vivo*, with 1.5% w/v chitosan hydrochloride increasing the absolute bioavailability of buserelin, following its intraduodenal application in rats, from 0.1% (in control buffer) to 5.1% (89). Application of a chitosan solution effectively enhanced nasal absorption of salmon calcitonin (sCT) *in vivo* in rats (90) and significantly increased the permeability of fluorescein isothiocyanate recombinant hirudin-2 (FITC-rHV2) across the excised rabbit nasal epithelium and its bioavailability following the nasal administration to rats (91). In addition to its ability to facilitate paracellular transport, chitosan can also be used to formulate microparticles or NPs. The permeability enhancing property of chitosan NPs in comparison to solution is investigated in this work and the results will be described and discussed in Chapter 6. Additionally, the

mechanisms thought to be involved in TJ-opening by chitosan will be discussed there.

Chitosan is a weak base and an acidic environment is required to transform it into the positively charged, water-soluble form; at neutral or physiological pH most chitosan molecules will lose their charge and precipitate from solution (92). The chitosan derivative ***N*-trimethyl chitosan chloride (TMC)** has been synthesised in an attempt to improve its solubility at neutral pH. In solutions in the 1.5–2.5% concentration range, at pH 7.4, TMC was found to markedly increase the permeability of peptide drugs (buserelin and porcine insulin) across Caco-2 cell monolayers (88). TMC, applied on Caco-2 cell monolayers at pH 7.4 provided permeability enhancement that was similar to chitosan that was applied at pH 5.6 (93). The degree of quarterization (DQ) and hence charge density, is a determinant factor for the permeability-enhancing property of TMC in neutral environments. The use of TMC derivative with a 60% degree of substitution (TMC60) at pH 7.2 was associated with a higher mannitol transport enhancement ratios across Caco-2 cells than TMC40 (40% DQ), whereas TMC with the lower degree of substitution (12.3%) was ineffective at neutral pH (94). Similarly, TMC afforded an improvement in bioavailability of buserelin by more than 7-fold and more than 16-fold, depending on the DQ, after intraduodenal administration in rats (95) and intratracheal instillation of octreotide in combination with TMC in rats resulted in a 2.5- and 3.9-fold increase in the AUC for TMC20 (20% DQ) and TMC60, respectively (96). Nevertheless, there is evidence that a higher of DQ in TMC leads to a greater toxicity (97).

**Poly-L-arginine** molecules of varying $M_{WS}$ were found to increase nasal absorption of the model drug, FITC-dextran of approximately 4 kDa, (FD4), in rats. The

observed bioavailability of FD4, shown to be dependent upon the $M_W$ of poly-L-arginine, was higher than that produced by chitosan (98). Nasal absorption in rats of recombinant human granulocyte colony-stimulating factor (RhG-CSF, $M_W$ of 18.8 kDa) was increased following its coadministration with 1% w/v poly-L-arginine, producing a bioavailability of about 11% (99). The absorption enhancing effect of poly-L-arginine was shown to be transient (100). Additionally, this molecule, was also demonstrated to increase the translocation of FD4 across excised rabbit nasal epithelium (101). The considerable correlation between the permeability and the electrical conductance of the membrane indicated that the enhancer exhibited its effect on the paracellular pathway. This pathway was also visualized by Confocal Laser Scanning Microscopy (CLSM), which showed that the use of poly-L-arginine was associated with a marked localisation of fluorescence in the paracellular space.

*1.5.1.4 Other TJ modulating agents*

A number of relatively novel experimental approaches (including RNA interference, gene cloning and high throughput tissue culture assays) have been used to identify TJ targets that are most suitable for pharmacological manipulation in order to enhance paracellular drug delivery. Dutzar *et al.* (102) evaluated the effects of siRNA knock down of claudins 1, 3, 4, 9, 12, 20, JAM-1 and occludin in functional assays for TJ formation and permeability. Knockdown of claudin 4 inhibited TJ formation and resulted in a significant decrease in transepithelial electrical resistance (TEER) and an increase in FD4 permeability. Combination knockdowns between claudin 4 and occludin or JAM-1 showed synergistic effects. Interestingly, Kondoh *et al.* (103) also confirmed the potential of claudin as a novel target for drug delivery system. The authors of this study found that the C-terminal fragment of *Clostridium perfringens*

enterotoxin (C-CPE) is a potent absorption enhancer with an enhancing activity of 400-fold greater compared to sodium caprate (a clinically used enhancer) without showing any mucosal toxicity in rat jejunum. The enhancing activity involved an interaction between C-CPE and claudin-4.

Johnson *et al.* (104) developed a novel TJ modulating peptide, PN159, the application of which was associated with a reduction in TEER across a tissue barrier and increased paracellular transport of dextran, with low cytotoxicity and no decrease in cell viability. In a subsequent study (105), this peptide, which is polycationic and amphipathic, was shown to afford a significant improvement in permeation of salmon calcitonin, parathyroid hormone 1-34 and peptide YY 3-36 across epithelial tissue. Additionally, the TJ modulating peptide, PN159, dramatically increased the bioavailability of peptide YY 3-36 when dosed intranasally in rabbits.

### 1.5.2 Bioadhesive polymers

There is some evidence that the interaction between various types of bio(muco)adhesive polymers and epithelial cells can affect mucosal permeability, with adhesion of the drug delivery system to the surface of intestinal epithelial cells leading to enhanced uptake by nonspecific receptor-mediated endocytosis (55). However, for this technology, there is a need for improvement in localization or retention of the drug delivery system at the desired mucosal region (106) as presently, mucoadhesive systems are susceptible to the sloughing of the mucosa (107) and displacement by mucus excretion (108).

The muco- or bio-adhesive nature of some materials has been explained through

different theories, amongst which the adsorption theory is the most widely accepted. This theory states that mucoadhesion occurs due to secondary forces such as hydrogen bonds, van der Waals interactions and ionic bonds (109). Anionic polymers such as poly(acrylic acid), poly(methacrylic acid), and others bearing carboxyl and hydroxyl groups have been shown to exhibit better bioadhesion than cationic or neutral polymers (110).

The mucoadhesive properties of **Carbopol®**, a derivative of poly(acrylic acid), providing an intimate and prolonged contact between the drug and the mucosal surface are potentially favourable for use in transmucosal drug delivery. Carbopol® has also been reported to open the paracellular spaces of Caco-2 cell monolayers, thereby enhancing the epithelial permeability (111) and inhibit calcium-dependent proteases, thus improving the stability of peptide/protein drugs at mucosal surface (112). Carbopol® has been demonstrated to enhance the intraduodenal absorption of the peptide buserelin in rats, with an increase in bioavailability from 0.1% (with control buffer) to 2.0% (with 0.5% w/v Carbopol® 934P) (89). Furthermore, the use of Carbopol® 971P in Calu-3 cell layers was associated with an increase in the apparent permeability of hydrophilic macromolecules such as mannitol, the peptide desmopressin (1-cys-deamino-8-Darginine-vasopressin), FD4, and FITC-dextran of approximately 10 kDa (FD10) across the cell layers, accompanied by a concomitant decrease in TEER (113).

In addition to its ability to open the intercellular TJs, **chitosan** possesses inherent mucoadhesive properties. These are attributed to its positive charges forming a strong electrostatic interaction with the negatively charged sialic acid residues of mucins

(114).

**Thiolated Polymers** seem to bind covalently to mucus through the thioldisulfide exchange reactions with mucin glycoproteins. Chitosan has been modified by immobilizing thiol groups on the polymer chain, with the purpose of improving its mucoadhesive and absorption-enhancing properties. Improved mucoadhesiveness results from exchange reactions between the thiol groups of the thiolated chitosan and disulfide groups within the mucus with formation of new disulfide bonds between the polymer and mucus (115). Nasal administration of chitosan-4-thio-butylamidine/reduced glutathione/insulin microparticles to rats was associated with a 1.6- to 3.5-fold increase in the absolute bioavailability compared to that seen with chitosan/insulin microparticles, and 4.3- to 7-fold higher bioavailability than that exhibited by mannitol/insulin microparticles (116, 117).

## 1.6 Crossing the mucosal barriers through the transcytotic route: cellular uptake and trafficking of protein drugs

Mucosal absorption through the transcellular route requires that the macromolecule must overcome the plasma membrane barrier once it reaches the surface of epithelial cells. Clathrin- or caveolin-mediated endocytosis, macropinocytosis and phagocytosis are all endocytic mechanisms which are known to play a role in the uptake of macromolecules (118). In addition to these, other clathrin- and caveolin-independent pathways have also been suggested to play a role in cellular uptake of material (119). The discussed uptake pathways are presented schematically in Figure 1.7. It should be emphasised that in the context of systemic mucosal drug delivery, in addition to effective uptake into the epithelial cell, therapeutic material has to be released into the

luminal side.

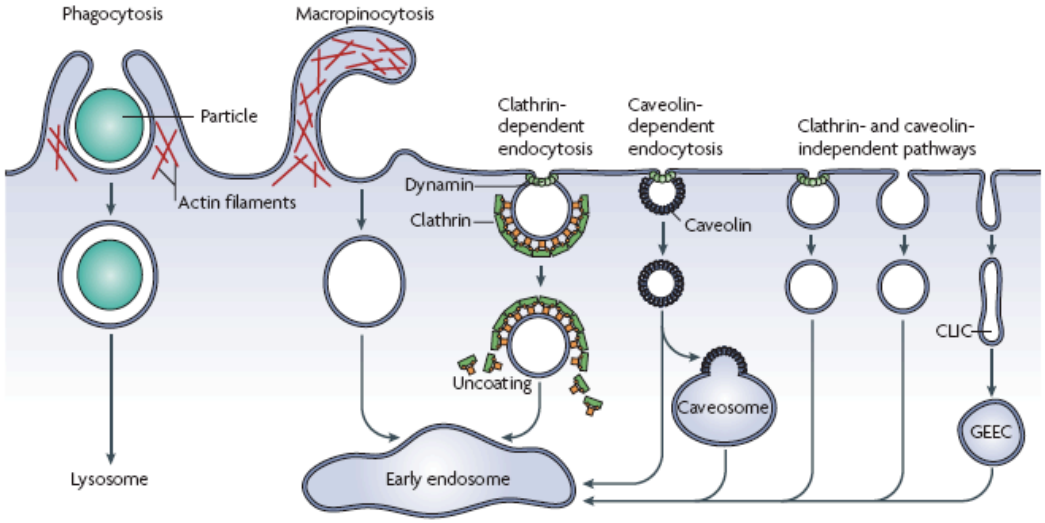


***Figure 1.7. Cell entry pathways. Large particles can be taken up by phagocytosis, whereas fluid uptake occurs by macropinocytosis. In comparison to other endocytic pathways, the size of the vesicles formed by phagocytosis and macropinocytosis is much larger. Cargoes can also be endocytosed by mechanisms that are independent of the coat protein clathrin and the fission GTPase, dynamin. Most internalised cargoes are delivered to the early endosome through vesicular (clathrin- or caveolin-coated vesicles) or tubular intermediates (known as clathrin- and dynamin-independent carriers (CLICs) that are derived from the plasma membrane. Some pathways may first traffic to intermediate compartments, such as the caveosome or glycosyl phosphatidylinositol-anchored protein enriched early endosomal compartments (GEEC), before reaching the early endosome. Taken from (119).***

### 1.6.1 Clathrin-independent endocytosis

Clathrin-independent endocytosis includes the constitutive pinocytotic pathway and endocytosis mediated by caveolae and glycolipid rafts (120). Caveolae are inverted omega-shaped invaginations with a maximal diameter of 50-100 nm connected to the plasma membrane or plasmalemma by a neck-like structure, which provides spatial continuity with the extracellular environment (121). The principal component, which is also a critical functional element is a protein called caveolin (122). Cholesterol is also very important component of caveolae and it is required to maintain structural integrity; caveolae disappear in cells that are depleted of cholesterol (123).

Caveolae can function as both intracellular and transcellular transport systems and they appear to be able to deliver their cargo either to endosomes or across the cell to opposite cell membrane surface (124). In contrast to classic clathrin-dependent endocytosis, there is evidence that caveolar internalization avoids lysosomes and hence the degradation of engulfed molecules (125).

The sensitivity of endocytosis *via* caveolae to cholesterol depletion with agents such as filipin, nystatin, or methyl-cyclodextrin distinguishes these pathways from both the clathrin-dependent and constitutive pinocytotic pathways. For example, Schnitzer *et al.* (124) showed the ability of filipin to disassemble endothelial noncoated vesicles, which selectively inhibits caveolae-mediated intracellular and transcellular transport of some macromolecules such as insulin and albumin in cultured endothelial cell monolayers. Filipin inhibits insulin uptake by endothelium for transcytosis, a cavelolae-mediated process, but not endocytosis for degradation, mediated by clathrin-coated pathway. The transcytosis process could occur by one of these two

mechanisms: caveolae could either pinch off from the plasma membrane, travel the short distance across the cell and fuse with the opposite surface, or, they may transiently fuse with each other producing channels through which ligands pass (126).

### 1.6.2 Uptake and transport of cargo in epithelial cells

The low rate of drug absorption through the mucosal surfaces is partly due to the low rate of endocytotic activity operating at the apical plasma membrane of epithelial cells. This phenomenon can be explained by the important physiological role of epithelia, and specifically the apical plasma membrane, filtering and repeling foreign substances in order to protect cells and organs from the external milieu (127). Endocytosis in non-polarised cells and at the basolateral plasma membrane of polarised epithelial cells was found to be several-fold faster than that operating at the apical plasma membrane (128, 129).

Polarized epithelial cells can internalize macromolecules from both apical and basolateral plasma membrane domains (130). In Madin-Darby canine kidney (MDCK) epithelial cells, used by many researches to study membrane protein trafficking in polarised epithelial cells (131), endocytosis occurs by both clathrin-dependent and independent mechanisms (132). The fate of material following endocytosis varies. After internalisation from the apical or basolateral sides of these cells, fluid-phase markers have been shown to enter distinct populations of apical early endosomes or basolateral early endosomes (133, 134). While a proportion of apically internalized fluid is thought to recycle or transcytose, some is delivered to a shared population of late endosomes and lysosomes (130).

*1.6.2.1 IgG/FcRn transcytotic pathway*

It has long been known that IgG is actively transferred from mother to offspring, conferring short-term passive immunity (135, 136). The transport of IgG is mediated by the neonatal Fc receptor (FcRn) (137, 138). This receptor is a potential candidate for mucosal delivery of therapeutic proteins as it is expressed in the lung (139) and the intestine (140) where it is involved in transepithelial transport of IgG. FcRn is known to undergo transcytosis in both apical-to-basolateral and basolateral-to-apical directions (141). Apical-to-basolateral transcytotic pathway of IgG/FcRn has been explored in various cell types, and is presented schematically in Figure 1.8. Briefly, IgG either binds to FcRn at the apical surface of the cells or is internalized by fluid-phase endocytosis, encountering FcRn in the apical early endosome (AEE). In the AEE, IgG/FcRn is sorted from fluid-phase markers and is either delivered to the apical recycling endosomes (ARE) or to the common recycling endosomes (CRE). Within the CRE, IgG/FcRn is sorted into coated vesicles that could serve as exocytic carriers to the basolateral cell surface (141) .

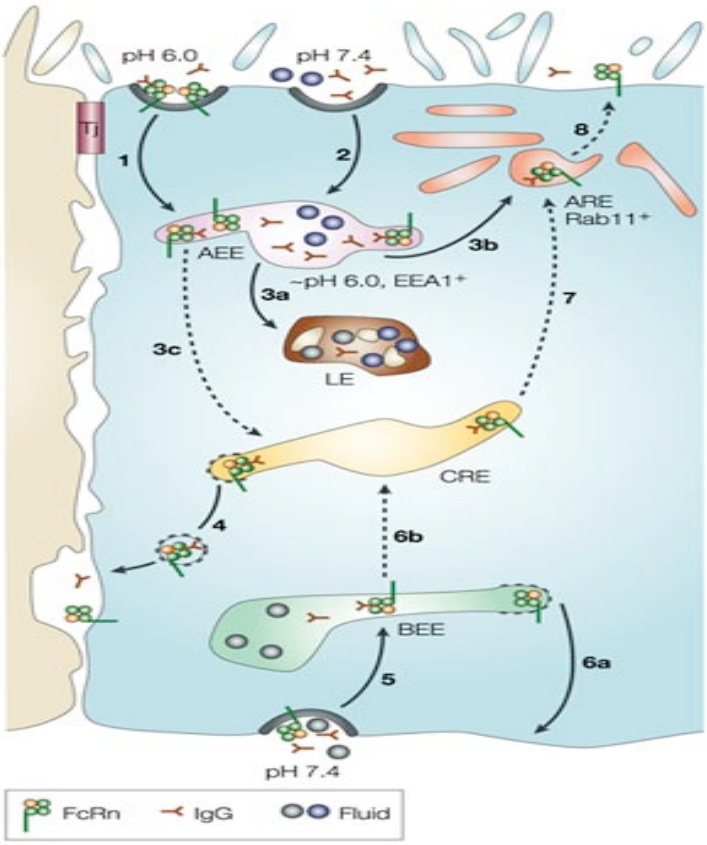


***Figure 1.8. IgG/FcRn transport pathway. IgG may bind to FcRn at the apical cell surface (step 1), or is internalized by fluid-phase endocytosis (step 2) (depending on the cell type) and encounters FcRn in the apical early endosome (AEE). In the AEE, FcRn–IgG is sorted from fluid-phase markers, which are delivered to late endosomes (LE) (step 3a) and lysosomes (not shown), and is either delivered to the apical recycling endosomes (ARE, step 3b) or delivered to the common recycling endosomes (CRE) (step 3c). In the CRE, FcRn–IgG is sorted into coated vesicles that probably serve as exocytic carriers to the basolateral cell surface (step 4). FcRn can also transport IgG in the basolateral-to-apical direction, although the intracellular pathway remains to be defined. A likely possibility is that IgG, internalized by fluid-phase endocytosis (step 5), binds to FcRn in the acidic pH of the basolateral early endosomes (BEE). FcRn–IgG either recycles (step 6a), or is delivered to the common recycling endosomes (CRE) (step 6b), ARE (step 7) and apical plasma membrane (step 8) where ligand dissociation and release occurs. Taken from (141).***

Recent studies investigating pulmonary absorption of therapeutic proteins (erythropoietin and follicle-stimulating hormone) through the FcRn pathway in non-human primates proved promising (142, 143). Furthermore, Bitonti *et al.* (144) investigated the prospect of exploiting this transcytotic pathway for absorption of protein drugs through the lung in healthy male volunteers and in doing so, demonstrated a dose-dependent absorption through the lungs. The potential of the IgG/FcRn pathway for mucosal delivery of macromolecules and NPs has been studied in this work and the results will be presented/discussed in Chapter 7.

*1.6.2.2 Vitamin $B_{12}$ transcytotic pathway*

Gastrointestinal absorption of vitamin $B_{12}$ ($VB_{12}$) occurs through receptor-mediated endocytosis. $VB_{12}$ is first bound to the intrinsic factor (IF), following which the $VB_{12}$-IF complex binds to the IF receptor located on the apical membrane of the villous enterocytes. The complex is subsequently endocytosed and transcytosed to the circulation (88). It is potentially possible to utilise $VB_{12}$ uptake mechanism to co-transport peptides and proteins. Russell-Jones and his coworkers (145-148) have demonstrated the potential of $VB_{12}$ to increase the oral uptake of various peptides such as luteinising hormone releasing hormone analogues, α-interferon, erythropoietin and granulocyte colony-stimulating factor by covalently linking the peptides to $VB_{12}$. Their later studies have focused on modifying the surface of the nanocarriers with $VB_{12}$, eliminating the need for conjugation and at the same time possibly increasing the transport capacity of the oral delivery system (145). Nevertheless, delivering drugs *via* $VB_{12}$ receptor-mediated transport is not without its associated problems. The limited transport capacity may be insufficient for less potent drugs and sharing a

physiological transport pathway of limited capacity, such that of $VB_{12}$ may lead to competition with other nutritional factors (149).

### 1.6.3 Other strategies for transcellular delivery of protein drugs

More recent strategies investigated for transmucosal delivery of proteins include the use of **cell-penetrating peptides (CPPs).** Recently, Khafagy *et al.* found that different forms of penetratin and octaarginine CPPs dramatically increased nasal absorption of insulin, with the most pronounced effect observed for L-penetratin. This compound exhibited a dose-dependent increase in insulin bioavailability from 1.7% (in control) to between 15.1% and 50.7% (depending on concentration) relative to the subcutaneous route. In a separate sudy by the same group, CPPs based on oligoarginines were investigated for their potential to improve intestinal absorption of insulin in rats. Insulin absorption increased dramatically after coadministration of oligoarginine of six residues of arginine in a dose-dependent manner, with resulting increase in bioavailability of up to 15.7% compared to the subcutaneous route (150). However, intestinal absorption of a larger molar mass interferon-β (23 kDa) was not affected by co-administration with oligoarginine, indicating that the $M_W$ of the protein therapeutic may present limitations to the usefulness of CPPs in their mucosal delivery.

**Dendrimers** possess unique characteristics and are considered to be promising candidates for biopharmaceutical delivery. The polyamidoamines (PAMAMs) are the most widely studied from a pharmaceutical perspective. A study by Wiwattanapatapee *et al*. (151) has demonstrated that PAMAM dendrimers crossed intestinal epithelial barriers at sufficient rates to act as potential drug delivery

systems, whereby anionic dendrimers were more efficient in crossing the epithelial barrier than cationic dendrimers. The uptake pathways were dependent on the sizes and charges of the dendrimers. On the other hand, Jevprasesphant *et al.* (152) revealed that cationic dendrimers were associated with a significantly greater permeability through Caco-2 cell monolayers than anionic dendrimers, an effect that was attributed to the interaction of cationic dendrimers with TJs, facilitating paracellular transport. In addition to paracellular movement, the studies discussed above indicate that transmucosal dendrimer transport may also occur *via* endocytic/transcytotic pathways.

**Lectins** are proteins or glycoproteins of plant, bacterial or vertebrate origin that recognise and bind to polysaccharide or glycoconjugate moieties (149). Plant lectins appear to be attractive carriers for oral drug delivery because of their ability to bind specifically to the sugar moieties of glycocalyx expressed on the intestinal epithelial cells and they are generally resistant to digestion within the gastrointestinal tract (149). Tomato lectin (TL) was one of the first lectins explored as a candidate in oral drug delivery because of its safety profile and resistance to gastrointestinal degradation (153). In the *in vivo* studies pioneered by Hussain *et al.* (154), although TL-conjugated NPs were entrapped within the mucus layer, they could efficiently penetrate the mucus gel and were transported across the epithelial cells. However, a major drawback of TL is its cross-reactivity with N-acetylglucosamine in mucus glycoprotein and a resultant reduction in the amount of TL conjugates available for interaction with epithelial cell surfaces (155).

## 1.7 Nanoparticles for mucosal delivery of protein therapeutics

Nanocarriers have great potential to improve the mucosal delivery of peptides and proteins (156). Polymeric NPs have been extensively investigated for the oral delivery of insulin. Insulin-loaded poly(*iso*-butylcyanoacrylate) (PIBCA) nanocapsules induced a reduction of glycemia in diabetic rats for up to 20 days (157). Their absorption has been shown to occur through the paracellular or transcellular pathways by enterocytes (and Goblet cells) (158). This nanoparticulate system, however, induced a variable therapeutic response when tested in dogs (159), which has limited its development. Coating of NPs with hydrophilic polymers, such as PEG (160) and chitosan (161) was found to improve the *in vivo* transport of proteins through preferential interaction with the mucus (mucoadhesion), and, in some cases, through the opening of TJs and paracellular transport.

Nanoparticulates were also used in an attempt to deliver peptide/protein drugs through the nasal mucosa. Nasal administration of chitosan NPs loaded with insulin resulted in a significant and relatively rapidly reduction of glycaemia compared to insulin mixed with soluble chitosan in rabbits (162). Coating of NPs with PEG and chitosan was found to increase their transport across the nasal mucosa, as demonstrated for PEGylated poly(lactide) (PLA) NPs (163) and chitosan-coated nanocapsules (164).

Administration of insulin-loaded poly(lactic-co-glycolic acid) (PLGA) NPs to guinea pig lungs resulted in a significant reduction in blood glucose level compared to insulin solution, an effect that lasted up to 48 hours (165). Similarly, pulmonary administration of insulin-loaded NPs of a different polymer, poly(butyl cyanoacrylate) (PBCA), were shown to extend the duration of a hypoglycemic effect (glucose level

below 80% of the original levels) over 20 hours, as compared to insulin solution (166). PLGA NPs coated with chitosan enhanced the absorption of calcitonin when delivered to the lungs of guinea pigs. This was attributed to a mucoadhesive effect and a possible opening of the TJs (167).

Recently, a rare study investigating the cellular uptake and transport of NPs (rather than soluble material) across MDCK polarised cells concluded that NP surface charge may significantly affect the mechanism of their internalization. Poly(ethylene glycol)-D,L-polylactide (PEG-PLA) NPs of both positive and negative surface charge (of approximately 90 nm and 96 nm, respectively) were found to mostly target the clathrin endocytic machinery, with a proportion internalized through a dynamin- and clathrin-independent process such as the macropinocytic pathway. The positive charge on the surface of NPs was seen to stimulate the movement of the NPs into clathrin-coated pits, with a fraction of internalized NPs following an endocytic pathway. A significant amount of cationic NPs and a fraction of the anionic NPs transcytosed and accumulated at the lateral plasma membrane. Importantly, cationic NPs were seen to avoid the lysosomal degradative pathway, which was not the case for anionic NPs (127).

Introducing hydrophilic PEG and hydrophobic alkyl side-chains potentially reduces adsorption of plasma proteins onto the NP surface (168, 169). PEG coated NPs offer greater stability against aggregation, minimal toxicity and diminished immunogenicity and thus have significant potential in controlled-release, targeted drug delivery. NP uptake by cells of the reticuloendothelial system can also be reduced by the presence of PEG on the surface, which ultimately extends the half-life

of NP-incorporated drugs and alters their tissue distribution (170), possibly improving the therapeutic profile of the drug.

## 1.8 General considerations in formulation design for mucosal delivery of proteins

In delivering protein therapeutics through the mucosal surfaces, several issues must be addressed. Firstly, the potential unwanted immunogenicity of protein pharmaceuticals in general seems very difficult to avoid (3), with evidence that the extent of this problem apparently depends on the route of administration. For example, the use of pulmonary insulin Exubera® was associated with a higher incidence of antibody formation compared to subcutaneous administration (3).

The safety of absorption enhancers has been assessed by various procedures, including the effect on ciliary beat frequency, reversibility of TEER, exclusion of membrane-impermeable compounds from epithelial cells, maintenance of morphological integrity and release of the intracellular enzyme, LDH (47). The use of some absorption enhancers, as discussed previously, gives rise to possible problems with toxicity. While the systemic toxicity of large, polymeric absorption enhancers is generally regarded as low (as because of their size they are not normally absorbed into systemic circulation) (47), absorption enhancers generally exert their effect by causing modification of the epithelial surfaces. This therefore raises concerns with regards to the maintenance of epithelial cell viability and the preservation of the physiological functionality. Furthermore, studies reported in the literature predominantly evaluate the toxicity of absorption enhancers following a single use (in epithelial cell lines or animals). In a clinical setting, however, repeated and often

long-term applications of the therapeutic system incorporating absorption enhancer(s) would be required; the long-term toxicity of such repeated application remains unknown.

Chitosans have in some cases been shown to produce dose-dependent toxicity on Caco-2 cells. Toxicity was directly related to the degree of deacetylation and, therefore, to the positive charge density of the polymer (171). Furthermore, an important factor affecting the extent of toxicity of chitosan towards buccal epithelial cells was the pH of the solution. As a more acidic pH leads to a higher charge density, this study confirmed that toxicity is related to positive charge density. Overall, the use of chitosan as an absorption enhancer is considered as substantially safe on the intestinal, nasal, ocular and buccal epithelia (47).

With regards to the use of nanoparticulates in an attempt to improve mucosal delivery of protein drugs, a major barrier is the lack of our understanding on how NPs interact with epithelial surfaces, the mechanism by which they traverse the epithelial barriers and ways to maximise transepithelial transport. Furthermore, a lot remains unknown about the toxicity and immunogenicity associated with the long-term use of nano-sized drug carriers.

Finally, the majority of studies investigating mucosal protein delivery, including those in this work, use mucosal models of various complexity. One must exercise caution in using the data generated in these studies, and even those performed in various animals *in vivo*, to make predictions in man.

## 1.9 Conclusion

In an era of biotechnology, the discovery of very specific and powerful protein drugs is proliferating, but their administration is presently limited to injections. Disadvantages associated with this method of drug administration make alternative ways of administering protein therapeutics greatly sought after. Mucosal surfaces offer high potential for delivery of this class of drugs, though biological barriers associated with this route present problems to the drug delivery scientist. Delivery of protein therapeutics across various mucosal surfaces, including gastrointestinal, respiratory, nasal and buccal is actively being researched by both the pharmaceutical industry and academia. Different strategies have been investigated in an attempt to improve the bioavailability of mucosally administered protein drugs. These include the use of absorption enhancers, mucoadhesive excipients and attempts to exploit epithelial transcytotic mechanisms, with or without the use of nanoparticulate drug delivery systems. While each of these approaches is not without its problems, significant progress has been achieved within this field. An ideal mucosal delivery strategy would incorporate systems that exhibit no toxicity upon repeated administration, preserve the biological activity of the therapeutic molecule, are applicable to most protein drugs, achieve acceptable bioavailability and do not substantially increase the cost of the formulation. Such a system would make mucosal administration of protein drugs widely available, which would be highly beneficial to both the patient and the pharmaceutical industry.

## 1.10 Project aims

The foregoing introduction argues that mucosal surfaces potentially provide non-invasive routes for administration of protein therapeutics. The main aim of this thesis

is to explore different strategies with a view to improving the transport of macromolecules (proteins and models of protein drugs) across mucosal surfaces. To this end, polarised epithelial cell layers will be adopted to serve as an *in vitro* model of airway epithelium. Initial work will focus on establishing and characterising this *in vitro* model, which will be based on the Calu-3 cell line. Thereafter, different strategies based on paracellular and transcellular transport pathways will be investigated for their potential to improve the translocation of macromolecules across the cell layers. These strategies will include the use of surfactants, tight junction modulation through the use of calcium depletion and chitosan, and lastly, exploitation of the IgG/FcRn transcytotic pathway for transmucosal protein and NP delivery.

## 1.11 References


1. PhRMA. Biotechnology Medicines in Development, *Medicines in Development*, The Pharmaceutical Research and Manufacturers of America, Washington, 2008.
2. N.A. Peppasand D.A. Carr. Impact of absorption and transport on intelligent therapeutics and nanoscale delivery of protein therapeutic agents. Chemical Engineering Science. 64:4553-4565 (2009).
3. E.H. Moellerand L. Jorgensen. Alternative routes of administration for systemic delivery of protein pharmaceuticals. Drug Discov Today. 5:89-94 (2008).
4. K. Mostov, T. Su, and M. ter Beest. Polarized epithelial membrane traffic: conservation and plasticity. Nat Cell Biol. 5:287-293 (2003).
5. R.J. Mrsny. Lessons from nature: "Pathogen-Mimetic" systems for mucosal nano-medicines. Adv Drug Deliv Rev. 61:172-192 (2009).
6. F.W. Merkus, J.C. Verhoef, N.G. Schipper, and E. Marttin. Nasal mucociliary clearance as a factor in nasal drug delivery. Adv Drug Deliv Rev. 29:13-38 (1998).
7. V.H. Lee. Protease inhibitors and penetration enhancers as approaches to modify peptide absorption. J Control Release. 13:213-223 (1990).
8. L. Illum. Transport of drugs from the nasal cavity to the central nervous system. Eur J Pharm Sci. 11:1-18 (2000).
9. S. Stolnikand K. Shakesheff. Formulations for delivery of therapeutic proteins. Biotechnol Lett. 31:1-11 (2009).
10. R. Bansiland B.S. Turner. Mucin structure, aggregation, physiological functions and biomedical applications. Curr Opin Colloid Interface Sci. 11:164-170 (2006).
11. D.J. Thorntonand J.K. Sheehan. From mucins to mucus: toward a more coherent understanding of this essential barrier. Proc Am Thorac Soc. 1:54-61 (2004).
12. G. Lafitte, K. Thuresson, and O. Soderman. Mixtures of mucin and oppositely charged surfactant aggregates with varying charge density. Phase behavior, association, and dynamics. Langmuir. 21:7097-7104 (2005).
13. C.T. Albanese, M. Cardona, S.D. Smith, S. Watkins, A.G. Kurkchubasche, I. Ulman, R.L. Simmons, and M.I. Rowe. Role of intestinal mucus in transepithelial passage of bacteria across the intact ileum in vitro. Surgery. 116:76-82 (1994).
14. K. Khanvilkar, M.D. Donovan, and D.R. Flanagan. Drug transfer through mucus. Adv Drug Deliv Rev. 48:173-193 (2001).
15. Y. Cuand W.M. Saltzman. Drug delivery: Stealth particles give mucus the slip. Nat Mater. 8:11-13 (2009).
16. W.M. Saltzman, M.L. Radomsky, K.J. Whaley, and R.A. Cone. Antibody diffusion in human cervical mucus. Biophys J. 66:508-515 (1994).
17. S.K. Lai, D.E. O'Hanlon, S. Harrold, S.T. Man, Y.Y. Wang, R. Cone, and J. Hanes. Rapid transport of large polymeric nanoparticles in fresh undiluted human mucus. Proc Natl Acad Sci U S A. 104:1482-1487 (2007).
18. Y.Y. Wang, S.K. Lai, J.S. Suk, A. Pace, R. Cone, and J. Hanes. Addressing the PEG mucoadhesivity paradox to engineer nanoparticles that "slip" through the human mucus barrier. Angew Chem Int Ed Engl. 47:9726-9729 (2008).

19. Y. Cuand W.M. Saltzman. Controlled surface modification with poly(ethylene)glycol enhances diffusion of PLGA nanoparticles in human cervical mucus. Mol Pharm. 6:173-181 (2009).
20. Y. Huang, W. Leobandung, A. Foss, and N.A. Peppas. Molecular aspects of muco- and bioadhesion: Tethered structures and site-specific surfaces. J Control Release. 65: (2000).
21. T.Y. Ma, D. Tran, N. Hoa, D. Nguyen, M. Merryfield, and A. Tarnawski. Mechanism of extracellular calcium regulation of intestinal epithelial tight junction permeability: role of cytoskeletal involvement. Microsc Res Tech. 51:156-168 (2000).
22. J.M. Andersonand C.M. Van Itallie. Tight junctions and the molecular basis for regulation of paracellular permeability. Am J Physiol. 269:G467-475 (1995).
23. B.M. Denkerand S.K. Nigam. Molecular structure and assembly of the tight junction. Am J Physiol. 274:F1-9 (1998).
24. P. Claude. Morphological factors influencing transepithelial permeability: a model for the resistance of the zonula occludens. J Membr Biol. 39:219-232 (1978).
25. J.L. Madaraand K. Dharmsathaphorn. Occluding junction structure-function relationships in a cultured epithelial monolayer. J Cell Biol. 101:2124-2133 (1985).
26. S.C. Chen-Quay, K.T. Eiting, A.W. Li, N. Lamharzi, and S.C. Quay. Identification of tight junction modulating lipids. J Pharm Sci. 98:606-619 (2009).
27. B.R. Stevensonand B.H. Keon. The tight junction: morphology to molecules. Annu Rev Cell Dev Biol. 14:89-109 (1998).
28. S. Tsukita, M. Furuse, and M. Itoh. Multifunctional strands in tight junctions. Nat Rev Mol Cell Biol. 2:285-293 (2001).
29. L. Gonzalez-Mariscal, A. Betanzos, P. Nava, and B.E. Jaramillo. Tight junction proteins. Prog Biophys Mol Biol. 81:1-44 (2003).
30. J.L. Madara. Regulation of the movement of solutes across tight junctions. Annu Rev Physiol. 60:143-159 (1998).
31. W. Rubas, M.E. Cromwell, Z. Shahrokh, J. Villagran, T.N. Nguyen, M. Wellton, T.H. Nguyen, and R.J. Mrsny. Flux measurements across Caco-2 monolayers may predict transport in human large intestinal tissue. J Pharm Sci. 85:165-169 (1996).
32. D. Ruppar. Oral delivery. Drug Delivery Technology. 8:50-51 (2008).
33. D. Guggi, A.H. Krauland, and A. Bernkop-Schnurch. Systemic peptide delivery via the stomach: in vivo evaluation of an oral dosage form for salmon calcitonin. J Control Release. 92:125-135 (2003).
34. E. Perakslis, A. Tuesca, and A. Lowman. Complexation hydrogels for oral protein delivery: an in vitro assessment of the insulin transport-enhancing effects following dissolution in simulated digestive fluids. J Biomater Sci Polym Ed. 18:1475-1490 (2007).
35. Diabetology. http://www.diabetology.co.uk/oral.htm (accessed 23/12/09 2009).
36. H. Itoh, M. Nishino, and H. Hatabu. Architecture of the lung: morphology and function. J Thorac Imaging. 19:221-227 (2004).

37. E.R. Weibeland D.M. Gomez. Architecture of the human lung. Use of quantitative methods establishes fundamental relations between size and number of lung structures. Science. 137:577-585 (1962).
38. IUPUI. http://anatomy.iupui.edu/courses/histo_D502/D502f04/lecture.f04/Respsystemf04/respiratory.html (accessed 07/01/2010 2010).
39. D.R. Owens, B. Zinman, and G. Bolli. Alternative routes of insulin delivery. Diabet Med. 20:886-898 (2003).
40. T. Neithercott. Diabetes Meds on the Horizon. (accessed 23/12/09 2009).
41. M.I. Ugwoke, N. Verbeke, and R. Kinget. The biopharmaceutical aspects of nasal mucoadhesive drug delivery. J Pharm Pharmacol. 53:3-21 (2001).
42. Y. Chugh, P. Kapoor, and A.K. Kapoor. Intranasal drug delivery: a novel approach. Indian J Otolaryngol Head Neck Surg. 61:90-94 (2009).
43. R. Dahland N. Mygind. Anatomy, physiology and function of the nasal cavities in health and disease. Adv Drug Deliv Rev. 29:3-12 (1998).
44. T. Kisseland U. Werner. Nasal delivery of peptides: an in vitro cell culture model for the investigation of transport and metabolism in human nasal epithelium. J Control Release. 53:195-203 (1998).
45. P. Arora, S. Sharma, and S. Garg. Permeability issues in nasal drug delivery. Drug Discov Today. 7:967-975 (2002).
46. S. Senel, M. Kremer, K. Nagy, and C. Squier. Delivery of bioactive peptides and proteins across oral (buccal) mucosa. Curr Pharm Biotechnol. 2:175-186 (2001).
47. G. Di Colo, Y. Zambito, and C. Zaino. Polymeric enhancers of mucosal epithelia permeability: synthesis, transepithelial penetration-enhancing properties, mechanism of action, safety issues. J Pharm Sci. 97:1652-1680 (2008).
48. D. Harrisand J.R. Robinson. Drug delivery via the mucous membranes of the oral cavity. J Pharm Sci. 81:1-10 (1992).
49. Y. Kurosakiand T. Kimura. Regional variation in oral mucosal drug permeability. Crit Rev Ther Drug Carrier Syst. 17:467-508 (2000).
50. T. Nagai. [Drug delivery systems by controlled release]. Yakugaku Zasshi. 108:613-624 (1988).
51. H.H. Alur, J.D. Beal, S.I. Pather, A.K. Mitra, and T.P. Johnston. Evaluation of a novel, natural oligosaccharide gum as a sustained-release and mucoadhesive component of calcitonin buccal tablets. J Pharm Sci. 88:1313-1319 (1999).
52. M.K. Gutniak, H. Larsson, S.J. Heiber, O.T. Juneskans, J.J. Holst, and B. Ahren. Potential therapeutic levels of glucagon-like peptide I achieved in humans by a buccal tablet. Diabetes Care. 19:843-848 (1996).
53. V.H.L. Lee. Peptide and protein drug delivery: Opportunities and challenges. Pharm Int. 7:208-212 (1986).
54. J.A. Fix. Oral controlled release technology for peptides: status and future prospects. Pharm Res. 13:1760-1764 (1996).
55. R. Singh, S. Singh, and J.W. Lillard, Jr. Past, present, and future technologies for oral delivery of therapeutic proteins. J Pharm Sci. 97:2497-2523 (2008).
56. V.R. Sinhaand A. Trehan. Biodegradable microspheres for protein delivery. J Control Release. 90:261-280 (2003).
57. V.M. Leitner, D. Guggi, and A. Bernkop-Schnurch. Thiomers in noninvasive polypeptide delivery: in vitro and in vivo characterization of a polycarbophil-

cysteine/glutathione gel formulation for human growth hormone. J Pharm Sci. 93:1682-1691 (2004).
58. A. Bernkop-Schnurch, A.H. Krauland, V.M. Leitner, and T. Palmberger. Thiomers: potential excipients for non-invasive peptide delivery systems. Eur J Pharm Biopharm. 58:253-263 (2004).
59. F. Ahsan, J. Arnold, E. Meezan, and D.J. Pillion. Enhanced bioavailability of calcitonin formulated with alkylglycosides following nasal and ocular administration in rats. Pharm Res. 18:1742-1746 (2001).
60. J. Arnold, F. Ahsan, E. Meezan, and D.J. Pillion. Nasal administration of low molecular weight heparin. J Pharm Sci. 91:1707-1714 (2002).
61. J.J. Arnold, F. Ahsan, E. Meezan, and D.J. Pillion. Correlation of tetradecylmaltoside induced increases in nasal peptide drug delivery with morphological changes in nasal epithelial cells. J Pharm Sci. 93:2205-2213 (2004).
62. S. Takatsuka, T. Morita, Y. Horikiri, H. Yamahara, and H. Saji. Absorption enhancement of poorly absorbed hydrophilic compounds from various mucosal sites by combination of mucolytic agent and non-ionic surfactant. Int J Pharm. 338:87-93 (2007).
63. T. Matsuyama, T. Morita, Y. Horikiri, H. Yamahara, and H. Yoshino. Influence of fillers in powder formulations containing N-acetyl-L-cysteine on nasal peptide absorption. J Control Release. 120:88-94 (2007).
64. T. Matsuyama, T. Morita, Y. Horikiri, H. Yamahara, and H. Yoshino. Improved nasal absorption of salmon calcitonin by powdery formulation with N-acetyl-L-cysteine as a mucolytic agent. J Control Release. 115:183-188 (2006).
65. A. Bernkop-Schnurch, C. Valenta, and S.M. Daee. Peroral polypeptide delivery. A comparative in vitro study of mucolytic agents. Arzneimittelforschung. 49:799-803 (1999).
66. A. Bernkop-Schnurch, H. Zarti, and G.F. Walker. Thiolation of polycarbophil enhances its inhibition of intestinal brush border membrane bound aminopeptidase N. J Pharm Sci. 90:1907-1914 (2001).
67. A. Bernkop-Schnurch. The use of inhibitory agents to overcome the enzymatic barrier to perorally administered therapeutic peptides and proteins. J Control Release. 52:1-16 (1998).
68. T. Loftssonand M.E. Brewster. Pharmaceutical applications of cyclodextrins. 1. Drug solubilization and stabilization. J Pharm Sci. 85:1017-1025 (1996).
69. N.N. Salama, N.D. Eddington, and A. Fasano. Tight junction modulation and its relationship to drug delivery. Adv Drug Deliv Rev. 58:15-28 (2006).
70. E.K. Anderbergand P. Artursson. Epithelial transport of drugs in cell culture VII: effects of pharmaceutical surfactant excipients and bile acids on transepithelial permeability in monolayers of human intestinal epithelia. J Pharm Sci. 81:879-887 (1992).
71. J.A. Fix, K. Engle, P.A. Porter, P.S. Leppert, S.J. Selk, C.R. Gardner, and J. Alexander. Acylcarnitines: drug absorption-enhancing agents in the gastrointestinal tract. Am J Physiol. 251:G332-340 (1986).
72. J.H. Hochman, J.A. Fix, and E.L. LeCluyse. In vitro and in vivo analysis of the mechanism of absorption enhancement by palmitoylcarnitine. J Pharmacol Exp Ther. 269:813-822 (1994).
73. E.K. Anderbergand P. Artursson. Epithelial transport of drugs in cell culture. VIII: Effects of sodium dodecyl sulfate on cell membrane and tight junction

permeability in human intestinal epithelial (Caco-2) cells. J Pharm Sci. 82:392-398 (1993).

74. E.S. Swenson, W.B. Milisen, and W. Curatolo. Intestinal permeability enhancement: efficacy, acute local toxicity, and reversibility. Pharm Res. 11:1132-1142 (1994).
75. E. Duizer, C. van der Wulp, C.H. Versantvoort, and J.P. Groten. Absorption enhancement, structural changes in tight junctions and cytotoxicity caused by palmitoyl carnitine in Caco-2 and IEC-18 cells. J Pharmacol Exp Ther. 287:395-402 (1998).
76. S. Gizurarson, C. Marriott, G.P. Martin, and E. Bechgaard. The influence of insulin and some excipients used in nasal insulin preparations on mucociliary clearance. Int J Pharm. 65:243-247 (1990).
77. P.C. Braga, L. Allegra, C. Rampoldi, G. Beghi, A. Ornaghi, G. Caminiti, Y.R. Zheng, and F. Bartucci. Topical tolerability of salmon calcitonin assessed by mucociliary transport velocity investigation. Arzneimittelforschung. 40:938-941 (1990).
78. D.J. Pillion, S. Hosmer, and E. Meezan. Dodecylmaltoside-mediated nasal and ocular absorption of lyspro-insulin: independence of surfactant action from multimer dissociation. Pharm Res. 15:1637-1639 (1998).
79. D.J. Pillion, J.A. Atchison, C. Gargiulo, R.X. Wang, P. Wang, and E. Meezan. Insulin delivery in nosedrops: new formulations containing alkylglycosides. Endocrinology. 135:2386-2391 (1994).
80. D.J. Pillion, P. Wang, J. Yorks, P. McCann, and E. Meezan. Systemic absorption of insulin and glucagon applied topically to the eyes of rats and a diabetic dog. J Ocul Pharmacol Ther. 11:283-295 (1995).
81. L. Gonzalez-Mariscal, B. Chavez de Ramirez, and M. Cereijido. Tight junction formation in cultured epithelial cells (MDCK). J Membr Biol. 86:113-125 (1985).
82. S. Citi. Protein kinase inhibitors prevent junction dissociation induced by low extracellular calcium in MDCK epithelial cells. J Cell Biol. 117:169-178 (1992).
83. M. Cereijido, E.S. Robbins, W.J. Dolan, C.A. Rotunno, and D.D. Sabatini. Polarized monolayers formed by epithelial cells on a permeable and translucent support. J Cell Biol. 77:853-880 (1978).
84. A. Martinez-Palomo, I. Meza, G. Beaty, and M. Cereijido. Experimental modulation of occluding junctions in a cultured transporting epithelium. J Cell Biol. 87:736-745 (1980).
85. M. Tomita, M. Hayashi, and S. Awazu. Absorption-enhancing mechanism of sodium caprate and decanoylcarnitine in Caco-2 cells. J Pharmacol Exp Ther. 272:739-743 (1995).
86. J. Raiman, S. Tormalehto, K. Yritys, H.E. Junginger, and J. Monkkonen. Effects of various absorption enhancers on transport of clodronate through Caco-2 cells. Int J Pharm. 261:129-136 (2003).
87. V. Dodaneand V.D. Vilivalam. Pharmaceutical applications of chitosan. Pharm Sci Tech Today. 1:246-253 (1998).
88. A.F. Kotze´, B.J. de Leeuw, H.L. Lueßen, A.G. de Boer, J.C. Verhoef, and H.E. Junginger. Chitosans for enhanced delivery of therapeutic peptides across intestinal epithelia: In vitro evaluation in Caco-2 cell monolayers. Int J Pharm. 159:243-253 (1997).

89. H.L. Luessen, B.J. de Leeuw, M.W. Langemeyer, A.B. de Boer, J.C. Verhoef, and H.E. Junginger. Mucoadhesive polymers in peroral peptide drug delivery. VI. Carbomer and chitosan improve the intestinal absorption of the peptide drug buserelin in vivo. Pharm Res. 13:1668-1672 (1996).
90. P. Sinswatand P. Tengamnuay. Enhancing effect of chitosan on nasal absorption of salmon calcitonin in rats: comparison with hydroxypropyl- and dimethyl-beta-cyclodextrins. Int J Pharm. 257:15-22 (2003).
91. Y.J. Zhang, C.H. Ma, W.L. Lu, X. Zhang, X.L. Wang, J.N. Sun, and Q. Zhang. Permeation-enhancing effects of chitosan formulations on recombinant hirudin-2 by nasal delivery in vitro and in vivo. Acta Pharmacol Sin. 26:1402-1408 (2005).
92. I.M. van der Lubben, J.C. Verhoef, G. Borchard, and H.E. Junginger. Chitosan and its derivatives in mucosal drug and vaccine delivery. Eur J Pharm Sci. 14:201-207 (2001).
93. A.F. Kotze, H.L. Luessen, B.J. de Leeuw, B.G. de Boer, J.C. Verhoef, and H.E. Junginger. N-trimethyl chitosan chloride as a potential absorption enhancer across mucosal surfaces: in vitro evaluation in intestinal epithelial cells (Caco-2). Pharm Res. 14:1197-1202 (1997).
94. A.F. Kotze, M.M. Thanou, H.L. Luebetaen, A.G. de Boer, J.C. Verhoef, and H.E. Junginger. Enhancement of paracellular drug transport with highly quaternized N-trimethyl chitosan chloride in neutral environments: in vitro evaluation in intestinal epithelial cells (Caco-2). J Pharm Sci. 88:253-257 (1999).
95. M. Thanou, B.I. Florea, M.W. Langemeyer, J.C. Verhoef, and H.E. Junginger. N-trimethylated chitosan chloride (TMC) improves the intestinal permeation of the peptide drug buserelin in vitro (Caco-2 cells) and in vivo (rats). Pharm Res. 17:27-31 (2000).
96. B.I. Florea, M. Thanou, H.E. Junginger, and G. Borchard. Enhancement of bronchial octreotide absorption by chitosan and N-trimethyl chitosan shows linear in vitro/in vivo correlation. J Control Release. 110:353-361 (2006).
97. N. Hagenaars, R.J. Verheul, I. Mooren, P.H. de Jong, E. Mastrobattista, H.L. Glansbeek, J.G. Heldens, H. van den Bosch, W.E. Hennink, and W. Jiskoot. Relationship between structure and adjuvanticity of N,N,N-trimethyl chitosan (TMC) structural variants in a nasal influenza vaccine. J Control Release. 140:126-133 (2009).
98. H. Natsume, S. Iwata, K. Ohtake, M. Miyamoto, M. Yamaguchi, K. Hosoya, D. Kobayashi, K. Sugibayashi, and Y. Morimoto. Screening of cationic compounds as an absorption enhancer for nasal drug delivery. Int J Pharm. 185:1-12 (1999).
99. M. Miyamoto, H. Natsume, I. Satoh, K. Ohtake, M. Yamaguchi, D. Kobayashi, K. Sugibayashi, and Y. Morimoto. Effect of poly-L-arginine on the nasal absorption of FITC-dextran of different molecular weights and recombinant human granulocyte colony-stimulating factor (rhG-CSF) in rats. Int J Pharm. 226:127-138 (2001).
100. K. Ohtake, H. Natsume, H. Ueda, and Y. Morimoto. Analysis of transient and reversible effects of poly-L-arginine on the in vivo nasal absorption of FITC-dextran in rats. J Control Release. 82:263-275 (2002).
101. K. Ohtake, T. Maeno, H. Ueda, H. Natsume, and Y. Morimoto. Poly-L-arginine predominantly increases the paracellular permeability of hydrophilic

macromolecules across rabbit nasal epithelium in vitro. Pharm Res. 20:153-160 (2003).
102. B. Dutzar, L. Chen, and S.C. Chen. siRNA knockdown of claudin expression inhibits tight junction formation and induces loss of differentiation in respiratory epithelia, *The 2004 AAPS National Biotechnology Conference*, Boston, 2003.
103. M. Kondoh, A. Takahashi, M. Fujii, K. Yagi, and Y. Watanabe. A novel strategy for a drug delivery system using a claudin modulator. Biol Pharm Bull. 29:1783-1789 (2006).
104. P.H. Johnsonand S.C. Quay. Advances in nasal drug delivery through tight junction technology. Expert Opin Drug Deliv. 2:281-298 (2005).
105. S.C. Chen, K. Eiting, K. Cui, A.K. Leonard, D. Morris, C.Y. Li, K. Farber, A.P. Sileno, M.E. Houston, Jr., P.H. Johnson, S.C. Quay, and H.R. Costantino. Therapeutic utility of a novel tight junction modulating peptide for enhancing intranasal drug delivery. J Pharm Sci. 95:1364-1371 (2006).
106. U.B. Kompellaand V.H. Lee. Delivery systems for penetration enhancement of peptide and protein drugs: design considerations. Adv Drug Deliv Rev. 46:211-245 (2001).
107. C.M. Lehr, J.A. Bouwstra, J.J. Tukker, and H.E. Junginger. ntestinal transit of bioadhesive microspheres in an in situ loop in the rat. A comparative study with polymers and blends based on poly(acrylic acid). J Control Release. 13:51-62 (1990).
108. A. Allen, W.J. Cunliffe, J.P. Pearson, L.A. Sellers, and R. Ward. Studies on gastrointestinal mucus. Scand J Gastroenterol Suppl. 93:101-113 (1984).
109. Chickeringand Mathiowitz. Definitions, mechanisms, and theories of bioadhesion. In E. Mathiowitz, D.E. Chickering, and C.M. Lehr (eds.), Bioadhesive Drug Delivery Systems: Fundamentals, Novel Approaches, and Development, Marcel Dekker, New York, 1999.
110. N. Salamat-Miller, M. Chittchang, and T.P. Johnston. The use of mucoadhesive polymers in buccal drug delivery. Adv Drug Deliv Rev. 57:1666-1691 (2005).
111. B. Kriwetand T. Kissel. Poly(acrylic acid) microparticles widen the intercellular spaces of Caco-2 cell monolayers: An examination by confocal laser scanning microscopy. Eur J Pharm Biopharm. 42:233-240 (1996).
112. H.L. Luessen, B.J. de Leeuw, D. Perard, C.M. Lehr, A.G. de Boer, J.C. Verhoef, and H.E. Junginger. Mucoahesive polymers in peroral peptide drug delivery. I. Influence of mucoadhesive excipients on the proteolytic activity of intestinal enzymes. Eur J Pharm Sci. 4:171-128 (1996).
113. L. Li, N.R. Mathias, C.L. Heran, P. Moench, D.A. Wall, and R.L. Smith. Carbopol-mediated paracellular transport enhancement in Calu-3 cell layers. J Pharm Sci. 95:326-335 (2006).
114. R.B. Qaqishand M.M. Amiji. Synthesis of a fluorescent chitosan derivative and its application for the study of chitosan–mucin interactions. Carbohydrate Polymers. 38:99-107 (1998).
115. C.E. Kastand A. Bernkop-Schnurch. Thiolated polymers--thiomers: development and in vitro evaluation of chitosan-thioglycolic acid conjugates. Biomaterials. 22:2345-2352 (2001).
116. A.H. Krauland, D. Guggi, and A. Bernkop-Schnurch. Thiolated chitosan microparticles: a vehicle for nasal peptide drug delivery. Int J Pharm. 307:270-277 (2006).

117. A.H. Krauland, V.M. Leitner, V. Grabovac, and A. Bernkop-Schnurch. In vivo evaluation of a nasal insulin delivery system based on thiolated chitosan. J Pharm Sci. 95:2463-2472 (2006).
118. C. Le Royand J.L. Wrana. Clathrin and non-clathrin mediated endocytic regulation of cell signalling. Nat Rev Mol Cell Biol. 6:112-126 (2005).
119. S. Mayorand R.E. Pagano. Pathways of clathrin-independent endocytosis. Nat Rev Mol Cell Biol. 8:603-612 (2007).
120. I.R. Nabiand P.U. Le. Caveolae/raft-dependent endocytosis. J Cell Biol. 161:673-677 (2003).
121. M. Gumbleton, A.G. Abulrob, and L. Campbell. Caveolae: an alternative membrane transport compartment. Pharm Res. 17:1035-1048 (2000).
122. K.G. Rothberg, J.E. Heuser, W.C. Donzell, Y.S. Ying, J.R. Glenney, and R.G. Anderson. Caveolin, a protein component of caveolae membrane coats. Cell. 68:673-682 (1992).
123. G.J. Rodrigues, C.B. Restini, C.N. Lunardi, J.E. Moreira, R.G. Lima, R.S. da Silva, and L.M. Bendhack. Caveolae dysfunction contributes to impaired relaxation induced by nitric oxide donor in aorta from renal hypertensive rats. J Pharmacol Exp Ther. 323:831-837 (2007).
124. J.E. Schnitzer, P. Oh, E. Pinney, and J. Allard. Filipin-sensitive caveolae-mediated transport in endothelium: reduced transcytosis, scavenger endocytosis, and capillary permeability of select macromolecules. J Cell Biol. 127:1217-1232 (1994).
125. G. Bathori, L. Cervenak, and I. Karadi. Caveolae--an alternative endocytotic pathway for targeted drug delivery. Crit Rev Ther Drug Carrier Syst. 21:67-95 (2004).
126. P.L. Tumaand A.L. Hubbard. Transcytosis: crossing cellular barriers. Physiol Rev. 83:871-932 (2003).
127. O. Harush-Frenkel, E. Rozentur, S. Benita, and Y. Altschuler. Surface charge of nanoparticles determines their endocytic and transcytotic pathway in polarized MDCK cells. Biomacromolecules. 9:435-443 (2008).
128. C.H. von Bonsdorff, S.D. Fuller, and K. Simons. Apical and basolateral endocytosis in Madin-Darby canine kidney (MDCK) cells grown on nitrocellulose filters. EMBO J. 4:2781-2792 (1985).
129. H.Y. Naim, D.T. Dodds, C.B. Brewer, and M.G. Roth. Apical and basolateral coated pits of MDCK cells differ in their rates of maturation into coated vesicles, but not in the ability to distinguish between mutant hemagglutinin proteins with different internalization signals. J Cell Biol. 129:1241-1250 (1995).
130. M. Bomsel, K. Prydz, R.G. Parton, J. Gruenberg, and K. Simons. Endocytosis in filter-grown Madin-Darby canine kidney cells. J Cell Biol. 109:3243-3258 (1989).
131. G. Apodaca. Endocytic traffic in polarized epithelial cells: role of the actin and microtubule cytoskeleton. Traffic. 2:149-159 (2001).
132. P. Eker, P.K. Holm, B. van Deurs, and K. Sandvig. Selective regulation of apical endocytosis in polarized Madin-Darby canine kidney cells by mastoparan and cAMP. J Biol Chem. 269:18607-18615 (1994).
133. C. Bucci, A. Wandinger-Ness, A. Lutcke, M. Chiariello, C.B. Bruni, and M. Zerial. Rab5a is a common component of the apical and basolateral endocytic machinery in polarized epithelial cells. Proc Natl Acad Sci U S A. 91:5061-5065 (1994).

134. S.M. Leung, W.G. Ruiz, and G. Apodaca. Sorting of membrane and fluid at the apical pole of polarized Madin-Darby canine kidney cells. Mol Biol Cell. 11:2131-2150 (2000).
135. L.G. Morphisand D. Gitlin. Maturation of the maternofoetal transport system for human gamma-globulin in the mouse. Nature. 228:573 (1970).
136. F.W. Brambell. The transmission of immunity from mother to young and the catabolism of immunoglobulins. Lancet. 2:1087-1093 (1966).
137. N.E. Simisterand A.R. Rees. Isolation and characterization of an Fc receptor from neonatal rat small intestine. Eur J Immunol. 15:733-738 (1985).
138. N.E. Simisterand K.E. Mostov. An Fc receptor structurally related to MHC class I antigens. Nature. 337:184-187 (1989).
139. G.M. Spiekermann, P.W. Finn, E.S. Ward, J. Dumont, B.L. Dickinson, R.S. Blumberg, and W.I. Lencer. Receptor-mediated immunoglobulin G transport across mucosal barriers in adult life: functional expression of FcRn in the mammalian lung. J Exp Med. 196:303-310 (2002).
140. E.J. Israel, S. Taylor, Z. Wu, E. Mizoguchi, R.S. Blumberg, A. Bhan, and N.E. Simister. Expression of the neonatal Fc receptor, FcRn, on human intestinal epithelial cells. Immunology. 92:69-74 (1997).
141. R. Rojasand G. Apodaca. Immunoglobulin transport across polarized epithelial cells. Nat Rev Mol Cell Biol. 3:944-955 (2002).
142. A.J. Bitonti, J.A. Dumont, S.C. Low, R.T. Peters, K.E. Kropp, V.J. Palombella, J.M. Stattel, Y. Lu, C.A. Tan, J.J. Song, A.M. Garcia, N.E. Simister, G.M. Spiekermann, W.I. Lencer, and R.S. Blumberg. Pulmonary delivery of an erythropoietin Fc fusion protein in non-human primates through an immunoglobulin transport pathway. Proc Natl Acad Sci U S A. 101:9763-9768 (2004).
143. S.C. Low, S.L. Nunes, A.J. Bitonti, and J.A. Dumont. Oral and pulmonary delivery of FSH-Fc fusion proteins via neonatal Fc receptor-mediated transcytosis. Hum Reprod. 20:1805-1813 (2005).
144. A.J. Bitontiand J.A. Dumont. Pulmonary administration of therapeutic proteins using an immunoglobulin transport pathway. Adv Drug Deliv Rev. 58:1106-1118 (2006).
145. G.J. Russell-Jones, L. Arthur, and H. Walker. Vitamin B12-mediated transport of nanoparticles across Caco-2 cells. Int J Pharm. 179:247-255 (1999).
146. G.J. Russell-Jones. The potential use of receptor-mediated endocytosis for oral drug delivery. Adv Drug Deliv Rev. 46:59-73 (2001).
147. A. Habberfield, K. Jensen-Pippo, L. Ralph, S.W. Westwood, and D.L. Russell-Jones. Vitamin VB12-mediated uptake of recombinant therapeutic proteins from the gut. Int J Pharm. 145:1-8 (1996).
148. A. Habberfield, K. Jensen-Pippo, L. Ralph, S.W. Westwood, and G.J. Russell-Jones. Vitamin B12-mediated uptake of erythropoietin and granulocyte colony stimulating factor in vitro and in vivo. Int J Pharm. 145:1-8 (1997).
149. C.M. Lehr. Bioadhesion technologies for the delivery of peptide and protein drugs to the gastrointestinal tract. Crit Rev Ther Drug Carrier Syst. 11:119-160 (1994).
150. M. Morishita, N. Kamei, J. Ehara, K. Isowa, and K. Takayama. A novel approach using functional peptides for efficient intestinal absorption of insulin. J Control Release. 118:177-184 (2007).

151. R. Wiwattanapatapee, B. Carreno-Gomez, N. Malik, and R. Duncan. Anionic PAMAM dendrimers rapidly cross adult rat intestine in vitro: a potential oral delivery system? Pharm Res. 17:991-998 (2000).
152. R. Jevprasesphant, J. Penny, D. Attwood, N.B. McKeown, and A. D'Emanuele. Engineering of dendrimer surfaces to enhance transepithelial transport and reduce cytotoxicity. Pharm Res. 20:1543-1550 (2003).
153. D.C. Kilpatrick, A. Pusztai, G. Grant, C. Graham, and S.W. Ewen. Tomato lectin resists digestion in the mammalian alimentary canal and binds to intestinal villi without deleterious effects. FEBS Lett. 185:299-305 (1985).
154. N. Hussain, P.U. Jani, and A.T. Florence. Enhanced oral uptake of tomato lectin-conjugated nanoparticles in the rat. Pharm Res. 14:613-618 (1997).
155. C.M. Lehr, J.A. Bouwstra, W. Kok, A.B. Noach, A.G. de Boer, and H.E. Junginger. Bioadhesion by means of specific binding of tomato lectin. Pharm Res. 9:547-553 (1992).
156. H. Hillaireauand P. Couvreur. Nanocarriers' entry into the cell: relevance to drug delivery. Cell Mol Life Sci. 66:2873-2896 (2009).
157. C. Damge, C. Michel, M. Aprahamian, and P. Couvreur. New approach for oral administration of insulin with polyalkylcyanoacrylate nanocapsules as drug carrier. Diabetes. 37:246-251 (1988).
158. H. Pinto-Alphandary, M. Aboubakar, D. Jaillard, P. Couvreur, and C. Vauthier. Visualization of insulin-loaded nanocapsules: in vitro and in vivo studies after oral administration to rats. Pharm Res. 20:1071-1084 (2003).
159. C. Damge, D. Hillairebuys, R. Puech, A. Hoeltzel, C. Michel, and G. Ribes. Effects of orally-administered insulin nanocapsules in normal and diabetic dogs. Diabetes Nutr Metabolism. 8:3-9 (1995).
160. M. Tobio, A. Sanchez, A. Vila, I.I. Soriano, C. Evora, J.L. Vila-Jato, and M.J. Alonso. The role of PEG on the stability in digestive fluids and in vivo fate of PEG-PLA nanoparticles following oral administration. Colloids Surf B Biointerfaces. 18:315-323 (2000).
161. A. Vila, A. Sanchez, M. Tobio, P. Calvo, and M.J. Alonso. Design of biodegradable particles for protein delivery. J Control Release. 78:15-24 (2002).
162. R. Fernandez-Urrusuno, P. Calvo, C. Remunan-Lopez, J.L. Vila-Jato, and M.J. Alonso. Enhancement of nasal absorption of insulin using chitosan nanoparticles. Pharm Res. 16:1576-1581 (1999).
163. A. Vila, H. Gill, O. McCallion, and M.J. Alonso. Transport of PLA-PEG particles across the nasal mucosa: effect of particle size and PEG coating density. J Control Release. 98:231-244 (2004).
164. C. Prego, M. Garcia, D. Torres, and M.J. Alonso. Transmucosal macromolecular drug delivery. J Control Release. 101:151-162 (2005).
165. Y. Kawashima, H. Yamamoto, H. Takeuchi, S. Fujioka, and T. Hino. Pulmonary delivery of insulin with nebulized DL-lactide/glycolide copolymer (PLGA) nanospheres to prolong hypoglycemic effect. J Control Release. 62:279-287 (1999).
166. Q. Zhang, Z. Shen, and T. Nagai. Prolonged hypoglycemic effect of insulin-loaded polybutylcyanoacrylate nanoparticles after pulmonary administration to normal rats. Int J Pharm. 218:75-80 (2001).
167. H. Yamamoto, Y. Kuno, S. Sugimoto, H. Takeuchi, and Y. Kawashima. Surface-modified PLGA nanosphere with chitosan improved pulmonary

delivery of calcitonin by mucoadhesion and opening of the intercellular tight junctions. J Control Release. 102:373-381 (2005).

168. S. Sagnellaand K. Mai-Ngam. Chitosan based surfactant polymers designed to improve blood compatibility on biomaterials. Colloids and Surfaces B-Biointerfaces. 42:147-155 (2005).
169. M.M. Amiji. Synthesis of anionic poly(ethylene glycol) derivative for chitosan surface modification in blood-contacting applications. Carbohydrate Polymers. 32:193-199 (1997).
170. Y. Hu, Jiang, X. Q., Ding, Y., Zhang, L. Y., Yang, C. Z., Zhang, J. F., Chen, J. N., Yang, Y. H. Preparation and drug release behaviors of nimodipine-loaded poly(caprolactone)-poly(ethylene oxide)-polylactide amphiphilic copolymer nanoparticles. Biomaterials. 24:2395-2404 (2003).
171. N.G. Schipper, S. Olsson, J.A. Hoogstraate, A.G. deBoer, K.M. Varum, and P. Artursson. Chitosans as absorption enhancers for poorly absorbable drugs 2: mechanism of absorption enhancement. Pharm Res. 14:923-929 (1997).

# Chapter 2

# Materials and General Methods

## 2.1 Materials

### 2.1.1 Cells, culture media, media components and cell solutions

Calu-3 cells were obtained from the American Type Culture Collection (ATCC) and used at passages 19-48. Caco-2 and HT-29 cells were obtained from the European Collection of Cell Cultures (ECACC) and used between passages 44-58 and 142-160, respectively. Essential Minimum Eagle's Medium (EMEM) medium was obtained from ATCC-LGC standards. Dulbeco's Modified Eagles Medium (DMEM), McCoy's-5A medium, Hanks Balanced Salt Solution (HBSS) with sodium bicarbonate and without phenol red and HBSS with sodium bicarbonate, without phenol red, calcium chloride and magnesium sulfate (referred to as calcium-free HBSS, CFHBSS) were all obtained from Sigma Aldrich. Phosphate buffered saline (PBS) tablets were purchased from Oxoid (Basingstoke, UK). 2.5% Trypsin/EDTA solution, Antibiotic/Antimycotic solution (containing penicillin, streptomycin and amphotericin), L-glutamine and Foetal Bovine Serum (FBS, non-USA origin) were all obtained from Sigma Aldrich. All cell media (EMEM, DMEM and McCoy's-5A) were supplemented with penicillin, streptomycin and amphotericin at final concentrations of 100 units/ml, 0.1 mg/ml and 0.25 μg/ml, respectively, and FBS at final concentrations of 10% v/v. DMEM was further supplemented with L-glutamine

and 1 mM sodium pyrovate. Note that from this point onwards, supplemented media are referred to as cell media, DMEM, EMEM or McCoy's-5A. Dimethylsulphoxide (DMSO), used as cryopreservant, was purchased from Sigma Aldrich. 4-(2-hydroxyethyl)-1-piperazineethanesulfonic acid (HEPES) and 2-(N-Morpholino)ethanesulfonic acid (MES) were obtained from Sigma Aldrich.

### 2.1.2 Plasticware and glassware

Transwell® permeable supports, referred to in this thesis as 'filters', of 12 mm diameter, 0.4 μm pore size (with polystyrene membranes) were obtained from Corning Life Sciences (Holland). Cell culture flasks (75 $cm^2$, canted neck with vented caps), 96-well polystyrene microplates (black or clear, non-cell culture treated) and sterile pipettes, used routinely for the maintenance of cells, were also purchased from Corning Life Sciences. Clear, tissue culture treated 96-well plates and ELISA (Immuno 96 MicroWell™) plates were obtained from NUNC. Sterile centrifuge tubes (of 15 ml and 50 ml volume capacity) were purchased from Grainer (USA). Sterile universals (5 ml and 30 ml volume capacity) were obtained from Sterilin (UK). Sterile cryovials (1 ml capacity) were supplied by NUNC. Freezing container ('Mr Frosty'), providing 1°C per minute cooling rate was purchased from Nalgene® Labware. Haemocytometer (Improved Neubauer, to British Standard 748) was purchased from Scientific Laboratory Supplies (SLS), UK.

### 2.1.3 Cell toxicity assay reagents

AlamarBlue® reagent was obtained from AbD Serotec (UK), while 3-(4,5-dimethylthiazol-2-yl)-5(3-carboxymethonyphenol)-2-(4-sulfophenyl)-2H-tetrazolium (MTS) reagent (commercially known as 'CellTiter 96 AQueous One Solution Cell

Proliferation Assay') was purchased from Promega (USA). Lactate Dehydrogenase (LDH) assay kit (known commercially as '*In Vitro* Toxicology Assay Kit, TOX7') was purchased from Sigma Aldrich.

### 2.1.4 Antibodies

IgG from human serum (hereinafter referred to as 'IgG') and IgG from rabbit serum (rIgG), both as lyophilized powders, and fluorescein isothiocyanate (FITC)-labelled IgG (FITC-IgG) solution were purchased from Sigma Aldrich. FITC-IgG was dialysed extensively against PBS (to remove sodium azide from the solution) prior to its use in cell experiments. IgG Fc fragment and FITC-labelled IgG Fc fragment were obtained from Jackson Immunoresearch Europe Ltd. Anti-human IgG, horseradish peroxidase (HRP)-conjugated, was purchased from The Binding Site, UK. Mouse, anti-human Zonula Occludens-1 (ZO-1, TJ protein) was purchased from Zymed (part of Invitrogen). Goat, anti-mouse FITC-IgG and goat, anti-mouse Cy5-IgG were purchased from Sigma Aldrich and Invitrogen, respectively. Goat, anti-human FcRn antibody (polyclonal IgG) and donkey, anti-goat TRITC-IgG were purchased from Santa Cruz (USA). Mouse, anti-human mucin-1 (MUC-1) was purchased from AbD Serotec, UK. Anti-mouse FITC-IgG was obtained from Sigma Aldrich. Investigational therapeutic (anti-cancer) antibodies, hCTMO1 (whole antibody, $M_W$ 147033), hCTMO1 (Fab, $M_W$ 95815), mA33γ1 (Fab, $M_W$ 24724.67) and mA33γ1 Fab-diPEG (Fab conjugated to PEG, $M_W$ 64724.67), were supplied by UCB (Slough, UK).

### 2.1.5 Chemicals

FITC-labelled dextrans ('FDs') of approximate average $M_W$ of 4 kDa (FD4), 10 kDa (FD10), 20 kDa (FD20), 40 kDa (FD40), 70 kDa (FD70) and 150 kDa (FD150), and FITC-labelled insulin (FITC-insulin) were supplied by Sigma Aldrich. n-Dodecyl-ß-D-maltoside (DDM), n-Tridecyl-ß-D-maltoside (TriDM) and n-Tetradecyl-ß-D-maltoside (TDM) were obtained from Anatrace (USA). Ethylene diamine tetraacetic acid (EDTA) was obtained from Sigma Aldrich. Fluo-4 fluorescent calcium-sensing dye was obtained from Invitrogen (Paisley, UK). Polyacrylic acids (PAA) of varying average $M_W$, namely 100 kDa, 250 kDa and 450 kDa were purchased from Polysciences Europe GmbH (Eppelheim, Germany). Ultrapure chitosan chloride (commercially known as 'Protasan UP CL 113', 75-90% deacetylated, with $M_W$ in the range of 50-150 kDa) was obtained from NovaMatrix (Norway). Pentasodium tripolyphosphate (TPP) was purchased from Sigma Aldrich. Fluorescein isothiocyanate (FITC, Type I) was purchased from Molecular Probes (Paisley, UK). Paraformaldehyde, osmium tetroxide, Triton X-100, Bovine Serum Albumin (BSA), Tween 20, FITC-phalloidin, glutaraldehyde and 1,4-Diazabicyclo-octane (DABCO, UV mountant) were all obtained from Sigma Aldrich. 3,3,5,5-tetramethylbenzidine (TMB) was purchased from Autogen Bioclear Ltd (UK). DAPI (4',6-diamidino-2-phenylindole) with antifade mounting media (commercially known as Slowfade Gold®) and CellTracker™ Green were obtained from Invitrogen. Fluorescent and non-fluorescent polystyrene nanoparticles (NPs) used in this work were purchased from different sources. Sulfate-modified, red NPs of 30 nm nominal diameter were obtained from Sigma Aldrich; sulfate-modified, yellow-green (YG) NPs (FluoSpheres®) of 20 nm diameter were obtained from Invitrogen (California, USA); carboxy-modified, YG NPs (Fluoresbrite®) of 50 nm diameter and non-fluorescent

carboxy-modified NPs of 50 nm (Polybead®) were supplied by Polysciences Europe GmbH (Eppelheim, Germany). All other chemicals were obtained from Sigma Aldrich.

## 2.2 Methods

### 2.2.1 Maintenance of cells

*2.2.1.1 Maintenance of cells in culture flasks*

All cell lines were routinely cultured in 75 $cm^2$ flasks at 5% $CO_2$, 95% relative humidity and 37°C until confluence (in this work confluence was considered as approximately 75-95% coverage of the flask surface by cells). Cell culture media was replaced every other day by aspirating the old culture media from the flasks, followed by the addition of 12-15 ml of fresh media, pre-warmed to 37°C. Cell growth was monitored regularly by viewing the cells under an optical microscope. Once confluent, cells were passaged using the following procedure: culture medium was removed (aspirated) from the flask and cells washed with PBS (5 ml, pre-warmed to 37°C), which was added to the flask and the flask gently swirled. PBS removes any dead cells remaining in the flask and traces of media; it was important to perform this step prior to the addition of trypsin/EDTA solution to cells since FBS present in the cell culture media inhibits the action of trypsin. PBS was then aspirated and replaced with 2.5-3 ml of pre-warmed (37°C) 2.5% trypsin/EDTA solution. The flask was gently swirled to ensure that trypsin/EDTA solution covered the cells and then transferred to the incubator at 37°C. The flask was observed at regular intervals for cell detachment from the tissue culture flask plastic. The period of incubation with trypsin/EDTA solution was dependent on the cell line and the extent of confluence. Generally, for HT29 and Caco-2 cells an incubation period of approximately 10 min was sufficient,

resulting in complete cell detachment from the flask plastic. On the other hand, Calu-3 cells required up to 15-20 min incubation with trypsin/EDTA for complete detachment from the flasks. Following cell detachment, approximately 10 ml of pre-warmed (37°C) culture medium was added to the flasks in order to dilute the cell suspension and deactivate trypsin (different media were used for each cell line, as will be described later). The resulting cell suspension was transferred to a sterile centrifuge tube and the cells centrifuged (pelleted) at 250g for 5 min. Trypsin-containing supernatant was aspirated and prewarmed culture medium (37°C, 5-10 ml) added to the cell pellet to create a cell suspension. A proportion of the resulting cell suspension was transferred to a new flask (containing prewarmed culture medium appropriate for the cell line) for further culturing. Split ratios between 1:3 and 1:5 were normally used for Calu-3 cells, while ratios between 1:4 and 1:8 were typically used for both HT29 and Caco-2 cells. Calu-3, Caco-2 and HT29 cells were cultured in EMEM, DMEM and McCoy's-5A medium, respectively. Culture media were supplemented with various components as described above (section 2.1.1).

*2.2.1.2 Frozen storage of cells*

Cells were cultured to confluence and then detached from the flask in the manner described previously (section 2.2.1.1). Following centrifugation of the cell suspension, the supernatant was aspirated, and the cell pellet was re-suspended in 1 ml of complete culture medium containing sterile DMSO. The concentration of DMSO used was 5% v/v for Calu-3 and Caco-2 cells and 7.5% v/v for HT29 cells. The cell suspension was added to a sterile cryovial (clearly labelled with the cell type, passage number, user name and date), which was placed into a freezing container ('Mr Frosty') in a -80°C freezer for a gradual, controlled temperature decrease. Cells were stored at –80°C for up to 4 weeks.

Thereafter, cells were transferred into a liquid nitrogen cell storage tank. Note that cells from a single confluent monolayer in *one* 75 $cm^2$ tissue culture flask were transferred and stored frozen in *one* cryovial; multiple flasks of cells were routinely detached and transferred into the equivalent number or sterile cryovials for frozen storage.

*2.2.1.3 Cell revival*

Cryovials containing frozen cells were removed from the liquid nitrogen-containing storage tank and thawed by placing the cryovial in the incubator at 37°C for approximately 5 min. DMSO-containing medium was removed by transferring the cell suspension into a centrifuge tube containing approximately 10 ml of warm (37°C) culture medium, centrifuging the resulting suspension at 250g for 5 min and aspirating the supernatant. The cell pellet was thereafter suspended in approximately 5 ml of culture medium and transferred into a 75 $cm^2$ flask containing approximately 10 ml of fresh, warmed (37°C) culture medium. Note that cells from *one* cryovial were revived and transferred into *one* tissue culture flask.

*2.2.1.4 Culture of cells on transwells*

2.2.1.4.1 Calu-3 cells

Calu-3 cells were cultured to confluence in 75 $cm^2$ flasks at 5% $CO_2$ and 37°C. Cells were then detached from the flasks using the method described above (2.2.1.1). Transwell® filters were incubated with EMEM (250 µl and 1.5 ml on the apical and basolateral chambers, respectively) at 37°C for approximately 15 min prior to the addition of cells. This was performed in order to coat the surface of the filter plastic with proteins present in the culture medium (serum), possibly resulting in improvement of cell attachment to plastic. Cells were counted using a

haemocytometer and the volume of the cell suspension containing the required number of cells was calculated. These volumes were subsequently added to the donor compartments of the transwells. The number of cells added ('seeding density') was $10^5$ per 1 $cm^2$ of the Transwell® filter area. The apical chamber volume was made up to 500 µl by adding warmed EMEM. After seeding on filters, cells were maintained at 5% $CO_2$, 37°C with EMEM.

Following the initial seeding on filters, Calu-3 cells were cultured in two ways: 1) cells were continuously exposed to culture medium on both apical and basolateral sides (0.5 ml and 1.5 ml, respectively), i.e. cells were grown using liquid covered culture (LCC); and 2) cells were cultured on transwells with medium present in the basolateral (acceptor) chamber only. The latter culture condition where the cells are exposed to the culture medium on their basal surface only is known as air-interfaced culture (AIC) or air-liquid interface (ALI) (note that the abbreviation AIC will be used in this work). Following their seeding on filters, cells were cultured using LCC conditions for two days. Thereafter, AIC conditions were created where cells were cultured with the culture medium (0.5 ml) present in the basolateral chamber only; cells were maintained at AIC for the remainder of the culture period.

For both culture conditions (LCC and AIC), the culture medium was subsequently replaced with fresh medium periodically (every other day). It is worth noting at this stage that, in this thesis, Calu-3 cells were typically cultured using AIC conditions only. However, in some cases cells were also cultured using LCC conditions for the purpose of comparison (of barrier properties and receptor expression) with AIC cells, as it will be apparent from Chapter 3 and 7. In cases where Calu-3 cells were cultured

using LCC conditions, this will be clearly stated; where culture conditions are not specified, cells were cultured using AIC. Calu-3 cells were typically cultured on filters for a period of 9-14 days prior to their use in experiments as confluent and polarised cell layers; work detailed in Chapter 7 was exclusively conducted on Calu-3 cells cultured on filters for 13-14 days.

2.2.1.4.2 Caco-2 cells

Caco-2 cells were seeded on filters in a similar way to Calu-3 cells, except that a density of $2x10^5$ cells/$cm^2$ was used. Caco-2 cells were cultured using LCC conditions only, with DMEM as the culture medium and were routinely grown on filters for 21-23 days (with culture medium replaced every other day) prior to their use in experiments as confluent, polarised cell monolayers.

### 2.2.2 Measurement of TEER

Transepithelial Electrical Resistance (TEER) is a measure of resistance to ion flux across an epithelial layer largely reflecting the degree of confluence of the cells and the paracellular pathway. TEER measurement has in the last two decades become universally established as the most convenient, reliable and non-destructive method to monitor the growth of epithelial tissue cultures *in vitro*, evaluate cell layer integrity and determine the presence and the tightness of the cellular tight junctions (TJs) (1). Measurements of TEER were conducted using the system depicted in Figure 2.1. Briefly, the chopstick electrodes were firstly sterilised by immersing in absolute ethanol for approximately 30 min prior to their use. The electrodes were then washed with PBS and carefully placed in the culture medium bathing the cell layers; the shorter electrode was submerged in the medium bathing the cells on the apical side,

while the longer electrode was placed in medium present on the basolateral chamber. The resulting readings were recorded. TEER was measured immediately upon removal of the cells from the incubator in all cases, in an attempt to minimise variability in observed TEER arising due to differences in temperature (TEER is affected by changes in temperature).

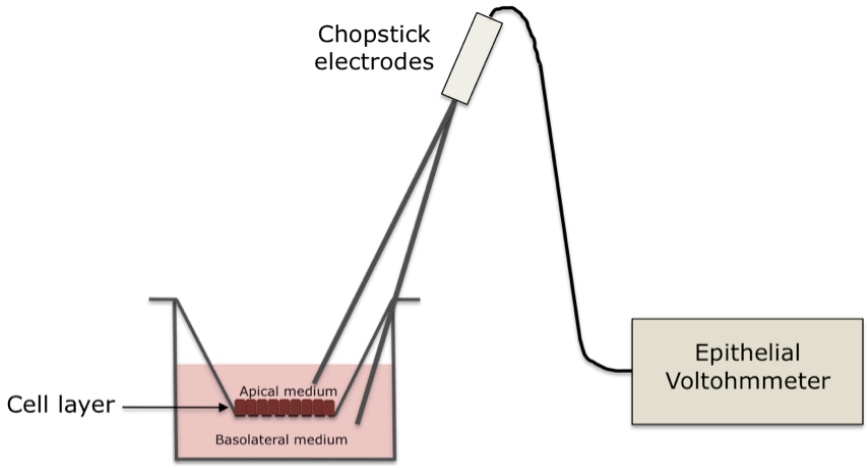


***Figure 2.1. Schematic representation of the Epithelial Voltohmmeter system used to measure TEER of the cell layers***.

In situations where measurements were conducted for the sole purpose of monitoring the cell growth, TEER was measured in the culture medium. For Calu-3 cells cultured using AIC conditions, culture medium was removed from the basolateral side and replaced with fresh, warmed medium on both apical and basolateral sides (0.5 ml and 1.5 ml, respectively). TEER was then measured following the incubation of cells with the culture medium on both sides (apical and basolateral) for approximately 45 min. This was done in order to minimise any possible effect that the physical shock resulting from replacement of the culture medium may have on TEER. In order to prevent any damage that may result from a possible leakage of ions from the electrodes, the culture medium was replaced following TEER measurements.

During the initial culture of Calu-3 cells on filters, TEER was measured every other day starting from day 2 to 15 of culture (daily measurements were avoided due to the possibility of cell damage from the measurement process and leakage of ions from electrodes). This step was repeated and the TEER development profile was found to be reproducible. TEER was subsequently only measured prior to the use of cell layers in experiments in order to establish cell confluence, cell layer intactness and TJ formation.

TEER values reported in this work take into account the area of the cell layer (assumed to amount to the area of the Transwell® filter) and are expressed as $\Omega cm^2$. Furthermore, electrical resistance across the cell-free Transwell® filters (background resistance) was also measured on every batch of Transwell® filters used in the experiments. This value (typically 100-110 $\Omega cm^2$, depending on the batch) was subtracted from the measured cell layer TEER in all experiments in this work; background filter resistance is therefore accounted for in all the reported values in this thesis.

### 2.2.3 Evaluation of TJ modulation through measurement of TEER

The purpose of these experiments was to assess the TJ modulating (opening) capacity of various compounds. Considering the nature of the experiments, only filter-cultured cell layers exhibiting TEER of 500 $\Omega cm^2$ or above were considered adequate for the purpose of these studies. Note that filter-cultured cells with a TEER $\geq$500 $\Omega cm^2$ are referred to as 'confluent cell layers' throughout this thesis. The experiments were conducted in HBSS, which was buffered at pH 6.0 (with 10 mM MES) or pH 7.4 (using 25 mM HEPES). Prior to application of the test samples to cells, the culture

medium was removed, cells washed with PBS and HBSS (warmed to 37°C; pH 7.4) added to both sides of the cell layers. Cells were equilibrated in HBSS (i.e. incubated at 37°C, 5% $CO_2$) for approximately 45 min, following which initial TEER measurements were conducted; the recorded values were considered as baseline TEER. HBSS was then removed from the apical side of the cell layers and replaced with the test samples (previously warmed to 37°C). Unless otherwise stated, cells were incubated with the samples for 2 hours, with TEER measurements at times 0.5, 1, 1.5 and 2 hours following sample application in the presence of the tested samples in HBSS. The samples were removed from the cells 2 hours post-application and cells washed with PBS (3 times). Culture medium (appropriate for the cell line, see section 2.2.1.1) was then added to the cell layers and cells incubated with the culture medium overnight. In order to determine whether the effect of the tested samples on TEER (if any) was reversible, TEER was measured (in culture medium) 4 hours and 24 hours (the following day) after test sample application. TEER changes are reported as percentage of the baseline value (i.e. TEER value before sample addition). In some cases confluent cell layers incubated with HBSS instead of the test samples were used as controls. All experiments were conducted in triplicate or quadruplicate.

### 2.2.4 FITC-dextran (FD) permeability experiments

In a similar way to TJ modulation experiments (in the previous section), only filter-cultured cell layers exhibiting TEER ≥500 $\Omega cm^2$ (i.e. 'confluent cell layers') were considered adequate for FD permeability experiments. TEER measurements were conducted prior to the permeability experiments in order to ensure that the cell layers were confluent and intact. TEER was also recorded after the permeability experiment

in order to confirm intactness of the cell layers throughout the experimental period and hence validate the permeability data.

Fluorescein isothiocyanate (FITC)–labeled dextrans (FDs) of varying $M_W$s were used in this work as macromolecular tracers (also referred to as 'solutes' and 'penetrants') modelling hydrophilic, large $M_W$ protein drugs. The availability of FDs in different $M_W$s and being fluorescent (enabling a relatively simple quantification) makes these molecules ideal for use in experiments investigating macromolecular permeability across epithelial cell layers.

HBSS is the most commonly used medium in drug transport experiments (2). To enable comparison of the data obtained in this work with those reported in the literature, HBSS was used in all transport experiments described in subsequent chapters. The availability of HBSS without fluorescent phenol red (present in the culture media), which would interfere with the fluorescent macromolecular tracers is another advantage associated with the use of HBSS. In order to maintain a desired pH, HBSS was supplemented with buffer systems. As described in the previous section, HEPES (25 mM) was added to HBSS to maintain a physiological pH 7.4, whereas MES (10 mM) was used to supplement HBSS in order to maintain a slightly acidic pH 6.0. In the subsequent chapters of this thesis, HBSS is sometimes referred to as the 'transport medium'. HBSS buffered at pH 6.0 and 7.4 represents HBSS supplemented with MES and HEPES, respectively. Note that 'HBSS pH 6.0' signifies the use of MES-buffered HBSS in the forthcoming Chapters; where the pH is not specified, HBSS was buffered (pH 7.4) by supplementing with HEPES.

Unless otherwise stated in individual chapters, permeability experiments were conducted in the following way. Culture medium was removed from the cell layers and cells washed with warm (37°C) PBS. HBSS was then added to the apical (0.5 ml) and basolateral (1.5 ml) chambers of the Transwell® system. Cells were incubated (at 37°C/5% $CO_2$) with HBSS for approximately 45 min for the purpose of equilibration. TEER was then measured in order to confirm the 'confluence' and the intactness of the cell layers, following which HBSS was removed from the apical side. Unless otherwise stated, permeability experiments were started by applying 0.5 ml of the test solution to the apical side of the cells (donor compartment of the transwells). Test solutions contained a FD with or without a compound that was investigated for its permeability enhancing effect. The final concentration of FDs in the apical chamber was kept constant at 500 µg/ml in all FD permeability experiments.

FD permeability was determined by sampling the basolateral solution at regular time intervals. More specifically, 100 µl volumes were removed from the basolateral chamber of the Transwell® system every 30 min for 3 hours. The sampled solutions were immediately replaced with equal volumes of the transport medium (HBSS). Between sampling times, cells were incubated at 37°C/5% $CO_2$. To ensure that the cell layer integrity remained intact during the permeability experiment, TEER was measured following the final sampling point. Sampled solutions were transferred into a black 96-well plate, which was then covered with aluminium foil to protect from light. Sample solution fluorescence (485 nm excitation, 535 nm emission) was then determined using an MFX microtiter plate fluorometer (Dynex Technologies, USA).

FD in the basolateral solutions was quantified by converting the fluorescence readings

into FD concentrations and ultimately amounts, through construction of calibration curves. Briefly, this involved measuring the fluorescence intensity of progressively diluted FD solutions of known FD concentrations. At least three such calibration curves were established; the mean values were then calculated and used for FD quantitation in each experiment.

FD permeability is expressed as the apparent permeability coefficient ($P_{app}$), calculated using the following equation:

$$P_{app} = \left(\frac{\Delta Q}{\Delta t}\right) x \left(\frac{1}{A x C_0}\right)$$

Where:

- $P_{app}$ is the apparent permeability in cm/s
- $\Delta Q/\Delta t$ is the permeability rate [amount FD (µg) traversing the cell layers over time (s)]. This was determined by plotting the amount of transported solute over time and calculating the gradient of the straight-line (i.e. steady state) portion (typically transport over time points 30 min – 3 h) of the resulting curve
- A is the diffusion area of the layer ($cm^2$), and
- $C_o$ is the initial FD concentration (500 µg/ml)

### 2.2.5 Cell toxicity studies

*2.2.5.1 Background information on toxicity tests*

**AlamarBlue® assay**, which was first described by Fields *et al.* (3), involves the addition of a fluorogenic redox indicator to growing cells in culture. The oxidized

form of alamarBlue®, which has a dark blue color, has little intrinsic fluorescence. However, in response to a chemical reduction of growth medium resulting from cell growth, the dye is reduced and turns red. The reduced form of alamarBlue® is highly fluorescent. The extent of this conversion is a reflection of cell metabolic activity and can be quantified by fluorescence.

There are many advantages associated with the use of the alamarBlue® assay to determine cell proliferation or toxicity, including its simplicity (the indicator is added directly to cells in culture) and non-toxicity to the cells and the user. Furthermore, it has been reported that the alamarBlue® assay is comparable in sensitivity to the thymidine incorporation and tetrazolium reduction assays for the measurement of cell proliferation and cytotoxicity (4, 5).

The **MTS** assay is also a colorimetric method for determining the number of viable cells in proliferation or cytotoxicity assays, containing a novel tetrazolium compound, 3-(4,5-dimethylthiazol-2-yl)-5-(3-carboxymethoxyphenyl)- 2-(4-sulfophenyl)-2H-tetrazolium (inner salt), and an electron coupling reagent (phenazine ethosulfate; PES). PES has enhanced chemical stability allowing its combination with MTS to form a stable solution. The MTS tetrazolium compound is bioreduced by cells into a colored formazan product that is soluble in tissue culture medium. This conversion is thought to occur by NADPH or NADH produced by dehydrogenase enzymes in metabolically active cells (6).

**Lactate dehydrogenase (LDH)** assay is a simple and convenient method for assessing cytotoxicity or cell viability. This assay, first described as a cytotoxicity test by Legrand *et al.* (7), can be used as an indicator of relative cell viability as well as a

function of membrane integrity of cells. With respect to the latter, the LDH assay is particularly valuable for testing compounds that perturb the cell membrane. The assay is based on the reduction of NAD by the action of LDH. The resulting reduced NAD (NADH) is used in the conversion of a tetrazolium dye into a coloured compound, which can then be measured spectrophotometrically. The extent of membrane damage results in a concomitant change in the amount of substrate converted. In this work, the LDH assay was used to test cell membrane integrity as a function of the amount of cytoplasmic LDH released into the medium relative to controls (described later).

*2.2.5.2 AlamarBlue® Cell Metabolic Activity Assay*

This assay was used to test the cytotoxicity of compounds on confluent Calu-3 layers or cells cultured on multiwell plates. In the first scenario, cell layers were incubated with the tested compounds and controls, followed by washing with PBS (three times). HBSS and Triton X-100 (0.1% v/v in HBSS) were used as the negative and positive control, respectively. AlamarBlue® *stock solution* was diluted 1 in 10 in HBSS to produce alamarBlue® *working solution*; this solution was then applied above and below the cell layers (0.5 ml and 1.5 ml, respectively). Cells were incubated with the alamarBlue® reagent for 90 min following which 100 µl samples were collected (from the apical side) and transferred into a black 96-well plate (covered with aluminium foil to protect from light). Sample fluorescence (Ex 560 nm/ Em 590 nm) was then measured using an MFX microtiter plate fluorometer (Dynex Technologies, USA).

AlamarBlue® assay was also conducted on cells cultured on 24-multiwell plates. Cells were incubated with the tested compounds and controls, followed by washing with PBS. 1 ml of the alamarBlue® working solution was then applied to the wells. Cells

were incubated with the alamarBlue® reagent for 90 min following which 100 µl volumes of this solution were collected and tested for fluorescence as before.

The relative cell metabolic activity (%) was calculated using the following equation:

$$\text{Relative metabolic activity} = \frac{S - T}{H - T} \times 100$$

Where:

- S is the fluorescence of the tested samples
- T is the fluorescence of cells incubated with Triton X-100, and
- H is the fluorescence of cells incubated with HBSS

*2.2.5.3 MTS Cell Metabolic Activity Assay*

The MTS assay was performed on Calu-3 cells. Unless otherwise stated, the assay was conducted in the following way. Cells were seeded on 96-well plates (sterile, cell culture treated) at a density of $10^4$ cells per well and incubated at 37°C/5%$CO_2$ for 24 hours. This seeding density was chosen (optimised) as it produced an absorbance value within the linear range of the assay, as recommended by the manufacturer. Culture medium was carefully aspirated (while making sure that the sterile pasteur pipette used for this purpose did not touch the cells) and replaced with test sample solutions (at different concentrations), dissolved in HBSS (at pH 6.0 or 7.4, as specified in the individuals chapters). Cells incubated with HBSS (at the same pH as the test samples) were used as the negative control, whereas cells incubated with Triton X-100 (0.1% v/v in HBSS at pH identical to that of the test samples) were used as the positive control. Samples and controls were previously warmed and applied to cells at 37°C. Following the application of the samples and controls, cells were

incubated at 37°C/5%$CO_2$ for 2 hours. Sample solutions (and controls) were then aspirated and cells washed with PBS. 100 µl of culture medium (at 37°C) was added onto each well, followed by application of 20 µl of the MTS reagent. Cells were incubated with the culture medium/MTS reagent for 1-4 hours (more typically 2-3 hours), following which absorbance at 492 nm was measured using a Dynex absorbance microplate reader (Dynex Technologies, USA).

The relative cell metabolic activity (%) was calculated using the following equation:

$$\text{Relative metabolic activity} = \frac{S - T}{H - T} \times 100$$

Where:

- S is the absorbance with the tested samples
- T is the absorbance with Triton X-100
- H is the absorbance with HBSS

*2.2.5.4 LDH assay*

The LDH assay was performed to test the membrane toxicity of different compounds on Calu-3 cells. Cells were seeded on 96-well plates (sterile, cell culture treated) at a seeding density of $10^4$ cells per well and cultured for 24 hours before the assay. Culture medium was removed and cells washed with PBS. Test compounds of different concentrations dissolved in HBSS (pH 6.0 or 7.4, at 37$^o$C) were then applied. Triton X-100 (0.1% v/v in HBSS) was used as the positive control to induce LDH release, whereas HBSS (pH 6.0 or 7.4) was used as the negative control. Cells were incubated with samples and controls for 2 hours, after which 50 µl of the solutions were removed from each well and placed onto a new 96-well plate. 100 µl

of the LDH reagent was added to the samples and an incubation time of 20-30 min at room temperature was allowed. After this period, absorbance at 490 nm was measured using the Dynex absorbance microplate reader. LDH release was calculated as the percentage relative to the controls, using the following equation:

$$\text{Relative LDH release} = \frac{S - H}{T - H} \text{ x } 100$$

Where:

- S is the absorbance obtained with the tested samples
- H is the absorbance with HBSS
- T is the absorbance with Triton X-100

### 2.2.6 Cell imaging and labelling

*2.2.6.1 Scanning Electron Microscopy (SEM)*

Filter-cultured confluent Calu-3 layers were fixed by replacing the culture medium with 1:1 mixture of culture medium and fixing solution, which comprised 2.5% v/v glutaraldehyde in 0.1 M sodium cacodylate buffer (pH 7.2) on both apical and basolateral sides of the transwells. Following an incubation interval of 5 min, this solution was removed and replaced with 100% of the fixing solution. The fixing solution was then removed and replaced with 1% w/v osmium tetroxide in water; cell samples were incubated with this solution at room temperature for 90 minutes. Osmium tetroxide is used in electron microscopy both as a fixative and a heavy metal stain for lipids in membranous structures and vesicles (8). Osmium tetroxide solution was then removed and samples dehydrated in progressively increasing concentrations of ethanol in water (25%, 50%, 75%, 95% and 100% v/v). Samples were dried using a

critical point dryer before filters were removed and mounted on aluminium stubs with adhesive double-sided carbon tape. The samples were gold coated for 3 minutes under an argon atmosphere in a Blazers Union SCD030 sputter coater unit (Blazers Ltd, UK). Coated samples were examined with a JEOL 6060LV (JEOL, Welwyn, UK) variable pressure scanning electron microscope operating at an accelerating voltage of 10 kV. Image analysis was carried out using the in-built SEM control user interface software (version 6.57) and digital imaging system.

*2.2.6.2 Transmission Electron Microscopy (TEM)*

Confluent Calu-3 layers were fixed with 4% paraformaldehyde and then washed with 0.1 M phosphate/cacodylate buffer. Cells were post fixed with 1% aqueous osmium tetroxide for 30 mins, followed by extensive washing (5x1 min) with distilled water. Samples were then dehydrated in a graded ethanol series by washing the cells for 5 min (twice) with 50% ethanol, followed by 70% ethanol, followed by 90% ethanol and then finally with 3x10 min washes with 100% ethanol. Finally, two 5 min washes were performed with 100% dried acetone. Cell samples were then infiltrated with resin for a duration of 30 minutes in 1:3 resin:acetone mix, 1 hour in 1:1 resin:acetone mix and 3x1 hour incubations in pure resin. Samples were embedded in the resin and left in the embedding oven for 48 hours at 60°C. Once the resin block polymerised, the substrate was removed from the cells by immersing the block in liquid nitrogen and snapping the substrate from the block. The block was then embedded in a microcentrifuge tube containing fresh resin and was polymerised as before, enclosing the cell layer in a resin block. The layer was cut out of the block by sawing either slide of it to give a disc of resin with the layer running through the middle. The disc was cut in half to form 2 semi-circles, which were stuck onto the top of a blank resin

block (using Araldite® epoxy resin). The Araldite® was left to set for a period of 1 hour. Ultrathin sections were cut using a cryoultramicrotome (Leica EM, UC6/FC6, Milton Keynes, UK) and viewed by TEM (Jeol JEM 1010 Electron Microscope, Japan). Note that some aspects of sample preparation for TEM were performed by the Advanced Microscopy Unit group, School of Biomedical Sciences, University of Nottingham.

*2.2.6.3 CellTracker™ staining*

CellTracker™ reagents pass through the cell membranes and once inside the cells they are converted into cell membrane-impermeant products. These dyes contain a chloromethyl or bromomethyl group that reacts with thiols, which is thought to occur in a glutathione *S*-transferase–mediated reaction since this has been shown to occur *in vitro* (9). Since glutathione levels are high (up to 10 mM) in most cells and glutathione transferase is ubiquitous, the reagent is transformed into a cell-impermeant fluorescent dye–thioether product.

50 µg of CellTracker™ Green stock solution was dissolved in high quality DMSO to produce a 10 mM solution. This solution was subsequently diluted to 10 µM with serum-free culture media and warmed to 37°C. Filter-cultured, confluent Calu-3 layers were washed with PBS, following which 500 µl of the labelling solution was added to the apical side of the cells; cells were incubated with CellTracker™ green solution for 45 min. The labelling solution was then removed and replaced with culture medium (EMEM). Cells were incubated with EMEM for 30 min. EMEM was then aspirated and cells fixed by incubating with 4% paraformaldehyde in PBS for approximately 10 min. Transwell® filters (containing cells) were then excised and

mounted (using DABCO mounting medium) on glass slides for confocal imaging. Cells were imaged using a Leica TCS SP2 system mounted on a Leica DMIRE2 inverted microscope.

*2.2.6.4 Actin staining*

Calu-3 cells were cultured on filters until confluent cell layers were formed, as described previously. Culture medium was removed and cells washed with BSA 1% w/v in PBS (BSA/PBS). Cells were then fixed in 4% paraformaldehyde (in PBS) for approximately 10 min at room temperature. The fixative was then removed and cells washed (3 times) with 1% BSA/PBS. Cells were permeabilised by applying cold permeabilising solution (consisting of 20 mM HEPES, 300 mM sucrose, 50 mM NaCl, 3 mM $MgCl_2$ and 0.5% v/v Triton X-100; in PBS at pH 7.4); cells were incubated with the permeabilising solution for 5 min in the freezer (-20°C), ensuring that the solution did not freeze. The permeabilising solution was then removed and cells washed three times with 1% BSA/PBS. Cells were incubated with 10 µg/ml FITC-phalloidin for 20 min at room temperature. FITC-phalloidin solution was then removed and cells washed with 1% BSA/PBS (3 times). Cell layer-containing filters were then excised carefully with a scalpel and placed on glass slides. Samples were mounted on glass slides with DABCO and covered with glass cover slips. Cells were imaged using the Leica confocal system, described in the previous section.

*2.2.6.5 MUC-1, mucus protein staining*

Calu-3 cells were cultured on filters as before. Confluent cell layers were fixed in paraformaldehyde (by incubating for approximately 10 min) at room temperature. Cells were then washed with PBS and permeabilised by incubating with Triton X-100

(0.1% v/v in PBS) for approximately 10 min. Cells were then washed and incubated with 1% w/v BSA in PBS for approximately 1 hour; this step was performed to block/minimise any non-specific antibody binding. BSA/PBS was then removed and cells incubated with mouse, anti-human MUC-1 (primary) antibody for approximately 1 hour. Following the incubation with the primary antibody, cells were washed extensively (5 times) with PBS, following which goat, anti-mouse FITC-IgG (secondary antibody) was added and cells incubated with the secondary antibody for approximately 1 hour. Cells were then washed extensively and Transwell® filters excised and mounted on glass slides (using DAPI-containing, ProLong® Gold antifade/mounting medium) for confocal imaging. Confocal imaging was performed using the Leica TCS SP2 confocal system.

*2.2.6.6 Zonula Occludens (ZO-1) TJ staining*

Confluent, filter-cultured cell layers were fixed in paraformaldehyde for approximately 10 min at room temperature. Cells were then washed with PBS and permeabilised by incubating with Triton X-100 (0.1% v/v in PBS) for approximately 10 min. Cells were then washed with PBS, followed by the application of 1% BSA/PBS for approximately 1 hour. Thereafter, BSA/PBS solution was aspirated and replaced with mouse, anti-human ZO-1 (primary) antibody, diluted in 1% BSA/PBS to a final concentration of 10 µg/ml. Cell samples were incubated with the primary antibody for 1 hour. The primary antibody solution was then removed and cells washed with PBS (5 times). FITC- or Cy5-labelled goat, anti-mouse (secondary) antibody, diluted according to manufacturer's instructions in 1% BSA/PBS was then applied to the cells for 1 hour. The secondary antibody solution was then aspirated and cells washed with PBS extensively. The Transwell® filter membrane was excised

and mounted on glass slides (using the ProLong® Gold mounting medium) for confocal imaging, which was performed using the confocal system described in section 2.2.6.3.

### 2.2.7 Antibody quantitation

*2.2.7.1 Quantitation of IgG by ELISA following transport experiments*

Basolateral solutions (100 µl volumes), sampled following IgG transport experiments (see Chapter 7) were placed on 96-well polystyrene ELISA plates and incubated overnight at 4°C; this was performed so that any IgG present in the basolateral solutions coated the surfaces of the multiwell plate. The following day, sample solutions were removed and the plate washed three times with the wash buffer consisting of Tween 20, 0.05% v/v in PBS. The wells were then blocked by applying 200 µl of 1% BSA w/v in PBS (blocking buffer) for 1 hour at room temperature. Blocking buffer was then removed and the wells washed (with the wash buffer) as before. 100 µl of anti-human IgG conjugated to horseradish peroxidase (HRP), diluted 1:1000 in blocking buffer was added to individual wells; the plate was incubated for 2 hours at room temperature. Anti-human IgG-HRP solution was then removed and the plate wells washed with the wash buffer (3 times). TMB substrate (100 µl) was added into each well for approximately 10 min. The reaction was stopped by adding 20 µl of 2.5 M sulphuric acid, following which the plates were transferred into the Dynex microplate reader for determination of absorbance (measured at 450 nm).

IgG was quantified by converting the absorbance readings into concentrations (and eventually amounts) through preconstructed calibration curves. In a similar way to FD calibrations curves, ELISA was performed on series of progressively diluted solutions

of known IgG concentrations. The resulting absorbance readings were plotted against concentrations. Calibration curves were constructed in triplicate and the calculated mean value was used for quantitation. The straight-line segment of the resulting curve was used to convert the absorbance readings of samples (i.e. basolateral solutions containing unknown IgG levels) into IgG concentrations. Note that calibration curves were created for each IgG transport experiment and that ELISA was performed in the same manner for both calibration curves and samples containing unknown IgG concentrations.

*2.2.7.2 Quantitation of investigational therapeutic antibodies by HPLC*

hCTMO1 antibody, hCTMO1 Fab, murine mA33γ1 Fab and murine mA33γ1 Fab-diPEG) were quantified by high-pressure liquid chromatography (HPLC) using a Gilson Model 600 pump equipped with a Gilson photodiode array detector, a 20 µl loop injection autosampler and Empower software. For analysis, a Zorbax GF250 size exclusion column was eluted with 0.2 M sodium phosphate buffer (prefiltered using 0.2 µm filters and degassed) at pH 7.0 in isocratic mode. The flow rate of 1 ml/min was maintained and the column eluent was monitored continuously at 277 nm. Quantitation of the compounds was carried out by measuring the peak areas in relation to those of the calibration curves (i.e. series of progressively diluted antibody solutions of known concentrations) chromatographed under the same conditions.

### 2.2.8 Statistical analysis

Statistical comparisons were performed by Student's t-test. Values of $p<0.05$ were considered statistically significant.

## 2.3 References


1. WPI. http://www.wpi-europe.com/en/products/tissue/evom2.shtml (accessed 02/01/2010 2010).
2. S. Tavelin, J. Grasjo, J. Taipalensuu, G. Ocklind, and P. Artursson. Applications of epithelial cell culture in studies of drug transport. Methods Mol Biol. 188:233-272 (2002).
3. R.D. Fieldsand M.V. Lancaster. Dual-attribute continuous monitoring of cell proliferation/cytotoxicity. Am Biotechnol Lab. 11:48-50 (1993).
4. S.A. Ahmed, R.M. Gogal, Jr., and J.E. Walsh. A new rapid and simple non-radioactive assay to monitor and determine the proliferation of lymphocytes: an alternative to [3H]thymidine incorporation assay. J Immunol Methods. 170:211-224 (1994).
5. R. de Friesand M. Mitsuhashi. Quantification of mitogen induced human lymphocyte proliferation: comparison of alamarBlue assay to 3H-thymidine incorporation assay. J Clin Lab Anal. 9:89-95 (1995).
6. M.V. Berridgeand A.S. Tan. Characterization of the cellular reduction of 3-(4,5-dimethylthiazol-2-yl)-2,5-diphenyltetrazolium bromide (MTT): subcellular localization, substrate dependence, and involvement of mitochondrial electron transport in MTT reduction. Arch Biochem Biophys. 303:474-482 (1993).
7. C. Legrand, J.M. Bour, C. Jacob, J. Capiaumont, A. Martial, A. Marc, M. Wudtke, G. Kretzmer, C. Demangel, D. Duval, and et al. Lactate dehydrogenase (LDH) activity of the cultured eukaryotic cells as marker of the number of dead cells in the medium [corrected]. J Biotechnol. 25:231-243 (1992).
8. O. Zrihan. http://www.emsdiasum.com/microscopy/products/sem/QX102/OsmiumTetroxideStainingFcells.pdf (accessed 02/01/2010 2010).
9. Y.Z. Zhang. New fluorescent probes for long-term tracing of living cells. FASEB J. 6:A1835 (1992).

# Chapter 3

# Calu-3 Layer Model: Morphological and Barrier Characteristics

## 3.1 Introduction

An essential prerequisite for investigation of mucosal drug absorption *in vitro* for the purpose of predicting *in vivo* absorption is a mucosal tissue model. An ideal model is simple, economical and represents the *in vivo* conditions as closely as possible. Different mucosal tissue models are available. These include excised mucosal tissues, three dimensional models based on multiple cell types and epithelial cell layers of primary cells and those based on cancerous cell lines. There are advantages and disadvantages associated with the use of each of these models. For example, although the *in vivo* conditions are most closely represented by an excised tissue of interest (usually from animals with similar tissue characteristics to humans'), this model usually requires animal sacrifice and suffers from limited viability of the tissue *ex vivo*.

*In vitro* models based on epithelial cell lines are popular in studies of drug transport processes. This is because, compared to an *in vivo* approach, these models offer the simplicity, reduced operational costs, robustness and better control in experiments. Furthermore, they minimize animal usage and eliminate variation among animals (1).

*In vitro* cell systems can be manipulated in ways not possible *in vivo*, allowing researchers to study the effects of different variables (such as temperature, pharmacological agents, etc.), which is particularly useful in investigating the mechanisms of drug transport processes.

A considerable amount of knowledge about active and passive drug transport mechanisms has been obtained from studies in various epithelial cell cultures. In fact, both cell culture and drug transport experiments across epithelial cultures have been automated, with these models being used as a screening tool in the pharmaceutical industry for the prediction of intestinal drug absorption (2). This is due to an observed good correlation between passive drug transport through various epithelial cell monolayers and that observed across the human intestine *in vivo* (3-5). The importance and credibility of the data obtained from drug transport experiments on epithelial cell monolayers is highlighted by the fact that both the FDA and the European Medicines Agency (6) recommend the use of monolayers of suitable epithelial cells for classifying the permeability of drug compounds. However, it is of utmost importance to highlight the fact that homogenous epithelial cell cultures lack the structural complexity and variability found *in vivo* and for this reason it is important to be cautious in extrapolating *in vitro* results to the *in vivo* situation and to compare results obtained in the two systems.

The Calu-3 cell line has been extensively researched in the past, partly due to the expression of the cystic fibrosis transmembrane conductance regulator (CFTR) protein (7, 8), which is important in studies related to cystic fibrosis. Calu-3 cells are derived from submucosal gland acini (9) and have been shown to express secretory

component, secretory leukocyte protease inhibitor, lysozyme and lactoferrin in addition to CFTR (7, 10, 11), which are all markers of serous submucosal gland cells (12). On the other hand, Calu-3 cell do not express the epithelial surface marker 15-lipoxygenase (11). Expression of the mucin gene, muc-2, found in surface goblet cells and gland mucous cells of native epithelium, has also been reported (11). Microscopic examinations of Calu-3 cells have shown that they contain granules typical of mucus-secreting cells (9). In culture, the Calu-3 cell line produces features of differentiated, functional human airway epithelial cells (7) including the formation of tight junctions (TJs), making it one of the few available respiratory cell lines exhibiting this property (13-23). It is the combination of all these characteristics and the fact that the Calu-3 cell line has demonstrated excellent *in vitro–in vivo* correlation (24) that enables utilization of the Calu-3 cell line as a model of the airway epithelium in mucosal drug delivery research.

There is reported evidence to suggest that the characteristics of the Calu-3 layers are determined upon the culture conditions employed for their growth (25, 26). Some researchers argue that, when grown under air-interfaced culture (AIC) conditions, the resulting cell layer resembles the native epithelium (27-29) to a greater extent than cells grown using liquid-covered culture (LCC). A study by Grainger *et al.* has reported increased mucus secretion, and more physiological TEER values in cell layers cultured using AIC compared to LCC-grown cells (9).

However, marked inconsistencies exist in the literature with regards to the morphology and permeability of the Calu-3 layers cultured using AIC and LCC. While Fiegel *et al*. reported a greater abundance of mucus-related acidic glycoproteins

in Calu-3 layers cultured using AIC compared to LCC (19) and Florea *et al*. found a reduced differentiated morphology for Calu-3 cultured using LCC (30), other studies have indicated no difference between AIC and LCC conditions (18). Furthermore, Pezron *et al*. and Patel *et al.* reported the appearance of abundant cilia and visible mucus production in Calu-3 cells grown using LCC (17, 18). Likewise, while some groups reported similar expression of the TJ protein, ZO-1, in AIC and LCC cells (19), others have shown a higher expression of this protein in LCC compared to AIC cells (9). Inconsistencies in the literature also exist with regards to the presence of cilia in Calu-3 cells, with some studies reporting their presence (17, 18) and other work reporting no such findings (7, 19, 21, 31). It is because of these inconsistencies that, to date, there is no generally accepted consensus on the culture conditions that should be followed in growing Calu-3 cells on filters. As a consequence of inter-laboratory variation in culture conditions, it has been argued that it is important to characterise the filter-cultured Calu-3 layers before using them as a model of the airways (9). This, therefore, is the rationale for the work detailed in this chapter.

In this part of the project, Calu-3 cells grown using AIC and LCC conditions were compared with respect to their TEER profiles (development of TEER with culturing time) and the barrier they present to the permeability of hydrophilic macromolecules and nanoparticles (NPs). To obtain morphological information, filter-cultured (using AIC conditions) Calu-3 layers were characterised by imaging the cells by different microscopic techniques. Furthermore, the effect of a mucolytic compound on the permeability of a hydrophilic solute across Calu-3 layers was also tested with the aim to assess whether the presence of mucus provides a barrier to translocation of macromolecules. The barrier properties of Calu-3 layers were also compared with

those of Caco-2 cells. As noted previously (section 2.2.1), AIC conditions were normally employed for growth of Calu-3 cells in filters; in cases where cells were cultured using LCC, this will be clearly stated.

## 3.2 Methods

### 3.2.1 TEER profiles of filter-cultured Calu-3 cells: AIC and LCC conditions

Calu-3 cells were cultured on flasks until confluence. Thereafter cells were detached from the flasks, seeded and cultured on filters using AIC and LCC conditions following the methods detailed previously (section 2.2.1). TEER measurements were conducted (in the manner described in section 2.2.2) every 2 or 3 days, starting from day 2 to day 15 of culture.

### 3.2.2 Morphological characterisation of filter-cultured Calu-3 cells

Calu-3 cells were grown using AIC conditions as per usual protocol (section 2.2.1). Cells were imaged once they formed confluent and polarised layers (as judged by TEER measurements). SEM, TEM, CellTracker$^{TM}$ Green labelling, F-actin staining, MUC-1 (mucus protein) staining and Zonula Occludens-1 (ZO-1) staining were performed according to methods described in section 2.2.6.

### 3.2.3 Permeability studies

*3.2.3.1 FD4 permeability across AIC and LCC Calu-3 layers*

Calu-3 cells (of the same passage number) were cultured on filters using AIC and LCC conditions. Both AIC- and LCC-grown cell layers were in this instance used for FD4 permeability experiment at day 10 of culture. Culture medium was initially replaced with warmed (37°C) HBSS (transport medium). Cells were allowed to equilibrate in HBSS for approximately 30 min, following which TEER measurements were conducted in order to confirm cell layer intactness and select those with the desired values (see sections 2.2.3 and 2.2.4 for further information on TEER values that were considered appropriate for TEER and permeability studies). HBSS was then removed from the apical side of the cells and replaced with a solution of FD4 dissolved in the HBSS (500 μg/ml). The rest of the experiment was conducted in the manner described previously (section 2.2.4).

*3.2.3.2 Effect of N-acetyl cysteine on FD4 permeability*

Calu-3 cells were cultured on filters using AIC conditions and were used in this experiment as confluent layers. Culture medium was removed and replaced with a solution containing N-acetyl cysteine (NAC), dissolved in HBSS at 0.3% w/v, on the apical side and HBSS only on the basolateral compartment of the transwells. Cells were incubated with NAC for 30 min after which NAC-containing apical solution was removed. Fresh solution of NAC in HBSS was re-applied to the apical side and cells incubated with NAC for a further 30 min. Preservation of the intactness of the cell layers following the incubation with NAC was assessed by TEER measurements, which were conducted before the application of NAC (baseline value) and at the end of the incubation period with NAC. NAC-containing solution was then removed from

the apical side of the cells and replaced with solutions of FD4 in HBSS (500 μg/ml). FD4 permeability was measured by sampling the basolateral solution in the way described previously (section 2.2.4). TEER was measured again immediately after the last sampling point.

A control experiment was performed by measuring FD4 permeability across the cell layers incubated with HBSS for 1 hour, with its replacement at 30 min, to replicate the conditions followed for NAC (above). For the purpose of comparison, TEER measurements were also performed on control cell layers at the same intervals as on the cells exposed to NAC.

*3.2.3.3 Permeability of varying $M_W$ FDs across Calu-3 layers*

Confluent Calu-3 layers cultured using AIC conditions were evaluated for their permeability characteristics with respect to the molar mass of the macromolecular solutes (penetrants). FDs with a different molar mass were used as tracer solutes to test the effect of $M_W$ on permeability. Prior to the application of the tracers, culture medium was removed and replaced with HBSS; cells were equilibrated in HBSS for approximately 45 min. HBSS was then removed from the apical side and replaced with FD solutions, comprising of FD20, FD40, FD70 and FD150 dissolved in HBSS (37°C) at 500 μg/ml. The permeability of different FDs was determined by regular sampling of the basolateral solution and quantitation by measurement of fluorescence in the same way as for FD4, which was described previously (section 2.2.4).

*3.2.3.4 Insulin translocation across Calu-3 layers*

Calu-3 cells were cultured on filters as before and used as confluent layers. Permeability experiments were commenced after replacement of the culture medium with HBSS and equilibration in HBSS (for approximately 45 min). Stock solutions of FITC-insulin dissolved in HBSS at pH 6.0 at a concentration of 160 μg/ml were prepared on the day of the permeability experiment. FITC-insulin solution was applied to the apical side of the cells at a final concentration of 80 μg/ml (in HBSS; pH 6.0) and its transport across the cell layers was determined by sampling (100 μl volumes) the basolateral solution at regular time intervals. The sampled volumes from the basolateral chamber were replaced with fresh HBSS. Insulin was quantified by fluorescence measurements (485 nm excitation, 535 nm emission) in a similar way to quantitation of FDs (described in section 2.2.4). The results were expressed as apparent permeability coefficient ($P_{app}$), calculated according to the equation in section 2.2.4.

*3.2.3.5 Comparison of FD permeability across Calu-3 and Caco-2 layers*

FD20 and FD40 were used as large molar mass tracer solutes for the purpose of this experiment. Calu-3 cells were cultured using AIC conditions in a way described previously, while Caco-2 cells were cultured on filters in the manner described in section 2.2.1.4.2 prior to their use. The experiment was conducted in an identical way for the cell layers of both cell lines: HBSS was used as the transport medium for both Calu-3 and Caco-2 cells and both cell lines were equilibrated in the transport medium for the same period of time (approximately 45 min) prior to the start of the experiment. Additionally, FDs were used at an equal concentration (500 μg/ml) and the permeability was assessed over the same time period (3 hours), with sampling at

the same time intervals (every 30 min). FDs were quantified by fluorescence using the method described previously (section 2.2.4).

### 3.2.4 Nanoparticle translocation across Calu-3 and Caco-2 layers

Calu-3 and Caco-2 cells were cultured on filters in the manner described previously (section 2.2.1). Calu-3 cells were cultured using both AIC and LCC conditions. Cell layers were equilibrated in HBSS for approximately 45 min. TEER was measured just before the addition of NPs; Calu-3 layers with a TEER ≥500 and Caco-2 monolayers with a TEER ≥1000 $\Omega cm^2$, were included in the experiment. Carboxy-modified, fluorescent (yellow-green) polystyrene NPs (Fluoresbrite®) of 50 nm nominal diameter, were diluted in HBSS (1 in 100) and applied to the apical side of the cell layers. Apical-to-basolateral translocation was measured by sampling the basolateral solution (i.e. removing 100 µl volumes) at 30 min intervals for 2 hours. The extent of NP translocation across the cell layers was determined by measuring the fluorescence (485 nm excitation, 535 nm emission) of the basolateral solutions and converting the obtained values into concentrations and percent amount relative to that applied apically through pre-constructed calibration curves (based on the same principle as for FD quantitation). NP transport across the cell layers is expressed as % of the applied amount.

## 3.3 Results

### 3.3.1 TEER profiles of filter-cultured Calu-3 cells: AIC and LCC conditions

Figure 3.1 compares changes in TEER over time observed for Calu-3 layers cultured using AIC and LLC conditions. No meaningful increase in TEER was observed until day 6 of culture for cell layers cultured using either AIC or LCC conditions. Thereafter, TEER increased sharply, but subsequently plateaued after day 10 in culture, for both AIC and LCC cells. Of notable difference are the maximal TEER values reached in different culture conditions; these equated to 817 $\Omega cm^2$ and 1525 $\Omega cm^2$ in AIC and LLC cells, respectively.

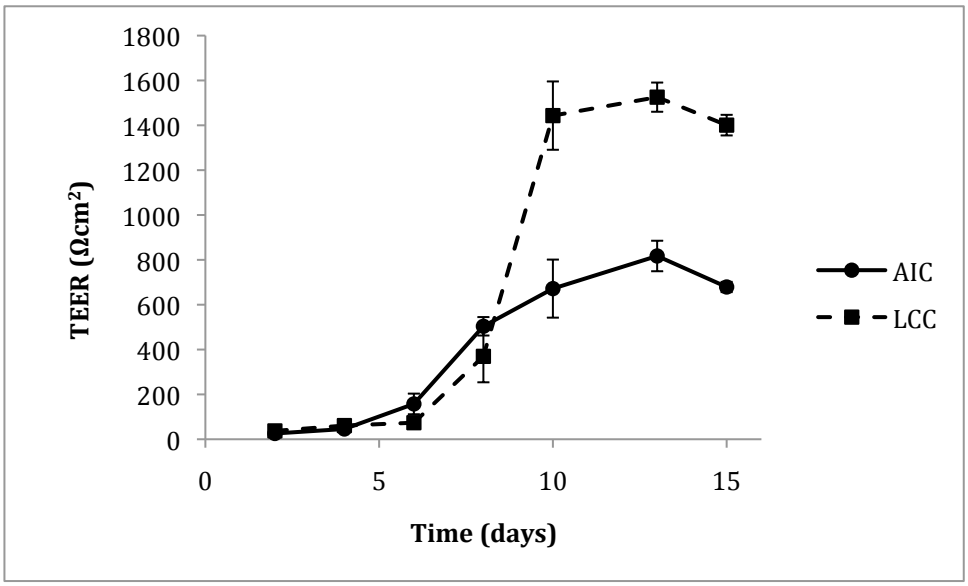


***Figure 3.1. TEER profiles of Calu-3 cells cultured on filters using AIC and LCC conditions. TEER is expressed as the measured resistance per area ($cm^2$) of the cell layer. Background TEER due to the filter was subtracted from the reported TEER values. Data presented as the mean ± SD (n=5).***

### 3.3.2 Morphological characterisation of filter-cultured Calu-3 cells

*3.3.2.1 SEM*

SEM revealed that Calu-3 cells form a tightly packed layer of cells when cultured on filters using AIC conditions (Figure 3.2). Furthermore the presence of microvilli can be observed from the figure. Apical projections on the surface of the cells and cilia were, however, not observed.

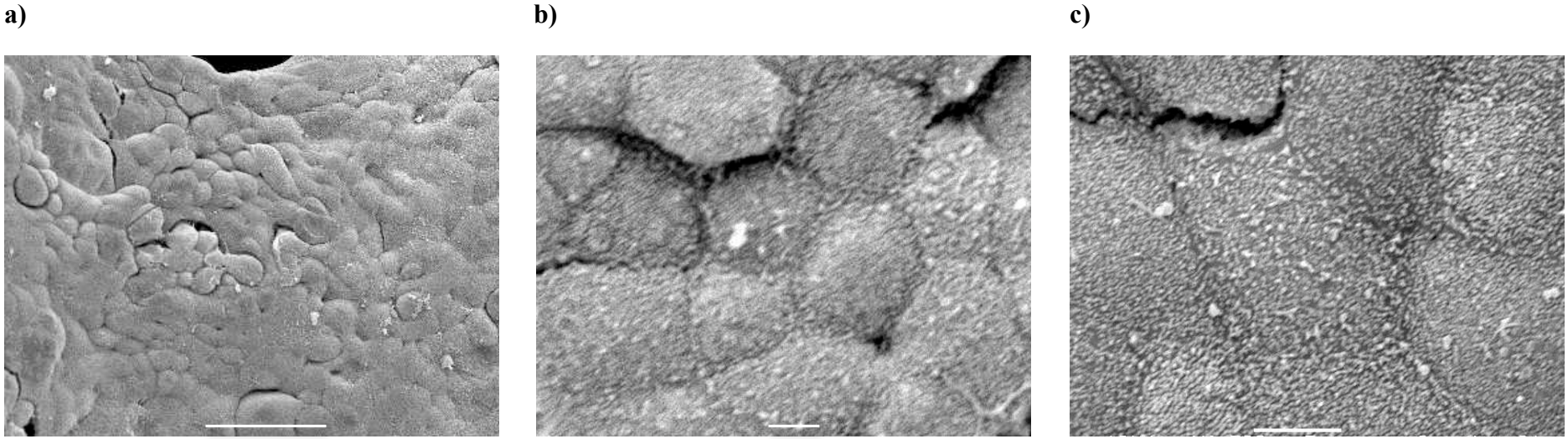


*Figure 3.2. Characterisation of the Calu-3 layer model by SEM. a) Imaging of a larger area showing closely packed cells, b) Magnified image, and c) A further magnified image showing the presence of microvilli on the surface of the cells. The observed cracks are artifacts resulting from sample processing for imaging. Cell-cell boundaries can be seen in all images. While lines represent scale bars of 50 µm (a) and 5 µm (b and c).*

*3.3.2.2 TEM*

TEM micrographs (Figure 3.3) indicated that filter-cultured Calu-3 cells express round granules of approximately 1 $\mu$m diameter, which were located apically (3.3a and 3.3c). These granules were electron-translucent, with some exhibiting an electron dense core (3.3c). Furthermore, cellular tight junctions ('TJ') and desmosomes ('DES') interconnecting adjacent cells can clearly be seen (3.3b). The presence of microvilli ('MV') on the apical membrane is also apparent (3.3 a and c), as are the cell boundaries ('CB') (3.3 a and b). The Transwell® filter ('filter') can also be seen on the micrographs.

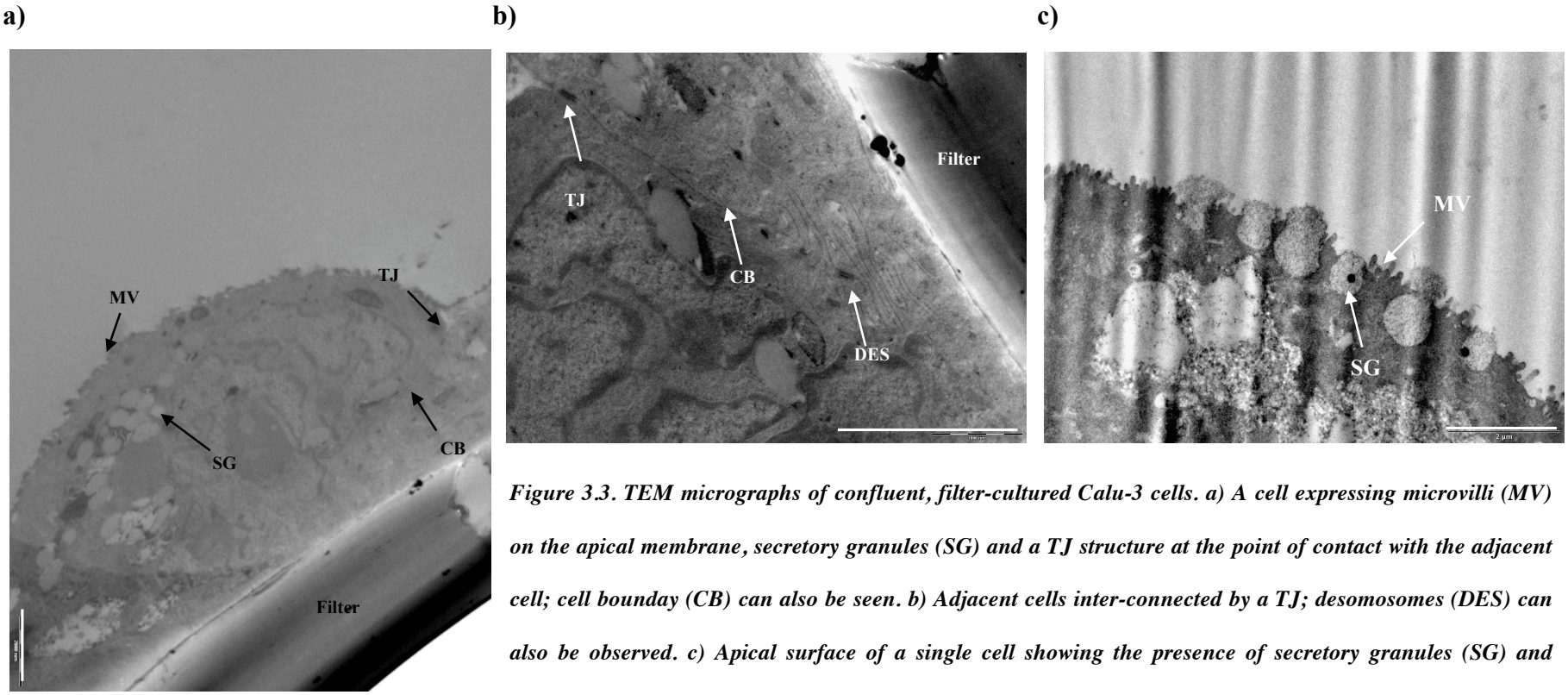


*Figure 3.3. TEM micrographs of confluent, filter-cultured Calu-3 cells. a) A cell expressing microvilli (MV) on the apical membrane, secretory granules (SG) and a TJ structure at the point of contact with the adjacent cell; cell bounday (CB) can also be seen. b) Adjacent cells inter-connected by a TJ; desomosomes (DES) can also be observed. c) Apical surface of a single cell showing the presence of secretory granules (SG) and microvilli (MV). White lines represent scale bars of 2 µm.*

*3.3.2.3 Whole cell labelling and staining for F-actin and MUC-1, mucus protein*

Figure 3.4 shows confocal micrographs of Calu-3 layers. More specifically, Figure 3.4a depicts cells labelled with CellTracker$^{TM}$ Green, a non-specific whole cell label. Closely packed cells covering the whole imaged area can be seen from the figure.

Confocal imaging of the cells, following their staining for cytoskeletal F-actin revealed the presence of perijunctional rings of F-actin, seen as continuous rings of fluorescence at cell-cell contacts (Figure 3.4b).

Figure 3.4c, on the other hand, shows a confocal micrograph of Calu-3 cells stained for MUC-1, mucus protein. Green fluorescence, apparent on the micrograph, shows distribution of the MUC-1 protein (more specifically it shows the distribution of FITC-IgG, targeted towards anti-MUC-1 antibody), while blue fluorescence is that resulting from cell nuclei label, DAPI. It is apparent from the image that green fluorescence is predominantly distributed on the apical side of the cells (labelled A).

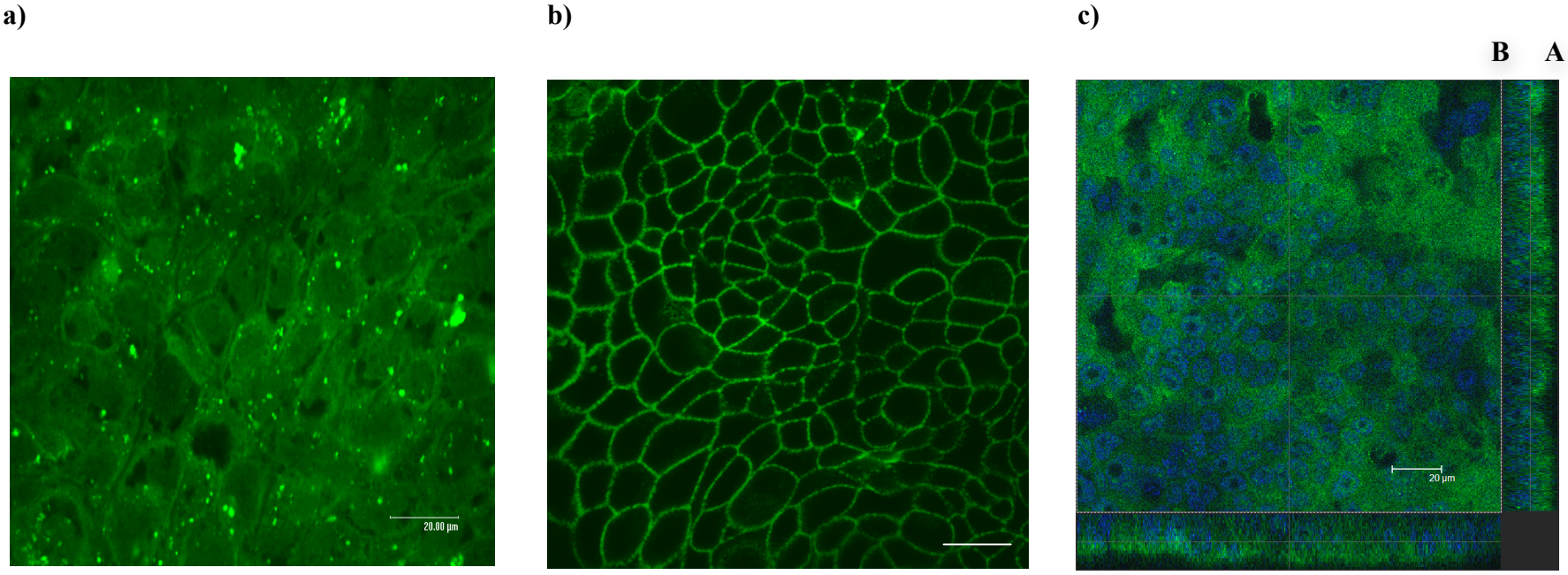


*Figure 3.4. Confocal micrographs of confluent, filter-cultured Calu-3 layers: a) Cells following staining with CellTracker™ Green, b) Cells following their staining with FITC-phalloidin, and c) Staining for the mucus protein, MUC-1, where green fluorescence is that resulting from goat, anti-mouse IgG FITC, which is a secondary antibody to mouse, anti-human MUC-1 and blue fluorescence is due to DAPI used to label the cell nuclei (A = apical side, B = basolateral side). White lines represent scale bars of 20 µm.*

*3.3.3.4 Zonula Occludens-1 (ZO-1) staining*

Immunostaining of confluent, filter-cultured Calu-3 cells with an antibody to ZO-1 protein, a structural and functional component of TJs, revealed the distribution of this protein as continuous 'rings' at cell-cell contacts. This is shown in Figure 3.5.

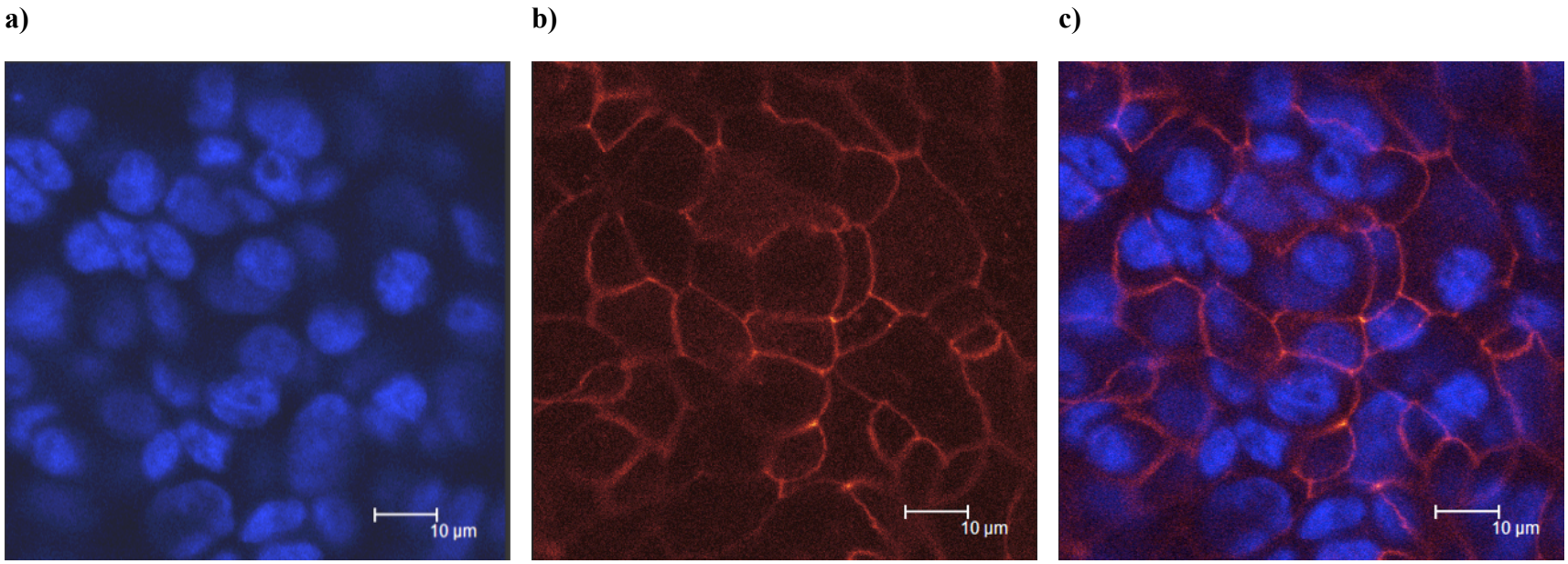


*Figure 3.5. Staining of a confluent, filter cultured Calu-3 layer for Zonula Occludens-1 (ZO-1) TJ protein. i) Blue channel showing DAPI-labelled cell nuclei, ii) Far red channel showing ZO-1 distribution (specifically the fluorescence pattern is that of Cy5-labelled goat, anti-mouse IgG, an antibody to mouse, anti-human ZO-1), and iii) Overlay image (Blue cell nuclei and Red ZO-1)*

### 3.3.3 Permeability studies

*3.3.3.1 FD4 permeability across AIC and LCC Calu-3 layers*

Permeability of FD4 across filter-grown Calu-3 cells cultured using AIC and LCC conditions is shown in Figure 3.6. Confluent cell layers grown at AIC presented a greater barrier to FD4 translocation compared to cells cultured using LCC. The obtained fluorescence readings resulting from gradual accumulation of FD4 in the periodically sampled basolateral solution were converted into apparent permeability coefficients ($P_{app}$). These values were calculated to be approximately $1.7x10^{-7}$ cm/s and approximately $5.7x10^{-7}$ cm/s for AIC and LCC layers, respectively, revealing an approximately 3-fold higher rate of FD4 permeability across the cell layers cultured using LCC compared to those cultured using AIC.

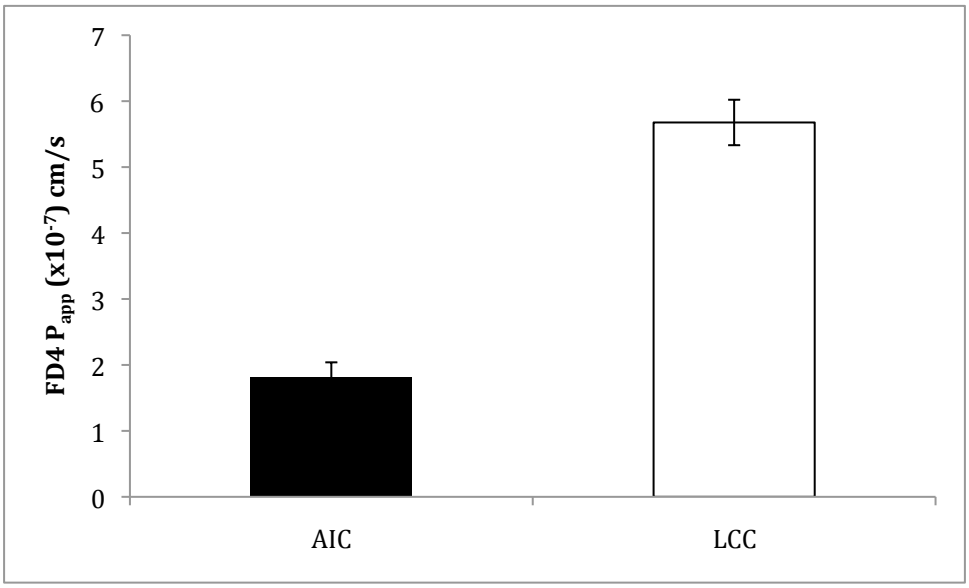


***Figure 3.6. Effect of culture conditions on FD4 permeability across Calu-3 layers. Black bar (labelled AIC) represents permeability across cells cultured under AIC conditions and empty bar (labelled LCC) represents permeability across cells cultured using LCC conditions. FD4 permeability expressed as $P_{app}$, calculated using the equation in section 2.2.4. Results presented as the mean ± SD (n=3).***

*3.3.3.2 Effect of N-acetyl cysteine on FD4 permeability*

FD4 permeability across Calu-3 layers that were previously incubated with NAC is shown in Figure 3.7. This is compared with FD4 permeability in cell layers not subjected to NAC treatment (control). FD4 traversed the cell layers pre-incubated with NAC more readily compared to cells not subjected to NAC treatment. The apparent permeability coefficient ($P_{app}$) values obtained were $6.1x10^{-8}$ cm/s and $1.7x10^{-8}$ cm/s and, respectively, revealing a 3.6-fold higher permeability in cells exposed to NAC.

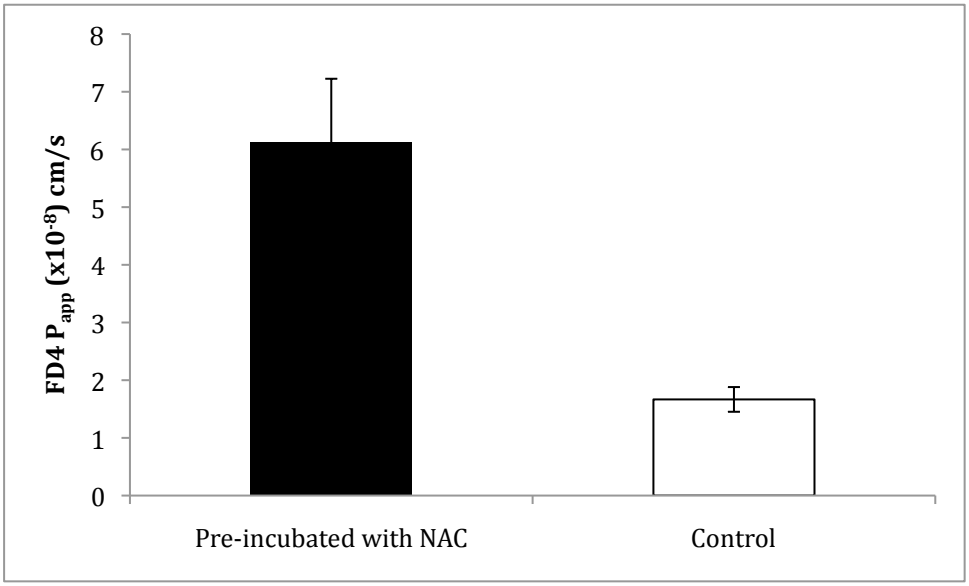


***Figure 3.7. Effect of NAC on FD4 permeability across Calu-3 layers. Black bar represents cells treated with NAC, whereas empty bar (control) represents untreated cells. Calu-3 cells were cultured using AIC conditions. FD4 permeability is expressed as $P_{app}$, calculated according to the equation in section 2.2.4. Data presented as the mean ± SD (n=4).***

Treatment of cells with NAC, however, resulted in a decrease in TEER (shown in Figure 3.8). A drop in TEER by approximately 44% compared to the baseline value and by approximately 29% compared to the control (i.e. decrease in TEER resulting from the application of HBSS) was observed at the end of incubation with NAC.

However, measurements at the end of the permeability experiment revealed a recovery in TEER within the permeability study period (3 hours), with the TEER values of the cell layers pre-incubated with NAC reaching 103% of the baseline value, while the TEER of control cell layers reverted to approximately 99% of the baseline value.

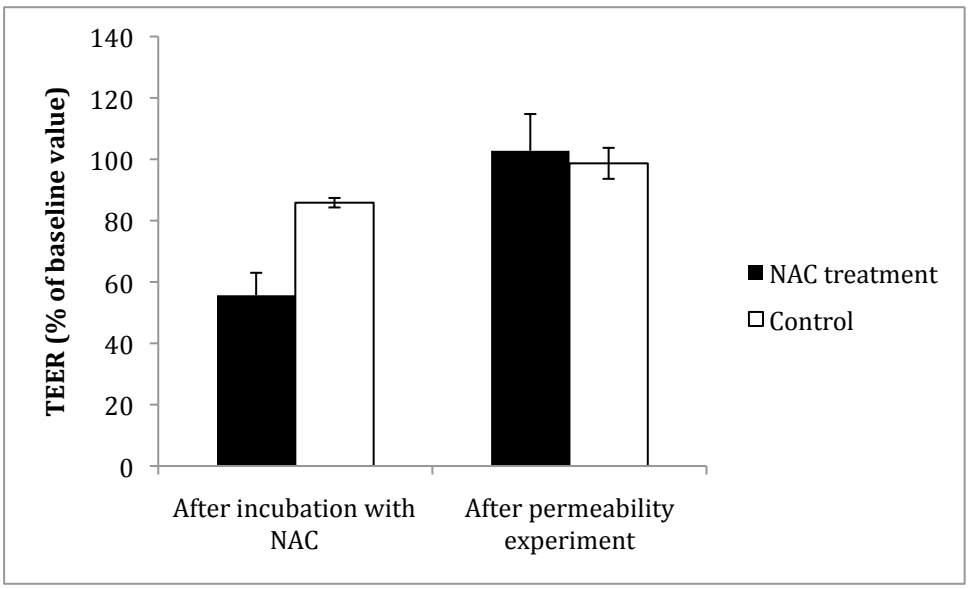


***Figure 3.8. Effect of NAC on TEER of Calu-3 layers. TEER was measured after incubation of the cells with NAC and again at the end of the permeability experiment. TEER was also monitored in control cells (incubated with HBSS). Changes in TEER are reported as % change compared to the TEER measured before the application of NAC (baseline value). Results are presented as the mean ± SD (n=4).***

*3.3.3.3 Permeability of varying $M_W$ FDs across Calu-3 layers*

Permeability of FDs with a different molar mass across the Calu-3 layers is shown in Figure 3.9. It is apparent from the figure that the permeability of FDs decreased with an increasing $M_W$, with FD20 ($M_W$ 20 kDa) permeating the cell layers most readily ($P_{app}$ approximately $6.5x10^{-9}$ cm/s), and the largest dextran, FD150 ($M_W$ 150 kDa), exhibiting the lowest permeability ($P_{app}$ $1.4x10^{-9}$ cm/s).

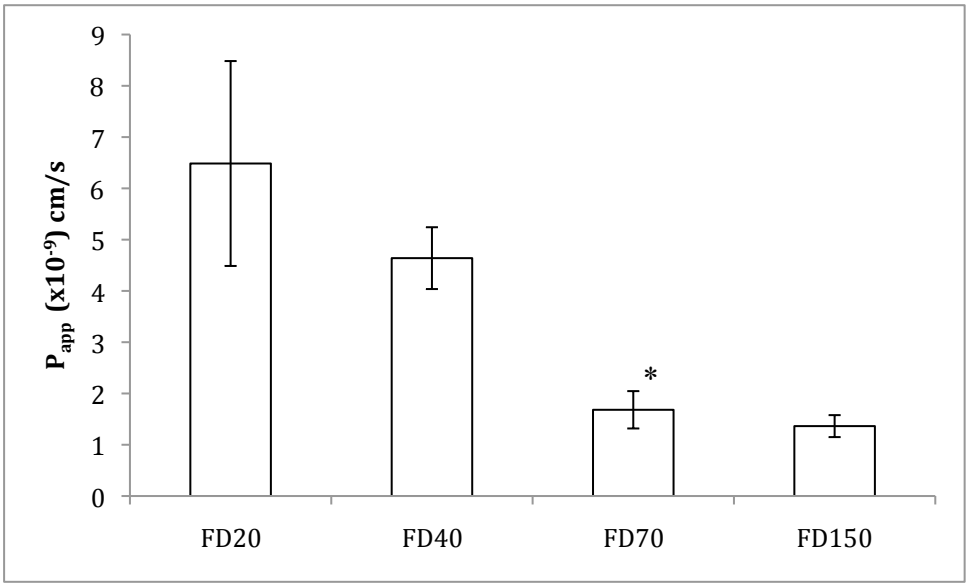


***Figure 3.9. Permeability of varying $M_W$ FDs (FD20, FD40, FD70 and FD150) across Calu-3 layers. Permeability expressed as apparent permeability coefficient ($P_{app}$), calculated according to the equation in section 2.2.4. Data presented as the mean ± SD (n = 3). * denotes statistically different (p=0.011) from the preceding bars.***

*3.3.3.4 Insulin translocation across Calu-3 layers*

The calculated $P_{app}$ for translocation of FITC-insulin across the Calu-3 layers was found to equate $1.01x10^{-8}$ cm/s ± $2.89x10^{-9}$ (n=3).

*3.3.3.5 Comparison of FD permeability across Calu-3 and Caco-2 layers*

Figure 3.10 compares the rate of permeability of two FDs (FD20 and FD40) across confluent Calu-3 and Caco-2 layers. Again there was a $M_W$ effect on permeability,

with FD20 observed to permeate the cell layers more readily than FD40 in both cell lines. There was a marked difference in the extent of permeability for both solutes between Calu-3 and Caco-2 layers, with a 15-fold and 13-fold higher permeability observed across Caco-2 monolayers compared to Calu-3 for FD20 and FD40, respectively.

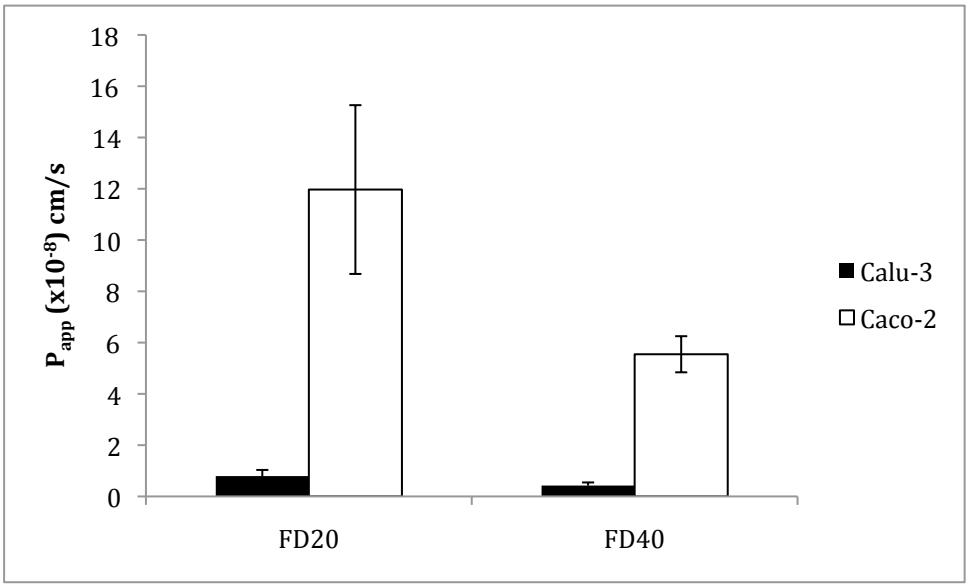


***Figure 3.10. Permeability of FD20 and FD40 across Calu-3 and Caco-2 layers. Permeability is expressed as apparent permeability coefficient ($P_{app}$), calculated according to the equation in section 2.2.4. Data presented as the mean ± SD (n = 3).***

*3.3.3.6 Nanoparticle transport across Calu-3 and Caco-2 layers*

Transport of polystyrene NPs (nominal diameter of 50 nm) across Calu-3 cells cultured on filters using AIC or LCC-conditions and Caco-2 cells is depicted in Figure 3.11. Data shows a low level of NP transport across the cell layers of both cell lines. Two important observations can be made from the figure: 1) Calu-3 layers cultured using AIC presented a greater barrier to NP translocation compared to those grown using LCC, and 2) Calu-3 layers cultured using either AIC or LCC conditions, presented a greater barrier to NP movement than Caco-2 monolayers.

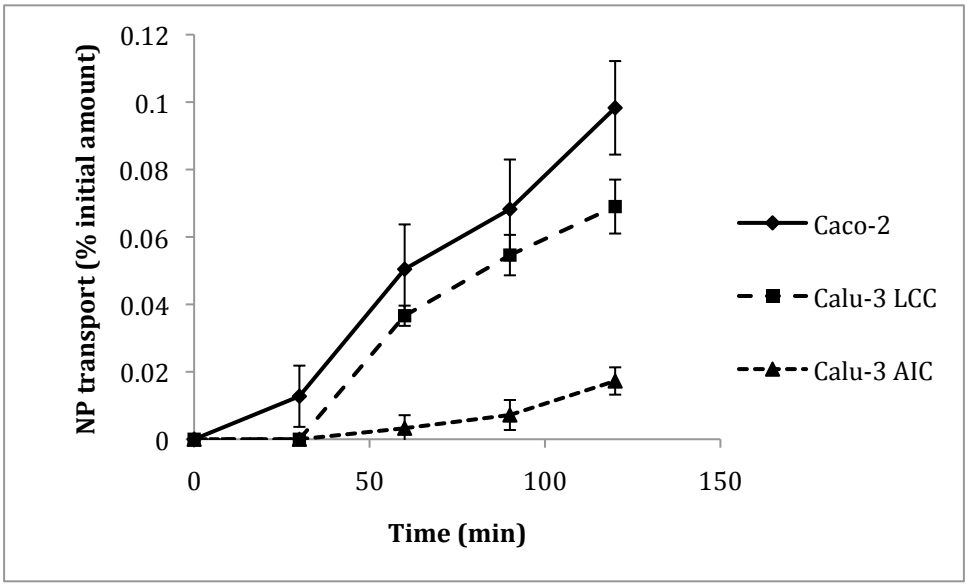


***Figure 3.11. Apical-to-basolateral transport of polystyrene NPs (carboxy-modified; 50 nm nominal diameter) across Calu-3 (grown using AIC and LCC conditions) and Caco-2 layers. NP transport expressed as % relative to the NP amount applied apically. Data presented as the mean ± SD (n=3).***

## 3.4 Discussion

The Calu-3 cell line is generally considered as one of the few respiratory cell lines to express features of the airway epithelium, including expression of TJs and mucus production, when appropriately cultured *in vitro*. Although this cell line has been relatively well characterised, large inconsistencies exist in the literature regarding its barrier and morphological properties, as discussed in section 3.1. Initial work therefore focused on determining the morphological and barrier characteristics of the cell culture model used in this project, whereby the suitability of the model system was investigated.

When Calu-3 cells were cultured on permeable supports using either AIC or LCC conditions, cell layer TEER was found to increase with time in culture. The observed

increase in TEER, which was eventually seen to plateau, suggests formation of polarised, confluent and restrictive cell layers. Since functional structures providing this restrictiveness in epithelial cells are the intercellular TJs (the expression of which was shown, as will be discussed below), high TEER values are therefore suggestive of cells that express and are interconnected by functional TJs. Continuous monitoring of the TEER while culturing cells on filters provided information regarding the time course needed for Calu-3 cells to form confluent cell layers. This time, which was found to be at least 9 days, proved to be consistent throughout the project. Establishing this information at an early stage of the project was therefore important with regards to planning experiments. (In practice, in subsequent experiments, cells were cultured on filters for 9-14 days without regular TEER measurements; to minimise culture handling and possible damage to the cells by the measurement process, TEER was only recorded prior to the experiments in order to confirm confluence and therefore the suitability of the cell layers for inclusion in experiments.)

It is interesting to note that the maximal TEER values obtained for Calu-3 cells cultured using AIC (approximately 800 $\Omega cm^2$) and LCC (approximately 1500 $\Omega cm^2$) differ significantly, with these values being nearly two-fold higher for cells cultured using LCC compared to AIC. The reasons behind this difference are not clear, but other groups have reported similar results (9). TEER values obtained in this work are higher than those found in some studies (7, 14, 16, 20, 32), but fall within the range of values (between 700 and 2500 $\Omega cm^2$) reported by Loman *et al*. (32). TEER variability in the literature was observed by Foster *et al*. (31), depending on the technique employed for measurements. Furthermore, other effects such as cell passage number,

filter type and filter coating are likely to affect the TEER, creating difficulties in comparing reported TEER values across labs.

The gradual decrease in TEER following attainment of a peak value is consistent with previous studies (14). This observation has been explained to possibly result from an increase in number of cells packed within the layer, increasing the total length of cell perimeter per area of the layer (TEER developed by an epithelial cell layer is determined to a large extent by the nature of its cell boundaries), as growth arrested cells have been shown not to exhibit such a reduction in TEER as cells age (33).

Cell imaging by different techniques revealed valuable morphological information. SEM and confocal microscopy showed that, when cultured on filters (under AIC conditions), Calu-3 cells predominantly grow as single layers (multilayer formation was evident in limited areas) whereby cells are closely packed. SEM further revealed the presence of microvilli on the apical surface of the cells, while ciliated structures were not observed. Electron-translucent granules, with some exhibiting an electron dense core (Figure 3.9c) were clearly seen by TEM. These granules, which resemble mucin granules of airway mucous goblet cells in organization and size (34), were also reported by other groups (7, 9, 35). Imaging of the cell layer by confocal microscopy following immunostaining for the ZO-1 protein, which is a structural component associated with functional epithelial TJs, clearly showed its expression and presence as continuous 'belts' at cell-cell contacts. In combination with the measured TEER, this confirms that the restrictiveness of the cell layers is mediated by the presence of the functional intercellular TJs. Immunostaining for MUC-1, a mucin protein, on the other hand revealed heavy presence of this mucus protein, which is in agreement with

a study by Kreda *et al.* (35). Additionally, its predominant distribution on the apical side of the cells confirmed cell polarity.

Although TEER is an easily measurable parameter that is an indicator of cell layer intactness and presence of functional TJs, it may not always correlate with the paracellular permeability of large hydrophilic molecules (36), which is another parameter used to characterise the formation of the cell layer barrier. Therefore, in addition to monitoring the ion permeability of TJs (i.e. TEER), the paracellular permeability of hydrophilic tracers was also established in this work to complement the TEER and provide more complete information on TJ functionality. One such hydrophilic tracer is dextran, which is commercially available in different $M_W$s and fluorescent forms allowing an easy quantitation through measurement of fluorescence.

The low permeability rate of a modestly sized macromolecule, FD4, across the Calu-3 layers confirms the barrier properties of the cell layer. The calculated apparent permeability coefficients ($P_{app}$) of $1.7x10^{-7}$ cm/s for AIC and $5.7x10^{-7}$ cm/s for LCC cells, are somewhat larger than those reported in the literature. $P_{app}$ values of $6x10^{-9}$ (AIC), $1.3x10^{-8}$ (AIC), $5.1x10^{-8}$ (culture conditions not specified) and $9.9x10^{-8}$ cm/s (culture conditions not specified) have been reported by Florea *et al.* (30), Li *et al.* (37), Chono *et al.* (38) and Seki *et al.* (39), respectively. Similarly to data variability with regards to TEER, large discrepancies in reported permeability values exist due to inter-laboratory differences in culture conditions, including the type of the filter and its coating to promote cell adherence, cell passage number, media, experimental procedures used to determine the permeability, etc. Therefore, caution must be exercised in comparing these values. Furthermore, it must be noted that, as it will be

apparent from the future chapters of this thesis, calculated $P_{app}$ values for FD4 in other experiments in this thesis are variable and range from approximately $1.7x10^{-7}$ to about $1x10^{-8}$ cm/s (in cells cultured using AIC conditions). This variability in data is likely to be a result of different factors, with cell culture age (i.e. time in culture) at the time when permeability experiments were conducted likely to play an important role.

Of particular interest is the finding that FD4 permeability was about 4-fold lower in Calu-3 cell layers cultured using AIC compared to cells cultured at LCC. This is rather surprising, considering that significantly higher TEER values were observed in LCC cells, suggesting a more restrictive barrier. There are conflicting reports in the literature regarding the permeability characteristics of Calu-3 cell layers cultured using AIC and LCC. While notable differences in permeability to sodium fluorescein between Calu-3 cell layers grown using AIC and LCC have been found (16), with Grainger *et al.* (9) reporting higher permeabilities of sodium fluorescein and FDs of varying $M_W$s in AIC cells compared to LCC, others found similar permeabilities (19, 20), attributing the finding to the existence of a threshold TEER barrier above which the rates of transport are similar. For example, Foster *et al*. (31) reported an inverse relationship between TEER and Lucifer yellow flux up to TEER of approximately 300 $\Omega cm^2$, but once the cell layers achieved a higher TEER, there was very little change in Lucifer yellow flux.

Lower FD4 permeability in AIC cells may possibly result from a greater presence of mucus in cell layers cultured using these conditions. Numerous groups have found that AIC growth conditions are favourable for mucus production. Grainger *et al*. (9) observed heavier glycoprotein staining in Calu-3 layers grown using AIC compared to

those cultured using LCC, arguing that, any secreted mucus under LCC conditions, is likely to disperse into the culture medium and is removed by medium exchange. Furthermore, Fiegel *et al*. (19) examined the impact of direct deposition of aerosolized poly(lactic-co-glycolic)acid (PLGA) microparticles on Calu-3 cell layers grown under AIC or LCC conditions. Determined $P_{app}$ for disodium fluorescein (FNa, 376 Da) across the layers following the particle deposition suggested that cells grown under AIC conditions remained unaltered following microparticle deposition, while a significant increase in $P_{app}$ was observed in the cells cultured under LCC condition. The authors attributed this finding to existence of a dense mucus coating developed during the AIC which may have protected the cell surface from the deposition insult.

To test whether the presence of mucus presents a barrier to the translocation of macromolecules across the cell layers, in this work FD4 permeability was measured following the incubation of cell layers grown at AIC with N-acetyl cysteine (NAC). NAC is a mucolytic agent that reduces mucus viscosity by splitting disulfide bonds linking proteins present in the mucus (mucoproteins) (40). A relatively low concentration of NAC (0.3% w/v) was used for this purpose to ensure that its addition caused minimal damage or disruption of the cell layer integrity, which would affect FD4 permeability; this was determined by measuring changes in TEER following the addition of NAC. A considerably higher rate (4-fold) of FD4 permeability was observed in cell layers pre-incubated with NAC. It is possible that reduction of mucus viscosity by the action of NAC, and its resulting removal from the cell layers (with replacement of NAC solution prior to the permeability experiment) may have played a role in the observed higher rate of FD4 permeability in NAC-incubated cells compared to control. It could be argued that higher penetrant permeability associated

with the application of NAC may have resulted from TJ opening and/or compromised cell layer integrity as application of NAC resulted in a decrease in cell layer TEER. Nevertheless, the decrease in TEER was relatively modest and recovered within the time frame of the permeability experiment.

Measurement of the permeabilities of varying $M_W$ FITC-dextrans (20 kDa-150 kDa) revealed an inverse relationship between the $M_W$ of the solute and its extent of permeability ($P_{app}$ value). Similar results are reported in the literature. For example, the permeability $P_{app}$ of differently sized FDs across the Calu-3 cell layers was shown to decrease from $2x10^{-9}$ cm/s to $1x10^{-9}$ cm/s and to $0.2x10^{-9}$ cm/s as the $M_W$ of the solutes increased from 10 kDa to 20 kDa and to 70 kDa, respectively (30). With respect to our data, it is interesting to note that with the largest two FDs, namely FD70 and FD150, the decrease in permeability with $M_W$ is not as marked as that observed between FD20 and FD40, and the difference between FD40 and FD70. This finding is in agreement with a previously reported study investigating dextran transport across rat alveolar epithelial cell monolayers (41). The authors of this study describe that FD $P_{app}$ decreased gradually from $1.35x10^{-8}$ cm/s for FD4 to $0.32\ x10^{-8}$ cm/s for FD40. In contrast, the calculated $P_{app}$ values for FD70 and FD150 were almost identical at $0.13x10^{-8}$ cm/s. Furthermore, when FD transport was tested at 4°C, $P_{app}$ decreased in a size-dependent manner, with observed decreases of approximately 40% for FD4 to FD40 and >80% for FD70 and FD150, compared to transport at 37°C (41). Observation of these phenomena was explained by the authors through the possibility that smaller macromolecules (radius <5 nm) translocated across the cell monolayers through the paracellular pathway, whereas larger macromolecules were likely to traverse the cells *via* other pathways such as pinocytosis.

Permeability of FITC-insulin, as an example of a therapeutic macromolecular protein, was tested in order to assess whether the Calu-3 layers present a similar barrier to its movement compared to FDs, which were used as model drugs throughout this thesis. The calculated $P_{app}$ value for FITC-insulin movement across the Calu-3 layers (cultured using AIC) amounted to $1.01 \times 10^{-8}$ cm/s ± $2.89 \times 10^{-9}$. This is lower than the $P_{app}$ for FD4 observed in the experiment in this chapter ($1.7 \times 10^{-7}$ cm/s), but falls within the range of FD4 $P_{app}$ values obtained throughout the project (approximately $2.5 \times 10^{-7}$ to $1 \times 10^{-8}$ cm/s). However, it must be noted that a direct comparison in permeability between insulin and FD4 and is not possible considering the different molecular structure of the two compounds. More specifically, insulin is a globular molecule existing in aqueous environment as dimers, tetramers, and hexamers in equilibrium (42), with the hexameric conformation having a hydrodynamic radius of 2.8 nm (43), while FD4 has a linear geometry with a hydrodynamic radius estimated to be 1.8 nm (44). Furthermore, FITC-insulin and FD4 permeability experiments were conducted on cells of different passage number. Observed FITC-insulin $P_{app}$ value is higher than $P_{app}$ of $0.41 \times 10^{-8} \pm 0.02 \times 10^{-8}$ cm/s reported by Pezron *et al*. (18) when determining insulin permeability across the Calu-3 cell layers and $P_{app}$ of $1.28 \times 10^{-9}$ cm/s, reported by Seki and co-workers (39).

In comparing the barrier properties of the Calu-3 layers with those of the intestinal Caco-2 cell line, which is a well-established cell line and widely-used in drug transport studies, FD was found to traverse the Caco-2 monolayers considerably more readily than the Calu-3 layers. This was the case for two tested FDs, FD20 and FD40, with calculated $P_{app}$ values approximately 12-fold higher in Caco-2 cell monolayers

compared to Calu-3 cells, for both dextrans. This finding is particularly interesting considering the substantially higher measured TEER in Caco-2 monolayers (approximately 2000 $\Omega cm^2$). Although the Caco-2 cell line has been reported to form looser TJs than Calu-3 cells (45), it is unclear why, in this work, this was not reflected in the TEER profile of the two cell lines. It has been shown that paracellular permeation of hydrophilic molecules is directly related to the number of tight junctional strands between epithelial cells and their density (46). Epithelial cells with a high number of tight junctional strands, such as gall bladder epithelia, have a low paracellular permeability (47), whereas those having a low number of tight junctional strands, such as the intestinal epithelia, have a high permeability (48). It is possible that the Calu-3 cell layers present a greater barrier to the movement of FDs due to morphological differences, including the number of tight junctional strands, between the two cell lines. Furthermore, other differences in cellular morphology, structural organisation and physiological functions (including the production of mucus by Calu-3 cells) may account for the observed differences in permeability.

Transport of NPs (polystyrene, 50 nm diameter) across the cell layers was investigated in order to test the extent of the barrier presented by Calu-3 and Caco-2 epithelial cells to the movement of small NPs. Mucosal transport of nanoparticulate materials, as potential drug carriers, has been researched previously (49-54) and in fact it is also the focus of this thesis (Chapters 6 and 7). Comparison of NP transport across Calu-3 cells cultured at AIC and LCC conditions and Caco-2 monolayers revealed a very low rate of NP translocation in all cases, highlighting the fact that cell layers severely restrict NP movement. However, it is interesting to note that the proportion of applied NPs traversing the cell layers was found to be moderately

higher across Caco-2 cell monolayers compared to Calu-3 cells cultured under LCC conditions and significantly higher compared to the NP translocation seen in AIC Calu-3 cells. It should be stressed that a similar trend was described above for FD4 permeability across the Calu-3 layers, with a notably lower permeability across AIC cells. Although transport of NPs is likely to occur through a different route to FD4, with NPs likely to traverse the cell layers through the transcellular route (across the cell) and FD4 predominantly *via* the paracellular pathway, the possible presence of a denser layer of mucus in AIC cells may impede transport of both FD4 and NPs.

As mentioned earlier, previous reports found that AIC Calu-3 layers exhibit a more physiological TEER and ultrastructure (9). Notably, a detailed study by Grainger *et al.* (9) comparing the effect of AIC and LCC conditions on the properties of the Calu-3 cell layers, found that AIC conditions produced cells with characteristics more similar to the tracheobronchial epithelium compared to cells grown using LCC. The authors consequently concluded that AIC conditions produced Calu-3 cell layers that are more suitable as a model of the tracheobronchial epithelium than LCC. Although AIC and LCC conditions were not directly compared in terms of the resulting cellular morphology, present work confirmed previous reports of a more physiologically relevant TEER observed in AIC compared to LCC grown cells. Combined with the finding that AIC cells presented a greater barrier to the movement of macromolecules and desirable morphological features, AIC conditions were therefore considered more appropriate for producing cell layers modeling the airway epithelium, which is in agreement with the aforementioned study. AIC conditions were therefore normally employed in culturing Calu-3 cells on filters in the subsequent experiments in this thesis.

## 3.5 Conclusion

Work presented in this chapter focused on characterising filter-cultured Calu-3 layers, which were adopted in this thesis to serve as a mucosal model. This was deemed necessary as, although the Calu-3 epithelial cell line has been (and continues to be) used extensively as a mucosal model, there is a large body of evidence suggesting that culture conditions (which vary between labs) influence their morphological characteristics and the barrier property of the model. Our work showed that filter-cultured Calu-3 cells exhibited TEER, which increased with time in culture and that cells cultured using AIC conditions exhibited a lower TEER, than those grown under LCC. Microscopic examination showed that cells cultured under AIC conditions formed polarized layers of tightly packed cells that express features found in the native airway epithelium, including cell microvilli, secretory granules, TJs and mucus protein. AIC conditions produced cell layers that presented a greater barrier to the translocation of macromolecules and NPs compared to LCC conditions. Calu-3 layers in general (cultured under AIC or LCC conditions) presented a greater barrier to the movement of dextrans and NPs compared to intestinal Caco-2 cells. Owing to observations of a more physiological TEER and a greater barrier to macromolecular transport and observation of relevant cell ultrastructure, Calu-3 cells grown using AIC conditions were regarded as a suitable mucosal model for the purpose of the investigations performed in this thesis.

## 3.5 References


1. P.L. Tumaand A.L. Hubbard. Transcytosis: crossing cellular barriers. Physiol Rev. 83:871-932 (2003).
2. S. Tavelin, J. Grasjo, J. Taipalensuu, G. Ocklind, and P. Artursson. Applications of epithelial cell culture in studies of drug transport. Methods Mol Biol. 188:233-272 (2002).
3. P. Arturssonand J. Karlsson. Correlation between oral drug absorption in humans and apparent drug permeability coefficients in human intestinal epithelial (Caco-2) cells. Biochem Biophys Res Commun. 175:880-885 (1991).
4. S. Tavelin, V. Milovic, G. Ocklind, S. Olsson, and P. Artursson. A conditionally immortalized epithelial cell line for studies of intestinal drug transport. J Pharmacol Exp Ther. 290:1212-1221 (1999).
5. J.D. Irvine, L. Takahashi, K. Lockhart, J. Cheong, J.W. Tolan, H.E. Selick, and J.R. Grove. MDCK (Madin-Darby canine kidney) cells: A tool for membrane permeability screening. J Pharm Sci. 88:28-33 (1999).
6. U. Bock, T. Kottke, C. Gindorf, and E. Haltner. Validation of the Caco-2 cell monolayer system for determining the permeability of drug substances according to the Biopharmaceutics Classification System (BCS) http://www.acrossbarriers.de/uploads/media/FCT02-I-0305_BCS.pdf (accessed 25/11/2009 2009).
7. B.Q. Shen, W.E. Finkbeiner, J.J. Wine, R.J. Mrsny, and J.H. Widdicombe. Calu-3: a human airway epithelial cell line that shows cAMP-dependent Cl- secretion. Am J Physiol. 266:L493-501 (1994).
8. M.C. Lee, C.M. Penland, J.H. Widdicombe, and J.J. Wine. Evidence that Calu-3 human airway cells secrete bicarbonate. Am J Physiol. 274:L450-453 (1998).
9. C.I. Grainger, L.L. Greenwell, D.J. Lockley, G.P. Martin, and B. Forbes. Culture of Calu-3 cells at the air interface provides a representative model of the airway epithelial barrier. Pharm Res. 23:1482-1490 (2006).
10. C.B. Basbaum, J.M. Madison, C.P. Sommerhoff, J.K. Brown, and W.E. Finkbeiner. Receptors on airway gland cells. Am Rev Respir Dis. 141:S141-144 (1990).
11. W.E. Finkbeiner, S.D. Carrier, and C.E. Teresi. Reverse transcription-polymerase chain reaction (RT-PCR) phenotypic analysis of cell cultures of human tracheal epithelium, tracheobronchial glands, and lung carcinomas. Am J Respir Cell Mol Biol. 9:547-556 (1993).
12. C.T. Tseng, J. Tseng, L. Perrone, M. Worthy, V. Popov, and C.J. Peters. Apical entry and release of severe acute respiratory syndrome-associated coronavirus in polarized Calu-3 lung epithelial cells. J Virol. 79:9470-9479 (2005).
13. H.L. Winton, H. Wan, M.B. Cannell, D.C. Gruenert, P.J. Thompson, D.R. Garrod, G.A. Stewart, and C. Robinson. Cell lines of pulmonary and non-pulmonary origin as tools to study the effects of house dust mite proteinases on the regulation of epithelial permeability. Clin Exp Allergy. 28:1273-1285 (1998).
14. H. Wan, H.L. Winton, C. Soeller, G.A. Stewart, P.J. Thompson, D.C. Gruenert, M.B. Cannell, D.R. Garrod, and C. Robinson. Tight junction

properties of the immortalized human bronchial epithelial cell lines Calu-3 and 16HBE14o. Eur Respir J. 15:1058-1068 (2000).

15. M.E. Cavet, M. West, and N.L. Simmons. Transepithelial transport of the fluoroquinolone ciprofloxacin by human airway epithelial Calu-3 cells. Antimicrob Agents Chemother. 41:2693-2698 (1997).
16. D. Cooney, M. Kazantseva, and A.J. Hickey. Development of a size-dependent aerosol deposition model utilising human airway epithelial cells for evaluating aerosol drug delivery. Altern Lab Anim. 32:581-590 (2004).
17. J. Patel, D. Pal, V. Vangal, M. Gandhi, and A.L. Mitra. Transport of HIV-protease inhibitors across 1 alpha,25di-hydroxy vitamin D3-treated Calu-3 cell monolayers: modulation of P-glycoprotein activity. Pharm Res. 19:1696-1703 (2002).
18. I. Pezron, R. Mitra, D. Pal, and A.K. Mitra. Insulin aggregation and asymmetric transport across human bronchial epithelial cell monolayers (Calu-3). J Pharm Sci. 91:1135-1146 (2002).
19. J. Fiegel, C. Ehrhardt, U.F. Schaefer, C.M. Lehr, and J. Hanes. Large porous particle impingement on lung epithelial cell monolayers--toward improved particle characterization in the lung. Pharm Res. 20:788-796 (2003).
20. C. Ehrhardt, J. Fiegel, S. Fuchs, R. Abu-Dahab, U.F. Schaefer, J. Hanes, and C.M. Lehr. Drug absorption by the respiratory mucosa: cell culture models and particulate drug carriers. J Aerosol Med. 15:131-139 (2002).
21. N.R. Mathia, J. Timoszyk, P.I. Stetsko, J.R. Megill, R.L. Smith, and D.A. Wall. Permeability characteristics of calu-3 human bronchial epithelial cells: in vitro-in vivo correlation to predict lung absorption in rats. J Drug Target. 10:31-40 (2002).
22. T. Yang, F. Mustafa, S. Bai, and F. Ahsan. Pulmonary delivery of low molecular weight heparins. Pharm Res. 21:2009-2016 (2004).
23. R. Trehin, U. Krauss, A.G. Beck-Sickinger, H.P. Merkle, and H.M. Nielsen. Cellular uptake but low permeation of human calcitonin-derived cell penetrating peptides and Tat(47-57) through well-differentiated epithelial models. Pharm Res. 21:1248-1256 (2004).
24. M. Sakagami. In vivo, in vitro and ex vivo models to assess pulmonary absorption and disposition of inhaled therapeutics for systemic delivery. Adv Drug Deliv Rev. 58:1030-1060 (2006).
25. L.A. Sachs, W.E. Finkbeiner, and J.H. Widdicombe. Effects of media on differentiation of cultured human tracheal epithelium. In Vitro Cell Dev Biol Anim. 39:56-62 (2003).
26. J.H. Widdicombe, L.A. Sachs, and W.E. Finkbeiner. Effects of growth surface on differentiation of cultures of human tracheal epithelium. In Vitro Cell Dev Biol Anim. 39:51-55 (2003).
27. P.K. Jeffery. Morphologic features of airway surface epithelial cells and glands. Am Rev Respir Dis. 128:S14-20 (1983).
28. P.K. Jeffery, D. Gaillard, and S. Moret. Human airway secretory cells during development and in mature airway epithelium. Eur Respir J. 5:93-104 (1992).
29. A.V. Rogers, A. Dewar, B. Corrin, and P.K. Jeffery. Identification of serous-like cells in the surface epithelium of human bronchioles. Eur Respir J. 6:498-504 (1993).
30. B.I. Florea, M.L. Cassara, H.E. Junginger, and G. Borchard. Drug transport and metabolism characteristics of the human airway epithelial cell line Calu-3. J Control Release. 87:131-138 (2003).

31. K.A. Foster, M.L. Avery, M. Yazdanian, and K.L. Audus. Characterization of the Calu-3 cell line as a tool to screen pulmonary drug delivery. Int J Pharm. 208:1-11 (2000).
32. S. Loman, J. Radl, H.M. Jansen, T.A. Out, and R. Lutter. Vectorial transcytosis of dimeric IgA by the Calu-3 human lung epithelial cell line: upregulation by IFN-gamma. Am J Physiol. 272:L951-958 (1997).
33. C.A. Rabito. Reassembly of the occluding junctions in a renal cell line with characteristics of proximal tubular cells. Am J Physiol. 251:F978-987 (1986).
34. C.W. Davis, Randell S.H.,. Airway goblet and mucous cells: identical, similar, or different? In S. M (ed.), Cilia and Mucus: from Development to Respiratory Defense, Marcel Dekker, New York, 2001, pp. 195-210.
35. S.M. Kreda, S.F. Okada, C.A. van Heusden, W. O'Neal, S. Gabriel, L. Abdullah, C.W. Davis, R.C. Boucher, and E.R. Lazarowski. Coordinated release of nucleotides and mucin from human airway epithelial Calu-3 cells. J Physiol. 584:245-259 (2007).
36. M.S. Balda, J.A. Whitney, C. Flores, S. Gonzalez, M. Cereijido, and K. Matter. Functional dissociation of paracellular permeability and transepithelial electrical resistance and disruption of the apical-basolateral intramembrane diffusion barrier by expression of a mutant tight junction membrane protein. J Cell Biol. 134:1031-1049 (1996).
37. L. Li, N.R. Mathias, C.L. Heran, P. Moench, D.A. Wall, and R.L. Smith. Carbopol-mediated paracellular transport enhancement in Calu-3 cell layers. J Pharm Sci. 95:326-335 (2006).
38. S. Chono, R. Fukuchi, T. Seki, and K. Morimoto. Aerosolized liposomes with dipalmitoyl phosphatidylcholine enhance pulmonary insulin delivery. J Control Release. 137:104-109 (2009).
39. T. Seki, H. Kanbayashi, S. Chono, Y. Tabata, and K. Morimoto. Effects of a sperminated gelatin on the nasal absorption of insulin. Int J Pharm. 338:213-218 (2007).
40. F. Sun, S. Tai, T. Lim, U. Baumann, and M. King. Additive effect of dornase alfa and Nacystelyn on transportability and viscoelasticity of cystic fibrosis sputum. Can Respir J. 9:401-406 (2002).
41. Y. Matsukawa, V.H. Lee, E.D. Crandall, and K.J. Kim. Size-dependent dextran transport across rat alveolar epithelial cell monolayers. J Pharm Sci. 86:305-309 (1997).
42. C.M. Yu, S. Mun, and N.H. Wang. Phenomena of insulin peak fronting in size exclusion chromatography and strategies to reduce fronting. J Chromatogr A. 1192:121-129 (2008).
43. Malvern. Protein solutions in research and development. http://www.malvern.com/LabEng/industry/protein/protein_solutions.htm (accessed 03/01/2010 2010).
44. M.P. Bohrer, W.M. Deen, C.R. Robertson, J.L. Troy, and B.M. Brenner. Influence of molecular configuration on the passage of macromolecules across the glomerular capillary wall. J Gen Physiol. 74:583-593 (1979).
45. A.V. Kamath, R.A. Morrison, N.R. Mathias, S.A. Dando, A.M. Marino, and S. Chong. Modulation of tight junctions does not predict oral absorption of hydrophilic compounds: use of Caco-2 and Calu-3 cells. Arch Pharm Res. 30:1002-1007 (2007).

46. P. Claude. Morphological factors influencing transepithelial permeability: a model for the resistance of the zonula occludens. J Membr Biol. 39:219-232 (1978).
47. T.Y. Ma, D. Tran, N. Hoa, D. Nguyen, M. Merryfield, and A. Tarnawski. Mechanism of extracellular calcium regulation of intestinal epithelial tight junction permeability: role of cytoskeletal involvement. Microsc Res Tech. 51:156-168 (2000).
48. M.A. Marcial, S.L. Carlson, and J.L. Madara. Partitioning of paracellular conductance along the ileal crypt-villus axis: a hypothesis based on structural analysis with detailed consideration of tight junction structure-function relationships. J Membr Biol. 80:59-70 (1984).
49. G.P. Carino, J.S. Jacob, and E. Mathiowitz. Nanosphere based oral insulin delivery. J Control Release. 65:261-269 (2000).
50. P. Jani, G.W. Halbert, J. Langridge, and A.T. Florence. The uptake and translocation of latex nanospheres and microspheres after oral administration to rats. J Pharm Pharmacol. 41:809-812 (1989).
51. T. Jung, W. Kamm, A. Breitenbach, E. Kaiserling, J.X. Xiao, and T. Kissel. Biodegradable nanoparticles for oral delivery of peptides: is there a role for polymers to affect mucosal uptake? Eur J Pharm Biopharm. 50:147-160 (2000).
52. A. Vila, A. Sanchez, M. Tobio, P. Calvo, and M.J. Alonso. Design of biodegradable particles for protein delivery. J Control Release. 78:15-24 (2002).
53. J. Brooking, S.S. Davis, and L. Illum. Transport of nanoparticles across the rat nasal mucosa. J Drug Target. 9:267-279 (2001).
54. M. de la Fuente, N. Csaba, M. Garcia-Fuentes, and M.J. Alonso. Nanoparticles as protein and gene carriers to mucosal surfaces. Nanomed. 3:845-857 (2008).

# Chapter 4

# Evaluation of the Toxicity of Alkylglycoside Surfactants

## 4.1 Introduction

Alkylglycosides (AGs) are water-soluble, nonionic and amphipathic surfactant compounds containing alkyl chains of variable lengths, glycosidically attached to either a monosaccharide or disaccharide. They can be economically synthesised and purified, and are metabolised to non-toxic alcohols and sugars (1). AGs have been investigated, both *in vitro* and *in vivo*, for their potential to improve the systemic bioavailability of macromolecular peptides and proteins delivered mucosally (2-7). When included in nasal or ocular formulations, AGs were reported to significantly increase the systemic bioavailability of peptides such as insulin and calcitonin (4, 6). The potential of AGs for use as agents facilitating mucosal absorption of protein therapeutics was in fact considered high enough as to result in their commercial exploitation; the drug delivery platform of Aegis Therapeutics is based on these compounds (8).

The precise molecular mechanism by which AGs exert their absorption-enhancing effects *in vivo* is, however, unclear. It is believed that AGs increase drug absorption *via* a direct effect on the epithelium rather than through a specific interaction with the

drug itself because AGs have been shown to improve absorption of several different types of macromolecules (6, 9). AGs were found to increase the paracellular movement of mannitol by opening the tight junctions (TJs) between cultured bronchial epithelial cells, suggesting that the paracellular route may be predominantly involved in the movement of macromolecules in cells treated with AGs (2, 9). Nevertheless, other studies have demonstrated that AGs intercalate into the lipid bilayers and fluidise the membrane leading to induction of endocytosis, hence increasing transcellular drug movement (2). The ability of AGs to fluidise and/or subsequently solubilise artificial phospholipid bilayers *in vitro* has been established (2). Arnold *et al*. (10) suggest that the absorption-enhancing mechanism of alkylglycosides in the nose appears to involve a different types of interactions of the surfactant with the nasal surface, which includes mucus dilution, inhibition of ciliary clearance and improved paracellular and transcellular movement.

Although the absorption-enhancing properties of AGs have been relatively well documented, the data on their toxicity is somewhat limited. Most published studies investigating AGs *in vivo* measured the reversibility of increased mucosal absorption (absorption of macromolecules measured at a certain period after the application of the surfactants) as an indication of toxicity (7, 11, 12). *In vitro* studies with epithelial cell models on the other hand determined reversibility in TEER, as a demonstration of toxicity (13), while to the best of our knowledge, cell toxicity assays measuring the effect of AGs on cell viability were not included in any of the published *in vitro* studies of AGs.

Present work attempts to establish mechanism(s) by which AGs exhibit mucosal absorption enhancing effects. Furthermore, the toxicity of AG surfactants *in vitro* is evaluated in detail by commonly used cell toxicity assays. Three representative AGs, with relatively long alkyl chains, namely dodecylmaltoside (DDM, 12 carbons), tridecylmaltoside (TriDM, 13 carbons) and tetradecylmaltoside (TDM, 14 carbons) were selected in this work as these compound are the most extensively studied and also because longer chain AGs, such as those used in this work have been shown to produce a more potent absorption enhancing effect compared to those with shorter alkyl chains. The molecular structures of these compounds are depicted in Figure 4.1.

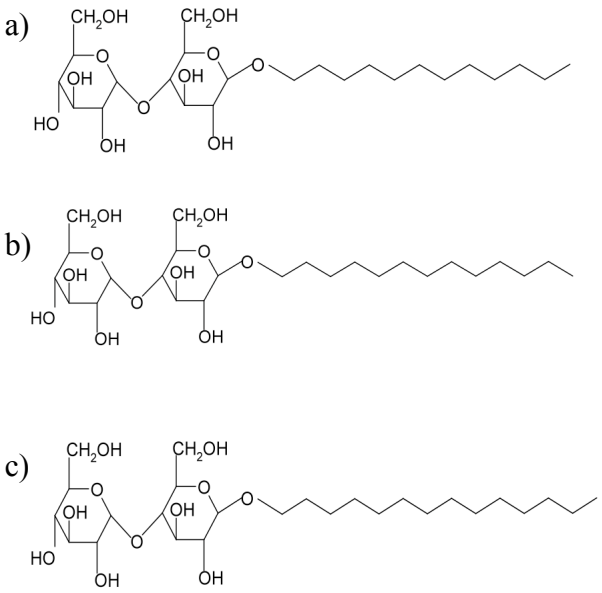


***Figure 4.1. Chemical structures of AGs. a) Dodecylmaltoside (DDM), b) Tridecylmaltoside (TriDM) and c) Tetradecylmaltoside (TDM), containing a 12, 13 and 14 carbon alkyl chain, respectively, linked to maltose.***

## 4.2 Methods

### 4.2.1 Effect of AGs on Calu-3 layer TEER

Calu-3 cells were cultured on filters (using AIC conditions) to produce confluent cell layers in the manner described previously (Chapter 2, section 2.2.1). Culture medium (EMEM) was aspirated from the cells and replaced with HBSS (0.5 ml and 1.5 ml in the apical and basolateral chambers of the Transwell™ system, respectively). Cells were equilibrated (incubated at 37°C) in HBSS for approximately 45 min. TEER was measured before the application of AGs and the recorded values were treated as the baseline TEER. Stock solutions of AGs were prepared fresh on the day of the experiment by dissolving each AG in HBSS at 0.25% w/v. AG sample solutions, which consisted of three AGs, DDM, TriDM and TDM, were applied to the apical side of the cells at a concentration of 0.125% w/v in HBSS. Triton X-100 (0.1% v/v, dissolved in HBSS) was used as a positive control causing cell death and therefore irreversible decrease in TEER, whereas HBSS *per se* was used as a negative control. TEER measurements were conducted 5 min, 15 min, 30 min and 45 min following the application of the samples (and controls). After the TEER measurement at time 45 min, AG solutions were removed from the apical side of the cell layers, while HBSS was removed from the basolateral chamber. Cell layers were washed with PBS and then culture medium was applied on both apical and basolateral sides of the cell layers; cells were incubated further in the culture medium. In order to determine whether any changes in TEER observed following the application of AGs were reversible, further measurements of electrical resistance were conducted at times 150 min, 180 min, 210 min and 24 hours.

### 4.2.2 Effect of AGs on Calu-3 metabolic activity: alamarBlue® assay

AlamarBlue® assay was conducted on filter-cultured Calu-3 cells once they formed confluent layers. Culture medium was aspirated from the cells and HBSS added to the basolateral side. Stock solutions of AGs were prepared fresh on the day of the experiment by dissolving each AG in HBSS at 0.25% w/v. AG solutions consisting of DDM, TriDM and TDM were applied to the apical side of the cells at a concentration of 0.125% w/v in HBSS for 45 min. Triton X-100 (0.1% v/v in HBSS) and HBSS were used as the positive and negative control, respectively. Following the incubation with AG solutions, cells were extensively washed with PBS. AlamarBlue® assay was then conducted following the method described in section 2.2.5.2.

### 4.2.3 Effect of AGs on HT29 metabolic activity: alamarBlue® assay

HT29 cells were seeded on a 24-well plate at a density of $5x10^4$ cells per well and cultured for 2 days in McCoy's 5A medium. Stock solutions of the AG surfactants were prepared by dissolving each AG in HBSS at 0.25% w/v and were used on the same day. Culture medium was replaced with pre-warmed (37°C) solutions of AGs (DDM, TriDM and TDM), used at 0.0625%, 0.125% and 0.25% w/v (in HBSS). HBSS and Triton X-100 (0.1% v/v in HBSS) served as negative and positive controls, respectively. HT29 cells were incubated (at 37°C/5%$CO_2$) with the test sample solutions for 45 min. AG solutions were then removed and cells washed with PBS. Thereafter, alamarBlue® assay was conducted in the manner described previously (section 2.2.5.2).

### 4.2.4 Effect of AGs on Calu-3 metabolic activity: MTS Assay

Calu-3 cells were seeded on a 96-well plate at a density of $10^4$ cells per well and the cells were incubated in the culture medium for 24 hours. AG sample solutions were prepared on the day of the experiment by dissolving each AG in HBSS. Culture medium was removed from each well and replaced with AG sample solutions, consisting of DDM, TriDM or TDM at concentrations of 0.0156%, 0.03125%, 0.0625% and 0.125% w/v (in HBSS). Triton X-100 and HBSS were used as the positive and negative control, respectively, as described in the preceding section. Cells were incubated with AG samples (and controls) for 2 hours. MTS assay was thereafter performed in the way detailed previously (section 2.2.5.3).

### 4.2.5 Effect of AGs on membrane toxicity: LDH assay

Calu-3 cells were seeded on a 96-well plate at a density of $10^4$ cells per well and incubated in the culture medium for 24 hours before the assay. AG stock solutions were prepared fresh on the day of the experiment by dissolving each AG (DDM, TriDM and TDM) in HBSS. Culture medium was removed and replaced with AG sample solutions at the following concentrations: 0.05%, 0.025%, 0.0125%, 0.00625% and 0.003125% w/v. Triton X-100 and HBSS were used as the positive and negative control, respectively, as described in section 4.2.3. Cells were incubated with AG solutions (and controls) for 2 hours, after which LDH assay was conducted according to the methods in section 2.2.5.4.

### 4.2.6 Effect of AGs on cell penetration of FD4

Calu-3 cells were cultured on filters and used in this experiment as confluent layers (i.e. exhibiting a TEER $\geq$ 500 $\Omega cm^2$). AG and FD4 stock solutions were prepared

fresh on the day of the experiment by dissolving DDM or TDM in HBSS at a concentration of 0.002% w/v and FD4 at a concentration of 1 mg/ml. Culture medium (EMEM) was firstly removed and cells washed with PBS. HBSS was then added to the basolateral compartment, whereas samples consisting of of DDM or TDM in combination with FD4 were added to the apical compartment of the Transwell®. The final concentrations of DDM or TDM and FD4 on the apical side of the cells were 0.001% w/v for AGs and 500 μg/ml for FD4. Cells were incubated with each AG in conjunction with FD4 for 1 hour. A control experiment was performed by applying FD4 at the same concentration (500 μg/ml in HBSS) without the presence of AGs and incubating the cells for the same duration (1 hour). AG/FD4 samples (and FD4 only, for the control experiment) were then removed from the apical side of the cell layers, followed by extensive washing of the cells with PBS. Cells were then fixed with 4% w/v paraformaldehyde (in PBS) for approximately 10 min. The filters were then excised and prepared for confocal imaging in the manner described previously (section 2.2.6.5).

## 4.3 Results

### 4.3.1 Effect of AGs on Calu-3 layer TEER

Addition of AG solutions to confluent Calu-3 layers resulted in an immediate and dramatic decrease of TEER (Figure 4.2). The observed effect on TEER was very similar for all three tested AGs, with a sharp decrease of TEER to approximately 3-4% of the baseline value within 5 min of their application. Furthermore, the TEER pattern resulting from application of the AGs paralleled that seen with Triton X-100. TEER values remained low even after removal of AG solutions and the replacement with culture medium (at time point of 45 min, indicated in Figure 4.2 by the arrow),

an effect also observed in cells incubated with Triton X-100, but not in control cell layers incubated with HBSS. TEER of control cell layers decreased by approximately 17% (in relation to the baseline value) initially, 5 min after application of HBSS, but recovered to levels near the baseline value within 30 min, following which it remained relatively constant throughout the experiment. Measurements conducted 24 hours following sample application (and 23.15 hours after their removal) revealed no recovery of TEER in cell layers incubated with AG samples, as well as Triton X-100. These values amounted to approximately 2-3% of the baseline TEER for all three AGs, which were comparable with the value recorded for Triton X-100 (2.6% of the baseline TEER). In contrast, control cell layers incubated with HBSS exhibited TEER similar to the baseline value (approximately 105% of the baseline figure).

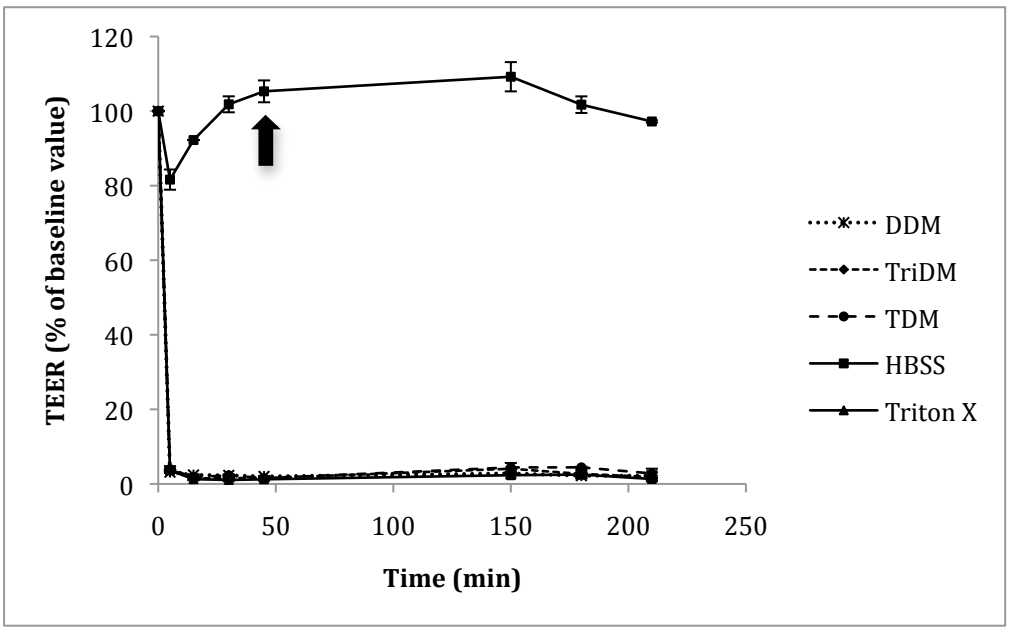


***Figure 4.2. Effect of AGs on Calu-3 layer TEER. Dodecylmaltoside (DDM), tridecylmaltoside (TriDM) and tetradecylmaltoside (DDM) were applied to confluent cell layers at 0.125% w/v. HBSS and Triton X-100 (0.1% v/v in HBSS), were used as the positive and negative control, respectively. Arrow indicates when AG sample solutions were removed and culture medium added. Data expressed as % of the baseline TEER and presented as the mean ± SD (n=3).***

### 4.3.2 Effect of AGs on Calu-3 metabolic activity: alamarBlue® assay

Figure 4.3 shows the effect of tested AG molecules on the metabolic activity of Calu-3 cells, as confluent, filter-cultured layers, as measured by the alamarBlue® assay. All three AGs were associated with a remarkable reduction of relative metabolic activity, amounting to more than 95% with DDM, TriDM and the two highest doses of TDM. The two lowest doses of TDM still produced a metabolic activity reduction of >85%. These values appeared to show a concentration-dependent effect. The diminution in cell metabolic activity caused by the highest concentration (0.125% w/v) of all AG compounds was greater than that seen with Triton X-100, resulting in negative metabolic activity values (Figure 4.4).

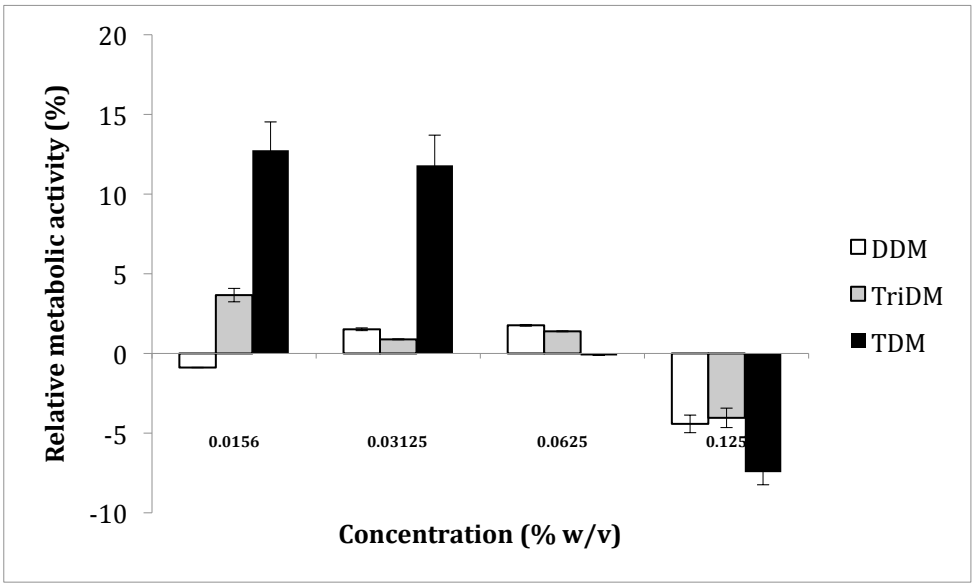


***Figure 4.3. Effect of AGs on Calu-3 metabolic activity, as determined by the alamarBlue® assay. Dodecylmaltoside (DDM), tridecylmaltoside (TriDM) and tetradecylmaltoside (TDM) were applied to cell layers at concentrations of 0.0625%, 0.125% and 0.25% w/v (in HBSS). Data expressed as % relative metabolic activity calculated in the manner described previously (section 2.2.5.2). Data presented as the mean ± SD (n=4).***

### 4.3.3 Effect of AGs on HT29 metabolic activity: alamarBlue® assay

Metabolic activity of intestinal HT29 cells following their incubation with AGs is shown in Figure 4.4. The dramatic metabolic activity-decreasing effect of the surfactants exhibited on Calu-3 cells was replicated on the HT29 cell line. Apart from the lowest concentrations of TriDM, calculated metabolic activity values were negative due to lower alamarBlue® fluorescence values obtained with AG samples compared to those seen with Triton X-100.

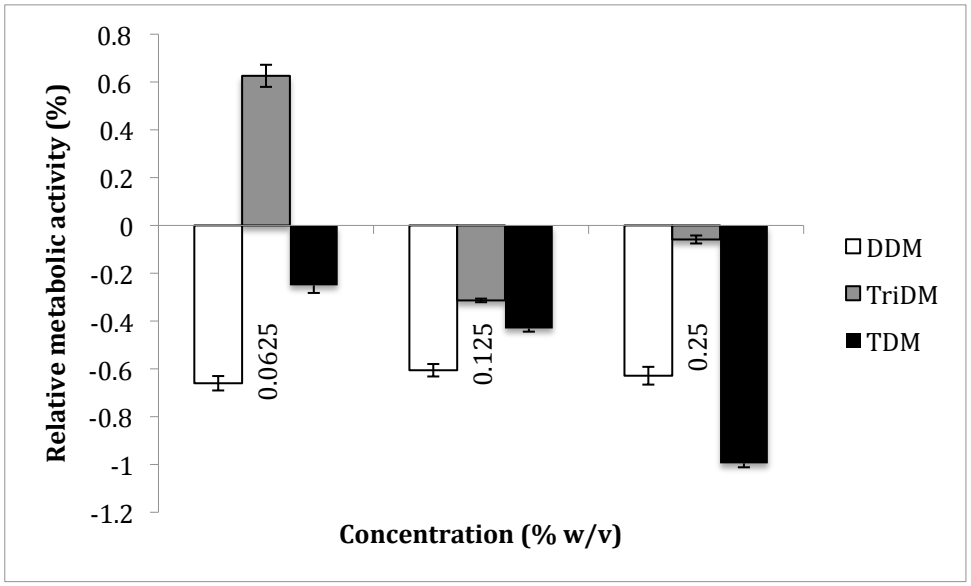


***Figure 4.4. Effect of AGs on HT29 metabolic activity. Dodecylmaltoside (DDM), tridecylmaltoside (TriDM) and tetradecylmaltoside (TDM) were used at concentrations of 0.0156%, 0.03125%, 0.0625% and 0.125% w/v. Data expressed as relative metabolic activity and presented as the mean ± SD (n=4).***

### 4.3.4 Effect of AGs on Calu-3 metabolic activity: MTS Assay

Figure 4.5 demostrates that the tested AGs showed a significant reduction in Calu-3 metabolic activity at tested concentrations, as measured by the MTS assay. Again, negative values were obtained, as MTS absorbance readings in some cases were lower for AG samples than those for Triton X-100. The MTS results therefore are in close

agreement with the previous assay (alamarBlue®) conducted on Calu-3 and HT29 cells.

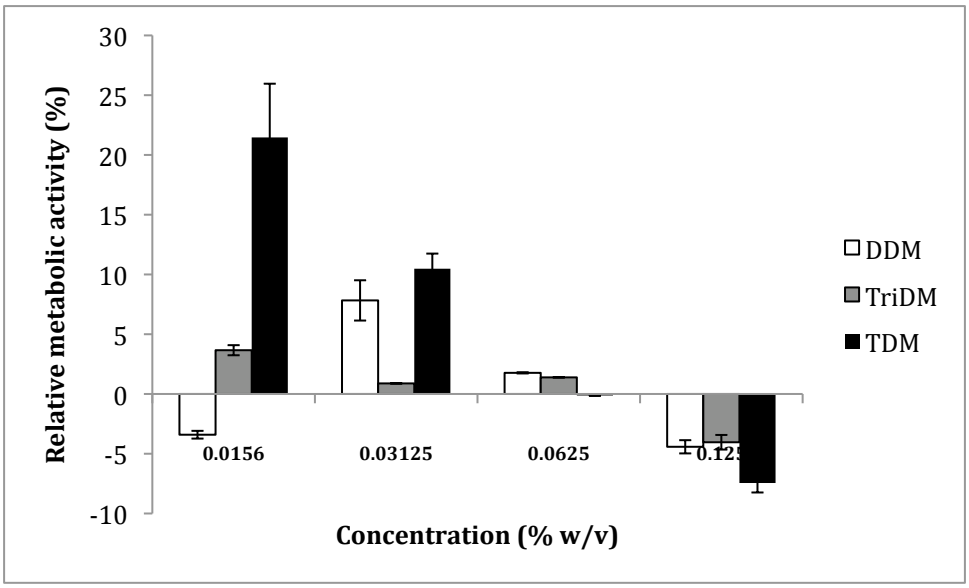


***Figure 4.5. Effect of AGs on Calu-3 metabolic activity, as determined by the MTS assay. Dodecylmaltoside (DDM), tridecylmaltoside (TriDM) and tetradecylmaltoside (TDM) were applied to cells at concentrations of 0.0156%, 0.03125%, 0.0625%, and 0.125% w/v. Data expressed as relative cell metabolic activity and presented as the mean ± SD (n=4).***

### 4.3.5 Effect of AGs on membrane integrity: LDH assay

Application of AGs to Calu-3 cells was associated with a dramatically significant release of the cytoplasmic enzyme, LDH (Figure 4.6). The extent of this release with two highest concentrations (0.05% and 0.025% w/v) of all three surfactants was greater than that observed with Triton X-100 (used as a positive control), resulting in relative LDH release values of greater than 100%. The degree of LDH release was concentration-dependent for TriDM and, to some extent, TDM. Even at the lowest concentrations of 0.003125% w/v, relative LDH release following the application of AGs amounted to approximately 100%, 71% and 84%, for DDM, TriDM and TDM, respectively.

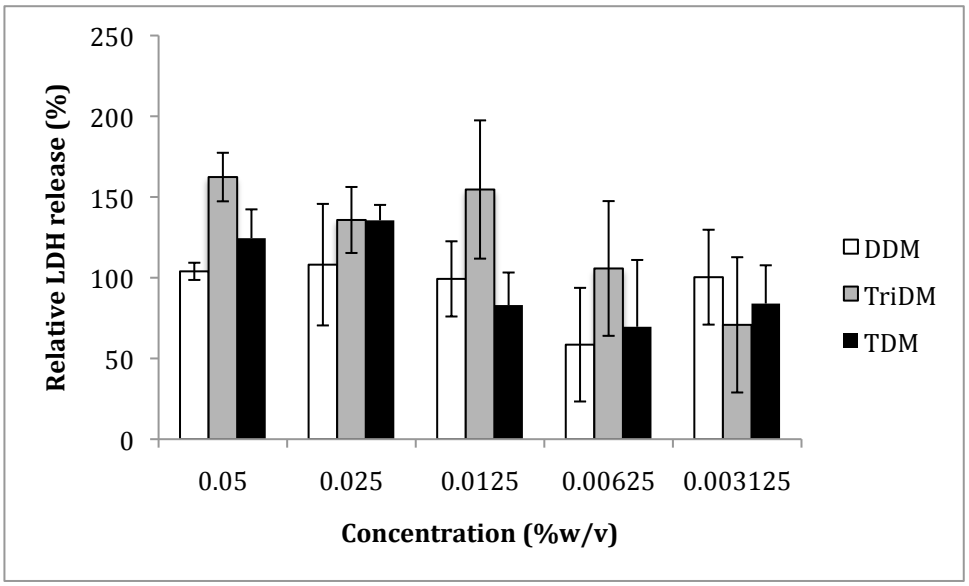


***Figure 4.6. Effect of AGs on LDH release from Calu-3 cells. DDM, Tri-DM and TDM were applied to cells at concentrations of 0.003125%, 0.00625%, 0.0125%, 0.025% and 0.05% w/v (in HBSS). Data expressed as relative LDH release, calculated using the equation described in section 2.2.5.4 and presented as the mean ± SD (n=4).***

### 4.3.6 Effect of AGs on cell penetration of FD4

Figure 4.7 shows the fluorescence distribution of the cell membrane impermeable compound, FD4, following its application to Calu-3 layers, on its own (4.6a) or in conjunction with AG compounds, DDM or TDM (4.6b and 4.6c, respectively). In the cell layer incubated with FD4 only, observed FD4 fluorescence (imaged in the red channel in this case) was limited. In contrast, large areas of FD4 fluorescence can be observed in cell layers subjected to concurrent FD4 and AG incubation.

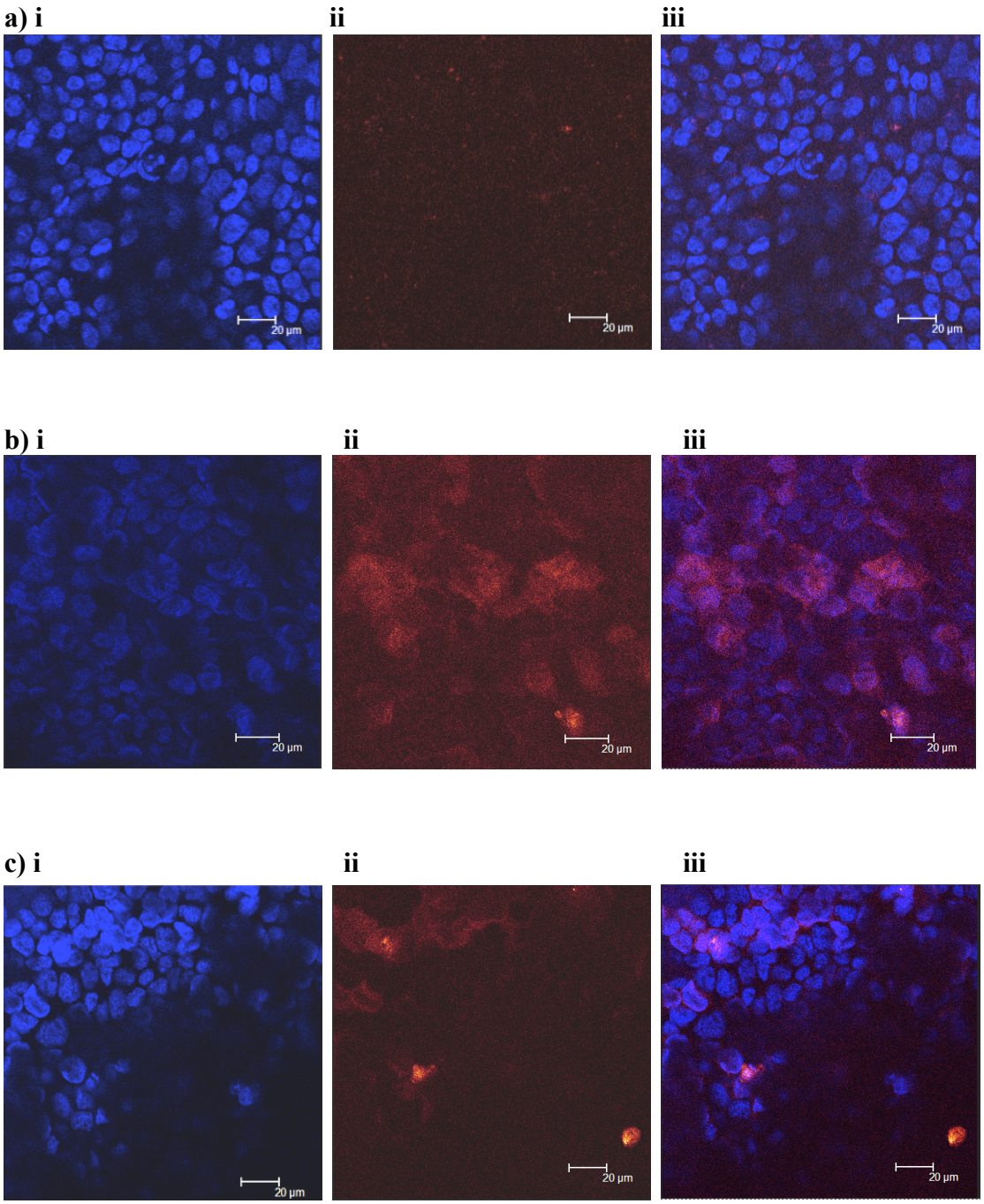


*Figure 4.7. Association of FD4 with Calu-3 layer following its application on its own or with AGs. a) FD4 in the absence of AGs (control), b) FD4 in conjunction with DDM, and c) FD4 in combination with TDM. AGs were applied to cells at 0.001% w/v and FD4 at 500 µg/ml. i) Blue channel: nuclei labelled with DAPI, ii) Red channel: FD4, and iii) Overlay image.*

## 4.4 Discussion

AG surfactants have recently been shown to improve transmucosal delivery of protein, peptide and non-peptide macromolecular therapeutics (7, 14) leading to their commercial exploitation. For example, Ahsan *et al*. (8) investigated the effect of TDM on translocation of insulin across the human bronchial epithelial cell line 16HBE14o$^{-}$. Application of TDM to the apical surface of cells decreased the TEER to approximately 60% of the baseline value and resulted in increased mannitol permeability (by approximately 3.2-fold). Furthermore, the authors reported a higher basolateral insulin recovery with application of TDM compared to control; this effect was attributed to loosening of the TJs.

While Aegis Therapeutics claim that their drug delivery technology, namely Intravail® absorption enhancing excipients based on AGs, effectively delivers protein and peptide drugs of up to 30 kDa through the nasal route without causing irritation of the nasal tissue (8), literature information on their toxicity is sparse. Furthermore, the mechanism of absorption-enhancing action of these molecules is not completely understood. Our work therefore aimed to fully evaluate these compounds for their toxicity towards epithelial cells *in vitro* and also attain information with regards to the mechanisms involved in their mucosal absorption enhancement.

Application of tested AGs to confluent Calu-3 layers, used as a model of the airway epithelium, resulted in an irreversible decrease in TEER, an early indication of toxicity of these compounds. The use of TEER as a sensitive measure of cell toxicity has been applied before. The application of membrane-perturbing toxicants, benzalkonium chloride and saponin was shown to rapidly decrease the TEER of the

intestinal Caco-2 cell monolayers. TEER values and released LDH (another cytotoxicity test also used in our work and will be discussed later) measured under various conditions were found to correlate negatively. However, the decrease in TEER was detectable at a lower concentration of a toxicant than that for LDH release (15). Similarly, *Clostridum difficile* toxin A was found to decrease the TEER values of human intestinal T84 cell monolayers, while the LDH release test was not always showing the toxic effect at the same concentration (16). A correlation between the TEER decrease and LDH release was also found when investigating the cytotoxic effect of heavy metals such as cadmium (Cd) (17). Prozialeck *et al.* (18) have demonstrated that the loss of the integrity of cell monolayers of the porcine renal epithelial cell line, LLC-PK1, caused by Cd occurred faster than cell disruption. While the LDH cytotoxicity assay requires increased membrane permeability and cell disruption as an indication of cell toxicity, measurement of TEER can detect early stages of the cytotoxic processes such as loss of cell layer integrity, making this a highly sensitive measure of cytotoxicity, particularly that caused by membrane-perturbing toxicants.

However, it may be possible that a decrease in TEER may arise from factors other than cell death. For example it could arise from an irreversible effect on TJ proteins (and opening of TJs) or cell detachment from the surface of the filter, leading to the loss of the barrier to the movement of ions across the filter/cell layer and therefore lower observed TEER. Further tests investigating the cell toxicity of AGs were therefore conducted, including the use of three different cytotoxicity assays in two epithelial cell lines (Calu-3 and HT29).

AlamarBlue® cell metabolic activity test was firstly performed on Calu-3 cells to test the toxicity of AGs exhibited towards cells cultured as polarised layers. The tested compounds showed a remarkable reduction in Calu-3 metabolic activity. In fact, the suppression of cell metabolic activity was in some cases (with the highest tested concentration) more potent than that of 0.1% Triton X-100. A similar effect was observed when testing the effect of AGs on the metabolic activity of intestinal HT29 cells (cultured in multiwell plates) through the same assay (AlamarBlue®). AGs were found to inhibit the metabolic activity of HT29 cells, used for corroboration, to an extent greater than Triton X-100, resulting in negative relative cell metabolic activity values. Determination of the effect of AGs on Calu-3 metabolic activity was repeated by applying the MTS assay, which works on the same principle (measures metabolic activity through an oxidation/reduction reaction) as AlamarBlue®. This test, used for corroboration, confirmed the previous observation of the dramatic negative effect of AGs on the metabolic activity of Calu-3 cells.

In addition to cell toxicity assays based on measurement of (products of) metabolic activity (MTS and AlamarBlue®), the LDH assay was further conducted to test any adverse effects that AGs may have on the membrane integrity of Calu-3 cells. LDH is a cytoplasmic enzyme ($M_W$ 140 kDa), which is released into the extracellular milieu when apical membrane of cells is damaged (19). The amount of enzyme detected in supernatant correlates to the proportion of lysed cells (20). This assay, first described by Legrand *et al.* (21), is therefore particularly useful for testing membrane perturbing effects of compounds. Application of AGs to Calu-3 cells was associated with remarkably high detection of cytoplasmic LDH, suggesting its release into the extracellular medium, which in turn indicates plasma membrane damage. Similarly to

findings obtained with the previous assays, higher concentrations of AGs caused a greater release of LDH than the positive control, indicating the severity of the effect of these molecules on Calu-3 cell membranes.

In investigating the effect of TDM on translocation of insulin across the human bronchial epithelial cell line 16HBE14o$^-$, Ahsan *et al.* (9) applied 0.125% w/v TDM to the apical surface of the cell layers. In our work, application of TDM to Calu-3 cells at this concentration was associated with a striking decrease in cell metabolic activity. In fact, much lower concentrations of TDM, namely 0.0156% and 0.03125%, also affected cell metabolic activity dramatically. The reasons behind such a marked difference in sensitivity towards TDM between the 16HBE14o$^-$ cell line in the above study and the Calu-3 cell line (also a bronchial cell line) in our work are not entirely clear. However, it must be noted that in the discussed work by Ahsan *et al.,* TDM was not fully evaluated for its toxicity towards cells, although it was shown that TEER recovered to >95% of initial values, though this recovery took place following a long interval (36-40 hours) post TDM application.

A study evaluating a series of AGs (13 compounds) for their ability to open the cellular TJs on intestinal epithelial cell lines, T-84 and HT29Cl19A (a subclone of HT29 cells) showed that the concentrations of AGs required to open the TJs with minimal disruption of cellular membranes were between 0.01% and 0.1% w/v (13). Of the 13 AGs tested, 4 caused permanent decrease in TEER, which the authors attributed to irreversible solubilisation of cell membranes, 5 resulted in a partial recovery of the cell monolayer TEER and 4 induced a decrease in TEER with a more complete recovery. The 4 AGs associated with an irreversible decrease in TEER

included TDM, applied at concentration of 0.01% w/v. The authors, however, found that TriDM, applied at 0.01% w/v, had no effect on TEER. Used at a higher concentration of 0.1% w/v, TriDM was associated with a decrease in TEER by 90%, but the recovery (measured 18 hours after its removal) was only partial (to 29% and 32% of the initial value in T-84 and HT29 cells, respectively). DDM, on the other hand, applied at 0.1% w/v, lowered the TEER by 95% and 88%, on T-84 cells and HT29Cl19A cells, respectively, with a recovery to 90% of the baseline value on both cell lines.

In a separate study, Tirumalasetty *et al.* (22) investigated the effect of octylglucoside (OG) on permeation of insulin across monolayers of two intestinal epithelial cell lines, T-84 and Caco-2. Application of OG at concentrations of 0.2% - 0.5% w/v was associated with a concentration-dependent reduction of TEER in both monolayers, with a full recovery of TEER observed only with 0.2% and 0.3% w/v OG. The authors speculated that the lack of TEER recovery is possibly a result of solubilisation of TJ-associated proteins (TJAPs) or ATP depletion, altering the phosphorylation state of TJAPs resulting in inactivation of kinases. With regards to permeability studies, the highest OG concentration associated with a reversible reduction of TEER (0.3% w/v) did not result in a significant enhancement in the permeability of insulin across the cell monolayers of both cell lines compared to controls. Although a noticeable increase in insulin permeability was observed with higher concentrations of OG (0.4% and 0.5% w/v), the authors note that basolateral accumulation of insulin after 4 hours was irregular (not steady state), indicating cell damage and disruption of the cell monolayers, revealing that the study was not able to find a compromise between a permeability-enhancing effect and an acceptable cellular toxicity.

A study by Hussain *et al.* (23) used 16HBE14o- and Calu-3 cells to assess the impact of octylmaltoside on insulin permeability across cell layers of these cell lines. It is interesting to note that octylmaltoside was applied to the cells at concentrations between 0.125% and 0.5% w/v. Although the addition of octylmaltoside was associated with a decrease in TEER and a significant increase in insulin permeability across both 16HBE14o- and Calu-3 layers, with both effects shown to be concentration-dependent, toxicity studies were not performed. A different study by Pillion *et al.* (4) investigated the effect of AGs on systemic absorption of insulin when administered *via* nosedrops in rats. The absorption-enhancing effect of AGs was found to be dose-dependent and varied with the alkyl chain length. DDM, TriDM and TDM were used in nosedrops at concentrations between 0.03% and 0.125% w/v and all three AGs at all concentrations were associated with a significant hypoglycemic response. Again, this study does not include any toxicity/irritancy tests performed on rats following the administration of AGs.

A study by Arnold *et al*. (2) evaluated the toxicity of TDM by determining the alterations in nasal morphology of rats, following treatment with this AG. Nasal formulations consisting of saline or TDM were administered, followed by animal sacrifice and removal of nasal septa, 15 min later. Light microscopy revealed that tissue samples from rats treated with 0.125% w/v TDM had less uniform cilia and increased endocytotic activity. In samples from rats exposed to 0.5% w/v TDM, cilia could not be observed at the apical surface of the septal tissue and an altered cellular morphology was apparent with both epithelial and goblet cells. Examination of the tissues by TEM showed that treatment with 0.125% TDM resulted in mild-to-

moderate morphological changes, with thinned cilia and appearance of numerous vesicles, which the authors attributed to stimulation of endocytosis by TDM.

Another study on AGs that addressed the assessment of their toxicity is that by Mustafa *et al.* (12). In this study, the authors assessed the effect of intranasally administered octylmaltoside (OM), decylmaltoside (DM), dodecylmaltoside (DDM) and tetradecylmaltoside (TDM) at concentrations 0.25%, 0.5% and 1% w/v in an attempt to improve the nasal absorption of enoxaparin in rats. The acute toxicity of the surfactants in this work was determined by 'reversibility studies', whereby absorption enhancers and drugs are administered separately at different time intervals. In this case, AGs were administered at 0.5% w/v, followed by the administration of enoxaparin at time zero (immediately afterwards), at 60 min or at 120 min. The authors reported a decrease in systemic absorption of enoxaparin when administered 120 min after the application of the surfactants compared to enoxaparin absorption immediately after application of the surfactant. However, the extent of this decrease was modest, with values of less than 2-fold with DDM and approximately 2-fold with TDM. Furthermore, absorption of enoxaparin following its administration 120 min after the application of AG remained significantly higher compared to control (where saline was administered instead of AG). In fact, the effects of DDM and TDM were sustained for >240 min, which could indicate toxicity effects towards the nasal epithelium.

One can assess membrane-disruptive effects of a compound by applying this compound to confluent, polarised cell layers in combination with a cell membrane-impermeable fluorescent probe, followed by measurement/observation of the

distribution of fluorescence in the cell layer. The distribution of the cell membrane-impermeable probes in living cells with intact plasma membrane is not expected to occur in significant levels within the interior of the cells due to the exclusion of the dye by the plasma membrane. On the other hand, any disruption of the plasma membrane will result in penetration of this marker into the interior of the cells, which can then be visualized by fluorescence microscopy. The use of this simple method, in conjunction with fluorescence microscopy, therefore provides visual information on cell membrane-disruptive effects of the tested compound. Due to their molecular size and hydrophilicity, FDs can be used as cell membrane-impermeable fluorescent markers (24). Application of a solution containing a combination of FD4 with either DDM or TDM (which were used at a low concentration of 0.001% w/v) to a confluent Calu-3 layer resulted in a widespread detection of FD4 fluorescence even after extensive washing of the cells following their incubation with FD4/AGs. This observation strongly indicated that AGs caused a cell membrane-disrupting effect, which resulted in penetration of FD4 into the interior of the cells. Conversely, in the cell layer incubated with FD4 only, lower levels of FD4 fluorescence were observed. This can be explained by the exclusion of FD4 from viable cells with intact plasma membranes in the control layer enabling its subsequent washing off following the incubation interval.

Although the present work set out to investigate the absorption enhancing mechanism of AGs, evaluation of their toxicity towards the epithelial cells (used as a mucosal model) highlighted severe adverse effects on cell metabolic activity and integrity of cell membranes. Considering this outcome, the mechanisms involved in permeability enhancement could not be fully elucidated. However, based on the toxicity data

obtained in this work, it could be speculated that the absorption-facilitating effect of AGs (found in the studies discussed above) results from their effect on cell membranes, leading to compromised integrity of epithelial cell barriers.

## 4.5 Conclusion

This work evaluated the toxicity of AG surfactants, as compounds that have recently been demonstrated to promote the mucosal absorption of peptide and protein drugs, towards the Calu-3 epithelial cells. A combination of different assays and methods indicating cellular toxicity were adopted. Permanent reduction in TEER, dramatic reduction in cell metabolic activity (as measured by two different assays), remarkable cell membrane disruption (indicated *via* the LDH assay) and penetration of otherwise cell membrane-impermeable FD4 into the cells were the experimental outcomes associated with the application of tested AG compounds. These phenomena were observed at AG concentrations lower than those typically used in the literature. This work therefore revealed that these compounds exhibited extremely high toxicity towards the Calu-3 cells (and also HT29 cells, used for corroboration), indicating the necessity for further evaluation of their chronic toxicity prior to the potential use of AGs as mucosal absorption enhancers in man. In the scope of the project described in this thesis, AGs were considered too toxic and therefore not investigated any further.

## 4.6 References


1. D.J. Pillion, F. Ahsan, J.J. Arnold, B.M. Balusubramanian, O. Piraner, and E. Meezan. Synthetic long-chain alkyl maltosides and alkyl sucrose esters as enhancers of nasal insulin absorption. J Pharm Sci. 91:1456-1462 (2002).
2. J.J. Arnold, F. Ahsan, E. Meezan, and D.J. Pillion. Correlation of tetradecylmaltoside induced increases in nasal peptide drug delivery with morphological changes in nasal epithelial cells. J Pharm Sci. 93:2205-2213 (2004).
3. D.J. Pillion, S. Hosmer, and E. Meezan. Dodecylmaltoside-mediated nasal and ocular absorption of lyspro-insulin: independence of surfactant action from multimer dissociation. Pharm Res. 15:1637-1639 (1998).
4. D.J. Pillion, J.A. Atchison, C. Gargiulo, R.X. Wang, P. Wang, and E. Meezan. Insulin delivery in nosedrops: new formulations containing alkylglycosides. Endocrinology. 135:2386-2391 (1994).
5. D.J. Pillion, P. Wang, J. Yorks, P. McCann, and E. Meezan. Systemic absorption of insulin and glucagon applied topically to the eyes of rats and a diabetic dog. J Ocul Pharmacol Ther. 11:283-295 (1995).
6. F. Ahsan, J. Arnold, E. Meezan, and D.J. Pillion. Enhanced bioavailability of calcitonin formulated with alkylglycosides following nasal and ocular administration in rats. Pharm Res. 18:1742-1746 (2001).
7. J. Arnold, F. Ahsan, E. Meezan, and D.J. Pillion. Nasal administration of low molecular weight heparin. J Pharm Sci. 91:1707-1714 (2002).
8. http://www.aegisthera.com/ (accessed 25/01/2010 2010).
9. F. Ahsan, J.J. Arnold, T. Yang, E. Meezan, E.M. Schwiebert, and D.J. Pillion. Effects of the permeability enhancers, tetradecylmaltoside and dimethyl-beta-cyclodextrin, on insulin movement across human bronchial epithelial cells (16HBE14o-). Eur J Pharm Sci. 20:27-34 (2003).
10. J.J. Arnold, M.D. Fyrberg, E. Meezan, and D.J. Pillion. Reestablishment of the nasal permeability barrier to several peptides following exposure to the absorption enhancer tetradecyl-beta-D-maltoside. J Pharm Sci (2009).
11. M.A. Bagger, H.W. Nielsen, and E. Bechgaard. Nasal bioavailability of peptide T in rabbits: absorption enhancement by sodium glycocholate and glycofurol. Eur J Pharm Sci. 14:69-74 (2001).
12. F. Mustafa, T. Yang, M.A. Khan, and F. Ahsan. Chain length-dependent effects of alkylmaltosides on nasal absorption of enoxaparin. J Pharm Sci. 93:675-683 (2004).
13. J.G. Eleyand P. Triumalashetty. In vitro assessment of alkylglycosides as permeability enhancers. AAPS PharmSciTech. 2:E19 (2001).
14. Z.M. Novakovic, M.C. Leinung, D.W. Lee, and P. Grasso. Intranasal administration of mouse [D-Leu-4]OB3, a synthetic peptide amide with leptin-like activity, enhances total uptake and bioavailability in Swiss Webster mice when compared to intraperitoneal, subcutaneous, and intramuscular delivery systems. Regul Pept. 154:107-111 (2009).
15. Narai A, Arai S, and S. M. Rapid decrease in transepithelial electrical resistance of human intestinal Caco-2 cell monolayers by cytotoxic membrane perturbents. Toxicology in Vitro. 11:347-354 (1997).
16. G. Hecht, C. Pothoulakis, J.T. LaMont, and J.L. Madara. Clostridium difficile toxin A perturbs cytoskeletal structure and tight junction permeability of

cultured human intestinal epithelial monolayers. J Clin Invest. 82:1516-1524 (1988).

17. Rossi A, Poverini R, Di Lullo G, Modesti A, Modica A, and Scarino M L. Heavy metal toxicity following apical and basolateral exposure in the human intestinal cell line Caco-2. Toxicology in Vitro. 10:27-31 (1996).
18. W.C. Prozialeck, D.R. Wellington, and P.C. Lamar. Comparison of the cytotoxic effects of cadmium chloride and cadmium-metallothionein in LLC-PK1 cells. Life Sci. 53:PL337-342 (1993).
19. C.M. Silva, F. Veiga, A.J. Ribeiro, N. Zerrouk, and P. Arnaud. Effect of chitosan-coated alginate microspheres on the permeability of Caco-2 cell monolayers. Drug Dev Ind Pharm. 32:1079-1088 (2006).
20. T. Deckerand M.L. Lohmann-Matthes. A quick and simple method for the quantitation of lactate dehydrogenase release in measurements of cellular cytotoxicity and tumor necrosis factor (TNF) activity. J Immunol Methods. 115:61-69 (1988).
21. C. Legrand, J.M. Bour, C. Jacob, J. Capiaumont, A. Martial, A. Marc, M. Wudtke, G. Kretzmer, C. Demangel, D. Duval, and et al. Lactate dehydrogenase (LDH) activity of the cultured eukaryotic cells as marker of the number of dead cells in the medium [corrected]. J Biotechnol. 25:231-243 (1992).
22. P.P. Tirumalasettyand J.G. Eley. Permeability enhancing effects of the alkylglycoside, octylglucoside, on insulin permeation across epithelial membrane in vitro. J Pharm Pharm Sci. 9:32-39 (2006).
23. A. Hussainand F. Ahsan. Indication of transcytotic movement of insulin across human bronchial epithelial cells. J Drug Target. 14:181-190 (2006).
24. D.N. Rhoads, S.G. Eskin, and L.V. McIntire. Fluid flow releases fibroblast growth factor-2 from human aortic smooth muscle cells. Arterioscler Thromb Vasc Biol. 20:416-421 (2000).

# Chapter 5

# Tight Junction Modulation by Calcium Depletion

## 5.1 Introduction

The presence of calcium in the extracellular environment of epithelial cells is essential for the maintenance of barrier function of the epithelium (1), with extracellular calcium depletion inducing opening of the cellular tight junctions (TJs) (2). The crucial role of extracellular calcium in regulating the TJ barrier function has been demonstrated in studies using different cell lines. Incubation of MDCK (Madin-Darby Canine Kidney) epithelial cells with a calcium-free medium containing a calcium-chelating agent prevented the formation of TJs (3) and incubation of confluent MDCK layers in a calcium-free solution resulted in increased TJ permeability (4, 5).

*In vitro* studies investigating the effects of extracellular calcium on TJs have often employed calcium-chelating compounds such as ethylenediaminetetra-acetic acid (EDTA) and ethylene glycol tetra-acetic acid (EGTA). The use of these agents has been demonstrated to result in opening of the TJs (6, 7) and an increased paracellular permeability of drug molecules (8, 9). For example, Tomita *et al.* (16) demonstrated that application of EDTA (0.25% w/v) to Caco-2 cell monolayers was associated with an increase in FD4 permeability, which was suppressed, concentration-dependently,

by addition of $CaCl_2$. Raiman *et al.* (17) assessed the effect of EGTA on the translocation of clodronate across Caco-2 monolayers. The transport experiments were performed in a medium containing normal calcium concentration (1.3 mM) and minimal calcium levels (calcium-free apically and 100 μM basolaterally). In the medium with normal calcium concentration, a strong improvement in permeability (190-fold and 130-fold for 1 mM and 10 mM clodronate, respectively) was observed with EGTA (2.5 mM). When the transport experiment was performed in medium containing a minimal calcium concentration, EGTA did not show such a potent effect on the permeability of clodronate, with observed permeability enhancement factors between 2 and 20.

The intracellular processes involved in extracellular calcium modulation of the TJ barrier have been examined by Ma *et al.* (10). In their study, incubation of filter-cultured Caco-2 monolayers in a calcium-free solution (modified Krebs-buffer solution containing no calcium and 1 mM EGTA), added on both apical and basolateral chambers resulted in a rapid drop in TEER (to <25% of the baseline value within 10 min) and an increase in the permeability of paracellular markers mannitol and inulin, indicating TJ opening. The increase in permeability was rapidly reversible with reintroduction of calcium (1.8 mM) into the incubation medium. Extracellular calcium removal produced a rapid centripetal retraction of the TJ proteins, as visualized by immunofluorescence/confocal microscopy, with formation of large paracellular openings between the adjoining cells, which was rapidly reversed by re-introduction of extracellular calcium.

As a result of a well-demonstrated effect of extracellular calcium depletion on TJ

modulation, different compounds with a capacity to bind calcium, reducing its extracellular levels, have been investigated for their potential to improve the mucosal absorption of macromolecules through the paracellular route. The use of older generation 'classical' absorption enhancers such as EDTA and EGTA is generally limited to *in vitro* experimental situations. This is as a result of their local intolerability, possibly related to a membrane damaging effect, and the possibility that they may penetrate into the cells where they interact with the intracellular calcium, causing cellular damage or even cell death (18). However, more recently, the absorption-enhancing mode of action of various compounds based on polymeric molecules has been attributed to extracellular calcium depletion. These compounds include carboxylic acid-containing polymers (11) such as poly(Acrylic acid) (PAA) and its derivatives (12).

Although the importance of extracellular calcium in maintaining the barrier property of the epithelium has been established long ago and the mechanisms involved in TJ modulation by extracellular depletion have been relatively well characterized (as discussed above), the conditions under which extracellular calcium depletion produces pronounced opening of the TJs are unclear from the literature. For example, it is not apparent whether lowering/exhausting calcium on the luminal side of the mucosal surfaces only, produces meaningful effects on TJs, whereby mucosal absorption of therapeutic macromolecules would be improved. Furthermore, with a newer generation of absorption enhancers based on calcium-binding polymers, there is insufficient evidence to clearly suggest that their absorption-promoting effect is wholly due to calcium depletion. Present work therefore attempts to address these points by investigating the settings in which depletion of extracellular calcium leads

to obvious effects on TJs and assessing the permeability-enhancing potential of a calcium-binding polymeric compound, PAA.

Present work investigated the effect of calcium depletion on the apical or basolateral, or both sides of confluent Calu-3 cell layers, on TEER and permeability of macromolecules (FITC-dextrans, FDs). Furthermore, changes in calcium levels following an initial depletion (achieved by different means) were also investigated using a fluorescent calcium-sensing probe. Calcium depletion was produced through the use of a calcium-free HBSS (CFHBSS) and EDTA. The effects of PAAs as a model polymeric compound shown to bind calcium, resulting in its depletion, were also investigated. For the purpose of corroboration, some experiments were additionally conducted on Caco-2 monolayers.

## 5.2 Methods

### 5.2.1 Cell culture

Calu-3 and Caco-2 cells were cultured (on flasks and filters) according to the protocols detailed in Chapter 2 (section 2.2.1).

### 5.2.2 Effect of calcium-free medium on TJ modulation

*5.2.2.1 Effect of CFHBSS on TEER*

Baseline TEER was measured after culture medium (EMEM and DMEM for Calu-3 and Caco-2 cells, respectively) was replaced with HBSS and an equilibration period of approximately 45 min was allowed. Following this, the experiments were conducted in three different ways:

1) HBSS was removed from both *apical and basolateral* sides of Calu-3 layers and replaced with CFHBSS. Cells were incubated with CFHBSS for 30 min, 60 min or 90 min, following which CFHBSS was removed and replaced with HBSS. TEER was measured at regular time intervals while cells were exposed to both, CFHBSS and HBSS.

2) HBSS solution was removed from the *apical* side of Calu-3 and Caco-2 layers and replaced with CFHBSS (i.e. cells were exposed to CFHBSS on their apical surface only). TEER was subsequently measured at regular intervals (every 30 minutes) for 3 hours.

3) In Caco-2 monolayers, HBSS was replaced with CFHBSS on both apical and basolateral sides and TEER was measured every 30 min for 3 hours.

It must be noted that CFHBSS used in this work was also $Mg^{2+}$-free. To establish whether the deficiency in $Mg^{2+}$ affected the TEER, control experiments were performed by incubating the cell layers with CFHBSS (Calcium/$Mg^{2+}$-free HBSS), supplemented with calcium (more specifically, CFHBSS was supplemented with 140 mg/L $CaCl_2$, which is found in HBSS) and measuring the effect of this solution on cell layer TEER.

*5.2.2.2 Effect of CFHBSS on permeability of FDs*

Permeability experiments were conducted in confluent cell layers (previously equilibrated in HBSS) in the following ways:

1) The effect of *apical* calcium depletion on FD4 permeability was measured by application of FD4 in CFHBSS (500 μg/ml) to the apical side of the cell layers, following which basolateral solution (HBSS) was sampled regularly (every 30 min) for 3 hours. The sampled volumes were immediately replaced with fresh HBSS.

2) Solution of FD4 in CFHBSS (500 μg/ml) was applied to the apical side of confluent Calu-3 layers as previously. However, this solution was replaced with fresh FD4/CFHBSS every 30 minutes. FD4 permeability was measured by sampling the basolateral solution (HBSS) at regular intervals as previously. The control experiment was in this instance conducted by replacing the apical solution, which consisted of FD4 in HBSS (500 μg/ml) every 30 min. Note that in this scenario the permeability coefficient ($P_{app}$) values could not be calculated as FD4 was removed and re-applied to the cells throughout the experiment. Therefore, for the purpose of this experiment, permeability is expressed as the cumulative FD4 amount traversing the layers.

### 5.2.3 Effect of EDTA on TJ modulation

*5.2.3.1 Effect of EDTA on TEER*

EDTA stock solution (0.5% w/v) was prepared by dissolving EDTA in HBSS (pH 8.0). EDTA (0.125% w/v in HBSS) was applied to the apical side of confluent Calu-3 and Caco-2 monolayers, which were previously equilibrated in HBSS (for approximately 45 min). Application of EDTA was followed by periodic

measurements of TEER (every 30 min for 3 hours), following which EDTA solution was removed and cells washed. Culture medium appropriate for the cell line was added to the cells and TEER measurements were also conducted 24 hours after the application of EDTA in order to measure cell recovery.

In a separate experiment, EDTA (0.125% w/v in HBSS) was applied to either the apical side or the basolateral side of confluent Caco-2 monolayers (previously equilibrated in HBSS). TEER was subsequently recorded periodically (every 30 min) for 3 hours.

*5.2.3.2 Effect of EDTA on permeability of FD4*

Effect of apical or basolateral addition of EDTA to confluent Calu-3 or Caco-2 layers on apical-to-basolatereal permeability of FDs was measured in the following ways:

1) EDTA was applied to the apical side of the cell layers in conjunction with FD4; final apical concentrations were 0.125% w/v and 500 μg/ml for EDTA and FD4, respectively (both in HBSS). Basolateral, solution was then sampled periodically for 3 hours.

2) EDTA solution (0.125% w/v in HBSS) was applied on the basolateral side of Calu-3 cell layers, whereas FD4 (in HBSS, at 500 μg/ml) was added on the apical surface of the cells. Apical-to-basolateral FD4 permeability was measured by regular sampling of the basolateral solution. The sampled solutions were immediately replaced with solutions containing EDTA 0.125% w/v in HBSS in order to maintain

sink conditions and basolateral concentration of EDTA constant throughout the experiment.

### 5.2.4 Effect of EDTA on cell metabolic activity: MTS assay

Calu-3 cells were seeded and cultured on 96-well plates according to the protocol described in Chapter 2 (section 2.2.5.3). Culture medium was removed and replaced with solutions of varying concentrations of EDTA (0.5%, 0.25%, 0.125% and 0.0625% w/v) in HBSS. Triton X-100 (0.1% v/v in HBSS) and HBSS were used as the positive and negative controls, respectively. Cells were incubated with EDTA solutions and the controls for 2 hours, following which the MTS assay was conducted following the protocol detailed on (section 2.2.5.3).

### 5.2.5 Changes in calcium levels following application of CFHSS and EDTA

*5.2.5.1 Changes in apical calcium levels with apical CFHBSS*

Confluent cell layers were equilibrated in HBSS for approximately 45 min prior to the addition of CFHBSS or EDTA in all cases. Changes in calcium levels in the apical medium were measured in the following way: CFHBSS or EDTA (0.125% w/v in HBSS or in CFHBSS) was added to the apical surface of the cell layers (with HBSS present on the basolateral side). The apical solution was subsequently withdrawn (50 µl volumes) regularly for a period of three hours and transferred onto a black 96-well plate. The calcium-sensing fluorescent probe, Fluo-4, was then applied (10 µM) to the sampled apical solutions and fluorescence was measured (485 nm excitation, 535 nm emission) using an MFX microtiter plate fluorometer (Dynex Technologies, USA). Cell layers incubated with HBSS (on apical and basolateral sides) served as a control,

with the apical solution removed at the beginning and at the end of the experiment and incubated with Fluo-4 for fluorescence determination.

*5.2.5.2 Changes in basolateral calcium with apical EDTA*

The change in *basolateral* calcium level following application of EDTA to the *apical* side of the cell layers was measured by applying EDTA (0.125% w/v) in HBSS to the apical side surface and sampling the basolateral medium (HBSS) at regular intervals. Fluo-4 was then added to the sampled solutions and fluorescence determined in the same way as in the preceding section. Control experiments were performed by measuring Fluo-4 fluorescence of basolateral solutions consisting of HBSS and EDTA in HBSS (0.125% w/v) (with apical HBSS in both cases).

### 5.2.6 Effect of polyacrylic acids of varying $M_W$s on TJ modulation

*5.2.6.1 Changes in TEER*

Stock solutions of polyacrylic acids (PAAs) of 125 kDa and 250 kDa were diluted in HBSS to a concentration of 0.25% w/v (pH 5.8) and applied to the apical side of confluent Calu-3 layers previously equilibrated in HBSS. This was followed by regular TEER measurements over 80 min. PAA solutions were removed from the cell layers after 80 min and cells washed with PBS. Culture medium was then added to the apical and basolateral sides of the cells and TEER was measured at 110 min, 140 min and 170 min in culture medium in order to determine TEER recovery. Control experiment was conducted by following similar experimental conditions as above, with the exception that HBSS (pH 5.8) was applied to the cells instead of PAA. Changes in TEER are reported as % relative to the baseline value, measured prior to sample addition.

*5.2.6.2 Effect of PAAs on FD4 permeability*

FD4 was added to the apical side of confluent Calu-3 layers in conjunction with solutions containing PAAs of 125 kDa, 250 kDa and 450 kDa. Both FD4 and PAAs of varying $M_W$s were dissolved in HBSS and applied to cells at concentrations of 500 μg/ml and 0.25% w/v, respectively (at a final solution pH of 5.8). FD4 permeability was determined over 3 hours, with regular sampling of the basolateral solution, as described previously.

## 5.3 Results

### 5.3.1 Effect of calcium-free medium on TJ modulation

*5.3.1.1 Effect of CFHBSS on TEER*

Figure 5.1 shows changes in TEER resulting from the application of CFHBSS to the *apical* and *basolateral* sides of Calu-3 layers. A sharp decrease in TEER following the incubation of cells with CFHBSS was apparent. A small decrease in TEER was also observed 5 min after the application of CFHBSS even for control cell layers (incubated with CFHBSS, supplemented with $CaCl_2$). However, in cells incubated with CFHBSS, TEER continued to decrease with time, reaching the lowest points (54%, 26% and 20% of the baseline value with cell layers incubated with CFHBSS for 30 min, 60 min and 90 min, respectively) at the measurement points prior to replacement of CFHBSS with HBSS. The TEER of control cells (those incubated with CFHBSS, supplemented with $CaCl_2$) on the other hand started to increase after the first measurement, reaching levels similar to the baseline value within 1 hour. The magnitude of TEER decrease was dependent on the time during which Calu-3 layers were incubated with CFHBSS, with more prominent decrease in TEER with longer

incubation with CFHBSS. Following the replacement of CFHBSS with HBSS, TEER started to increase in all cases. Measurement at 180 min, showed that TEER of cell layers previously incubated with CFHBSS reached levels similar or close to those of control.

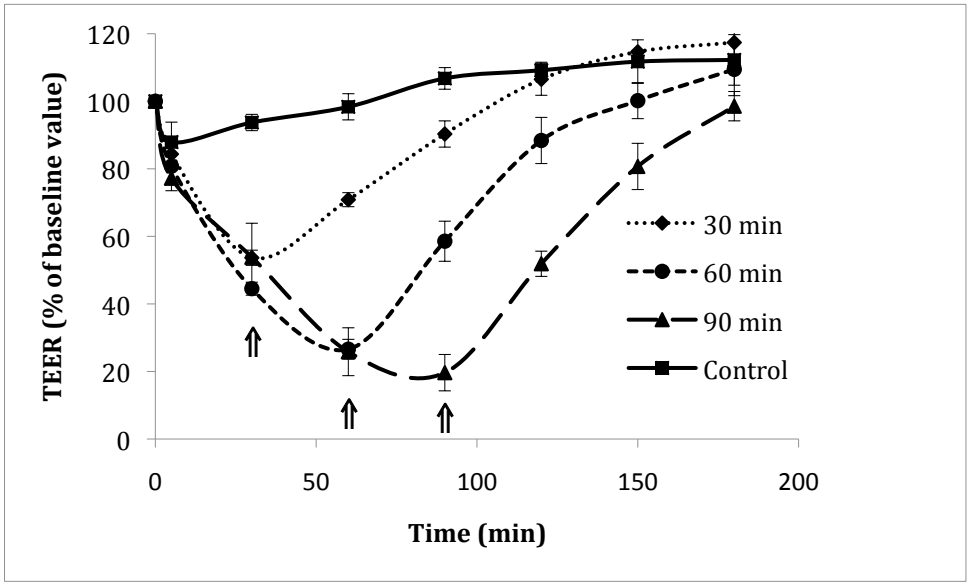


***Figure 5.1. Effect of CFHBSS, applied on the apical and basolateral sides of Calu-3 layers, on TEER. Arrows indicate replacement of CFHBSS with HBSS. Control represents cell layers incubated with CFHBSS supplemented with $CaCl_2$. TEER expressed as % relative to the baseline value. Results presented as the mean ± SD (n=3).***

Application of CFHBSS to the apical side of Calu-3 layers, while (calcium-containing) HBSS was present on the basolateral surface also produced measurable changes in TEER. The TEER pattern, illustrated in Figure 5.2 shows that apical addition of CFHBSS resulted in a drop of TEER to 42% of the baseline value, 30 min following its application. However, succeeding measurements revealed that this initial drop in TEER was followed by an increase, with measurements at 180 min reaching 97% of the baseline value. With regards to control cell layers, there was an initial

decrease in TEER amounting to 19% (i.e. TEER decreased to 81% of the baseline value), but subsequently this recovered to levels >100% of the baseline value.

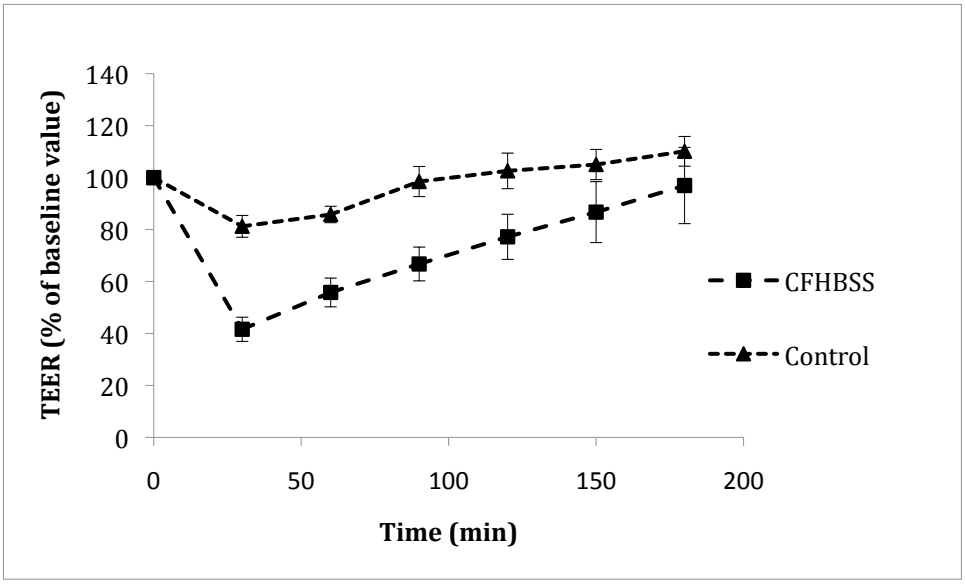


***Figure 5.2. TEER changes resulting from addition of CFHBSS to the apical side of Calu-3 layers. Control represents cell layers incubated with $CaCl_2$-supplemented CFHBSS. TEER expressed as % relative to the baseline value. Results presented as the mean ± SD (n=3).***

Using confluent Caco-2 monolayers, effects of CFHBSS application to the apical, or both apical and basolateral sides of the cells on TEER were further measured. The results, shown in Figure 5.3, show that both conditions produced an initial reduction of TEER, with application of CFHBSS to both apical and basolateral sides producing a somewhat larger effect. Addition of CFHBSS to the apical monolayer side only (with HBSS present on the basolateral chamber) resulted in a decrease of TEER to approximately 33% of the baseline value, while application of CFHBSS on both sides (apical and basolateral) produced a drop in TEER to levels approximating 25% of the baseline value, as measured 30 min following its application. However, subsequent measurements revealed an increase in TEER with time in cell monolayers exposed to CFHBSS apically only, with the measurement conducted at 180 min reaching 63% of the baseline TEER. On the other hand, in Caco-2 monolayers exposed to CFHBSS on

both apical and basolateral surfaces, TEER continued to drop to low levels of approximately 5% of the baseline value at 90 min, after which no further decrease was observed. In control cell monolayers incubated with HBSS, there was a 10% decrease in TEER at 30 min, but subsequent measurements revealed that the resistance remained stable (within 5% of the baseline value) throughout the experiment.

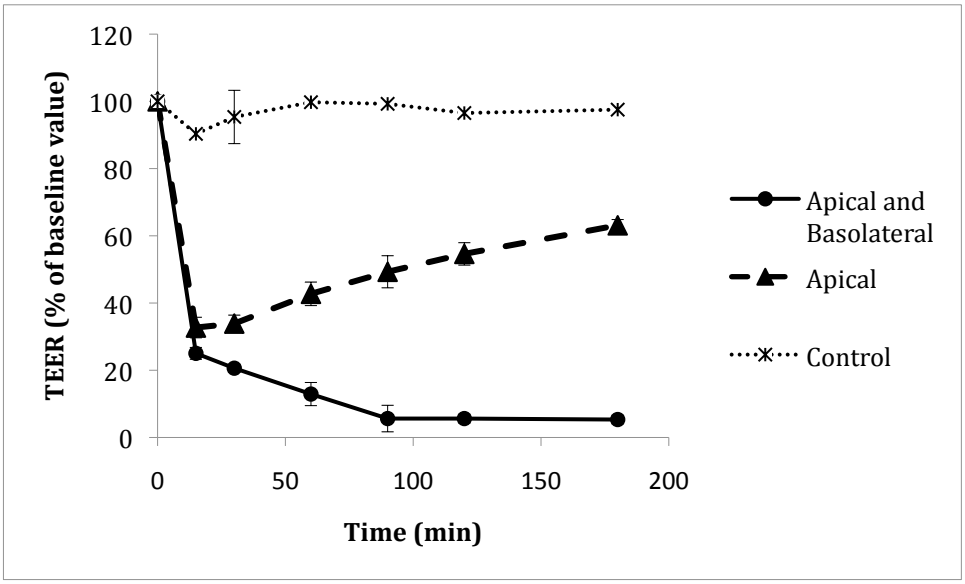


***Figure 5.3. Changes in TEER of Caco-2 monolayers following application of CFHBSS to the apical side only or both apical and basolateral sides. Control cell monolayers were incubated with HBSS. TEER expressed as % relative to the baseline value. Results presented as the mean ± SD (n=3).***

*5.3.1.2 Effect of CFHBSS on permeability of FDs*

The impact of calcium exhaustion by addition of CFHBSS apically on the permeability of FD4 across Calu-3 and Caco-2 layers (measured over a period of 3 hours) is depicted in Figure 5.4. There was a small (approximately 1.8-fold), but significant ($p=0.001$) increase in FD4 permeability across Calu-3 cell layers with apical CFHBSS compared to control (5.4a). A similar effect was observed in Caco-2 monolayers (5.4b), with apical CFHBSS giving rise to the same extent of increase in

FD4 permeability (approximately 1.8-fold, which was statistically significant, p=0.007) as in Calu-3 layers.

**a)**

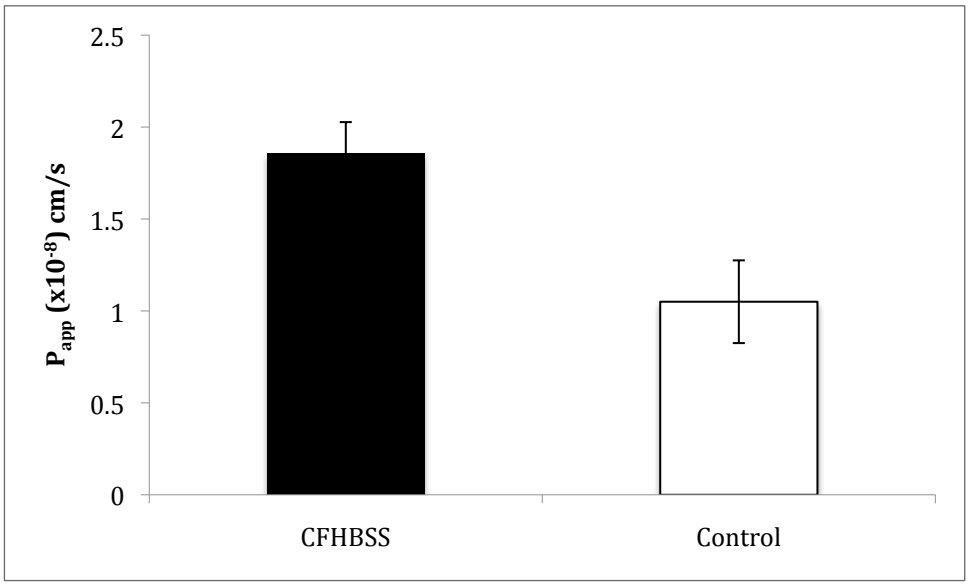


**b)**

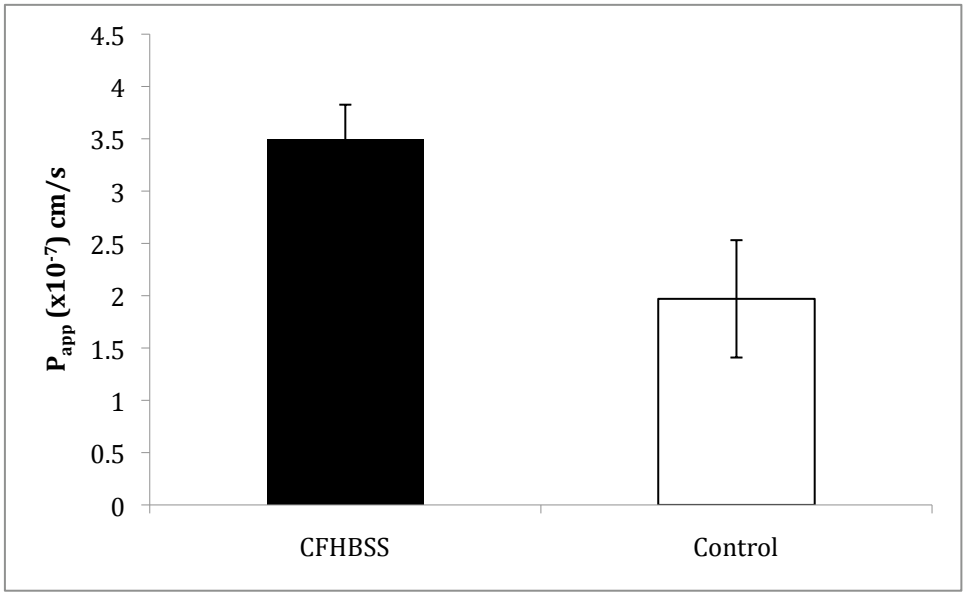


***Figure 5.4. Effect of apical CFHBSS on permeability of FD4 across cell layers. a) Calu-3 layers, and b) Caco-2 cell monolayers. Control represents FD4 permeability in HBSS. FD4 permeability expressed as apparent permeability ($P_{app}$), calculated in the manner described in section 2.2.4. Results presented as the mean ± SD (n=3).***

Regular replacement of the penetrant solution consisting of FD4 in CFHBSS on the apical surface of Calu-3 layers resulted in an increase of FD4 permeability compared to control (regularly replaced FD4/HBSS), as shown in Figure 5.5. Periodic measurement of FD4 in the basolateral solution demonstrated an increase in its amount with time when applied apically in both, CFHBSS and HBSS (control). However, accumulation of FD4 in the basolateral solution was observed to occur at a greater rate (0.52 μg/hour) following its apical addition in CFHBSS, which was replaced with fresh FD4/CFHBSS every 30 min compared to its application in (calcium-containing) HBSS (0.16 μg/min) (also replaced regularly to allow comparison), amounting to a 3.3-fold difference.

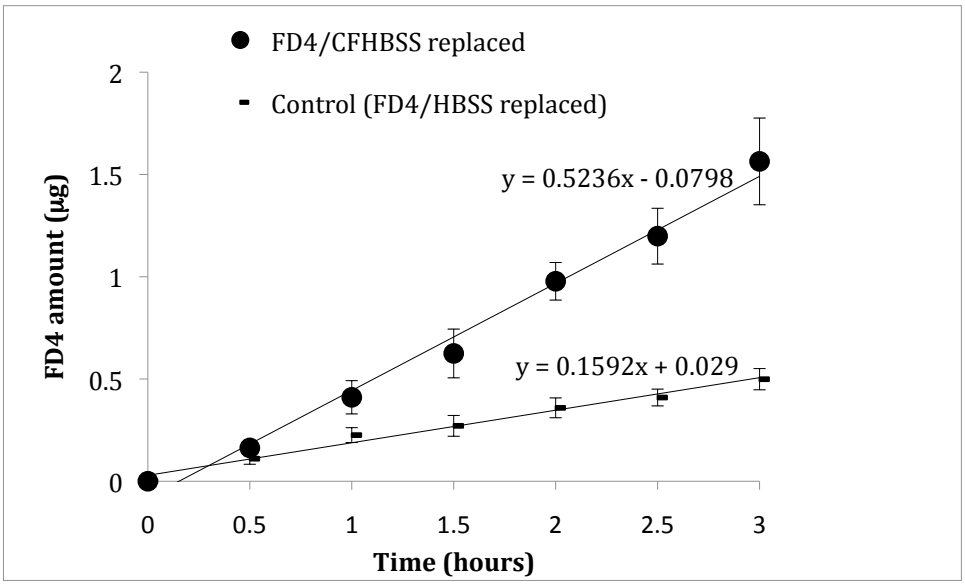


***Figure 5.5. FD4 permeability across Calu-3 layers subjected to regular replacement of apical penetrant solution consisting of FD4 dissolved in CFHBSS or HBSS (control). Results shown as amount of FDs (μg) accumulated in the basolateral chamber with time. Results presented as the mean ± SD (n=3).***

### 5.3.3 Effect of EDTA on TJ modulation

*5.3.3.1 Effect of EDTA on TEER*

A marked reduction of TEER with time was observed in the cell layers of both Calu-3 and Caco-2 cell lines following the application of EDTA to the apical side of the cells (Figure 5.6). The largest drop in TEER occurred at the measurement point of 30 min and was somewhat larger in Calu-3 layers (to 22% of the baseline value) compared to Caco-2 cells (to 28% of the baseline TEER). Thereafter, TEER decreased at a lower rate (from 22% to 17% and from 28% to 15% of the baseline value in Calu-3 and Caco-2 monolayers, respectively). Measurements at 24 hours following the application of EDTA to cells revealed that TEER reverted back to values similar to the baseline figure (±10%) in both Calu-3 and Caco-2 layers.

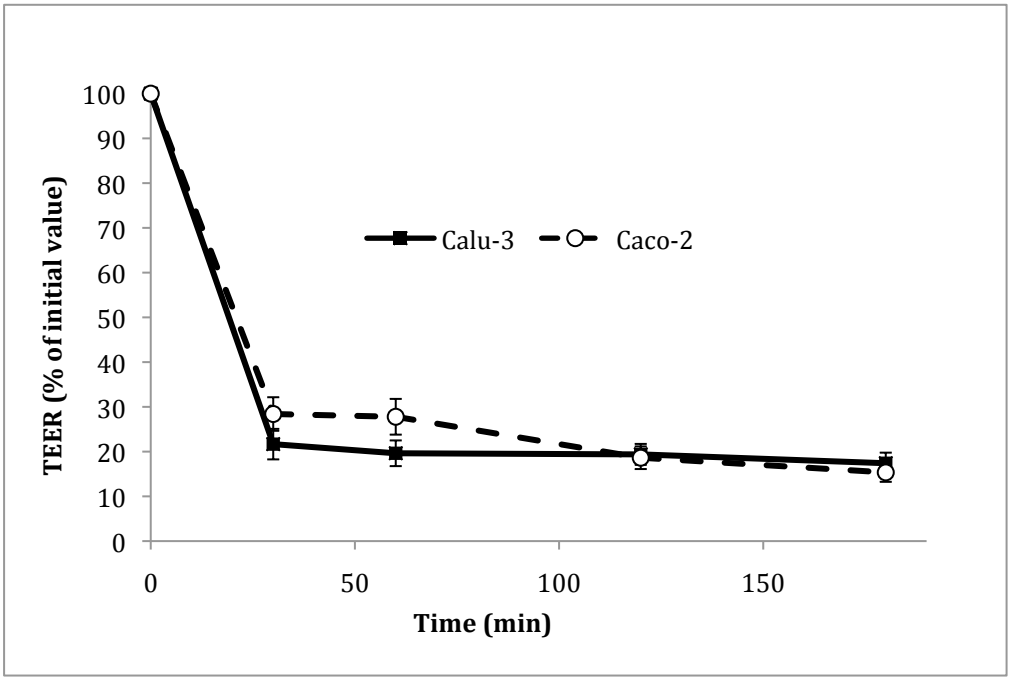


***Figure 5.6. Effect of apical addition of EDTA (0.125% w/v in HBSS) on TEER of Calu-3 and Caco-2 layers. TEER shown as % of the baseline value (prior to EDTA application). Results presented as the mean ± SD (n=3).***

Figure 5.7 compares the effects of apical and basolateral addition of EDTA (0.125% w/v in HBSS, pH 7.4, in both cases) on TEER of Caco-2 cell layers. Both apical and basolateral application of EDTA resulted in a decrease in TEER, with a steeper initial drop (observed in the first 15 min) obtained following the addition of EDTA on the apical surface of the cells. At measurement intervals of 60 min and 90 min following EDTA application, TEER reached similar values at 60 min, which amounted to approximately 35% and 40% of the baseline value with apical and basolateral EDTA, respectively. However, reductions in TEER at later measurement points were more prominent with basolateral EDTA, with a lower minimum TEER level (at 180 min) seen with basolateral EDTA (11% of the baseline value) compared to apical EDTA (23% of baseline TEER). Recordings of TEER 24 hours following the exposure of cells to EDTA revealed its reversibility to 93% and 132% of the baseline TEER for Caco-2 monolayers incubated with EDTA on the apical and basolateral surface, respectively.

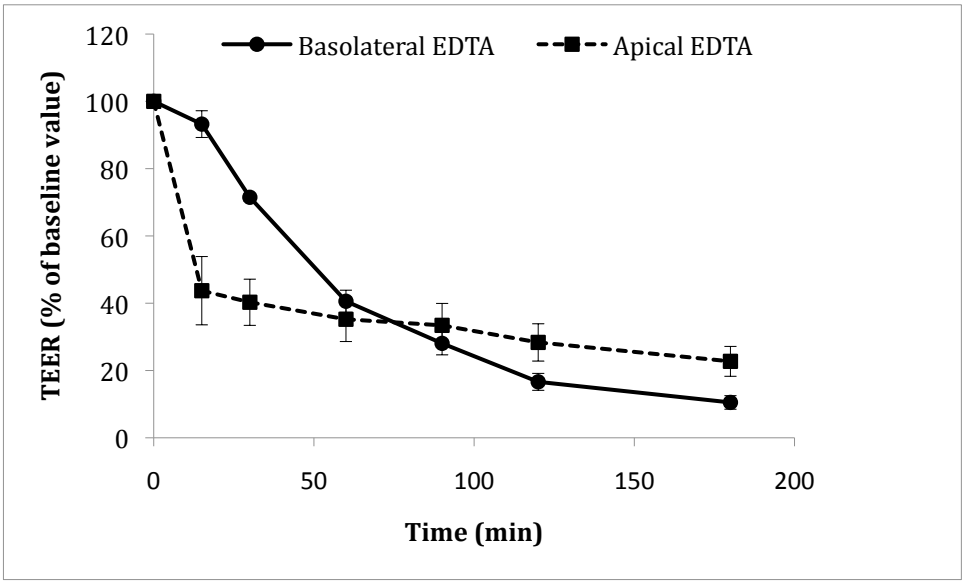


***Figure 5.7. Changes in TEER following the application of EDTA (0.125% w/v in HBSS) to the apical or basolateral side of Caco-2 monolayers. TEER shown as % of the baseline value. Results presented as the mean ± SD (n=3).***

*5.3.3.2 Effect of EDTA on the permeability of FD4*

Application of EDTA to the apical side of Calu-3 and Caco-2 layers resulted in a significant increase in FD4 permeability across the cell layers (Figure 5.8). In Calu-3 cells, this increase amounted to approximately 7-fold compared to control (5.8a), whereas the enhancement in FD4 permeability across the Caco-2 cell monolayers with EDTA was approximately 8-fold in comparison to control (5.8b).

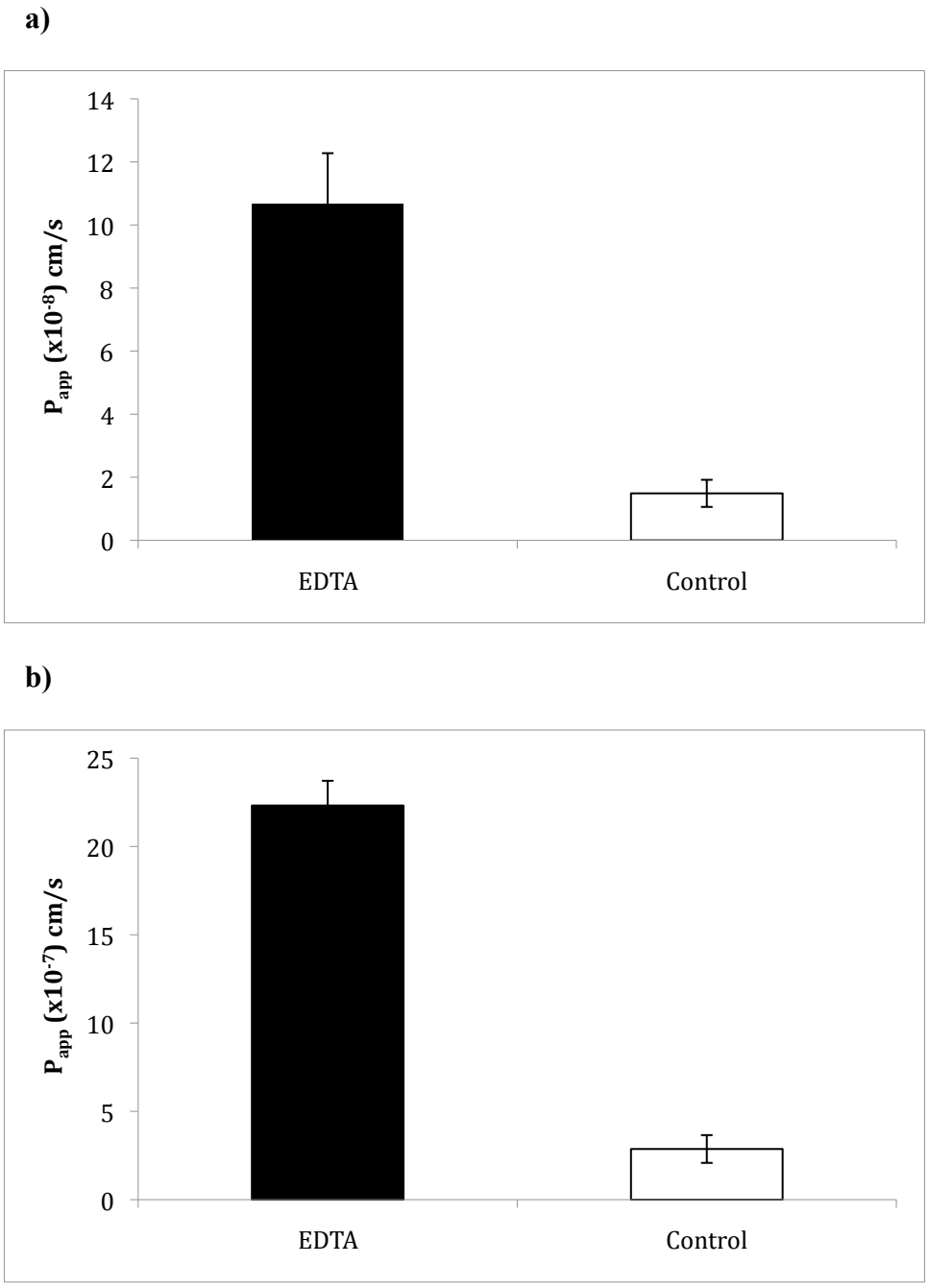


***Figure 5.8. FD4 permeability enhancement with EDTA. Permeability measured across Calu-3 layers (a) and Caco-2 monolayers (b). EDTA was added apically at 0.125% w/v in HBSS (pH 7.4). Control represents FD4 permeability when applied in HBSS (pH 7.4) in the absence of EDTA. FD4 permeability is expressed as apparent permeability coefficient ($P_{app}$), calculated using the equation shown in section 2.2.4. Results are presented as the mean ± SE; (n=4 and 3 for Calu-3 and Caco-2 layers, respectively).***

Figure 5.9 compares apical-to-basolateral FD4 permeability observed with application of EDTA to the apical, or basolateral sides of Calu-3 layers (0.125% w/v in both cases). Both apical or basolateral addition of EDTA produced an increase in FD4 permeability as compared to control (FD4 permeability in the absence of EDTA). However, addition of EDTA to the basolateral side induced a markedly greater permeability enhancing effect (45-fold compared to control) than apical EDTA (15-times higher than the control in the current experiment).

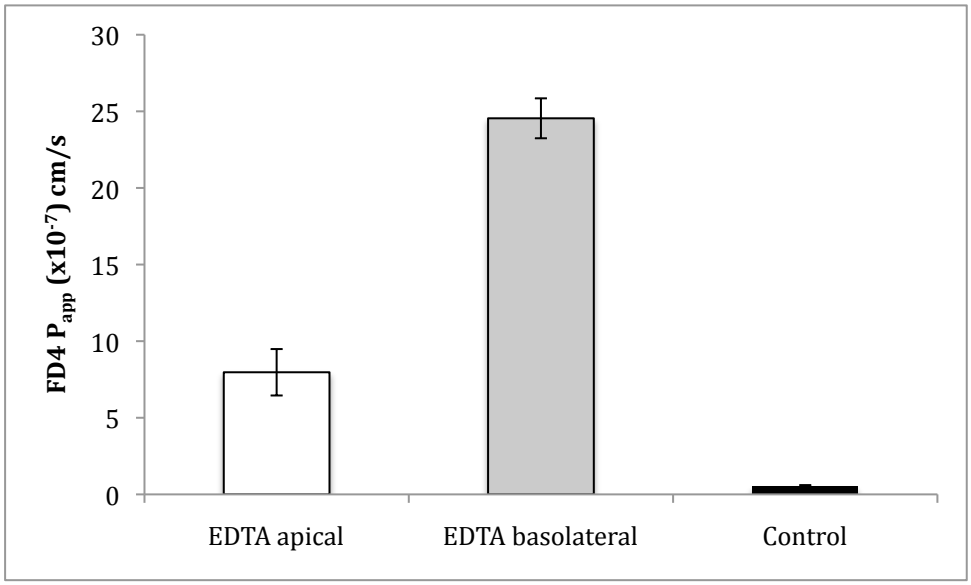


***Figure 5.9. Effect of apical or basolateral EDTA on FD4 permeability across Calu-3 layers. Cells were incubated with 0.125% w/v EDTA (in HBSS, pH 7.4) on the apical or basolateral sides. FD4 added on the apical side only. Control represents FD4 permeability in HBSS (pH 7.4) in the absence of EDTA. FD4 permeability is expressed as apparent permeability coefficient ($P_{app}$), calculated using the equation shown in section 2.2.4. Results are presented as the mean ± SE (n=3).***

### 5.3.4 Effect of EDTA on cell metabolic activity: MTS assay

EDTA exhibited a dose-dependent reduction in relative metabolic activity of Calu-3 cells, ranging from 22% with 0.0625% w/v to 92% with 0.5% w/v (applied in HBSS, pH 7.4), as determined by the MTS assay after 2-hour exposure. The concentration of EDTA used in TEER and permeability experiments (0.125% w/v) caused a 39% decrease in relative metabolic activity. The results are presented in Figure 5.10.

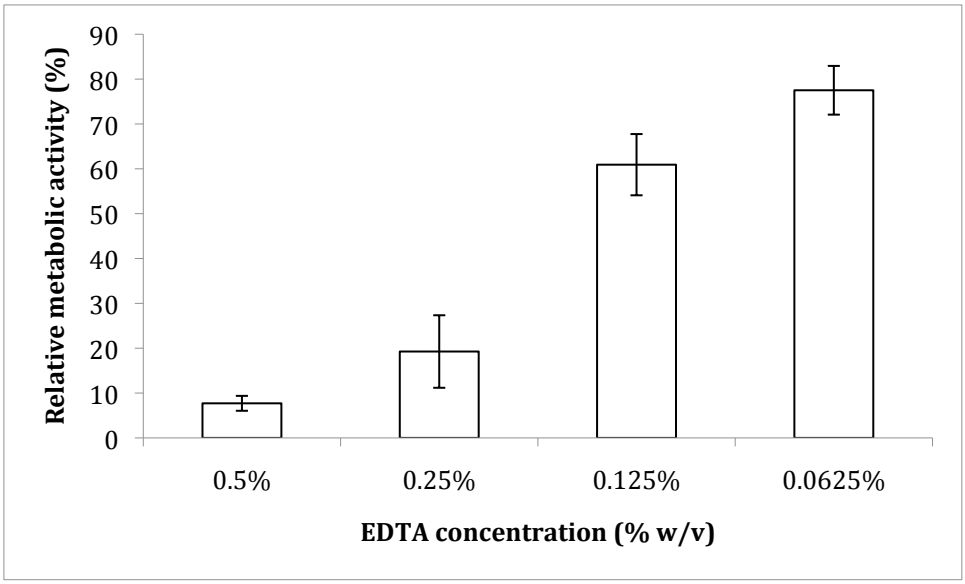


***Figure 5.10. Effect of varying concentrations of EDTA on Calu-3 metabolic activity as determined by the MTS assay. EDTA was applied to the cells at 0.0625, 0.125%, 0.25% and 0.5% w/v (in HBSS, pH 7.4) Results are expressed as relative metabolic activity, calculated in the manner described in section 2.2.5.3. Data presented as the mean ± SD (n=4).***

### 5.3.5 Changes in calcium levels following application of CFHBSS and EDTA

*5.3.5.1 Changes in apical calcium levels with apical CFHBSS*

Changes in fluorescence intensity of the calcium-sensing probe, Fluo-4, following its incubation with different solutions present on the apical side of Calu-3 layers, which were sampled at different time intervals, are shown in Figure 5.11. The apical solutions consisted of CFHBSS, 0.125% w/v EDTA in CFHBSS, 0.125% w/v EDTA in HBSS or HBSS. 5 min following the addition of CFHBSS to the apical side of the

cell layers, the fluorescence intensity of Fluo-4 was 3-fold lower in cells incubated with CFHBSS compared to the cells exposed to HBSS. However, Fluo-4 fluorescence intensity increased gradually with time eventually reaching a plateau at time 90 min, with no further significant increases beyond this time point. In sharp contrast, the fluorescence intensity of Fluo-4 incubated with apical samples containing EDTA (in HBSS, or CFHBSS) was significantly lower (up to approximately 30 and 50 times lower, respectively). In these scenarios, Fluo-4 fluorescence intensity remained at these low levels at all time points.

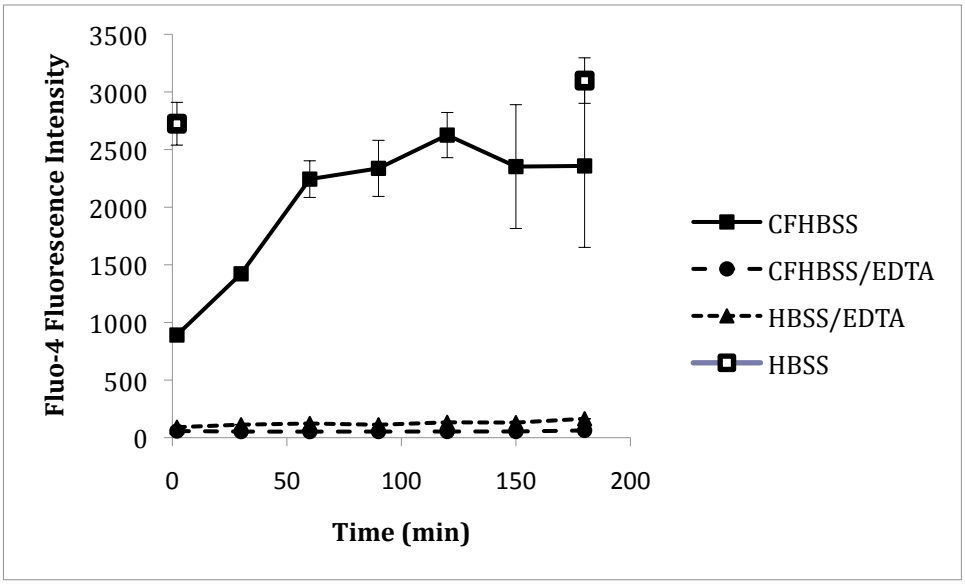


***Figure 5.11. Changes in fluorescence intensity of the calcium-sensing probe, Fluo-4, following its addition to apical solutions. These consisted of CFHBSS, CFHBSS/EDTA, HBSS/EDTA and HBSS, and were present on the apical side of Calu-3 layers for 3 hours, with sampling every 30 min. Results presented as the mean ± SD (n=3).***

*5.3.5.2 Changes in basolateral calcium with apical EDTA*

The effect of EDTA addition to the *apical* surface of Calu-3 cell layers on fluorescence intensity of Fluo-4 incubated with solutions sampled from the *basolateral* compartment (indicating basolateral calcium levels) is shown in Figure 5.12. There was no change in the fluorescence intensity of Fluo-4 incubated with basolateral solutions sampled in the first hour following the application of EDTA to the apical side of the cell layers. However, measurements at subsequent time intervals revealed a decrease in Fluo-4 fluorescence intensity, with levels measured at 180 min amounting to 75% of the initial value (measured at 5 min) or 69% of control cell layers (incubated with HBSS), measured at the same interval. In cell layers incubated with HBSS (control) the fluorescence intensity of basolateral solutions sampled at different intervals (and incubated with Fluo-4) remained high (approximately 2100-2200) and relatively constant. On the other hand, basolateral solutions consisting of HBSS/EDTA had low fluorescence intensity, ranging between 122-285.

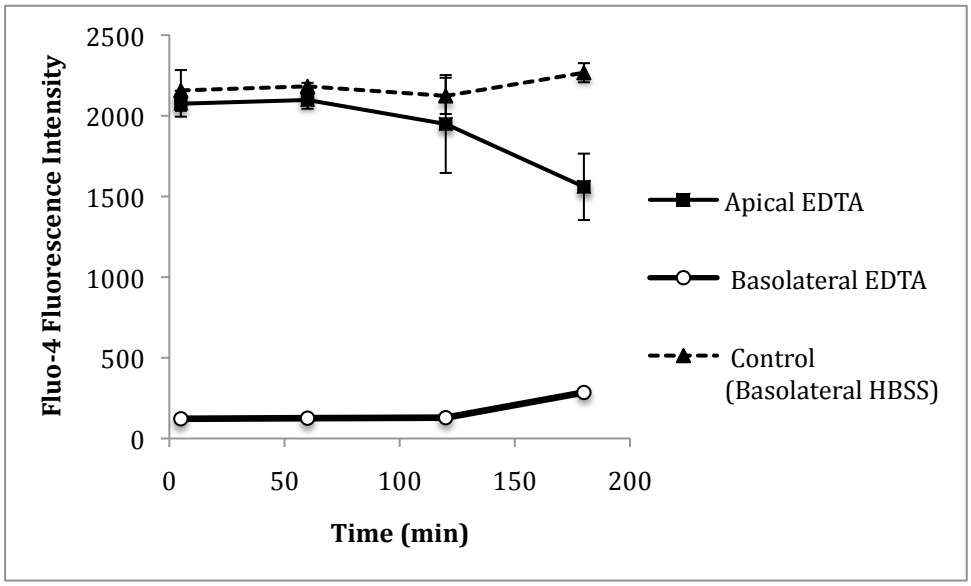


***Figure 5.12. Changes in fluorescence intensity of the calcium-sensing probe, Fluo-4, following its incubation with basolateral solutions. These were sampled at different intervals and consisted of HBSS while EDTA (in HBSS, 0.125% w/v) or HBSS (control) was present on the apical side of cell layers, or EDTA (in HBSS, 0.125% w/v) with HBSS on the apical side. Results presented as the mean ± SD (n=3).***

### 5.3.6 Effect of polyacrylic acids (PAAs) of varying $M_W$s on TJ modulation

*5.3.6.1 Changes in TEER*

Changes in TEER measured across the Calu-3 layers following the addition of PAA 100 kDa and PAA 250 kDa on the apical side of the cells is illustrated Figure 5.13. Application of both PAAs resulted in a reduction of TEER to approximately 71-77% and 59-77% of the baseline value for PAA 100 kDa and 250 kDa, respectively. The reduction in TEER was sustainable for the duration of cell incubation with PAA samples and started to revert back to baseline values following the replacement of PAA solutions with HBSS at 80 min. Subsequent TEER measurements (after the replacement of samples with the culture medium) revealed its recovery to 79% and

100% of the baseline value for PAA 100 kDa and 250 kDa, respectively, within 3 hours of their application.

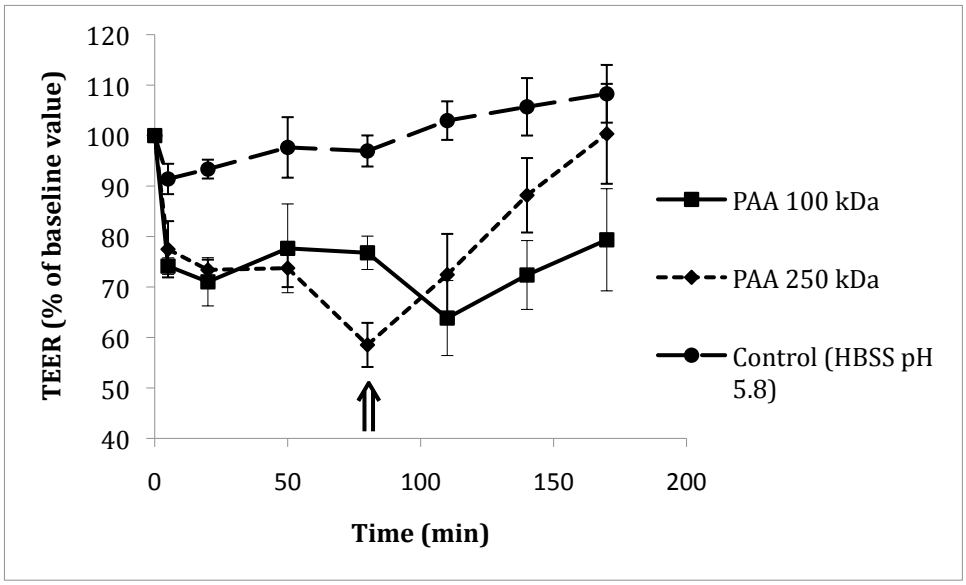


***Figure 5.13. Effect of PAAs on Calu-3 layer TEER. PAAs were applied to cells at pH 5.8 (0.25% w/v in HBSS). Arrow indicates removal of PAA samples, cell washing and application of the culture medium. Results expressed as % relative to the baseline value (before sample application). Data presented as the mean ± SD (n=3).***

*5.3.6.2 Effect of PAAs on FD4 permeability*

FD4 permeability following its application to the apical surface of Calu-3 layers in conjunction with one of the three tested PAAs is shown in Figure 5.14. It is apparent from the figure that PAAs produced an insignificant increase in FD4 permeability compared to control.

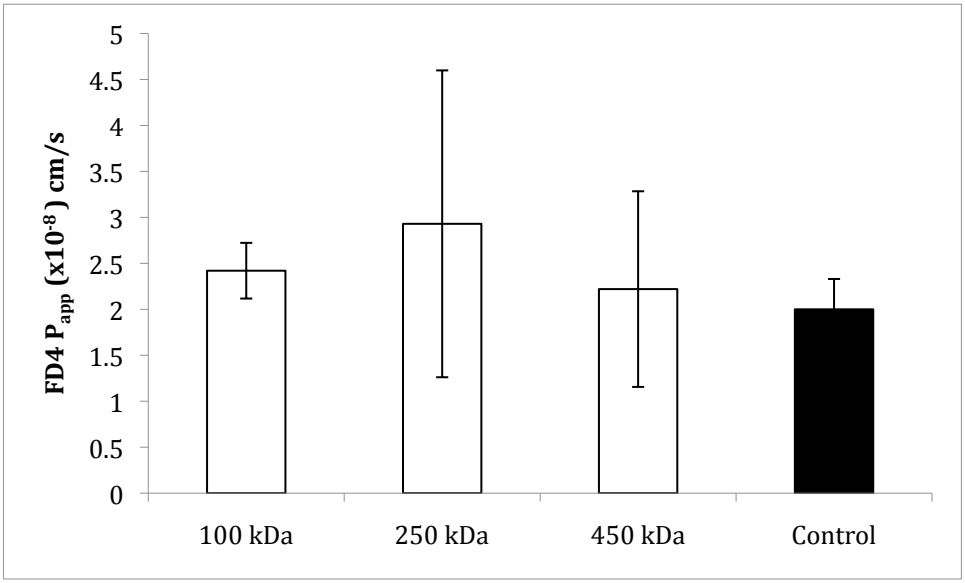


***Figure 5.14. Effect of PAAs on FD4 permeability across Calu-3 layers. PAAs of varying $M_W$s (100 kDa, 250 kDa and 450 kDa) were applied to cells at 0.25% w/v (in HBSS at pH 5.8). Control represents FD4 permeability in HBSS (pH 5.8). FD4 permeability expressed as apparent permeability coefficient ($P_{app}$), calculated using the equation shown in section 2.2.4. Results presented as the mean ± SD (n=3).***

## 5.4 Discussion

The property of the epithelium to function as a barrier to the movement of macromolecules is heavily dependent upon the presence of calcium in the extracellular environment of epithelial cells (1). As discussed above (section 5.1) different studies have demonstrated that exhaustion of extracellular calcium induces opening of the cellular TJs and increases the paracellular permeability. Observations of these phenomena have therefore led to investigation of different compounds possessing an ability to bind calcium, reducing or depleting its extracellular levels, in an attempt to induce TJ opening, potentially resulting in increased paracellular absorption of macromolecules.

Exhaustion of extracellular calcium has been shown to induce global changes in

epithelial cells, including disruption of actin filaments and adherent junctions, reduction of cell adhesion and activation of protein kinases (2). Citi *et al.* (13) proposed that the calcium-depleting EGTA affects the calcium-dependent adhesion molecules concentrated at adherens junctions and induces the contraction of the junction associated microfilament cytoskeleton (14, 15), whereby inducing TJ opening. Protein kinase C (PKC) is also thought to mediate TJ-opening caused by extracellular calcium depletion, as demonstrated in a study on MDCK cell monolayers where the removal of extracellular calcium was shown to stimulate PKC which then dissociates adhesion molecules from cell-cell sealing and loosens junctional strands (2). To add to the complexity of possible mechanisms involved in TJ opening by extracellular calcium depletion Ma *et al.* (10) demonstrated that the observed increase in epithelial permeability induced by calcium free medium was mediated by the activation of myosin light chain kinase and a resulting contraction of the peri-junctional actin-myosin filaments.

The use of polymeric compounds with a capacity to bind calcium, has recently been proposed as a strategy to improve mucosal absorption of macromolecules by the paracellular route (19, 20). Numerous studies involving the use of certain polymers as permeability enhancers attributed the permeability-improving mechanism of these compounds to calcium depletion. For example, the high capacity of poly(acrylic acid) (PAA) to bind calcium, depleting this ion from the extracellular cell medium, has been provided as an explanation for the increase in the paracellular permeability across epithelial cell layers observed with this polymer and its derivatives (21, 22).

The ability of polymeric powder formulations (microcrystalline cellulose,

semicrystalline cellulose, hydroxyethyl starch, cross-linked dextran, microcrystalline chitosan, pectin and alginic acid) to bind calcium ions was, in a study by Oechslein *et al*. (18), reported to be of major importance for their potential to enhance nasal absorption of the somatostatin analogue peptide, octreotide, when administered nasally to rats. The absorption-promoting effect of the powders in this study correlated directly with their calcium binding capacity, which led the authors to suggest that the absorption-enhancing effect was due to TJ opening through a local decrease in calcium concentration. In another study, Kriwet *et al.* (20) reported that the weakly crosslinked poly(acrylic acid), Polycarbophil (PC), chelated up to 80% of the total calcium concentration in a physiological buffer, leading the authors to attribute the observed increase in bioavailability of drugs with PC to complexation of calcium ions and its removal from the physiological solution by this polymer.

The access of a drug formulation incorporating an absorption enhancer is normally predominantly limited to the mucosal (apical) surface of the epithelium *in vivo*. This is especially true if the absorption enhancer is a large $M_W$ polymeric molecule such as those investigated in the studies discussed above. Therefore, in an *in vivo* situation, local reduction in extracellular calcium resulting from the mucosally administered polymeric (calcium depleting) absorption enhancer is likely to occur exclusively on the luminal side of the mucosal surfaces. But, importantly, there is some evidence from the literature, as will be discussed later, that meaningful improvements in paracellular transport induced by calcium chelators require calcium depletion on the serosal (basolateral) side of epithelial cells. The conditions under which removal of calcium gives rise to TJ-opening effects that are sufficiently pronounced as to produce meaningful improvements in mucosal permeability of macromolecules are therefore

not obvious. Additionally, and related to the previous point, it is unclear whether depletion of calcium exclusively on the apical side of epithelial cells (likely to be achieved by polymeric calcium binding molecules), produces opening of epithelial TJs resulting in enhanced macromolecular permeability.

Present work confirmed the importance of extracellular calcium in maintaining the barrier properties of epithelial cells, as tested in Calu-3 and Caco-2 cell layers. Calcium exhaustion by application of a calcium-free medium (CFHBSS) on both apical and basolateral surfaces of Calu-3 layers produced a rapid decrease in TEER, which was reversible upon reintroduction of a calcium-containing medium (HBSS) (Figure 5.1), suggesting TJ opening with calcium depletion. However, in Calu-3 layers, exhaustion of calcium on the apical side only, as achieved by the addition of CFHBSS apically, produced a short-lived and reversible reduction in TEER. Importantly, TEER reverted back to near-baseline value (97% of the baseline TEER) during the presence of CFHBSS on the apical side of the cell layers. This effect was also apparent in Caco-2 monolayers, although in this case a lower extent of TEER reversibility was observed (63% of the baseline value, Figure 5.3) compared to Calu-3 cells. Incubation of Caco-2 monolayers with CFHBSS on both apical and basolateral sides, on the other hand produced a marked reduction in TEER (reaching low levels amounting to approximately 5% of the baseline value) with no reversibility observed within the time frame of the experiment (Figure 5.3). The results therefore suggest that the TJs of epithelial cells recover from an initial effect caused by exhaustion of extracellular calcium on the apical side only.

The transient effect of apical calcium depletion on opening of the TJs, as observed through TEER measurements (discussed above), was reflected in permeability experiments. The data showed that apical calcium exhaustion (by application of CFHBSS on the apical side of cell layers) produced a modest increase (1.8-fold) in the permeability of FD4 across both Calu-3 and Caco-2 layers (Figure 5.4).

A possible reason for the relatively mild effect that apical calcium depletion with CFHBSS was seen to produce on TJ modulation may be that apical calcium is relatively unimportant for the maintenance of TJ integrity in epithelial cells. Indeed, there is evidence in the literature to support our findings. It was observed that in Caco-2 monolayers, enhancement of paracellular transport induced by calcium-depleting agents required their addition (i.e. calcium depletion) on the serosal side (25, 26). Using the same epithelial cell monolayer model, Tomita *et al*. (27) also found that basolateral calcium plays a more important role than apical calcium in maintenance of the barrier properties of the epithelium. In another study, Kamath *et al.* (28) incubated Caco-2 monolayers with CFHBSS supplemented with 2.5 mM EGTA (CFHBSS/EGTA) on the apical side and HBSS or CFHBSS on the basolateral side for 1 hour. Measurement of TEER 4 hours after the removal of these solutions and their replacement with HBSS revealed a TEER decrease of varying extents, depending on the condition. In cell monolayers incubated with CFHBSS/EGTA on the apical side and HBSS on the basolateral side, TEER amounted to 64% of the initial value (before application of the samples). However, cell monolayers exposed to CFHBSS/EGTA on the apical side and CFHBSS on the basolateral surface exhibited a TEER level amounting to 15% of the initial value.

Another factor that may possibly contribute to the unexceptional effect of apical calcium depletion with CFHBSS on TJ-opening *in vitro* is a recovery in apical calcium that may possibly occur following an initial depletion. This was investigated through the use of a calcium-sensing fluorescent marker, Fluo-4, and indeed proved to be the case. Measurement of Fluo-4 fluorescence following its incubation with apical CFHBSS present on Calu-3 layers, which was sampled at different intervals, was found to increase with time (Figure 5.12). This indicated rising apical calcium levels, following an initial depletion, to levels approaching those present in control cell layers (incubated with HBSS). In sharp contrast, apical EDTA led to permanently low Fluo-4 fluorescence, indicating low calcium levels throughout the experiment. The manner in which this reversibility in apical calcium levels arises is, at the present moment, unclear. However, it may be possible that calcium is transported in the basolateral-to-apical direction *via* the paracellular route, which has previously been demonstrated to occur (29).

To test whether prolonged apical calcium depletion produced more pronounced effects on TJs, the calcium-chelating compound, EDTA, was applied to the apical side of confluent Calu-3 and Caco-2 layers and the effect on TJs monitored through measurements of TEER and FD4 permeability. Apical EDTA produced a significantly larger reduction in TEER, compared to apical CFHBSS, in the layers of both cell lines. Furthermore, the decrease in TEER was sustainable for the duration that EDTA was present apically. Addition of EDTA to the apical side of cell layers (Calu-3 and Caco-2) also produced notable effects in FD4 permeability, with a significantly higher permeability enhancement (approximately 7-fold and 8-fold in Calu-3 and Caco-2

layers, respectively) than that resulting from apical CFHBSS (1.8-fold in layers of both cell lines).

It is possible that the larger effect produced by EDTA on TEER and FD4 permeability, compared to apical CFHBSS, may be a result of EDTA exhibiting a toxic/irritant effect on the cells, in addition to calcium depletion. In this scenario, the barrier property of the cell layer would be compromised resulting in a lower TEER and increased macromolecular permeability. In fact, EDTA was tested for its toxicity towards Calu-3 cells and found that, at the concentration used to test TJ modulation (0.125% w/v), it caused a decrease in relative cell metabolic activity by 39%. Reports in the literature also suggest toxicity associated with higher concentrations of EDTA, with Zakelj *et al*. (31) finding that concentrations above 3 mM had an unacceptable effect on the viability of rat jejunum. Despite the decrease in cell metabolic activity, application of EDTA to cell layers at the tested concentration was associated with a reversible decrease in TEER (measured 24 hours following its removal from the cells), suggesting cell recovery. Another possibility that potentially explains the difference in TEER and permeability effects between CFHBSS and EDTA is the prolonged apical calcium depletion associated with application of EDTA (as suggested by the fluorescence intensity of the calcium-sensing Fluo-4, Figure 5.11), which may produce a greater effect on TJs compared to a reversible decrease in calcium levels seen with CFHBSS. Prolonged depletion/marked decrease in apical calcium observed with EDTA is not surprising. This is because at the concentration used in this work (0.125% w/v, corresponding to 4.3 mM), EDTA is expected to have produced total apical calcium depletion as it exceeded the concentration of calcium

present in the system (1.26 mM), with EDTA chelating an equivalent molar amount of calcium.

In an attempt to deconvolute the impact that EDTA-induced prolonged apical calcium depletion produces on TJ modulation from other possible effects of EDTA (such as toxicity), which potentially influence the cell layer barrier and therefore macromolecular permeability, studies were conducted by applying the penetrant (FD4) in CFHBSS with regular replenishment on the apical side of cell layers. Any calcium reappearing in the apical solution with time, following an initial depletion achieved by applying CFHBSS, would therefore be removed regularly. The adoption of this experimental approach therefore permitted prolonged maintenance of minimal apical calcium levels. The extent of FD4 permeability enhancement achieved in this scenario was relatively higher (3.3-fold in Calu-3 cell layers, Figure 5.5) compared to that produced by a one-off application of CFHBSS (1.8-fold), suggesting that prolonged apical calcium removal produces a somewhat larger effect on opening of the epithelial TJs. However, it must be noted that the increase in FD4 permeability across the Calu-3 layers seen in this scenario was still lower than that achieved with apical addition of EDTA, suggesting that effects other than apical calcium depletion are likely to contribute towards the permeability-enhancing property of EDTA.

In addition to assessing the impact of apical calcium depletion on TJ modulation, the effect of basolateral calcium removal by EDTA on FD4 permeability was also investigated. The observation of a 3-fold larger permeability enhancement (of FD4) ensuing following the application of EDTA on the basolateral side of Calu-3 layers compared to its addition to the apical side (used at an identical concentration of

0.125% w/v in both scenarios) strongly suggested that depletion of extracellular calcium on the basolateral side induces greater TJ-opening effects compared to exhaustion of apical extracellular calcium. However, achieving depletion of extracellular calcium on the luminal side of mucosal surfaces *in vivo* is likely to be problematic. As discussed earlier, the calcium-depleting effect of the mucosally administered absorption enhancer is probably almost exclusively limited to the apical side of the mucosal surfaces. This is because, in the case of large $M_W$ absorption enhancers, their translocation from the apical side into the basolateral side is limited due to the presence of mucosal barriers including the mucus layer, the mucociliary mechanism and the TJs (as discussed in Chapter 1). Even for lower $M_W$ calcium-depleting agents, which can potentially traverse the epithelial layers through the paracellular route, exhaustion of extracellular calcium on the basolateral side is not viable due to the likely possibility of their passage into the bloodstream following translocation across the mucosal surface.

Our finding that application of EDTA to the basolateral side (producing serosal calcium depletion) leads to a more enhanced effect on TJs compared to apical EDTA is in agreement with previous studies. Tomita *et al*. (32) reported that application of EDTA to the apical side of Caco-2 monolayers increased FD4 permeability to a lower extent than its addition to the basolateral side. The authors attributed the permeability-enhancing mechanism of EDTA through its effect on the calcium susceptible adhesion molecule, uvomorulin, which is located in the basolateral membrane, maintaining TJ integrity (26, 33), with EDTA affecting this molecule more easily from the basolateral side of the cell monolayers.

Going back to the comparison of TEER and permeability effects between apical EDTA and CFHBSS, another possibility explaining the more pronounced action of EDTA is its apical to basolateral translocation following the addition on the apical side of cell layers. This possibility was tested experimentally through the use of calcium-sensing fluorescent probe, Fluo-4. Apical addition of EDTA produced a decrease (albeit modestly) in basolateral calcium levels (i.e. decreased the fluorescence intensity of Fluo-4) (Figure 5.12). The finding, firm evidence for apical-to-basolateral movement of EDTA, is not surprising given that EDTA is a relatively small molecule ($M_W$ 292 Da) and therefore may traverse the cell layers through the paracellular route. A reduction in basolateral calcium, even if not dramatic, may have a prominent effect on TJ opening and permeability enhancement.

This work finally assessed the potential of PAA, as an example of calcium binding polymeric compound investigated previously as a mucosal absorption enhancer, to open the cellular TJs and increase paracellular permeability. Several studies have demonstrated the ability of PAA to facilitate the absorption of drugs across the mucosal surfaces. For example, PAA has been reported to increase rectal absorption of calcitonin (34) and nasal absorption of insulin and calcitonin (35, 36). Furthermore PAA-based polymer, Carbopol®, prolonged the oro-caecal transit time (by approximately 25%) in rats, an effect suggested by the authors to result from a bioadhesive interaction (37). Kriwet *et al.* (20) however, postulated that the depletion of extracellular calcium and other metal ions by PAA could explain its biological effects, including the improvement of drug absorption. Similarly, in investigating the effect of the PAA derivative, carbomer (Carbopol® 934P), on the intactness of epithelial TJs on Caco-2 cell monolayers, Borchard *et al.* (19) reported a significantly

decreased TEER and markedly increased fluxes of [$^{14}$C]mannitol and FD4 associated with application of carbomer to the apical side of the cells, which the authors attributed to depletion of extracellular calcium.

Present work, however, showed that PAAs having a nominal $M_W$ of 100 kDa and 250 kDa had a moderate effect on cell layer TEER following their application to the apical surface of Calu-3 layers (Figure 5.13), suggesting a limited effect on TJs. This was indeed reflected in their impact on FD4 permeability, with PAAs of three $M_W$s (100 kDa, 250 kDa and 450 kDa) exhibiting a negligible effect on FD4 permeability (Figure 5.14). The lack of effect on TJs by PAA, as assessed through the measurements of TEER and FD4 permeability, is an interesting observation. Factors accounting for the difference in the extent of TJ modulation between apical calcium removal and PAA are, at the present moment, unclear. However, it is possible that at the conditions used (concentration and pH) PAAs did not produce a sufficient decrease in apical calcium levels to elicit a strong effect on TJs.

## 5.5 Conclusion

Using Calu-3 and Caco-2 epithelial layers, this work investigated different situations under which extracellular calcium depletion produces the largest effect on TJs. The data presented here suggested that an initial removal of apical calcium (by CFHBSS) produced limited effects on TJs, with observed reversible decrease in TEER and modest improvement of macromolecular permeability. However, sustainable apical calcium depletion produced an effect on TJs that was somewhat more pronounced though still moderate. Exhaustion of calcium on the basolateral side of the cell layers (by application of EDTA) produced a notably larger effect on TJs as compared to

apical calcium depletion. However, removal of extracellular calcium on the basolateral surface of the epithelium is difficult to achieve *in vivo*, especially in the case of large polymeric absorption enhancers. Calcium-depleting mucosal absorption enhancers are likely to reduce/exhaust calcium ions on the apical side and only for the duration that they are present at the mucosal surfaces. Considering the inadequate effect of apical calcium removal on TJ opening, the calcium depletion strategy can therefore be regarded as relatively inefficacious for mucosal delivery of therapeutic macromolecules.

## 5.6 References


1. C.A. Rabito, C.A. Rotunno, and M. Cereijido. Amiloride and calcium effect on the outer barrier of the frog skin. J Membr Biol. 42:169-187 (1978).
2. S. Citi. Protein kinase inhibitors prevent junction dissociation induced by low extracellular calcium in MDCK epithelial cells. J Cell Biol. 117:169-178 (1992).
3. L. Gonzalez-Mariscal, B. Chavez de Ramirez, and M. Cereijido. Tight junction formation in cultured epithelial cells (MDCK). J Membr Biol. 86:113-125 (1985).
4. M. Cereijido, E.S. Robbins, W.J. Dolan, C.A. Rotunno, and D.D. Sabatini. Polarized monolayers formed by epithelial cells on a permeable and translucent support. J Cell Biol. 77:853-880 (1978).
5. A. Martinez-Palomo, I. Meza, G. Beaty, and M. Cereijido. Experimental modulation of occluding junctions in a cultured transporting epithelium. J Cell Biol. 87:736-745 (1980).
6. M. Thanou, J.C. Verhoef, and H.E. Junginger. Chitosan and its derivatives as intestinal absorption enhancers. Adv Drug Deliv Rev. 50 Suppl 1:S91-101 (2001).
7. J.D. Schulzke, A.H. Gitter, J. Mankertz, S. Spiegel, U. Seidler, S. Amasheh, M. Saitou, S. Tsukita, and M. Fromm. Epithelial transport and barrier function in occludin-deficient mice. Biochim Biophys Acta. 1669:34-42 (2005).
8. D. Ameye, J. Voorspoels, P. Foreman, J. Tsai, P. Richardson, S. Geresh, and J.P. Remon. Trypsin inhibition, calcium and zinc ion binding of starch-g-poly(acrylic acid) copolymers and starch/poly(acrylic acid) mixtures for peroral peptide drug delivery. J Control Release. 75:357-364 (2001).
9. M. Roumi, E. Kwong, R. Deghenghi, V. Locatelli, S. Marleau, P. Du Souich, R. Beliveau, and H. Ong. Permeability of the peptidic GH secretagogues hexarelin and EP 51389, across rat jejunum. Peptides. 22:1129-1138 (2001).
10. T.Y. Ma, D. Tran, N. Hoa, D. Nguyen, M. Merryfield, and A. Tarnawski. Mechanism of extracellular calcium regulation of intestinal epithelial tight junction permeability: role of cytoskeletal involvement. Microsc Res Tech. 51:156-168 (2000).
11. H.L. Lueßen, C.M. Lehr, and C.O. Rentel. Bioadhesive polymers for the peroral delivery of peptide drugs. J Control Release. 29:329-338 (1994).
12. L. Li, N.R. Mathias, C.L. Heran, P. Moench, D.A. Wall, and R.L. Smith. Carbopol-mediated paracellular transport enhancement in Calu-3 cell layers. J Pharm Sci. 95:326-335 (2006).
13. S. Citiand N. Denisenko. Phosphorylation of the tight junction protein cingulin and the effects of protein kinase inhibitors and activators in MDCK epithelial cells. J Cell Sci. 108 ( Pt 8):2917-2926 (1995).
14. B. Gumbiner, B. Stevenson, and A. Grimaldi. The role of the cell adhesion molecule uvomorulin in the formation and maintenance of the epithelial junctional complex. J Cell Biol. 107:1575-1587 (1988).
15. B. Gumbinerand K. Simons. A functional assay for proteins involved in establishing an epithelial occluding barrier: identification of a uvomorulin-like polypeptide. J Cell Biol. 102:457-468 (1986).
16. M. Tomita, M. Hayashi, and S. Awazu. Absorption-enhancing mechanism of sodium caprate and decanoylcarnitine in Caco-2 cells. J Pharmacol Exp Ther. 272:739-743 (1995).

17. J. Raiman, S. Tormalehto, K. Yritys, H.E. Junginger, and J. Monkkonen. Effects of various absorption enhancers on transport of clodronate through Caco-2 cells. Int J Pharm. 261:129-136 (2003).
18. C.R. Oechslein, G. Fricker, and T. Kissel. Nasal delivery of octreotide: Absorption enhancement by particulate carrier systems. International Journal of Pharmaceutics. 139:25-32 (1996).
19. G. Borchard, H.L. Lueßen, A.G. de Boer, J.C. Verhoef, C.M. Lehr, and H.E. Junginger. The potential of mucoadhesive polymers in enhancing intestinal peptide drug absorption. III: Effects of chitosan-glutamate and carbomer on epithelial tight junctions in vitro. Journal of Controlled Release. 39:131-138 (1996).
20. B. Kriwetand T. Kissel. Interactions between bioadhesive poly(acrylic acid) and calcium ions. International Journal of Pharmaceutics. 127:135-145 (1996).
21. H.L. Lueßen, C.M. Lehr, C.O. Rentel, A.B. Noach, A.G. de Boer, J.C. Verhoef, and H.E. Junginger. Bioadhesive polymers for the peroral delivery of peptide drugs. Journal of Controlled Release. 29:329-338 (1994).
22. H.L. Lueßen, C.O. Rentel, A.F. Kotze, C.M. Lehr, A.G. de Boer, J.C. Verhoef, and H.E. Junginger. Mucoadhesive polymers in peroral peptide drug delivery. IV. Polycarbophil and chitosan are potent enhancers of peptide transport across intestinal mucosae in vitro. Journal of Controlled Release. 45:15-23 (1997).
23. J.F. Woodley. Enzymatic barriers for GI peptide and protein delivery. Crit Rev Ther Drug Carrier Syst. 11:61-95 (1994).
24. F. Madsenand N.A. Peppas. Complexation graft copolymer networks: swelling properties, calcium binding and proteolytic enzyme inhibition. Biomaterials. 20:1701-1708 (1999).
25. P. Arturssonand C. Magnusson. Epithelial transport of drugs in cell culture. II: Effect of extracellular calcium concentration on the paracellular transport of drugs of different lipophilicities across monolayers of intestinal epithelial (Caco-2) cells. J Pharm Sci. 79:595-600 (1990).
26. A.B. Noach, Y. Kurosaki, M.C. Blom-Roosemalen, A.G. de Boer, and D.D. Breimer. Cell-polarity dependent effect of chelation on the paracellular permeability of confluent Caco-2 cell monolayers. Int J Pharm. 90:229-237 (1993).
27. M. Tomita, M. Hayashi, and S. Awazu. Comparison of absorption-enhancing effect between sodium caprate and disodium ethylenediaminetetraacetate in Caco-2 cells. Biol Pharm Bull. 17:753-755 (1994).
28. A.V. Kamath, R.A. Morrison, N.R. Mathias, S.A. Dando, A.M. Marino, and S. Chong. Modulation of tight junctions does not predict oral absorption of hydrophilic compounds: use of Caco-2 and Calu-3 cells. Arch Pharm Res. 30:1002-1007 (2007).
29. S.L. Davies, C.E. Gibbons, M.C. Steward, and D.T. Ward. Extracellular calcium- and magnesium-mediated regulation of passive calcium transport across Caco-2 monolayers. Biochim Biophys Acta. 1778:2318-2324 (2008).
30. L. Illum. Transport of drugs from the nasal cavity to the central nervous system. Eur J Pharm Sci. 11:1-18 (2000).
31. S. Zakelj, L. Vadnjal, and A. Kristl. The effect of clodronate on the integrity and viability of rat small intestine in vitro-a comparison with EDTA. Biol Pharm Bull. 28:1249-1253 (2005).

32. M. Tomita, M. Hayashi, and S. Awazu. Absorption-enhancing mechanism of EDTA, caprate, and decanoylcarnitine in Caco-2 cells. Journal of Pharmaceutical Sciences. 85:608-611 (2000).
33. B. Gumbiner. Structure, biochemistry, and assembly of epithelial tight junctions. Am J Physiol. 253:C749-758 (1987).
34. K. Morimoto, H. Akatsuchi, R. Aikawa, M. Morishita, and K. Morisaka. Enhanced rectal absorption of [Asu1,7]-eel calcitonin in rats using polyacrylic acid aqueous gel base. J Pharm Sci. 73:1366-1368 (1984).
35. K. Morimoto, K. Morisaka, and A. Kamada. Enhancement of nasal absorption of insulin and calcitonin using polyacrylic acid gel. J Pharm Pharmacol. 37:134-136 (1985).
36. A. Rydenand P. Edman. Effect of polymers and microspheres on the nasal absorption of insulin in rats. Int J Pharm. 83:1-10 (1992).
37. D. Harris, J.T. Fell, D.C. Taylor, J. Lynch, and H.T. Sharma. GI transit of potential bioadhesive system in rat. J Control Release. 12:55-65 (1990).
38. M. Fujiwara, R.H. Grubbs, and J.D. Baldeschwieler. Characterization of pH-Dependent Poly(acrylic Acid) Complexation with Phospholipid Vesicles. J Colloid Interface Sci. 185:210-216 (1997).

# Chapter 6

# Permeability Enhancement with Chitosan Solution and Nanoparticles

## 6.1 Introduction

Chitosan has been shown to considerably enhance the mucosal (especially nasal) absorption of peptides and proteins, which are otherwise poorly absorbed. Chitosan is a cationic polymer (polysaccharide) produced by partial deacetylation of chitin and has been reported to be biocompatible, biodegradable and exhibiting a low toxicity (1-3). Its absorption-promoting effect is thought to result from a combination of mucoadhesion and the ability to open the intercellular tight junctions (TJs) (4-6). The mucoadhesive properties of chitosan have been attributed mainly to an interaction between its positively charged amino groups with negatively charged sialic acid groups on the mucus membrane (7). Application of therapeutic agents in combination with chitosan has been reported to prolong the contact time between the agent and the absorptive surface for up to 84 min in man for a chitosan powder formulation (8). The capacity of chitosan to transiently open the TJs has been associated with an interaction of chitosan with the Protein Kinase C pathway (9).

Different chitosan formulations, such as solutions, freeze dried or spray dried powders and nanoparticles (NPs) have been investigated for the potential improvement of nasal

absorption of various macromolecular drugs (6, 10). While chitosan solution and powder formulations improve mucosal absorption through mucoadhesion and TJ modulation, chitosan NP formulations have been developed in an attempt to deliver macromolecules across the mucosal surfaces by exploiting endocytic/transcytotic pathways (11-13). Potential advantages associated with the use of chitosan NPs encompass entrapment of the drug within the particle matrix, consequently ensuring protection against enzymatic degradation that may occur at the mucosal surface and the possibility of controlled drug release. However, despite these potential advantages, so far only one published study has shown superior mucosal drug absorption using chitosan NPs compared to chitosan solution (13).

Dyer *et al.* (6) showed that in the rat and sheep models, the pharmacological responses to an insulin-chitosan solution or insulin-chitosan powder formulation applied nasally were significantly higher compared to those resulting from an equivalent chitosan NP formulation. Similarly, Ma and Lim (14) showed that chitosan NPs did not mediate translocation of insulin across intestinal Caco-2 monolayers. Recently Sadeghi *et al.* (15) found that chitosan (and its derivatives) in a nanoparticulate form were less efficient in opening the TJs than their soluble form equivalents. The authors suggested that drug movement across the cell layers would be more likely to occur through the transcellular pathway rather than as a result of TJ opening.

The present work sets out to investigate the potential of chitosan NPs, formulated by the ionic gelation method, to improve the permeability of macromolecular compounds across biological membranes through TJ modulation, in comparison to the soluble

equivalent. Initial work assessed the effects of increasing concentrations of chitosan NPs and solutions on cell toxicity. The concentrations exhibiting minimal and reversible toxicity were then used to investigate TJ modulation and FITC-dextran (FD) permeability. Furthermore, the effect on structural changes in TJs is compared between chitosan solution and NPs. Finally, studies investigating the mucoadhesive property of chitosan are also included in this chapter.

## 6.2 Methods

### 6.2.1 Formulation and Characterisation of Chitosan NPs

*6.2.1.1 Formulation of chitosan NPs*

Chitosan NPs were prepared by the ionic gelation of tripolyphosphate pentasodium (TPP) and chitosan hydrochloride (CS), as described by Fernandez-Urrusuno *et al.* (13) and Dyer *et al*. (6). Preliminary experiments were performed with the objective of identifying the appropriate concentrations of chitosan and TPP producing NPs. Chitosan hydrochoride solutions of varying concentrations (2 mg/ml, 1.5 mg/ml, 1 mg/ml, 0.75 mg/ml and 0.5 mg/ml) and TPP, at 0.84 mg/ml, were prepared in ultrapure water. TPP solution was added dropwise to chitosan solution while stirring. The resultant mixtures were broadly characterized as either clear solutions, opalescent mixtures or phase-separated aggregates. The formation of NPs was confirmed through particle size analysis (by Dynamic Light Scattering, Viscotek, UK). Excess chitosan (not associated with NPs) was removed by centrifugation (at 13,000 rpm, for 30 minutes) of NP suspension until no chitosan was present in the supernatant. The concentration of chitosan in the supernatant was determined by a colorimetric method (based on the derivatization reaction of its primary amino groups with *o*-phthalaldehyde and N-acetyl-L-cysteine), as described by Muzzarelli (16). Chitosan

concentration in the NPs was calculated by subtracting the amount lost in the supernatant from the starting amount used to formulate the NPs. Note that chitosan NP formulation and characterisation (section 6.2.1.2, below) were performed by Ruth Harris, Institute for Biofunctional Studies, Physical Chemistry Department, Faculty of Pharmacy, Complutense University of Madrid, Madrid, Spain.

*6.2.1.2 Chitosan NP characterisation*

The mean diameter and size distribution of chitosan NPs were measured by DLS in HBSS at pH 6.0. The reported results represent the mean of ten measurements, performed at 25°C. Zeta potential of the NPs was measured in HBSS (pH 6.0) using a Zetasizer 2000 (Malvern Instruments, UK). Values reported are the mean of four measurements ±SD.

### 6.2.2 Synthesis of FITC-chitosan

100 mg of chitosan was dissolved in 10 ml of deionised water. 20 ml of DMSO was then added to this solution, followed by the slow addition of 5 mg of FITC, previously dissolved in DMSO, under continuous stirring. The reaction was carried out overnight at room temperature in the dark. The resulting solution was poured in an excess of acetone and then centrifuged for 10 min at 3000 rpm. The pellet was washed several times with fresh acetone until FITC fluorescence signal was no longer observed in the washing solution. The FITC-labelled polymer was then dissolved in water and dialysed against deionised water using a 1000 Da $M_W$ cut off (MWCO) membrane for three days while protecting from light. The labelled product was then freeze-dried for a further three days (17). FITC-chitosan was synthesised and FITC-chitosan NPs

(next section) were formulated by Luca Casettari, Pharmaceutical Chemistry Institute, University of Urbino 'Carlo Bo', Urbino, 61029, Italy.

### 6.2.3 Formulation of FITC-chitosan NPs

FITC-chitosan NPs were produced using the ionic gelation technique in a similar way to unlabeled chitosan NPs. Preliminary experiments were performed in order to identify the optimal concentrations of FITC-chitosan and TPP resulting in formation of nano-sized complexes as confirmed by DLS. The optimal polymer:TPP ratio was found to be between 6:1 and 4:1. Chitosan was dissolved in HBSS (pH adjusted to 5.0) at a concentration between 0.33 to 1.0 mg/ml. TPP solution of 0.5 mg/ml was added dropwise to 3 ml of the chitosan solution under mild magnetic stirring.

### 6.2.4 Cell culture

Calu-3 cells were cultured according to the method described previously (Chapter 2, section 2.2.1).

### 6.2.5 Cell toxicity studies

*6.2.5.1 MTS assay*

The MTS assay was performed to evaluate the effect of chitosan NPs on cell metabolic activity and compare this effect with that resulting from chitosan solution. Furthermore, this test was undertaken in order to identify the highest concentration of chitosan NPs and solution that exhibits insignificant toxicity towards Calu-3 cells. The MTS assay was performed according to the manner described previously (section 2.2.5.3). Sample solutions, the toxicities of which were tested, comprised of chitosan NPs or chitosan solution in HBSS (pH 6.0) of the following concentrations: 0.025%,

0.0125%, 0.006125%, 0.003% and 0.0015% w/v. Additionally, the effect of Triton X-100 (0.1% w/v in HBSS, pH 6.0) and the HBSS (pH 6.0) on cell metabolic activity was tested and used as the positive and negative control, respectively.

In order to assess whether cells recover following the application of chitosan, a further MTS assay was performed 15 hours after cells were exposed to the chitosan samples (incubated for 2 hours, as in the previous test). In the period between removal of the chitosan samples (NPs and solution) and the assay, cells were incubated with the culture medium (EMEM, at 37°C/5% $CO_2$).

*6.2.5.2 LDH assay*

The lactate dehydrogenase (LDH) release assay was conducted to assess membrane disruptive effects of chitosan NPs and chitosan solution. The LDH assay was performed in the manner described previously (section 2.2.5.4). Chitosan NPs and solutions tested using the LDH assay were used at the same concentrations (in HBSS, pH 6.0) as for the MTS assay (preceding section). Furthermore, the controls used for the LDH assay were the same (and at identical concentration) as those used in the MTS assay.

### 6.2.6 Effect of chitosan NPs and solution on TEER

*6.2.6.1 Calu-3 layers*

Confluent filter-cultured cell layers were used in these experiments. Prior to sample application, culture medium was removed and replaced with HBSS (pH 6.0 and 7.4 on the apical and basolateral side, respectively). Cells were equilibrated (incubated at 37°C, 5% $CO_2$) in HBSS for approximately 45 min, following which the first TEER

measurement was recoded; this was treated as the baseline TEER. HBSS was then removed from the apical side of the cells and replaced with chitosan NPs or chitosan solutions (visually transparent in HBSS, pH 6.0) of 0.003% w/v and 0.006% w/v. The rest of the experiment was conducted according to the method described in section 2.2.3. The reported changes in TEER are presented as percentage relative to baseline TEER. All experiments were performed in triplicates.

*6.2.6.2 Caco-2 monolayers*

The effect of chitosan NPs on TEER of Caco-2 cell monolayers was tested following similar procedures as those used for Calu-3 cells, with the following difference: only chitosan NPs were tested for their TEER-modulating effect and suspensions containing equivalent chitosan concentrations of 0.1%, 0.05%, 0.025% and 0.0125% w/v (i.e. higher concentrations than those used in Calu-3 cells) were used.

### 6.2.7 Permeability experiments

*6.2.7.1 Effect of chitosan NPs and solution on FD permeability: Calu-3 cells*

Permeability experiments were performed on confluent, filter-cultured Calu-3 layers. Prior to sample application, culture medium was removed and cells washed with PBS. HBSS was then applied (at pH 6.0 and 7.4 on the apical and basolateral sides, respectively) and cells equilibrated for a period of approximately 45 minutes. Chitosan NPs or chitosan solution in combination with FDs (FD4 or FD10), in HBSS at pH 6.0 were then applied to the apical side of the cells. The final concentration of chitosan (as NPs or solution) was 0.003% w/v while FDs were used at a final concentration of 500 µl/ml. FD permeability was determined by sampling the basolateral solution in the manner described earlier (section 2.2.4).

*6.2.7.2 FD4 permeability with chitosan NPs: Caco-2 cells*

Effect of chitosan NPs on FD4 permeability across Caco-2 cell layers was conducted in a similar manner as in the previous section, with the following exception: the tested concentration of NPs was that containing 0.0125% w/v chitosan.

### 6.2.8 Effect of FITC-chitosan on TJ modulation

Experiments evaluating the effects of FITC-chitosan on TEER and FD4 permeability were conducted (separately) in the same way as those for chitosan NPs and solution. FITC-chitosan was used at a concentration of 0.003% w/v in both cases.

### 6.2.9 Association of FITC-chitosan NPs with Calu-3 layers

FITC-chitosan NPs were diluted in HBSS (pH 6.0) to a concentration of 0.003% w/v chitosan and then applied to the apical side of confluent Calu-3 layers previously equilibrated in HBSS (for approximately 30 min). HBSS was present on the basolateral side. Cells were incubated with FITC-chitosan NPs at 37°C for 2 hours. NPs were then removed and cells washed extensively with PBS. Cell layers were then fixed with paraformaldehyde, processed for confocal imaging and imaged by confocal microscopy using the confocal system in the manner described previously (section 2.2.6.5).

### 6.2.10 Effect of chitosan NPs and solution on ZO-1 distribution

Chitosan in NP or solution form, of 0.003% w/v chitosan (in HBSS, pH 6.0), was applied to the apical side of confluent Calu-3 layers, following an equilibration step with HBSS. Cells were incubated with chitosan NPs or solution for a period of 1 hour followed by cell washing with PBS. Cells were then fixed with paraformaldehyde,

prior to staining for zonula occludens-1 (ZO-1) TJ protein. ZO-1 immunostaining, preparation of the samples for confocal imaging were conducted in the manner described in section 2.2.6.6. Confocal imaging was performed using the system described in section 2.2.6.3.

### 6.2.11 Association of FITC-chitosan with Calu-3 and Caco-2 layers

Caco-2 and Calu-3 cells were cultured on filters until confluence. In addition to normally employed AIC conditions, Calu-3 cells in this instance were also cultured using LCC conditions. Culture medium was removed and replaced with HBSS for equilibration (for approximately 30 min). Apical HBSS was then removed and replaced with a solution of FITC-chitosan (0.003% w/v in HBSS, pH 6.0). Cells were incubated with FITC-chitosan for 2 hours, following which chitosan solution was removed and cells washed with PBS extensively (at least 5 times in an attempt to remove the applied chitosan). Cells were then fixed with paraformaldehyde for 5-10 min and processed for confocal imaging in the manner described previously (section 2.2.6.5).

### 6.2.12 Effect of chitosan on the permeability of investigational antibodies

Antibody permeability experiments were conducted on confluent Calu-3 layers, equilibrated in HBSS for approximately 45 min. UCB antibodies, mA33γ1 Fab (6.52 mg/ml), mA33γ1 Fab-diPEG (10.3 mg/ml), hCTM01γ4 antibody (3.67 mg/ml) and hCTM01γ4 Fab (5.64 mg/ml), all diluted in HBSS (pH 6.0), were applied to the apical side of the cell layers, with chitosan, which was used at a final apical concentration of 0.003% w/v (in HBSS, pH 6.0). Antibody permeability was established by sampling the basolateral solution (HBSS) periodically. Sampled volumes were replaced with

fresh HBSS. Apical-to-basolateral translocation of the antibodies across the cell layers without the addition of chitosan was used as a control experiment; antibodies were applied at the same concentration and pH as above. Antibodies were quantified by HPLC (see section 2.2.7.2 for the method) in all cases.

## 6.3 Results

### 6.3.1 Chitosan NP characterisation

Following the initial screening experiments, the optimised preparation conditions (initial concentrations of chitosan and the polyphosphate salt) were identified as a final chitosan hydrochloride concentration of 1.5 mg/ml and a final TPP concentration of 1.8 mg/ml. Under these conditions, the NPs formed had a mean radius of 339±66 nm (Figure 6.1) and a surface potential of +11.3±2.7 mV, as measured in HBSS (pH 6.0). The final NPs suspension, after the removal of excess free chitosan, following the procedure described in the methods section, contained 0.56 ± 0.06 mg/ml of chitosan (in the form of NPs), as determined by the colorimetric assay.

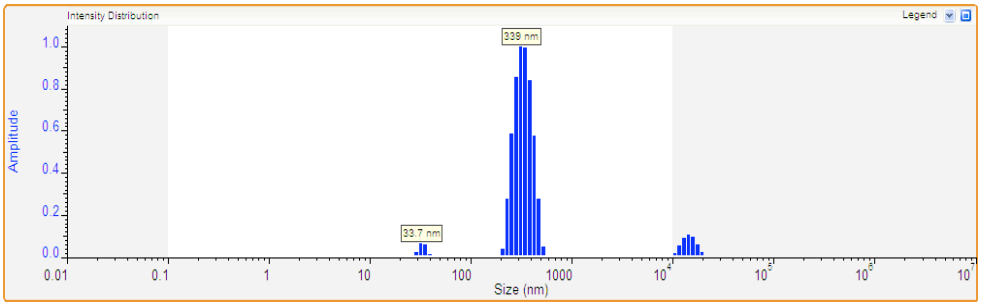


***Figure 6.1. Dynamic Light Scattering (DLS) measurement of the size distribution of chitosan NPs re-suspended in HBSS (at pH 6.0). The result represents a mean of ten measurements, performed at 25°C.***

### 6.3.2 Cell toxicity studies

*6.3.2.1 MTS assay*

The effect of chitosan NPs and chitosan solution on the relative metabolic activity of Calu-3 cells is shown in Figure 6.2. NP suspensions containing 0.0015% and 0.003% w/v chitosan, show no significant suppressive effect on Calu-3 metabolic activity, while NP suspensions containing chitosan concentrations greater than 0.006% w/v all exhibit significant reductions (>50%) in relative metabolic activity in a concentration-dependent manner. It should be noted that chitosan solutions at two highest concentrations (0.0125% and 0.025% w/v) exhibit significantly higher suppressive effect than corresponding NP concentrations, while for the lower three concentrations (0.006%, 0.003% and 0.0015% w/v), although the reduction in metabolic activity appears higher for chitosan solution, this difference is not statistically significant. According to this study, one can assign 0.003% w/v as the highest chitosan concentration, for both solution and NPs, exhibiting no statistically significant suppression on metabolic activity, as determined by the MTS assay.

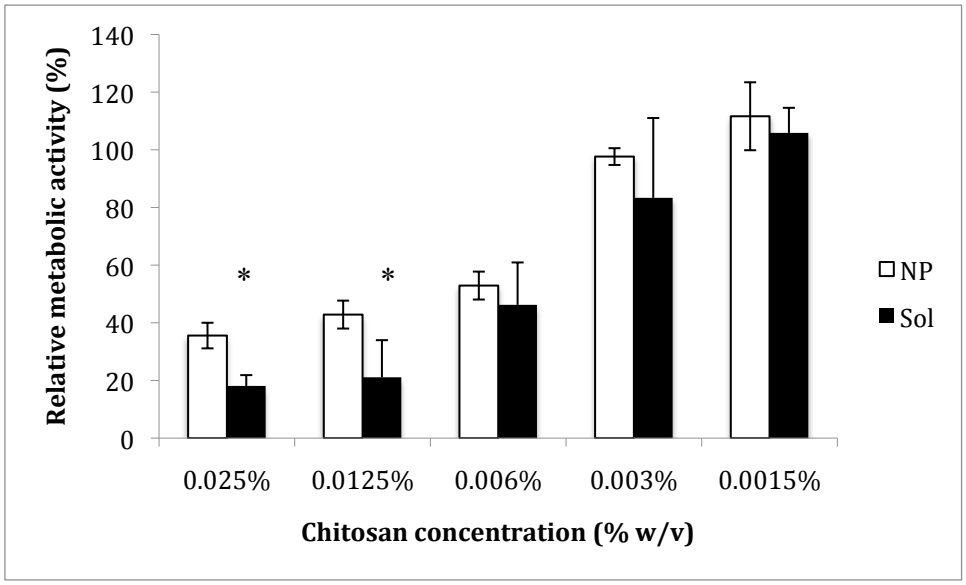


***Figure 6.2. Effect of chitosan NPs ('NP') and chitosan solution ('Sol') on the metabolic activity of Calu-3 cells, measured by the MTS assay following a 2-hour incubation of the cells with chitosan samples. Results expressed as % metabolic aactivity relative to controls (HBSS and Triton X-100), calculated according to the method described in section 2.2.5.3 and presented as the mean ± SD (n=5). * denotes statistically different effect between chitosan solution and NPs.***

The recovery of cells following the application of chitosan NPs and solution was also tested (Figure 6.3) by conducting the MTS assay 13 hours following the exposure of cells to chitosan. Although the data variability is higher than in Figure 6.2, it can nevertheless be noticed that in this cell recovery experiment, chitosan NP suspensions were typically associated with higher cell metabolic activity, relative to chitosan solutions of the corresponding concentration. Namely, for chitosan NPs statistically higher relative metabolic activity was observed for 0.003 and 0.0015% w/v tested concentrations, compared to chitosan solution.

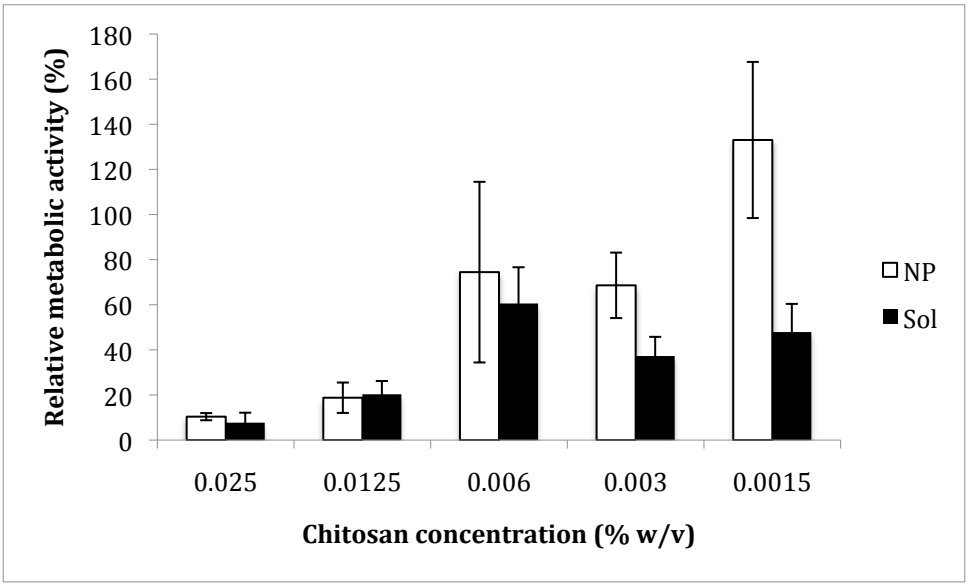


***Figure 6.3. Long term effect of chitosan NPs and chitosan solution on the metabolic activity of Calu-3 cells, measured by the MTS assay 13 hours following the incubation of cells with chitosan samples. Results expressed as % relative metabolic activity calculated according to the method described in section 2.2.5.3 and presented as the mean ± SD (n=5).***

*6.3.2.2 LDH assay*

Figure 6.4 shows the effect of chitosan NPs and chitosan solution on relative LDH release. The release of LDH from cells is generally considered as an indication of plasma membrane disruption. In essence, a concentration dependent LDH release (signifying membrane toxicity) was found for both chitosan NPs and chitosan solution (apart from the highest concentrations of chitosan solution). Application of NP suspension equivalent to chitosan concentration of 0.003% w/v, identified using the MTS assay as the highest concentration that did not affect cell metabolic activity, caused a 10% increase in LDH release, whereas chitosan solution of the same concentration showed an increase of 11%. Both these values are significantly different to the HBSS control, indicating some extent of membrane disruption, however there is no statistically significant difference between chitosan NPs and solution ($p=0.33$). Applying higher concentrations, the membrane toxicity gradually increased for both

systems, reaching approximately 37% and 45% of LDH release (relative to the positive control) with NPs (at 0.025% w/v) and solution (at 0.0125% w/v), respectively. At the higher concentrations of NPs and solution, namely 0.006% and 0.0125% w/v, there was a statistically significant difference between NPs and solutions ($p=0.043$ and $p=0.004$ for 0.006% w/v and 0.0125% w/v, respectively), whereby at the same chitosan concentration solutions showed higher membrane toxicity.

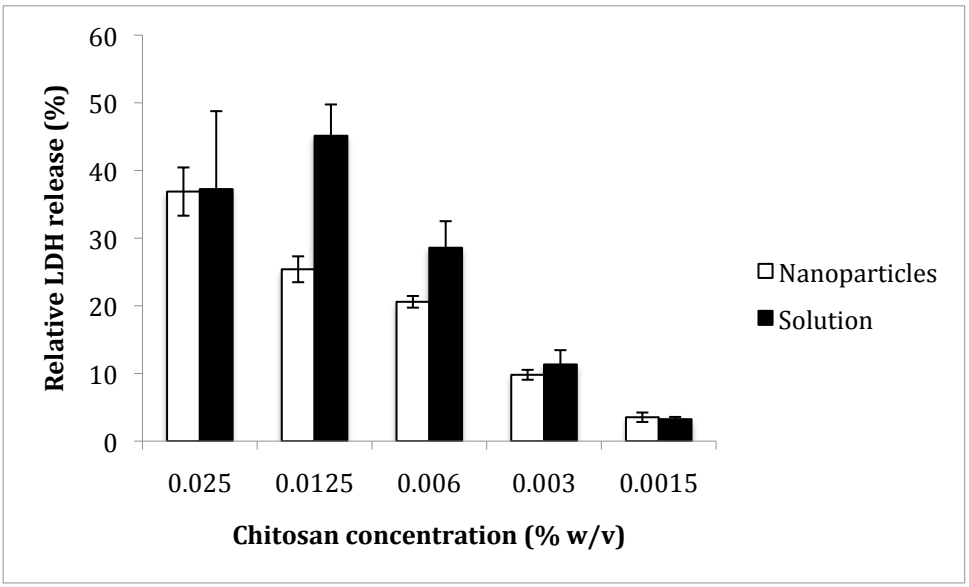


***Figure 6.4. Effect of chitosan NPs and solution on LDH release following a 2-hour incubation of Calu-3 cells with chitosan samples. Results expressed as relative LDH release calculated using the equation shown in section 2.2.5.4 and presented as the mean ± SD (n=4).***

### 6.3.3 Effect of chitosan NPs and solution on TEER

*6.3.3.1 Effect on Calu-3 layers*

The effect of chitosan NPs and chitosan solutions of two different concentrations (0.003% and 0.006% w/v) on the TEER of Calu-3 layers is presented in Figure 6.5 (6.5a and 6.5b for chitosan NPs and chitosan solution, respectively). Both profiles exhibit a typical pattern of a steep decrease in TEER to less than 10% of the baseline value for all the samples applied. TEER remained low (in the region <10% of the baseline figure) for the duration of cell incubation with the samples (2 hours). The largest recorded decrease in TEER was, however, significantly (statistical significance) larger for chitosan solution than for the NPs.

Reversibility of TEER following the removal of chitosan formulations from the cells was found to be concentration dependent, whereby the higher concentration of chitosan NPs and solution (0.006% w/v) was associated with an irreversible lowering of the TEER (Figure 6.5). Measured 20 hours after subjecting the cell layers to chitosan incubation, the TEER values were in the order of 10% and 5% of the baseline figure, respectively. TEER values for 0.003% w/v NP suspension showed a high level of recovery (to 92% of the baseline value) in the same time period (6.5a). Regarding chitosan solution, the concentration of 0.003% w/v again showed recovery, with TEER reaching 84% of the baseline value (6.5b). An interesting point to note is that the lower concentration (0.003% w/v chitosan) produced an initial TEER reduction similar in magnitude to that observed with the higher concentration (0.006% w/v) of both NPs and solution, which were associated with no recovery in TEER.

a)

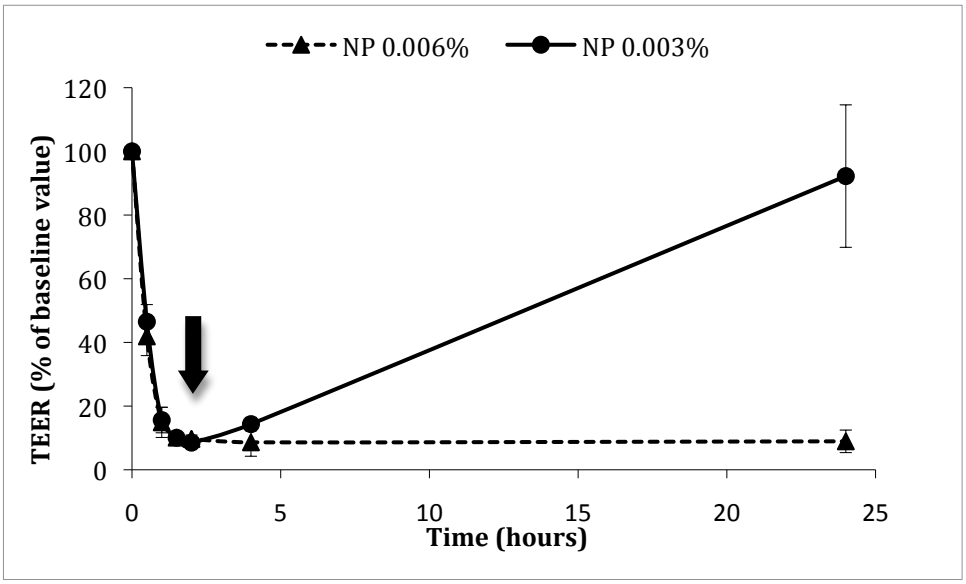


b)

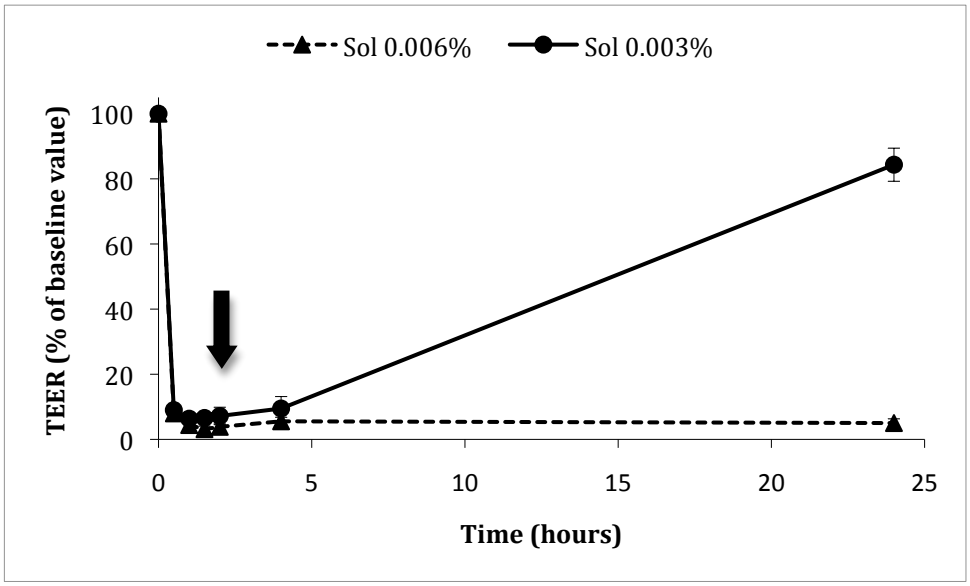


***Figure 6.5. Effect of chitosan NPs (a) and solution (b) on Calu-3 layer TEER. Chitosan NPs and chitosan solutions were used at concentrations 0.003% w/v and 0.006% w/v. Time 0 hrs represents baseline TEER (i.e. TEER in HBSS, prior to application of chitosan samples). Arrows indicate chitosan sample removal and replacement with culture medium. Results presented as the mean ± SD (n=3)***

*6.3.3.2 Effect on Caco-2 monolayers*

In order to determine whether the TEER-reducing effect of chitosan NPs was reproducible in a different cell line that also forms electrically tight polarised layers, this effect was tested on intestinal Caco-2 cells. Figure 6.6 shows that the application of chitosan NPs to Caco-2 monolayers was again associated with a decrease in TEER and that the extent of this reduction, similarly to Calu-3 cells, was large (to >80% of the baseline value). TEER recovery was again dependent upon the NP concentration. However, importantly, in Caco-2 cells a complete TEER recovery (tested 22 hours after a 2 hour incubation of cells with chitosan NPs) was observed with a 0.0125% w/v chitosan concentration of NPs. This is a four times higher concentration of material than the chitosan NP concentration exhibiting a reversible TEER reduction in Calu-3 cells. Furthermore, a partial TEER recovery was also evident with higher NP concentrations (to 64%, 53% and 29% of the baseline value with NP concentrations containing chitosan concentrations of 0.025%, 0.05% and 0.1% w/v, respectively).

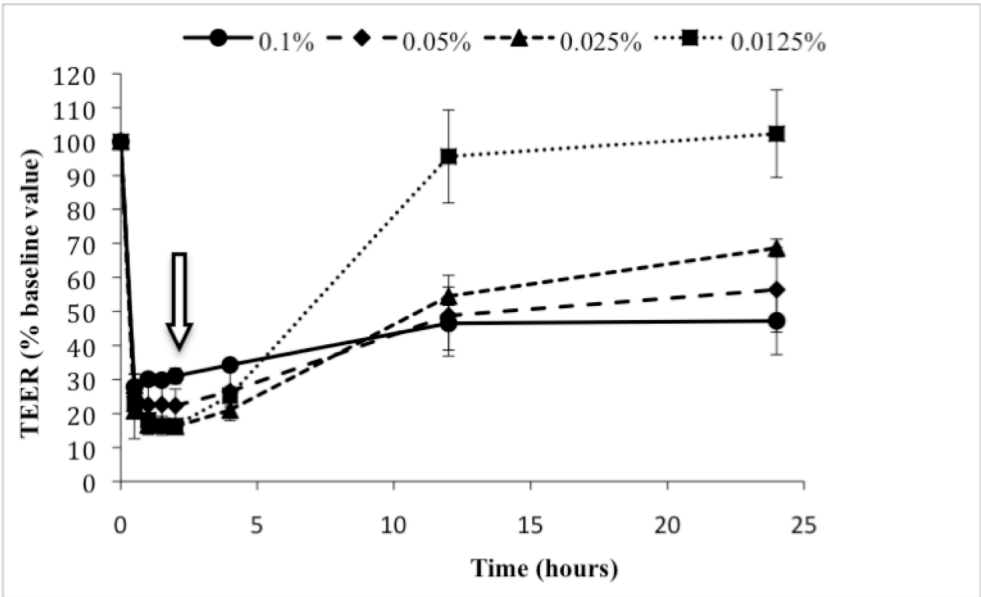


***Figure 6.6. Effect of chitosan NPs on Caco-2 monolayer TEER. Chitosan NPs were applied to cells at concentrations 0.1%, 0.05%, 0.025% and 0.0125% w/v. Time 0 hrs represents baseline TEER (i.e. TEER in HBSS, prior to application of chitosan NPs). Arrow indicates sample removal and replacement with culture medium. Results presented as the mean ± SD (n=3).***

### 6.3.4 Permeability experiments

*6.3.4.1 Effect of chitosan NPs and solution on FD permeability: Calu-3 cells*

The permeability study was conducted to compare suspension of chitosan NPs and a corresponding solution containing 0.003% w/v of chitosan. The selection was based on (i) the low toxicity of this chitosan concentration, as determined by the MTS assays, and (ii) the finding that this was the highest chitosan concentration that showed reversibility in TEER *versus* time profile, for both formulations. FD4 and FD10 were used as macromolecular tracers and the effect of chitosan NPs and solution of the equivalent concentration on their permeability was compared (Figure 6.7). The data clearly demonstrate that chitosan NPs significantly enhance the permeability of both FD4 and FD10, relative to the control. The extent of this effect is apparently dependent on the $M_W$ of the FD; the permeability of FD4 was 7.6-fold

higher than the control, while there was a 6.5-fold increase in the permeability of FD10, as compared to the control. Chitosan solution appears more efficient in improving the permeability of both FD4 and FD10, with a 10.1-fold improvement in permeability across the cells observed for both FDs, relative to their respective controls. However the difference between chitosan NPs and solution for the effect on FD4 transport was found to be statistically insignificant (p=0.074), though the data obtained are highly variable. In contrast, the improvement in FD10 permeability achieved with chitosan solution is significantly (p=0.018) higher than for the NPs. The data therefore clearly show that in the presence of chitosan NPs, FDs (coexisting in the same solution and not incorporated within the NPs) exhibit paracellular translocation across the Calu-3 layers and that this translocation is dependent upon their molecular size.

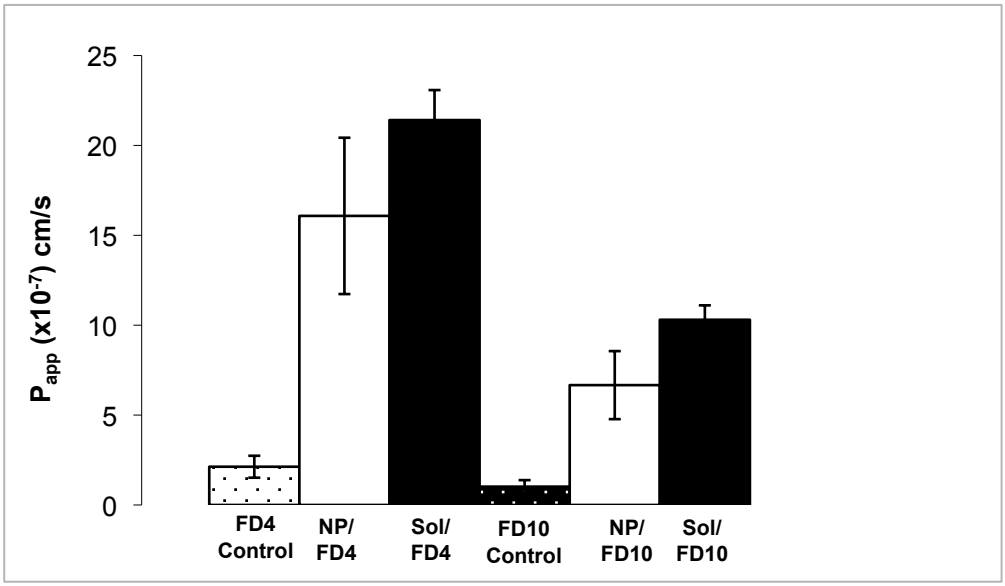


***Figure 6.7. Effect of chitosan NPs and solution (0.003% w/v) on the permeability of FD4 and FD10 across Calu-3 layers. Control represents FD4 and FD10 permeability (in HBSS) without the presence of chitosan NPs or chitosan solution. Permeability expressed as apparent permeability coefficient ($P_{app}$), calculated using the equation in section 2.2.4. Results presented as the mean ± SD (n=4).***

*6.3.4.2 FD4 permeability with chitosan NPs: Caco-2 cells*

Permeability-enhancing effect of chitosan NPs was also tested on Caco-2 monolayers for the purpose of corroboration. In presence of chitosan NPs at 0.0125% w/v, FD4 was found to traverse the Caco-2 monolayers significantly more readily compared to control (FD4 applied in absence on chitosan NPs), with the calculated $P_{app}$ values amounting to $3.72 \times 10^{-7}$ cm/s in control monolayers and $26.2 \times 10^{-7}$ cm/s when applied in combination with chitosan NP, producing a 7-fold improvement in FD4 permeability. The data are shown in Figure 6.8.

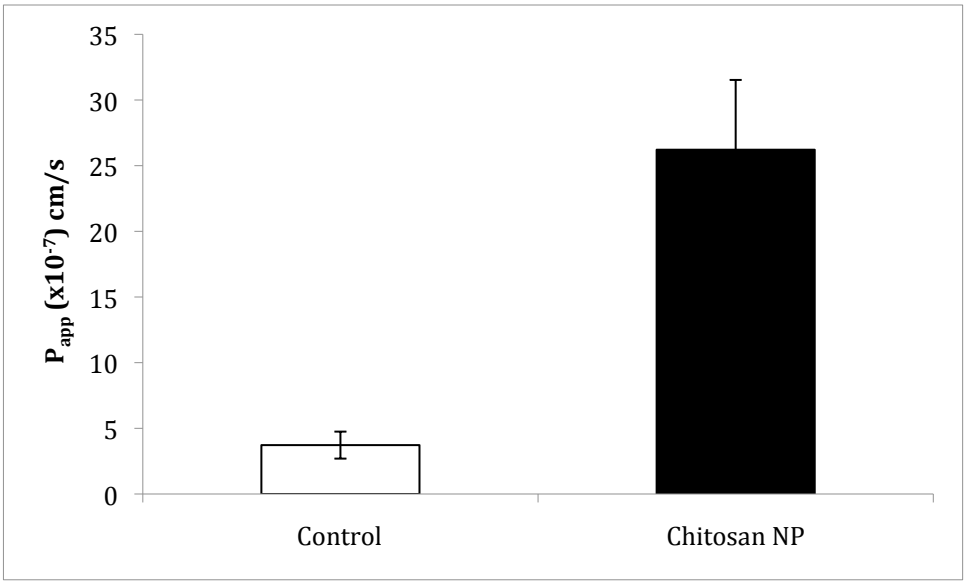


***Figure 6.8. Effect of chitosan NP on FD4 permeability across Caco-2 monolayers. NP suspensions containing an equivalent of 0.0125% w/v chitosan were used. Control represents FD4 permeability (in HBSS) without the presence of chitosan NPs. Permeability expressed as apparent permeability coefficient ($P_{app}$), calculated using the equation in section 2.2.4. Results presented as the mean ±SD (n=3).***

### 6.3.7 Effect of FITC-chitosan on TJ modulation

Changes in measurable indications of TJ modulation, namely TEER and paracellular permeability, observed following the application of FITC-chitosan to confluent Calu-3 layers are illustrated in Figure 6.9. The purpose of conducting these experiments was to determine whether chemical conjugation of FITC affected the TJ opening properties of chitosan. Application of FITC-chitosan to Calu-3 layers was associated with an immediate and drastic reduction in TEER, to levels <10% of the baseline value (6.9a). The decrease in TEER was fully reversible, with TEER value measured 24 hrs following the application of FITC-chitosan to the cells reaching approximately 99% of the baseline value. It must be noted that the TEER pattern seen with FITC-chitosan was similar to that observed with unlabeled chitosan solution. This is especially the case when considering the extent of TEER reduction achieved. TEER recovery on the other hand was more apparent with the labelled chitosan. The similarity in effect extends to FD4 permeability (6.9b), with FITC-chitosan showing a similar level of FD4 permeability enhancement (11-fold compared to control) as unlabeled chitosan (10-fold).

**a)**

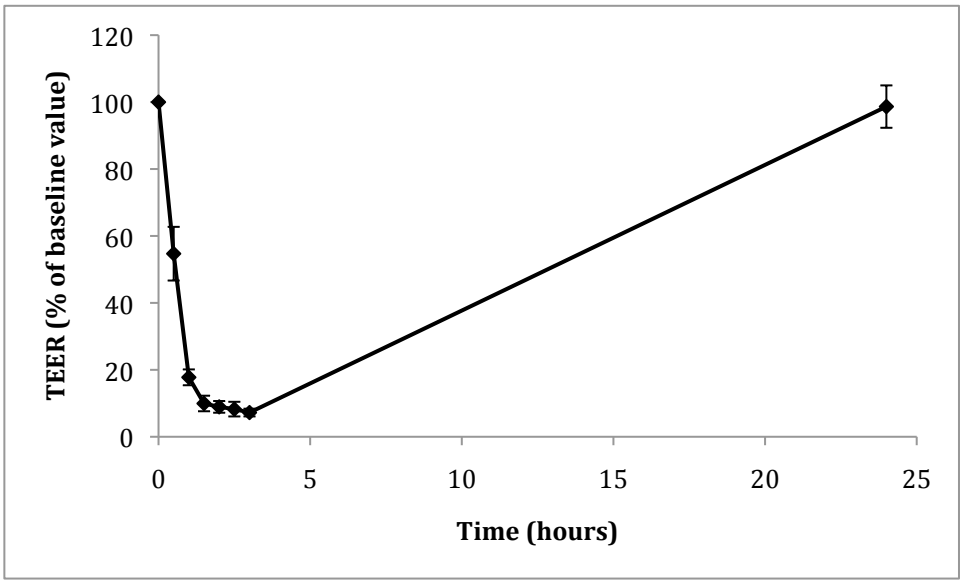


**b)**

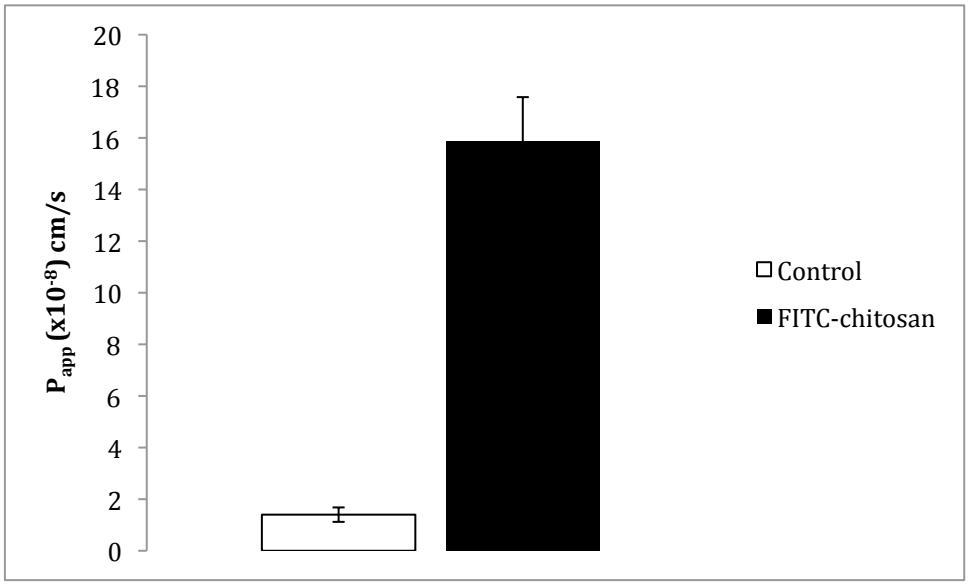


***Figure 6.9. Effect of FITC-chitosan on TJ modulation of Calu-3 layers. a) Changes in TEER following the application of 0.003% w/v FITC-chitosan, expressed as % of the baseline value; b) FD4 permeability in the presence of 0.003% w/v FITC-chitosan and in HBSS (pH 6.0; control). Results are expressed apparent permeability coefficient ($P_{app}$), calculated using the equation in section 2.2.4 and presented as the mean ± SD (n=3).***

### 6.3.8 Association of FITC-chitosan NPs with Calu-3 layers

The association of FITC-chitosan NPs with a confluent Calu-3 layer, following incubation and extensive cell washing, is shown in Figure 6.10. Green fluorescence, arising from FITC-labelled chitosan NPs is distributed throughout the imaged area of the cell layer. In some regions the fluorescence is concentrated, forming larger aggregates, while in other regions, punctate fluorescence indicating nano-sized species (NPs), could be observed. In some regions (arrow) the fluorescence appears to follow the contour of cells on the apical surface. With respect to NP fluorescence distribution across the vertical axis of the cell layer, NPs were mainly observed on the apical side of the cells (marked A), with some NP fluorescence also observed deeper, within the level of the cell nuclei and closer to the basolateral surface of the cells (marked B).

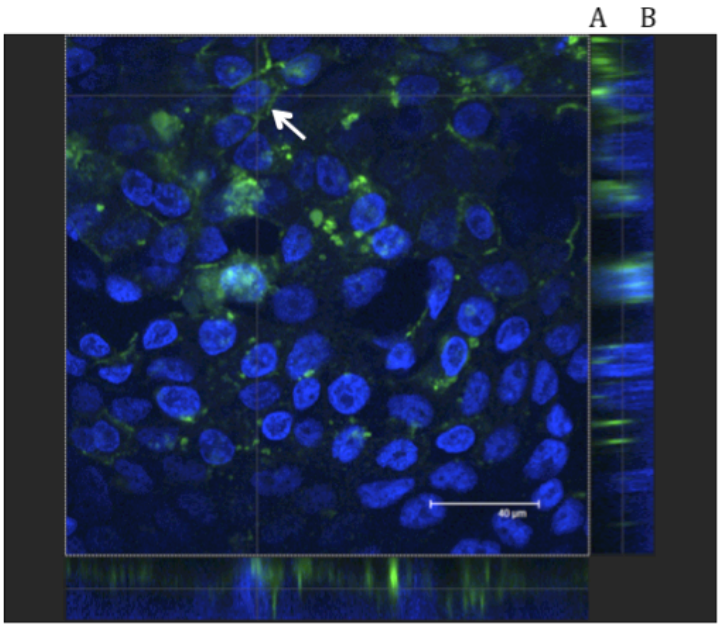


***Figure 6.10. Association of FITC-chitosan NPs with filter-cultured Calu-3 cells. Green: FITC-labelled NPs; and Blue: DAPI-labelled cell nuclei. Apical side of the cells is marked with A, whereas basolateral side is marked with B.***

### 6.3.9 Effect of chitosan NPs and solution on ZO-1 distribution

Structural changes at the level of the cellular TJs resulting from the application of chitosan as NPs and solution are shown in Figure 6.11. A continuous ring of fluorescence, arising from ZO-1 staining, at cell-cell contacts is clearly visible in the control cell layer (6.11a). Fluorescence at the point of contact between the cells can also be seen in the cell layer incubated with chitosan NPs (6.11b) and solution (6.11c). However, in comparison to the control cell layer, a considerable loss in continued fluorescence is clearly apparent, with observation of discontinuous pericellular rings of fluorescence for both, chitosan NPs and chitosan solution.

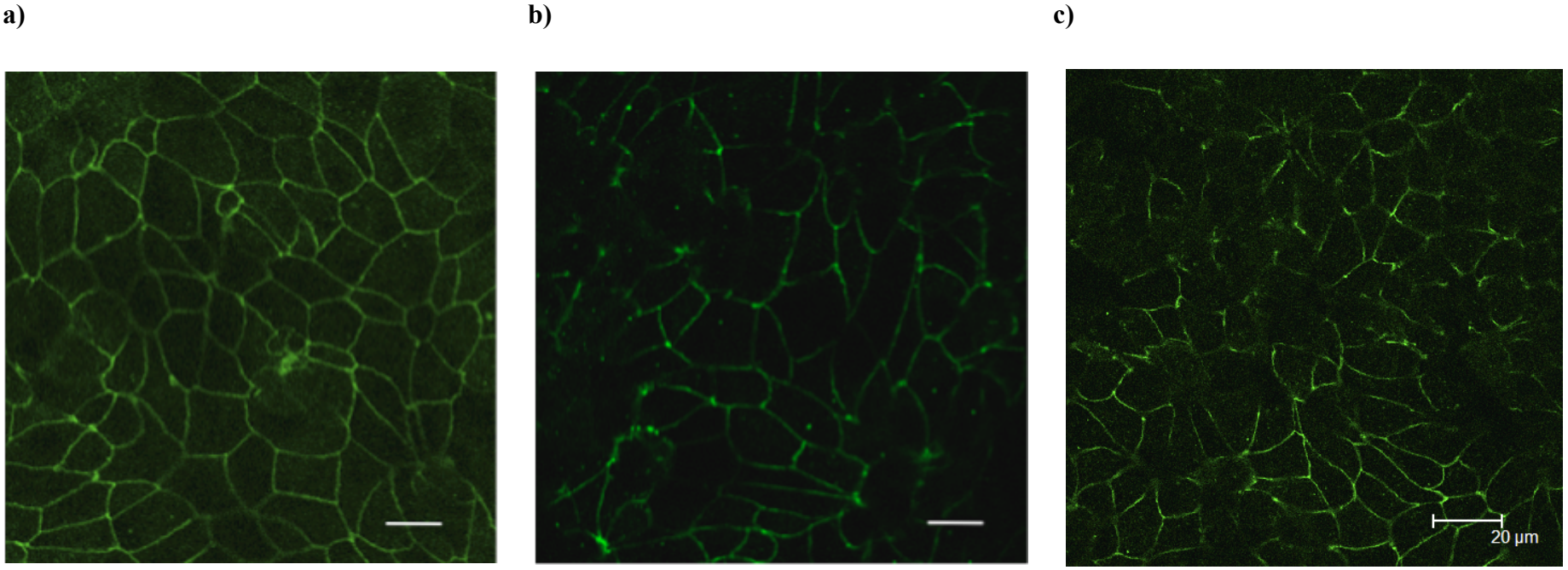


*Figure 6.11. Effect of chitosan NPs and solution on distribution of ZO-1 TJ protein in Calu-3 layers. a) ZO-1 staining in a control layer not subjected to chitosan incubation (white line represents a scale bar of 10 µm), b) ZO-1 staining in cells incubated with NPs of 0.003% w/v chitosan (white line represents a scale bar of 10 µm), and c) ZO-1 distribution in a cell layer incubated with chitosan solution of 0.003% w/v. ZO-1 immunostaining was performed in the same way (see section 2.2.6.6) for all conditions.*

### 6.3.10 Association of FITC-chitosan with Calu-3 and Caco-2 layers

Figure 6.12 shows the association of FITC-chitosan with Calu-3 layers cultured using AIC and LCC conditions and Caco-2 monolayers. In Calu-3 cells grown using AIC (6.12a), green fluorescence was in some regions observed as continuous 'rings' around individual cells. Areas of intense green fluorescence were also observed. Green fluorescence surrounding individual cells were also apparent in Calu-3 cells cultured using LCC (6.12b). However, in contrast to AIC conditions, areas of bright fluorescence were not observed in Calu-3 cells grown using LCC. FITC-chitosan fluorescence was distributed around the cells in the Caco-2 monolayer (6.12c) although this pattern of fluorescence distribution was somewhat less apparent than in Calu-3 cells (cultured using both AIC and LCC conditions).

**a) AIC Calu-3 cells**

**i)**

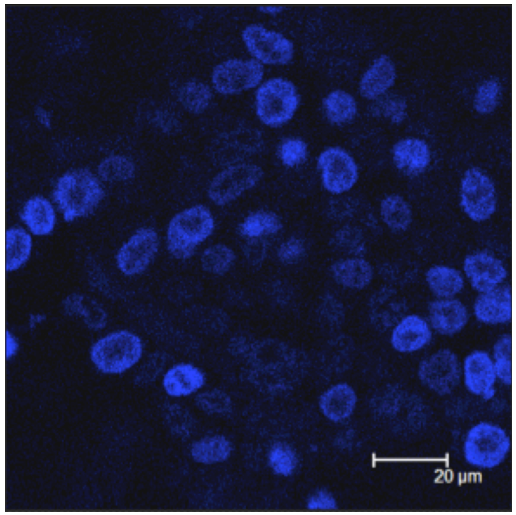


**ii)**

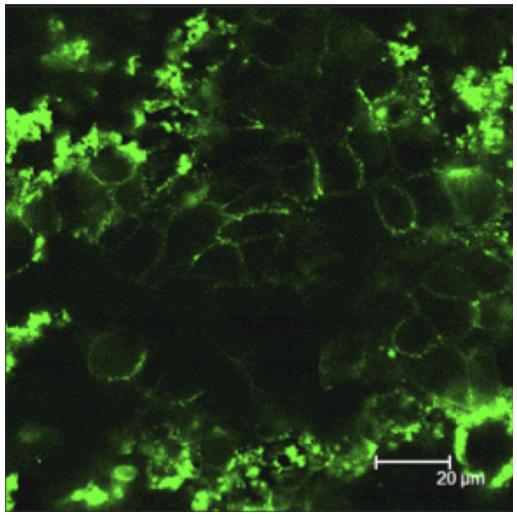


**iii)**

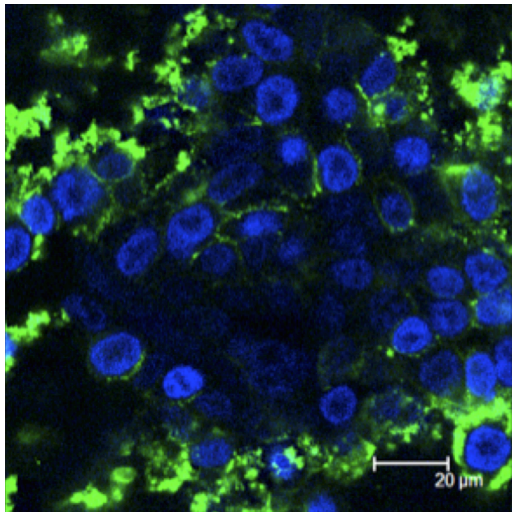


**b) LCC Calu-3 cells**

**i)**

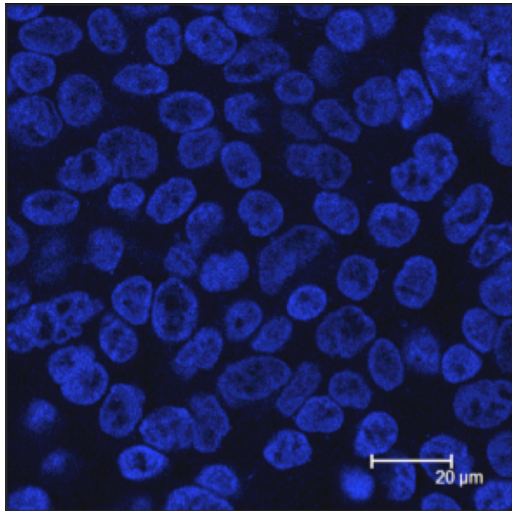


**ii)**

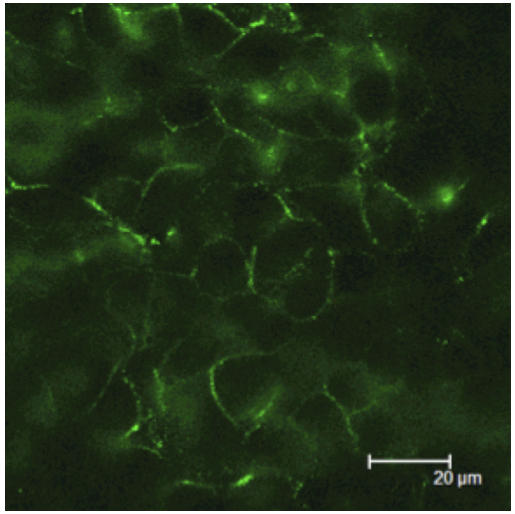


**iii)**

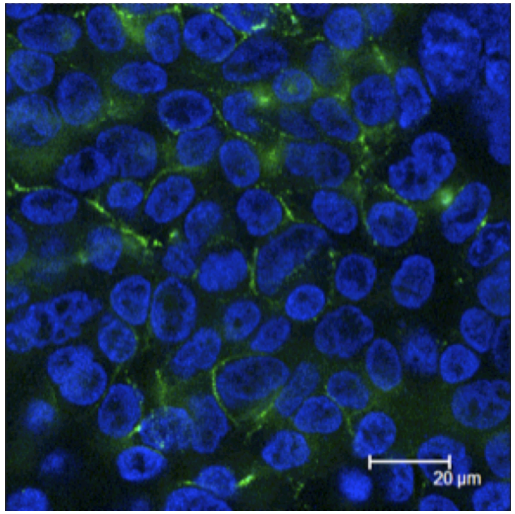

### c) Caco-2 cells

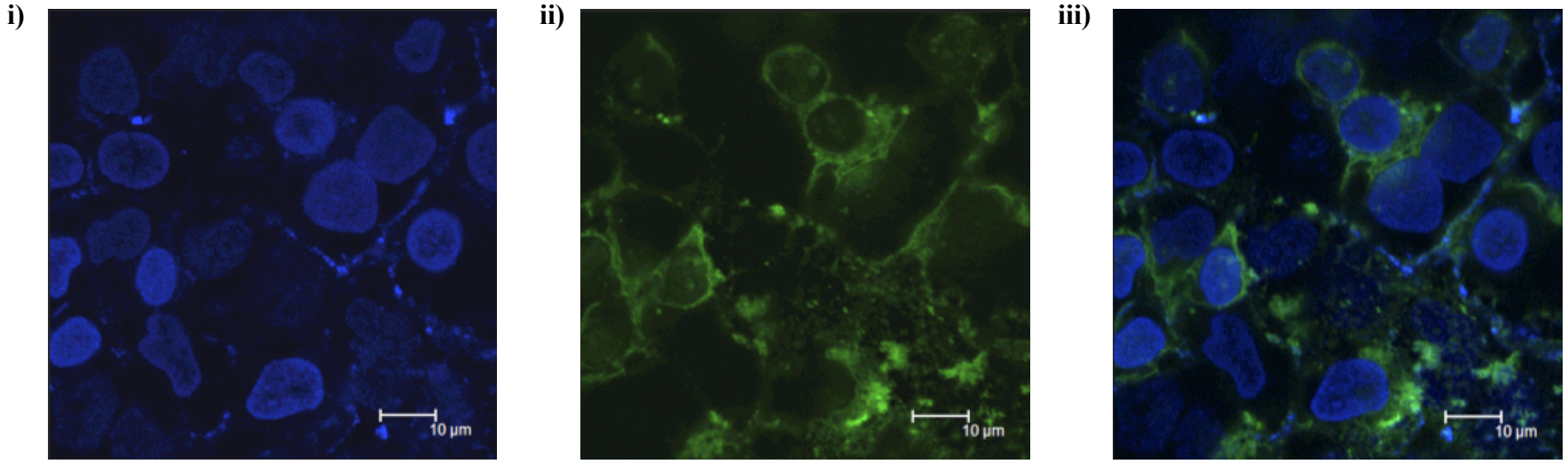


*Figure 6.12. Association of FITC-chitosan with confluent Calu-3 and Caco-2 layers. a) Calu-3 cells cultured using AIC conditions, b) Calu-3 cells grown using LCC, and c) Caco-2 cells. FITC-chitosan was applied to confluent cell layers at 0.003% w/v and incubated with the cells for 2 hours. i) Blue channel: Cell nuclei stained with DAPI, ii) Green channel: FITC-chitosan, and iii) Overlay images.*

### 6.3.11 Effect of chitosan on the permeability of investigational antibodies

Table 6.1 shows the effect of chitosan on the permeability of four investigational antibodies (property of UCB). It is important to note that the HPLC method used to quantify the antibodies suffered from limited detection sensitivity. Consequently, any low basolateral levels of antibodies could not be detected. In control cell layers where the transport of antibodies was tested in the absence of chitosan, none of the applied proteins (an antibody and three Fabs) were detected (marked by 'ND' in Table 6.1) in the basolateral solution, i.e. if any antibody translocation occurred, it was below the detection limit. (The detection limits for the antibodies were 1.95 μg/ml for hCTM01 antibody, 2.3 μg/ml for hCTM01 Fab, 1.7 μg/ml for mA33γ1 Fab and 15 μg/ml for A33γ1 Fab-diPEG.) On the other hand, application of the antibodies to the cell layers in combination with chitosan led to the detection of hCTM01 Fab (0.26% of the applied amount) and mA33γ1 Fab (0.49% of the applied amount) in the basolateral solution, while the whole antibody (hCTM01γ4), and the PEGylated antibody fragment (A33γ1 Fab-diPEG) were not detected after the incubation period with the cell layers.

| Name | Type | $M_W$ | Permeability (% of apical) | |
|---|---|---|---|---|
| | | | Control | Chitosan |
| hCTM01 antibody | Whole Antibody | 147033 | ND | ND |
| hCTM01 Fab | Fab | 95815 | ND | 0.26±0.167 |
| mA33γ1 Fab | Fab | 24725 | ND | 0.49±0.022 |
| mA33γ1 Fab-diPEG | PEGylated Fab | 64725 | ND | ND |

***Table 6.1. Effect of chitosan solution (0.003% w/v) on the permeability of therapeutic antibodies and antibody fragments. Types of antibodies (i.e. whole antibody or fragment) and their $M_W$ is also given. Permeability is expressed as % relative to the applied amount. 'ND' means none detected. Data presented as the mean ± SD (n=3).***

## 6.4 Discussion

The mucoadhesive and TJ opening functionalities of chitosan have especially been exploited in formulation of nasal macromolecular therapeutics, including peptides and proteins (18). In addition to the well-documented TJ opening and mucoadhesive properties of chitosan solutions (8, 9), it has been suggested that chitosan NPs, and NPs of other materials, may improve mucosal absorption by traversing the epithelial barriers. The concept of using nano-sized carriers to transport drugs across the epithelial layers, however remains controversial (10). The *in vivo* transport of 150-200 nm polylethylene glycol coated polylactide/glycolide NPs in the absence of any permeability enhancer was suggested by Vila *et al.* (12), although no evidence was shown of *in vitro* NP translocation, or indeed of a systemic effect of insulin *in vivo,* from insulin-chitosan complex NPs following nasal administration (19). It has also been suggested that a paracellular transport of NPs larger than 20 nm is not feasible due to a maximal widening of the intercellular spaces of about 15 nm (20). The efficacy of mucosal absorption of macromolecules using chitosan NPs as a carrier system has in general been shown to be inferior compared to that obtained with chitosan solution or chitosan powder formulations (6, 10). While a limited number of studies have reported opening of TJs by chitosan NPs, a large proportion of investigations, as will be discussed later, have shown no such effects.

The present work provides a comparison between the effect of chitosan NPs and solution on TJ opening, whereby the paracellular translocation of model therapeutic macromolecules across the mucosal surfaces is investigated. In this study the hydrophilic FDs (FD4 and FD10), serving as models for therapeutic biomacromolecules, were not incorporated within the interior of the chitosan NPs, but

applied to cells in conjunction with the chitosan solution and the NP suspension. This work therefore mimics a possible situation where the therapeutic macromolecule is released from, and resides at the mucosal surface alongside the NPs. FDs (FD4 and FD10) are transported across a cell layer predominantly *via* the paracellular route, but due to their large size the extent of this transport is limited. However their paracellular transport would be improved if the chitosan formulations exhibited a TJ-opening effect. The present experimental design eliminated the need to consider a contribution of possible transcellular transport of chitosan NPs on the overall translocation of macromolecules across the epithelial cell layer. Even if transcellular transport of chitosan NPs did occur, this would not contribute to the apical-to-basolateral translocation of the FDs.

Chitosan NPs were in this work prepared by the ionic gelation method, under relatively mild preparation conditions, which would enable incorporation of different therapeutic molecules (including labile protein macromolecules) within the interior of the NPs. Previous studies have incorporated several biomolecules, in addition to peptides and proteins, including tetanus toxoid (21) and siRNA (22) into similarly fabricated NPs. The concentrations of chitosan and TPP established as optimal for the production of NPs in this experiment are comparable to those reported previously (23), with the final chitosan and TPP concentrations in the order of 1–3 mg/ml and 0.2–1.0 mg/ml, respectively. The optimal chitosan:TPP ratio on a weight-to-weight basis in this study was found to be 4.0, which is again comparable to the above studies. The zeta potential of the chitosan NPs was, as expected, positive, under experimental conditions used in the measurements, which is believed to be important for maintaining the mucoadhesive and TJ-opening properties of chitosan (24). It

should be noted that the preparation of chitosan NPs was based on the interaction between positively charged chitosan groups and the negatively charged TPP, where a balanced ratio of the two compounds is needed to ensure both sufficient cross-linking and also NP charge stabilization and surface presence of excess charge. It was ensured by centrifuging and repeated washing of the NPs that no free chitosan was present in the NP formulations, which could have biased the results. In previous studies by other research groups it has often not been clear whether free chitosan was present in the formulations and hence these studies are not directly comparable with this work.

Systematic studies on cell toxicity (using two different cell toxicity assays, MTS and LDH, and in addition assessment of cell layer integrity through measurement of TEER) were conducted in this work to compare the effects of chitosan NPs with corresponding concentrations of chitosan solutions. From these studies the concentration of chitosan (in nanoparticulate and solution form) with minimal toxic effects and a reversible decrease in cell layer TEER was chosen. Performing such a selection was considered necessary in order to ensure that the observed effects on TEER and permeability were due to TJ opening and a resulting increased access to the paracellular route, and not because of cell toxicity and compromised cell layer integrity.

MTS and LDH assays are two commonly used methods of determining cell toxicity. A reduction in metabolic activity is an early indication of cellular damage (25). On the other hand, the LDH assay indicates plasma membrane damage (26). Changes in metabolic activity are superior indicators of early cell injury, whereas membrane effects indicate more serious damage, leading to cell death (27). In this work, both

MTS and LDH assays were used to test two different indicators of cell toxicity and also for corroboration.

It is interesting to note that the effect of chitosan solution and NPs towards the metabolic activity of Calu-3 cells was similar (Figure 6.2), despite the fact that chitosan is presented to the cells in different forms. The reasons behind observation of this phenomenon are, at the present point, unclear. A similar finding was described with application of chitosan solution and chitosan NPs produced by the same method as in our study (ionotropic gelation) to pulmonary epithelial A549 cells, as revealed by the MTT reduction assay (28). On the other hand, Silva *et al.* (29) observed a remarkable decrease in LDH release when chitosan was used as NP coating instead of a solution.

The data on the membrane-disruptive effects of chitosan NPs, as determined by the LDH assay, indicates that even at chitosan concentration of as low as 0.003% w/v, chitosan NPs exhibit some degree of membrane disruption. A similar effect is observed with chitosan solution of an equivalent concentration. Although there are a large number of reported studies on the permeability-promoting effect of chitosan, very few of these studies incorporated the LDH membrane toxicity test. In the above-mentioned study by Silva *et al*. (29) it was found that the application of chitosan solutions ($M_W$ 150 kDa and degree of deacetylation near 85%) to Caco-2 cells was associated with dose-dependent and significant membrane toxicity. The concentrations of chitosan used in these studies were 0.1%, 0.25% and 0.5% w/v. In another study, a 30 min exposure of Caco-2 monolayers with chitosan hydrochloride, used at concentrations 0.005%, 0.01% and 0.5% w/v, resulted in a slight increase in

extracellular LDH activity. However, when cells were allowed to recover for 8 hours or 24 hours following the incubation with 0.005 or 0.01% w/v concentrations of chitosan, the LDH activity at these time points was similar to control, suggesting cell membrane recovery (30). Schipper *et al.* (31) found a dose-dependent effect on intracellular dehydrogenase release from Caco-2 cells when exposed to chitosans having a low degree of acetylation (<35%).

It should be noted that the concentrations of chitosan, either in solution or NP form, used in this study (0.003 and 0.006% w/v) were significantly lower than those typically reported in the literature. Reports on the toxicity of chitosan on Calu-3 cells are sparse, despite chitosan being studied extensively as a mucoadhesive and absorption-enhancing agent. It has been reported that application of chitosan solution at a concentration of 1.5% (w/v) reduced the metabolic activity of Calu-3 cells to around 68% compared to control (32). Chitosan NPs prepared by a similar ionic gelation method, as used in the present study, were shown to induce a reduction in the viability of A549 cells (human alveolar epithelial carcinoma) to approximately 70% at a concentration of around 1 mg/ml (0.1% w/v) (28). The same authors also reported that chitosan, delivered as microparticles, induced pro-inflammatory responses in rat lungs (33). However, other studies have reported low toxicity of chitosan solution and NPs in respiratory cell lines (3, 9). In a recent publication, the authors noted that chitosan/cyclodextrin ('hybrid') NPs exhibited a significantly lower cytotoxicity than those based on chitosan only (34), whereby the $IC_{50}$ values (NP dose causing a 50% reduction in cell viability) were 3-fold higher for chitosan/cyclodextrin-containing NPs compared to the chitosan-only NPs. However, it should be emphasized that direct comparisons between these studies, and also with the present work, are problematic

due to the variabilities in the experimental parameters, including the use of different cytotoxicity assays, cell lines, different conditions employed, different chitosan forms, molecular weights and suppliers, and finally, differences in chitosan formulations.

Polycations are generally considered to be cytotoxic (35). Kissel *et al.* (26) studied the toxicity of TMC and they propose that, its cytotoxic effects arise from an interaction with anionic components (sialic acid) of the glycoproteins on the surface of epithelial cells, which is also applicable to most cationic macromolecules such as protamine and polylysine. The authors found a $M_W$ effect on toxicity, with an increase in cytotoxicity as a function of $M_W$.

Regarding the discrepancies in the tolerability of chitosan between different cell lines, the present work clearly demonstrates a significant difference in two cell lines, Caco-2 and Calu-3. Reversibility in TEER (indicating cell layer recovery) was seen in Caco-2 cells following NP application containing significantly higher concentrations of chitosan (0.0125% w/v) compared to that used in Calu-3 cells (0.003% w/v). This indicates a cell specific toxicity and emphasizes the importance of using a relevant cell culture model.

The TEER data in this study demonstrates that chitosan in nanoparticulate form, as *per* production method described, maintains its intrinsic capacity to open the cellular TJs. Application of chitosan NPs or chitosan solution to Calu-3 layers was shown to be associated with a dramatic decrease in TEER for both NPs and solution, whereby the effect of NP formulation is comparable, although somewhat reduced, to chitosan solution of a corresponding concentration. Our results are in discrepancy with a study

by Ma and Lim (14) where soluble chitosan was more effective at disrupting the intercellular TJ than chitosan NPs. This was explained by the possibility of a less effective interaction of chitosan NPs with the cellular proteins because of their TPP-crosslinked chains (14). Furthermore, in a recent publication investigating the effect of chitosan-TPP NPs incorporated into mannitol microspheres on TJ modulation of Calu-3 layers, the authors did not observe any effects (on TEER and permeability) for the maximum NP concentration tested (1.3 mg/ml of NPs in the formulation, corresponding to chitosan amount of 150 μg) (3). Discrepancy in the capacity to induce TJ opening between chitosan solution and NPs has also been explained by a restriction in the movement of the chitosan chains in the nanoparticulate form, hindering the contact of these chains with the plasma membranes and TJs (36).

Another recent study on the effect of chitosan solution and NP formulations on TEER of Caco-2 monolayers showed that, in comparison to the free-soluble polymers, NPs based on chitosan and its quaternized derivatives (prepared by the ionic gelation method as used in this study), had a much lower effect on decreasing the TEER (15). The authors explained the finding by the reduced available amount of positive charge (charge density) at the surface of the NPs, compared to the soluble form of chitosan.

In the present study an equivalent amount of chitosan in the nanoparticulate form (devoid of free chitosan) to that in the solution form was applied and therefore the argument that there would be a reduced exposure of positive charge in the NPs in comparison to the solution would stand. The TJ modulating effects of chitosan were shown to be mediated by its cationic charges in a study by Schipper *et al.* (24), where the authors demonstrate an inhibition of permeation-enhancing effect of chitosan by

addition of the highly negatively charged heparin. The same group also showed that chitosans with a lower degree of deacetylation, and therefore with less free positively charged amino groups, had a lower absorption promoting effect (31).

The present study uses mucus producing Calu-3 cell layers. The presence of mucus would be expected to promote association of chitosan NPs, as well as chitosan from solution, with the cells. Behrens *et al.* (11) demonstrated a strong association of chitosan NPs (prepared by the same method as in the present study) with mucus-secreting MTX-E12 cells (58%), an effect that was less apparent with non-mucus producing Caco-2 cells (7.8%). Their study further showed that the largest fraction of NPs was bound to mucus and that removal of the mucus layer prior to incubation of cells with NPs led to a 14% decrease of NP association with the cells.

The strong mucoadhesive properties of chitosan coated-poly(isobutylcyanoacrylate) NPs have also been suggested by Bravo-Osuna *et al*. (37). However, in this study, the authors argue that the mucoadhesive properties of chitosan-coated NPs lead to their immobilization in the mucus layer, and in doing so, hamper their diffusion within the layer, reaching the vicinity of the TJ proteins, which the authors consider to be a prerequisite for a TJ-modulating effect. This theory was provided as an explanation for their finding that chitosan-coated NPs were ineffective in opening of the TJs and improving the paracellular permeability.

The ability of chitosan-coated nanoparticles to open the TJs has previously been attributed to their calcium biding property (37). In fact, poly(isobutyl cyanoacrylate) core-shell NPs coated with chitosan were shown to possess a higher capacity to bind

calcium than the solution, which the authors explained by an improvement in the accessibility of binding sites of chitosan on the NP surface (38). This results in a higher calcium-depleting capacity of NPs compared to solution. However, despite the widely-acknowledged role of calcium in maintaining the TJ integrity and therefore the barrier property of the epithelium (39, 40), previous work (see Chapter 5) showed that a reduction of apical calcium levels in Calu-3 and Caco-2 layers led to a limited effect on TJ opening with a reversible TEER decrease and a modest increase in FD4 permeability (41).

In our study, confocal imaging of filter-cultured Calu-3 cells incubated with NPs formulated with FITC-labelled chitosan showed NP distribution throughout the viewed area of the cell layer. The widespread observation of chitosan NPs on the apical side of the cell layer, even after extensive washing of the cells, indicates a strong association of the NPs with the cell layer possibly arising due to mucoadhesion and/or bioadhesion, which is in agreement with the above study. However, in our study, chitosan NPs appear to reach the apical cell membrane level, with some evidence of NP uptake, as judged from observations of vertical (Z-sections) distribution of fluorescence in Figure 6.10. This suggests a close proximity of the NPs to the apical cell membrane and cellular TJs, enabling an interaction of chitosan with the TJ proteins and the resulting TJ opening effect, which was clearly demonstrated in this work.

Determination of structural changes in cellular TJs following the incubation of the cells with chitosan formulations (NPs and solution) revealed that chitosan NPs produced a change in the distribution of ZO-1 protein that was similar to that

observed with chitosan solution, if not greater (Figure 6.11). Importantly, this experiment showed that the TEER-reducing and permeability-enhancing effects of chitosan NPs do indeed result from an effect on TJs and, to the best of our knowledge, no previous studies in the literature had reported such structural changes in TJs with chitosan NPs.

Owing to the bioadhesive nature of chitosan NPs, which is demonstrated in this work, any TJ-opening effect that the NPs may have is therefore likely to be relatively sustainable. Provided that the therapeutic molecule is present in the vicinity (for example released from the drug-incorporated NPs), the mucoadhesive and TJ-opening effect of chitosan NPs would be expected to result in an improvement of its permeability across the mucosal surface.

Experiments evaluating the apical-to-basolateral translocation of FDs across the Calu-3 layers showed that chitosan NPs, devoid of free chitosan, significantly enhanced their permeability. In the case of the smaller penetrant macromolecule, FD4, the increase in permeability seen with chitosan NPs was similar to that observed with chitosan solution of corresponding concentration. For FD10, a significantly higher apparent permeability was seen with chitosan solution compared to NPs. Factors accounting for this observation are not clearly apparent at the present moment, especially considering that chitosan NPs produced clearly obvious changes in ZO-1 (TJ protein) distribution similar to, or more pronounced than chitosan solution (Figure 6.11).

Work described in this chapter therefore clearly demonstrates that chitosan NPs, devoid of free chitosan, reversibly open the TJs and enhance macromolecular permeability across the Calu-3 layers, without inducing irreversible toxicity to the cells at the optimized concentration used. Furthermore, the data shows that chitosan NPs have a permeability-increasing effect similar to chitosan solution for a 4 kDa macromolecular solute and somewhat inferior effect for a 10 kDa macromolecule. Although the work shows there is no improvement in permeability-enhancement of chitosan NPs compared to chitosan solution, it may be still advantageous to deliver proteins therapeutics through the mucosal surfaces by incorporating them within the NPs with the aim to provide protection from enzymatic degradation, prolong the presence time at the mucosa and achieve a controlled drug release.

Mucoadhesive chitosan would be expected to associate with mucus, which is present on Calu-3 layers. In fact, based on the data obtained by confocal imaging of Calu-3 and Caco-2 layers following their incubation with FITC-labeled chitosan, there is evidence of occurrence of this phenomenon. Fluorescence was clearly apparent in all cell layers incubated with FITC-chitosan, even after an extensive washing step following the exposure of the cells with fluorescent chitosan. However, larger and brighter areas of fluorescence, indicating a greater content of fluorescent material, was seen in Calu-3 cells cultured under conditions that facilitate mucus production (AIC) (42) compared to Calu-3 cells cultured using LCC and Caco-2 cells (Figure 6.12). It is possible that the presence of mucus in Calu-3 cell layers cultured using AIC leads to a greater retainment of chitosan on the apical surface of the cell layer. Note that to demonstrate that chemical conjugation of FITC to chitosan does not alter the effects of chitosan on cellular TJs, it was shown that application of FITC-chitosan

to Calu-3 layers leads to a reversible decrease in TEER and an increase in FD4 permeability across the cells (Figure 6.9); these effects were very similar to those encountered with unlabeled chitosan.

Considering its well-established permeation-enhancing effect, which was also demonstrated in our work, chitosan (as solution) was evaluated whether it improves the transport of very large $M_W$ proteins (antibodies) across the Calu-3 layers. More specifically, the tested biomolecules (supplied by UCB) consisted of investigational therapeutic antibodies or antibody fragments (one of which was PEGylated). Although the technique used to quantify the antibodies suffered from a poor sensitivity, two out of four tested antibodies were detected in the basolateral solution, suggesting their translocation across the cell layers. These included the antibody fragments (Fabs) hCTMO1 and mA33γ1 Fab. In the case of the latter molecule (mA33γ1 Fab), its detection is not surprising considering its $M_W$ of approximately 25 kDa (lowest $M_W$ out of the tested molecules). A lower level of transport across the cell layers was observed with the higher molar mass hCTMO1γ4 (approximately 96 kDa), suggesting a $M_W$ effect, which was also seen with FDs. It is apparent from section 6.3.11 that the permeability of antibodies/fragments was expressed as % amount relative to the apically-applied amount; this is because the apparent permeability coefficient ($P_{app}$) values could not be calculated due to the lack of sufficient detection points of the materials over time (the tested compounds were not detected in the basolateral solution in the first 2 hours of the sampling period). Furthermore, it was not possible to calculate the permeability enhancement ratios as antibody permeability values in the control experiment could not be established. Nevertheless, the findings suggest that chitosan facilitated the translocation of two

antibody fragments across the Calu-3 layers, with the extent of this translocation depending on the $M_W$ of the tested molecule.

## 6.5 Conclusion

This work demonstrated that chitosan NPs, formulated using an ionic gelation method, exhibited similar effects on cellular toxicity and TJs to chitosan solution, as tested on Calu-3 layers. When applied at a concentration associated with limited toxicity, chitosan NPs reversibly opened the cellular TJs, as demonstrated by a sharp and reversible decrease in cell layer TEER and an increase in the permeability of two FDs. Chitosan NPs displayed TJ opening effects of an almost similar magnitude to chitosan solution. Furthermore, the similarity in TJ effect between NPs and chitosan solution was demonstrated through the changes that the two formulations of chitosan produced in the distribution of ZO-1 TJ protein. The mucoadhesive nature of chitosan solution and NPs was evident through imaging of mucus producing cell layers incubated with FITC-labelled chitosan (NPs or solution). The permeability enhancing property of chitosan (solution) was confirmed when testing its effect on the translocation of investigational antibody fragments across the Calu-3 layers, with evidence that the improvement in permeability is dependent on the $M_W$ of the tested solute. While there was no improvement in the permeability with chitosan NPs compared to solution, the former provide the potential for drug incorporation with the possibility of providing controlled drug release and protection from enzymatic degradation.

## 6.6 References


1. S. Hirano, H. Seino, Y. Akiyama, and I. Nonaka. Chitosan: a biocompatible material for oral and intravenous administration. In C.G. Gebeleinand R.L. Dunn (eds.), Progress in Biomedical Polymers, Plenum Press, New York, 1990, pp. 283-289.
2. M. Dornish, M. Aarnold, and O. Skaugrud. Alginate and chitosan: Biodegradable biopolymers in drug delivery systems. Eur J Pharm. 4:S153-S153 (1996).
3. A. Grenha, C.I. Grainger, L.A. Dailey, B. Seijo, G.P. Martin, C. Remunan-Lopez, and B. Forbes. Chitosan nanoparticles are compatible with respiratory epithelial cells in vitro. Eur J Pharm Sci. 31:73-84 (2007).
4. P. Artursson, T. Lindmark, S.S. Davis, and L. Illum. Effect of chitosan on the permeability of monolayers of intestinal epithelial cells (Caco-2). Pharm Res. 11:1358-1361 (1994).
5. L. Illum. Chitosan and its use as a pharmaceutical excipient. Pharm Res. 15:1326-1331 (1998).
6. A.M. Dyer, M. Hinchcliffe, P. Watts, J. Castile, I. Jabbal-Gill, R. Nankervis, A. Smith, and L. Illum. Nasal delivery of insulin using novel chitosan based formulations: a comparative study in two animal models between simple chitosan formulations and chitosan nanoparticles. Pharm Res. 19:998-1008 (2002).
7. I. Fiebrig, S.E. Harding, and S.S. Davis. Sedimentation analysis of potential interaction between mucins and a putative bioadhesive polymer. Progr Colloid Polym Sci. 94:66-73 (1994).
8. R.J. Soane, M. Frier, A.C. Perkins, N.S. Jones, S.S. Davis, and L. Illum. Evaluation of the clearance characteristics of bioadhesive systems in humans. Int J Pharm. 178:55-65 (1999).
9. J.M. Smith, M. Dornish, and E.J. Wood. Involvement of protein kinase C in chitosan glutamate-mediated tight junction disruption. Biomaterials. 26:3269-3276 (2005).
10. L. Illum. Nanoparticulate systems for nasal delivery of drugs: a real improvement over simple systems? J Pharm Sci. 96:473-483 (2007).
11. I. Behrens, A.I. Pena, M.J. Alonso, and T. Kissel. Comparative uptake studies of bioadhesive and non-bioadhesive nanoparticles in human intestinal cell lines and rats: the effect of mucus on particle adsorption and transport. Pharm Res. 19:1185-1193 (2002).
12. A. Vila, A. Sanchez, M. Tobio, P. Calvo, and M.J. Alonso. Design of biodegradable particles for protein delivery. J Control Release. 78:15-24 (2002).
13. R. Fernandez-Urrusuno, P. Calvo, C. Remunan-Lopez, J.L. Vila-Jato, and M.J. Alonso. Enhancement of nasal absorption of insulin using chitosan nanoparticles. Pharm Res. 16:1576-1581 (1999).
14. Z. Maand L.Y. Lim. Uptake of chitosan and associated insulin in Caco-2 cell monolayers: a comparison between chitosan molecules and chitosan nanoparticles. Pharm Res. 20:1812-1819 (2003).
15. A.M. Sadeghi, F.A. Dorkoosh, M.R. Avadi, M. Weinhold, A. Bayat, F. Delie, R. Gurny, B. Larijani, M. Rafiee-Tehrani, and H.E. Junginger. Permeation enhancer effect of chitosan and chitosan derivatives: comparison of

formulations as soluble polymers and nanoparticulate systems on insulin absorption in Caco-2 cells. Eur J Pharm Biopharm. 70:270-278 (2008).
16. R.A. Muzzarelli. Colorimetric determination of chitosan. Anal Biochem. 260:255-257 (1998).
17. C. Colonna, B. Conti, P. Perugini, F. Pavanetto, T. Modena, R. Dorati, P. Iadarola, and I. Genta. Ex vivo evaluation of prolidase loaded chitosan nanoparticles for the enzyme replacement therapy. Eur J Pharm Biopharm. 70:58-65 (2008).
18. L. Illum. Nasal drug delivery--possibilities, problems and solutions. J Control Release. 87:187-198 (2003).
19. S. Mao, O. Germershaus, D. Fischer, T. Linn, R. Schnepf, and T. Kissel. Uptake and transport of PEG-graft-trimethyl-chitosan copolymer-insulin nanocomplexes by epithelial cells. Pharm Res. 22:2058-2068 (2005).
20. T. Jung, W. Kamm, A. Breitenbach, E. Kaiserling, J.X. Xiao, and T. Kissel. Biodegradable nanoparticles for oral delivery of peptides: is there a role for polymers to affect mucosal uptake? Eur J Pharm Biopharm. 50:147-160 (2000).
21. B. Sayin, S. Somavarapu, X.W. Li, M. Thanou, D. Sesardic, H.O. Alpar, and S. Senel. Mono-N-carboxymethyl chitosan (MCC) and N-trimethyl chitosan (TMC) nanoparticles for non-invasive vaccine delivery. Int J Pharm. 363:139-148 (2008).
22. H. Katasand H.O. Alpar. Development and characterisation of chitosan nanoparticles for siRNA delivery. J Control Release. 115:216-225 (2006).
23. P. Calvo, C. Remunan-Lopez, J.L. Vila-Jato, and M.J. Alonso. Chitosan and chitosan/ethylene oxide-propylene oxide block copolymer nanoparticles as novel carriers for proteins and vaccines. Pharm Res. 14:1431-1436 (1997).
24. N.G. Schipper, S. Olsson, J.A. Hoogstraate, A.G. deBoer, K.M. Varum, and P. Artursson. Chitosans as absorption enhancers for poorly absorbable drugs 2: mechanism of absorption enhancement. Pharm Res. 14:923-929 (1997).
25. NoAbBioDiscoveries. Cytotoxicity. http://www.noabbiodiscoveries.com/assays/invitro/cytotoxicity_studies.pdf (accessed 12/01/2010 2010).
26. S. Mao, X. Shuai, F. Unger, M. Wittmar, X. Xie, and T. Kissel. Synthesis, characterization and cytotoxicity of poly(ethylene glycol)-graft-trimethyl chitosan block copolymers. Biomaterials. 26:6343-6356 (2005).
27. J.C. Davila, C.G. Reddy, P.J. Davis, and D. Acosta. Toxicity assessment of papaverine hydrochloride and papaverine-derived metabolites in primary cultures of rat hepatocytes. In Vitro Cell Dev Biol. 26:515-524 (1990).
28. M. Huang, E. Khor, and L.Y. Lim. Uptake and cytotoxicity of chitosan molecules and nanoparticles: effects of molecular weight and degree of deacetylation. Pharm Res. 21:344-353 (2004).
29. C.M. Silva, F. Veiga, A.J. Ribeiro, N. Zerrouk, and P. Arnaud. Effect of chitosan-coated alginate microspheres on the permeability of Caco-2 cell monolayers. Drug Dev Ind Pharm. 32:1079-1088 (2006).
30. V. Dodane, M. Amin Khan, and J.R. Merwin. Effect of chitosan on epithelial permeability and structure. Int J Pharm. 182:21-32 (1999).
31. N.G. Schipper, K.M. Varum, and P. Artursson. Chitosans as absorption enhancers for poorly absorbable drugs. 1: Influence of molecular weight and degree of acetylation on drug transport across human intestinal epithelial (Caco-2) cells. Pharm Res. 13:1686-1692 (1996).

32. B.I. Florea, M. Thanou, H.E. Junginger, and G. Borchard. Enhancement of bronchial octreotide absorption by chitosan and N-trimethyl chitosan shows linear in vitro/in vivo correlation. J Control Release. 110:353-361 (2006).
33. Y.C. Huang, A. Vieira, K.L. Huang, M.K. Yeh, and C.H. Chiang. Pulmonary inflammation caused by chitosan microparticles. J Biomed Mater Res A. 75:283-287 (2005).
34. D. Teijeiro-Osorio, C. Remunan-Lopez, and M.J. Alonso. Chitosan/cyclodextrin nanoparticles can efficiently transfect the airway epithelium in vitro. Eur J Pharm Biopharm. 71:257-263 (2009).
35. D.M. Morgan, V.L. Larvin, and J.D. Pearson. Biochemical characterisation of polycation-induced cytotoxicity to human vascular endothelial cells. J Cell Sci. 94 ( Pt 3):553-559 (1989).
36. C. Prego, M. Garcia, D. Torres, and M.J. Alonso. Transmucosal macromolecular drug delivery. J Control Release. 101:151-162 (2005).
37. I. Bravo-Osuna, C. Vauthier, H. Chacun, and G. Ponchel. Specific permeability modulation of intestinal paracellular pathway by chitosan-poly(isobutylcyanoacrylate) core-shell nanoparticles. Eur J Pharm Biopharm. 69:436-444 (2008).
38. I. Bravo-Osuna, G. Millotti, C. Vauthier, and G. Ponchel. In vitro evaluation of calcium binding capacity of chitosan and thiolated chitosan poly(isobutyl cyanoacrylate) core-shell nanoparticles. Int J Pharm. 338:284-290 (2007).
39. C.A. Rabito, C.A. Rotunno, and M. Cereijido. Amiloride and calcium effect on the outer barrier of the frog skin. J Membr Biol. 42:169-187 (1978).
40. T.Y. Ma, D. Tran, N. Hoa, D. Nguyen, M. Merryfield, and A. Tarnawski. Mechanism of extracellular calcium regulation of intestinal epithelial tight junction permeability: role of cytoskeletal involvement. Microsc Res Tech. 51:156-168 (2000).
41. D. Vllasaliu, M.C. Garnett, C. Alexander, M. Eaton, and S. Stolnik. Enhancing Paracellular Permeability by Calcium Depletion, *2nd International Symposium on Cellular Delivery of Therapeutic Macromolecules (CDTM) 2008*, Cardiff, UK, 2008.
42. C.I. Grainger, L.L. Greenwell, D.J. Lockley, G.P. Martin, and B. Forbes. Culture of Calu-3 cells at the air interface provides a representative model of the airway epithelial barrier. Pharm Res. 23:1482-1490 (2006).

# Chapter 7

# The potential of IgG transcytosis pathway for mucosal protein and nanoparticle delivery

## 7.1 Introduction

While it is potentially feasible to achieve mucosal absorption of smaller peptides and proteins by inducing transient opening of the epithelial tight junctions (TJs), this strategy is inefficient for larger protein therapeutics such as antibodies ($M_W$ approximately 150 kDa) (1), or delivery systems based on nano-sized carriers larger than 20 nm (2). It is also important to remember that the surface area defined by the TJs (i.e. the paracellular route), represents only a small proportion of the overall surface area of the epithelia that is potentially accessible to the mucosally-administered drug (3). Indeed, in the gut this amounts to around 1% of the overall area (4). Transcytosis would potentially overcome this problem. Furthermore, unlike paracellular transport, receptor-mediated transcytosis is specific (5) to molecules (ligands) that are able to recognize and bind to receptors involved in the process, making this pathway selective to ligands or ligand-coupled therapeutic molecules or carrier systems. Therefore receptor-mediated transcytosis is potentially an attractive route for mucosal absorption of protein therapeutics.

IgG has long been known to be actively transferred from mother to offspring,

confering short-term passive immunity (6, 7). Its transport is carried out by the neonatal Fc receptor (FcRn) (8, 9). The FcRn is a potential candidate for mucosal delivery of therapeutic proteins, because it is expressed in several organs and tissues, including the placenta (10), lung (11), kidney (12) and intestine (13) in which it is involved in IgG transport. Exression of FcRn in epithelia is thought to play an important role in the function of IgG in immune surveillance and host defense at mucosal surfaces (14).

FcRn-mediated transport pathway across the lung epithelium may potentially be a useful route to deliver biological agents. Recent studies attempting to achieve pulmonary delivery of erythropoietin and follicle-stimulating hormone (FSH) in non-human primates through this route proved promising (15, 16). These studies indicated that delivery of Fc-fusion proteins (therapeutic proteins conjugated to the Fc domain of IgG) to the upper airway results in an Fc-dependent, saturable uptake of these proteins into the systemic circulation (15-19). Furthermore, alveolar epithelial cells have also been shown to transcytose IgG *in vitro* (20). Therefore, considering that the surface area of the alveolar epithelium is much larger compared to the upper airway epithelium, the alveolar surface may contribute considerably to the amount of IgG absorbed through the pulmonary route (21).

IgG is taken into epithelial cells from the external milieu by pinocytosis through formation of coated vesicles by invagination of the plasma membrane (22-24). Some binding of IgG to FcRn may occur at the plasma membrane (25), though it is more likely that binding predominantly takes place intracellularly as there is evidence that the majority of FcRn appears to be localized within acidic endosomal vesicles within

the cell, with little FcRn being detectable at the cell surface (26). Rather than fusing with the degradative lysosomes, the vesicles containing IgG bound to FcRn pass through the epithelial cell in the apical to basolateral direction, eventually releasing intact IgG to the interstitial space. This process is predominantly unidirectional in a physiological setting, being driven by a strong pH dependence of the binding of IgG to FcRn (as will be discussed below), and the pH gradient between the luminal and serosal sides of the epithelial cells.

The Fc portion of IgG binds with high affinity to FcRn, with a 1:2 stoichiometry (21, 27), at an acidic environment of the endosome (pH<6.5) (21), but not at a physiological pH (7.4) (8, 28, 29). The strict pH dependence of the FcRn–Fc interaction is mediated by the titration of histidine residues in the $C_H2$–$C_H3$ hinge region of IgG and their subsequent interaction with acidic residues on the surface of FcRn (21). The neutral (to slightly alkaline) pH found in the interstitial space enables the release of IgG from FcRn after fusion of the IgG-containing transport vesicles with the plasma membrane at the basolateral side of epithelial cells (18). Passage of IgG into the circulation is likely to occur largely through the paracellular route because of the absence of TJs between endothelial cells (30).

Work described in this chapter investigated the transport of IgG across Calu-3 layers. Furthermore, this work assessed the potential of the IgG/FcRn transcytotic pathway for cellular uptake and transcellular transport of nanoparticles (NPs), which to the best of our knowledge has not been attempted previously. The use of Calu-3 cells for the purpose of this work was possible as this cell line has been shown to express FcRn (11). Initial work examined FcRn expression in Calu-3 cells (to confirm previous

reported findings), followed by characterisation of IgG transport across the cell layers. Uptake and transport of model NPs across the cell layers was then investigated by adsorbing IgG, or Fc portion of IgG, onto the surface of NPs. Certain studies were repeated in Caco-2 monolayers for the purpose of comparison.

## 7.2 Methods

### 7.2.1 Immunostaining for FcRn

Filter-cultured Calu-3 cells in the form of polarised layers were fixed in parafomaldehyde, washed with PBS and permeabilized by incubating with Triton X-100 (0.1% v/v in PBS) for approximately 10 min. Cells were washed again with PBS and incubated for 1 hour with BSA in PBS (1% w/v). Goat, anti-human FcRn primary antibody was diluted to 10 μg/ml in 1% BSA/PBS and incubated with the cells for 30-60 min at room temperature. Cells were then washed extensively with PBS (5x) and treated with donkey, anti-goat TRITC-IgG (secondary antibody, diluted according to supplier's instructions in 1% BSA/PBS) for 30-60 min. Thereafter, cells were washed extensively with PBS and filters excised and mounted on a glass slide (using the DAPI-containing ProLong® Gold antifade mounting medium) for confocal imaging, which was performed using the confocal system described in section 2.2.6.3.

Calu-3 cells cultured on filters under LCC conditions and Caco-2 cell monolayers were also immunostained for FcRn (and thereafter imaged using CLSM). This was conducted in the same manner as above.

### 7.2.2 Association of FITC-IgG with cell layers

*7.2.2.1 Effect of pH on FITC-IgG association with cells*

Calu-3 cells, as confluent layers, were serum starved by incubating with HBSS for 1 hour. To ensure maximal removal of the residual bovine IgG (bIgG, present in FBS, used to supplement the culture medium), HBSS was replaced (in both, apical and basolateral compartment) twice during the serum-starving period (at 15 min and 30 min). FITC-IgG (human, 5 μg/ml) was applied to the apical side at pH 6.0 or 7.4 (in MES- or HEPES-buffered HBSS, respectively). Following a 3-hour incubation of the cells with FITC-IgG, 100 μl volumes were removed from the apical side of the cell layers and transferred to a black 96-well plate for fluorescence measurements. FITC-IgG was quantified by fluorescence (485 nm excitation, 535 nm emission; using an MFX microtiter plate fluorometer from Dynex Technologies, USA) through pre-constructed calibration curves. Note that to account for pH sensitivity of FITC, in cases where FITC-IgG was applied at pH 6.0, the calibration curves were constructed by serially diluting FITC-IgG in HBSS at pH 6.0.

*7.2.2.2 Association of FITC-IgG with cells: competition with unlabelled IgG*

A solution of human FITC-IgG (5 μg/ml) and human IgG (referred to as 'IgG' in this thesis, 20 μg/ml) in HBSS (pH 6.0) was added to confluent cell layers and cells incubated for 3 hours. Apical solutions were then sampled (by removing 100 μl volumes) and transferred into a black 96-well plate. FITC-IgG was quantified by fluorescence in the manner described in the preceding section.

*7.2.2.3 Cell uptake of FITC-IgG: effect of pH and competition with unlabelled IgG*

Cell uptake of FITC-IgG was assessed on the same confluent Calu-3 layers used in the preceding two experiments (section 7.2.3.2 and 7.2.3.3). As described above, cell layers were incubated with FITC-IgG (5 μg/ml) at pH 6.0 or pH 7.4 for 3 hours. Additionally, some cell layers were incubated with a solution containing a combination of FITC-IgG (5 μg/ml) and unlabelled IgG (20 μg/ml), at pH 6.0. After sampling of the apical solution for the purpose of FITC-IgG quantitation in experiments detailed in the preceding two sections, the apical solution was aspirated and cells washed with PBS extensively (5x). Cells were then permeabilised with Triton X-100 (0.1% v/v), which also produced cell detachment from the filters. Cells were collected from the filters, transferred into microcentrifuge tubes and centrifuged (13,000 rpm) to form cell pellets. The supernatants were transferred into a black 96-well plate following which FITC-IgG was quantified by fluorescence as before (see section 7.2.2.1). Note that the calibration curve used to quantify FITC-IgG was in this instance constructed by measuring the fluorescence of known concentrations of FITC-IgG progressively diluted in a solution of Triton X-100, 0.1% v/v in HBSS.

### 7.2.3 IgG transport experiments

*7.2.3.1 IgG transport across Calu-3 layers*

Culture medium was removed from confluent cell layers and cells washed with PBS. Cells were then serum starved by incubating with HBSS (pH 6.0 and 7.4 on the apical and basolateral side, respectively) for 1 hour prior to the transport experiments. In an attempt to remove the residual bIgG present in FBS, HBSS was replaced twice during the serum-starving period as described in section 7.2.2.1. 1 μg/ml of IgG (human) was applied on the apical side of the cells and IgG transport across the cell layers was

measured for the duration of two hours by regular sampling of the basolateral solution (with replacement of the sampled volumes). HBSS (pH 6.0 and pH 7.4, on the apical and basolateral side, respectively) was used as the transport medium. IgG was quantified by ELISA, in the manner detailed in section 2.2.7.1.

*7.2.3.2 Transport saturation*

IgG was applied to the apical side of serum-starved Calu-3 layers at the following concentrations: 50 ng/ml, 500 ng/ml and 5 µg/ml (in HBSS, pH 6.0). Its apical-to-basolateral translocation was determined by quantifying IgG present in the basolateral medium (HBSS) at different time intervals (every 30 min). However, in contrast to the experiment above, transport was assessed over 3 hours and the basolateral solution was completely exchanged at each sampling interval. IgG was quantified by ELISA, as described in section 2.2.7.1.

*7.2.3.3 Receptor competition*

IgG (1 µg/ml) was added to the apical side of confluent (serum-starved) Calu-3 layers in conjunction with rabbit IgG (rIgG, 50 µg/ml), both in HBSS at pH 6.0. The basolateral medium (HBSS) was then sampled regularly (every 30 min) over 2 hours (with replacement of the sampled volumes). (Human) IgG specific ELISA was then conducted on the sampled solutions, as described in section 2.2.7.1.

*7.2.3.4 IgG transport across Caco-2 monolayers*

Caco-2 cells were cultured on filters for 21-23 days as per protocol detailed before (section 2.2.1). Apical-to-basolateral IgG transport experiment was conducted in the same way as for Calu-3 cells (described in Section 7.2.3.1).

### 7.2.4 Adsorption of IgG or Fc to NPs

FITC-IgG was adsorbed on the surface of sulfate-modified, polystyrene NPs of 30 nm diameter (Red, Sigma). To achieve this, the stock suspension of NPs (containing 2.5% w/v solid) was diluted in 1:50 in distilled water (sterile filtered). The use of HBSS or PBS for dilution of NPs was not appropriate due to the colloidal instability (coagulation) of the NPs in these buffers. The resulting diluted NP suspension was added to FITC-IgG stock solution (10 mg/ml in 0.01 M PBS). An overall amount of FITC-IgG used per 1 ml of diluted NP solution was 1 mg (equivalent to 50 mg FITC-IgG per 1 ml of 2.5% w/v stock NP suspension). NPs were incubated with IgG at room temperature for 3 hours, with gentle magnetic stirring. The suspension was then centrifuged at 14,000 rpm for 30 min. The supernatant was removed and the NP pellet re-suspended in HBSS (pH 6.0), the volume of which was equal to the volume of removed supernatant.

The amount of IgG added to the NPs was selected based on the hypothetical number of IgG molecules adsorbing on the surface of one NP, which was calculated by, firstly, determining the number of NPs in 1 ml of the stock solution using the equation provided by the manufacturer (Sigma):

$$NP_n = \frac{6.03 \times 10^{10} \times S}{3.3 \times d^3} = 1.692 \text{ x } 10^{15}$$

($NP_n$ is NP number, $S$ is % solids in NP stock solution, and $d$ is the diameter, μm.)

Thereafter, the surface area of one NP was determined using this equation:

$$SA = 4\pi r^2 = 2827.43 \text{ nm}^2$$

(SA is the surface area and $r$ is the NP radius.)

Based on the literature data (31), the minimal molecular area of the native 'T'-shaped IgG in the adsorbed closely-packed monolayer, calculated from X-ray diffraction data, should be approximately 7100 $Å^2$ when the molecules are attached to the surface by the 'leg' (Fc fragment) or by the 'cap' ('end-on' disposition), approximately 4200 $Å^2$ at the 'side-on' disposition, and approximately 12100 $Å^2$ at the flat disposition. Therefore, a theoretical estimate (range) of the number of IgG molecules adsorbing per one NP can be calculated in the following way:

$$\text{AC} = \text{between} \quad \frac{2827.43 nm^2}{12100 A^2} \text{ and } \frac{2827.43 nm^2}{4200 A^2} = 23\text{-}67$$

(AC is adsorption capacity in terms of number of IgG molecules per 1 NP.)

The number of IgG molecules adsorbed on the surface of NPs present in 1 ml of NP suspension (undiluted 2.5% w/v stock) was calculated to be between $3.892 \times 10^{16}$ and $1.134 \times 10^{17}$ ($AC \times NP_n$), amounting to a range between $6.463 \times 10^{-8}$ M and $1.883 \times 10^{-7}$ M

(calculated using Avogadro's constant) or between approximately 9.7 mg and approximately 28.2 mg. The higher ratio of 50 mg per 1 ml of NP suspension (undiluted stock containing 2.5% w/v solid) was used to ensure maximal NP surface coverage.

FITC-Fc or (unlabelled) Fc fragment of IgG (Jackson Immunoresearch, USA) were adsorbed on three types of fluorescent polystyrene NPs: red, sulfate modified, 30 nm diameter NPs (used above, Sigma), yellow-green (YG), 20 nm, sulfate modified (FluoSpheres®, Invitrogen) and YG, 50 nm, carboxy-modified (Fluoresbrite®, Polysciences Europe). Additionally, Fc was also adsorbed on non-fluorescent, carboxy-modified NPs of 50 nm (Polybead®, Polysciences Europe). The adsorption was performed by incubating the NPs, which were diluted 1 in 20 in distilled water (sterile filtered) with Fc in a similar way as for IgG, described above, with the following exceptions. 20 mg of Fc (in PBS) was used per 1 ml of 2% w/v and 2.5% w/v solid NP stock suspension, for FluoSpheres® and Fluoresbrite® NPs, respectively. This amounted to approximately 5.3 and 13.2 molecules of Fc per one 20 nm (sulfate-modified) and 50 nm (carboxy-modified) NP, respectively, as calculated by determining the number of NPs per 1 ml (using manufacturer's information, in a similar way to above) and the number of individual Fc molecules (by employing Avogadro's constant). The amount of Fc used for coating of the NPs was probably lower than the adsorption capacity of NPs. However, this was done intentionally in order to achieve sub-total decoration of the NP surfaces, leaving exposed surface charges in an attempt to maximise the colloidal stability (charge repulsion) of NPs. Consequently, the decision was made not to centrifuge the NP suspensions following the incubation with Fc solution to remove the excess of free (not adsorbed) Fc as no

significant amount of free Fc was expected. Omitting the centrifugation step was considered advantageous as to prevent NP aggregation, which was noted following centrifugation of IgG-coated NPs. After incubation with Fc, the resulting suspension was diluted (1 in 5) in HBSS (pH 6.0) to achieve an overall dilution of 1 in 100 for all NP stock suspensions; NPs were applied to cells at this concentration.

Note that protein-adsorbed NPs were applied to cells in HBSS (pH 6.0) in all cases. A control experiment, which potentially indicates successful adsorption of Fc onto the NP surface, was in some cases performed by adding HBSS to 'uncoated' NP suspension (of the same concentration), with evident immediate aggregation. Out of the different NPs used in this work, colloidal stability in HBSS in the absence of Fc was only apparent with those having a carboxy-modified surface (as judged by observation of visually transparent solution following the addition of HBSS to NPs).

#### *7.2.4.1 Nanoparticle size characterisation*

The mean diameter and size distribution of NPs after their incubation with IgG or Fc was determined by Dynamic Light Scattering (DLS) using a Viskotec system. Protein-adsorbed NPs were analysed by DLS suspended in HBSS at pH 6.0 (to replicate the conditions in which NPs were applied to the cells). The results represent the mean of ten measurements, performed at 25°C.

### 7.2.5 Confocal microscopy analysis of cellular uptake of IgG- or Fc-NPs

#### *7.2.5.1 Cell uptake of IgG-adsorbed NPs*

Confluent cell layers were serum-starved (in the way described in section 7.2.3.1) for 1 hour. HBSS was then removed from the apical side of the layers and replaced with

IgG-adsorbed NP suspension (red, 30 nm, sulfate-modified) in HBSS (pH 6.0). The incubation with NPs continued for 2 hours. NP suspension was then removed and cells washed extensively (5x) with PBS. Cells were then fixed with 4% paraformaldehyde and processed for confocal imaging (in the way described in section 2.2.6.5). Confocal imaging was performed using the Leica system described in section 2.2.6.3.

*7.2.5.2 Cell uptake of Fc-adsorbed NPs*

The method detailed in section 7.2.5.1 for the uptake of IgG-coated NPs was followed, i.e. FITC-Fc- or Fc-adsorbed NPs, were applied to confluent, serum-starved cell layers (in HBSS, pH 6.0) for 2 hours. Cells were then washed (with PBS, 5x) and fixed with paraformaldehyde as before. Fixed cells were either processed for confocal imaging (as described in section 2.2.6.5) or in some cases, stained for ZO-1 TJ protein (following the method detailed in section 2.2.6.6) prior to processing for confocal microscopy. YG, Fc-adsorbed NPs were used in addition to red NPs (both sulfate modified). Adsorption of Fc on NPs was conducted according to the method described in section 7.2.4.

*7.2.5.3 LysoTracker® staining*

Fc-adsorbed NPs (YG, sulfate modified), prepared as described in section 7.2.4 were applied to the cells in a similar manner as in the preceding section, but in combination with the LysoTracker® probe. The concentration of the probe in the apical solution (containing NPs in HBSS, pH 6.0) was 100 nM. (A higher than the manufacturer's recommended concentration of 50-75 nM was used due to the lack of observed staining with the recommended concentration range). Cells were incubated with the

NPs and the LysoTracker® probe for 2 hours. The apical solution was thereafter removed and cells washed extensively with PBS. Cells were fixed with paraformaldehyde and processed for confocal imaging as described in section 2.2.6.5. Cell samples were imaged by CLSM using the system described in section 2.2.6.3.

### 7.2.6 Cell uptake of Fc-NPs: measurement of NP fluorescence

*7.2.6.1 Cell uptake of Fc-NPs, comparison with unmodified NPs, and effect of IgG*

YG, carboxy-modified NPs were used for the purpose of this experiment due to their colloidal stability in HBSS in the absence of Fc (see section 7.2.4). Fc-adsorbed and unmodified (non-coated) NPs were applied to confluent, serum-starved cell layers. Additionally, Fc-NPs were applied to cell layers in the presence of soluble, 'free' IgG (5 μg/ml, added separately prior to the application of Fc-NPs). NP concentration was identical in all three situations. Cells were incubated with NPs for 3 hours, following which apical solutions were removed and cells extensively washed with PBS. Triton X-100 (0.1 v/v in PBS) was then applied to the cells for approximately 10 min. Application of Triton X-100 resulted in cell membrane permeabilisation and cell detachment from the filters. Cells were collected, transferred into microcentrifuge tubes and centrifuged at 13,000 rpm for 5 min. 100 μl of the supernatant from each pelleted cell layer was transferred to a 96-well plate for fluorescence determination. Cell uptake of NPs was quantified by fluorescence (485 nm excitation, 535 nm emission) using an MFX microtiter plate fluorometer (Dynex Technologies, USA), through preconstructed calibration curves. NP solution applied to cells was progressively diluted in a solution of 0.1% v/v Triton X-100 in HBSS and the resulting curve (a mean of three) was used to quantify NP uptake in terms of % relative to the applied amount.

*7.2.6.2 Effect of non-fluorescent Fc-NPs on cell uptake of fluorescent Fc-NPs*

Fluorescent (YG) and non-fluorescent NPs (both carboxy-modified, 50 nm) were used for the purpose of this experiment. Adsorption of Fc to NPs was conducted in the same manner for both, fluorescent and non-fluorescent NPs, as described in section 7.2.4. Confluent cell layers were serum-starved for 1 hour before the experiment as described in section 7.2.3.1 and NP suspensions (in HBSS, pH 6.0) were applied to the apical side of the cell layers. Fluorescent Fc-NPs (i.e. Fc adsorbed on fluorescent NPs) were applied to the cells either on their own or with non-fluorescent Fc-NPs (used at a 5-fold higher concentration than fluorescent Fc-NPs). The concentration of fluorescent Fc-NPs was kept identical in both scenarios. The incubation lasted for 3 hours at usual cell culture conditions (37°C/5%$CO_2$), following which the apical solution was aspirated and cell layers washed. Cells were then permeabilised and detached from filters with Triton X-100, pelleted by centrifugation and the supernatant collected. NP uptake was quantified by measuring the fluorescence of the supernatant using the method described in section 7.2.6.1. NP uptake is expressed as % relative to the applied amount, as determined through calibration curves in the manner detailed in section 7.2.6.1.

### 7.2.7 Fc-coated NP transport across the cell layers

*7.2.7.1 Transport of Fc-NPs and unmodified NPs*

YG, carboxy-modified NPs were used in this experiment. Transport of Fc-NP (prepared as described in section 7.2.4) across the Calu-3 layers was determined simultaneously to NP uptake (section 7.2.6.1). Following the application of NPs on the apical side of the cell layers (as detailed in section 7.2.6.1), the basolateral solution was sampled regularly for 3 hours (with replacement of the sampled

volumes). NPs were quantified in the sampled basolateral solutions by fluorescence (see section 3.2.4); the extent of transport is expressed as % relative to the applied amount.

*7.2.7.2 Effect of IgG on Fc-NP transport*

YG, sulfate-modified, Fc-NPs (prepared as described in Section 7.2.4) were applied to the apical side of the cell layers and incubated with the cells for 3 hours. In some cases NPs were added to the cells in combination with soluble IgG (5 μg/ml, added separately prior to the application of Fc-NPs). Cells were incubated with NPs for three hours, after which the basolateral medium was collected and transferred into a black 96-well plate. The presence of NPs in the basolateral medium was determined and quantified (relatively to the NP amount applied apically) through measurement of fluorescence (485 nm excitation, 535 nm emission) using an MFX microtiter plate fluorometer, based on calibration curves of known concentrations of Fc-NPs serially diluted in HBSS.

*7.2.7.3 Effect of non-fluorescent Fc-NPs on transport of fluorescent Fc-NPs*

Fluorescent (YG) and non-fluorescent NPs (both carboxy-modified, 50 nm) were used for the purpose of this experiment. The transport of fluorescent Fc-NPs (prepared as described in section 7.2.4) across the cell layers was established in the same experiment as their uptake (as described in section 7.2.6.2). Following NP application to the apical side of the cell layers (as detailed in section 7.2.6.2), their transport across the layers was determined by sampling the basolateral medium (100 μl volumes) every 30 min for 3 hours (with replacement of the sampled volume with fresh HBSS). NP transport was determined by measuring the fluorescence of the

sampled basolateral solutions using preconstructed calibration curves (as described in the preceding section) and is expressed as % relative to the applied amount.

*7.2.7.4 Co-adsorption of Fc and an investigational therapeutic protein on the NPs and transport across the cell layers*

Carboxy-modified (YG) NPs (50 nm in diameter) were coated with Fc only (as described in section 7.2.4) or with equal amounts (20 mg protein per 1 ml of 2.5% w/v NP stock suspension) of Fc and an investigational therapeutic antibody fragment (Fab), hCTM01 (supplied by UCB, Slough), for 3 hours. Fc-NPs, hCTM01-Fc-NPs and unmodified NPs were applied on the apical surface of confluent, serum-starved Calu-3 layers. Apical-to-basolateral NP transport was determined by sampling the basolateral solution at regular intervals and fluorescence measurement of these solutions (as described in section 7.2.7.2).

*7.2.7.5 Association of NPs with filter (Transwell®) plastic*

Following the measurement of NP transport in the preceding section (7.2.7.4) cells were detached from the filters by incubation with Triton X-100. The filters were then excised from the Transwell® and the fluorescence associated with the filters was assessed by lysis of the NPs with 50% acetone to release the entrapped fluorochrome (32) followed by fluorescence measurement (485 nm excitation, 535 nm emission). NPs associated with the filters are expressed as % relative to the applied amount, calculated through calibration curves (constructed in 50% acetone).

## 7.3 Results

### 7.3.1 Immunostaining for FcRn

Figure 7.1 shows confocal micrographs of Calu-3 cell layers cultured under AIC (7.1 a and b) or LCC conditions (7.1c). Intensive punctate red fluorescence was observed in cells treated with both, primary (anti-FcRn) and TRITC-labelled secondary antibody (7.1a and 7.1b). Red fluorescence was observed in the region around the cell nuclei (cytosol), apparent from the micrographs as large blue areas (DAPI-stained) and also across the vertical axis (7.1b), implying that the receptor is distributed on both apical and basolateral sides of the cells. Considerably less fluorescence was observed in Calu-3 cells cultured using LCC (7.1c) and no red fluorescence was detected in control cells (grown using AIC) treated with the secondary (TRITC-labelled) antibody only (Figure 7.1d).

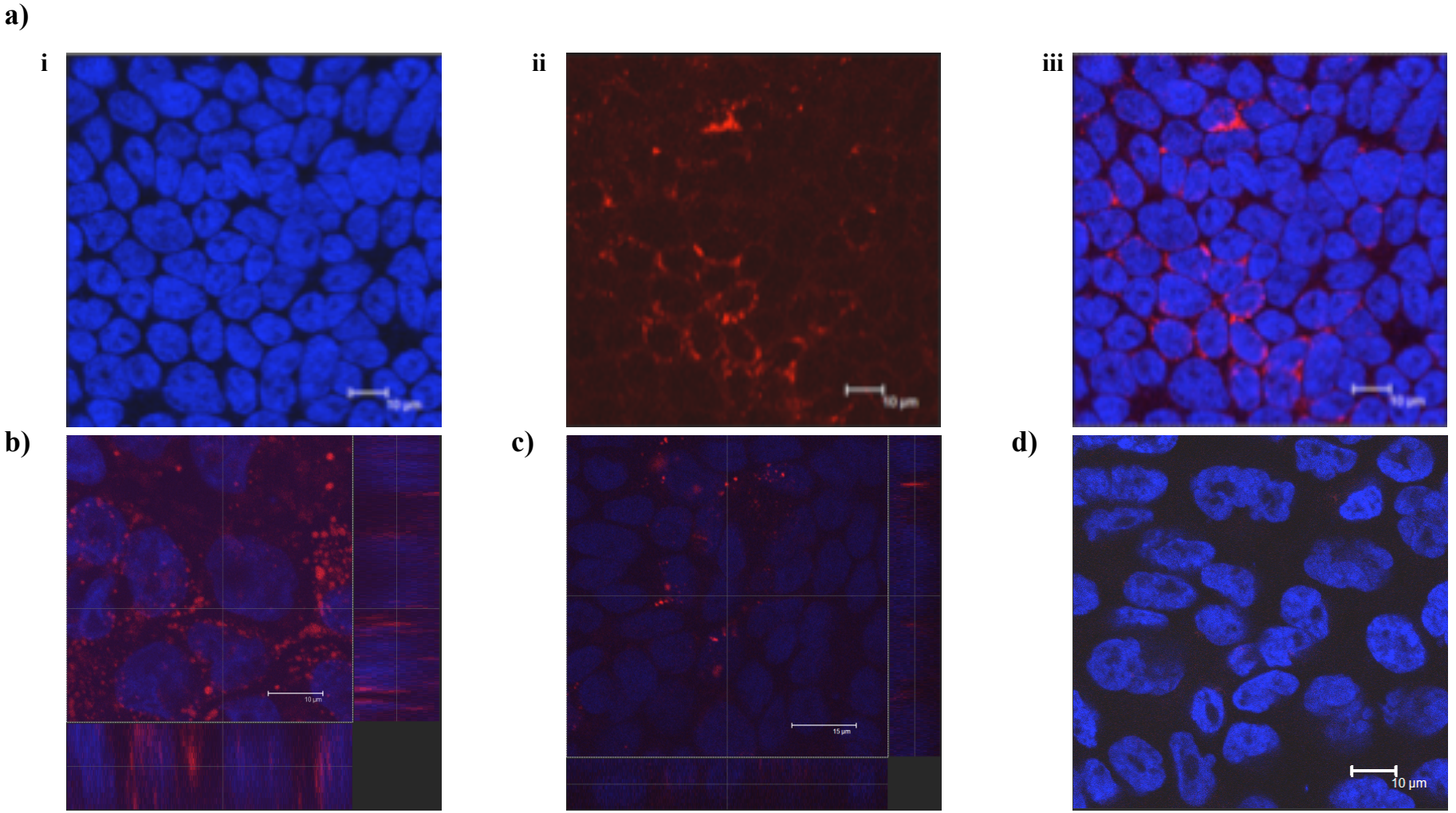


*Figure 7.1. Immunostaining for FcRn in filter-cultured Calu-3 cells. a) AIC Calu-3 cells subjected to incubation with goat, anti-human FcRn (primary) antibody and donkey, anti-goat TRITC-IgG (secondary antibody); i) Blue channel: cell nuclei stained with DAPI, i) Red channel: TRITC fluorescence, and iii) Overlay image (Blue and Red channel). b) Three dimensional image of a Calu-3 cell layer cultured under AIC, showing vertical ('z-axis') on the bottom and the right hand side. c) Calu-3 cells cultured using LCC conditions. d) Calu-3 cells (AIC) incubated with donkey, anti-goat TRITC-IgG (secondary antibody) only.*

Similar results were obtained with confluent Caco-2 cells cultured as monolayers (Figure 7.2). Again, red fluorescence due to donkey, anti-goat TRITC-IgG, was distributed in the regions around the nuclei. This fluorescence was only observed in cells incubated with both, primary and secondary antibodies (7.2a ii and iii); in control cells where incubation with the primary antibody was omitted (i.e. cells were exposed to donkey, anti-goat TRITC-IgG only) no red fluorescence was detected (Figure 7.2b).

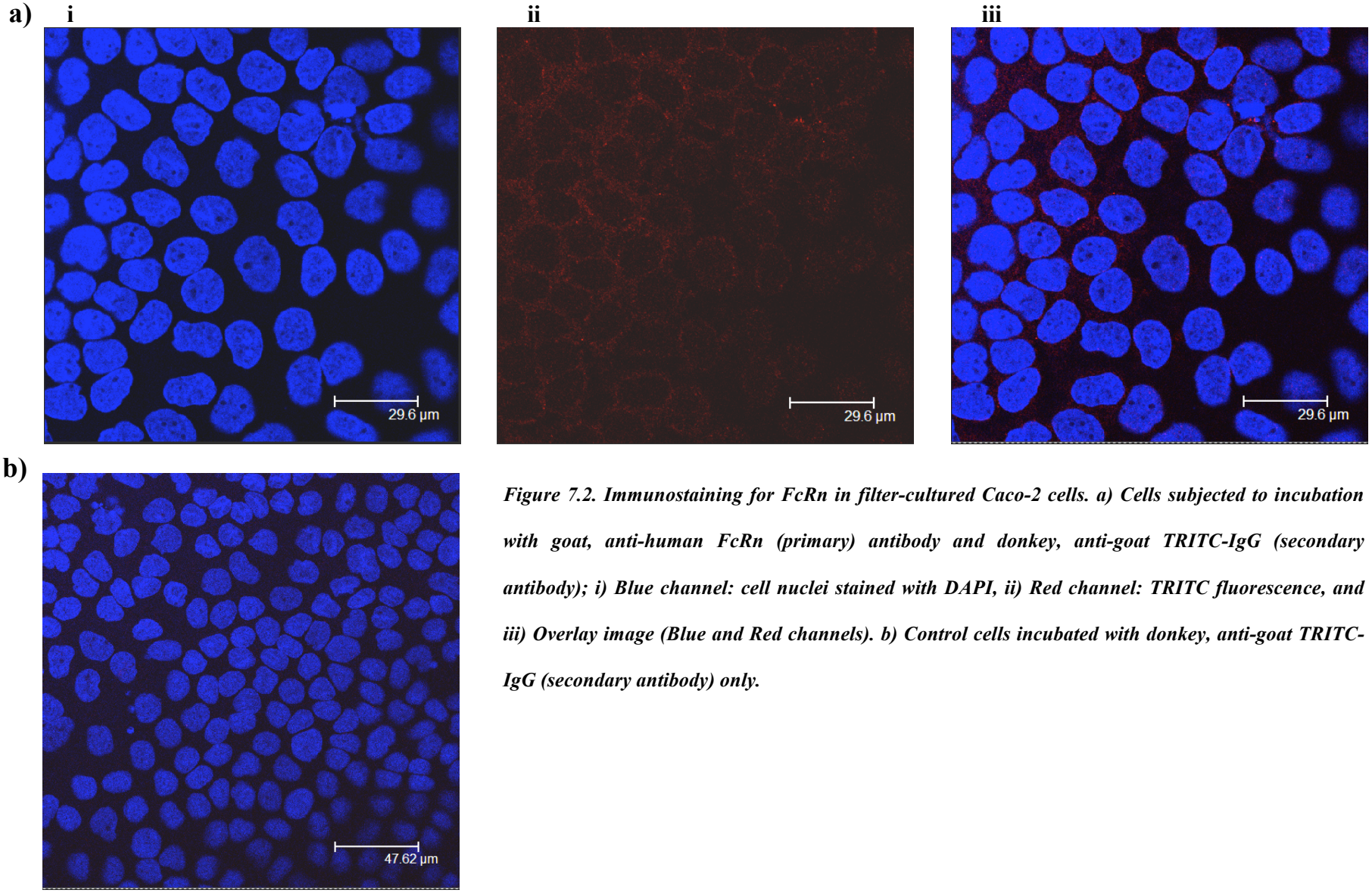


*Figure 7.2. Immunostaining for FcRn in filter-cultured Caco-2 cells. a) Cells subjected to incubation with goat, anti-human FcRn (primary) antibody and donkey, anti-goat TRITC-IgG (secondary antibody); i) Blue channel: cell nuclei stained with DAPI, ii) Red channel: TRITC fluorescence, and iii) Overlay image (Blue and Red channels). b) Control cells incubated with donkey, anti-goat TRITC-IgG (secondary antibody) only.*

### 7.3.2 Association of FITC-IgG with cell layers

*7.3.2.1 Effect of pH on FITC-IgG association with cells*

Levels of cell-associated FITC-IgG following its incubation with Calu-3 layers in either a slightly acidic or physiological pH (6.0 and 7.4, respectively) for 3 hours are shown in Figure 7.3. Approximately 76% of the applied dose of FITC-IgG was present in the apical solution 3 hours after its application at pH 6.0, compared to 87% following its application to cells at pH 7.4; this difference was statistically sigificant (p=0.04).

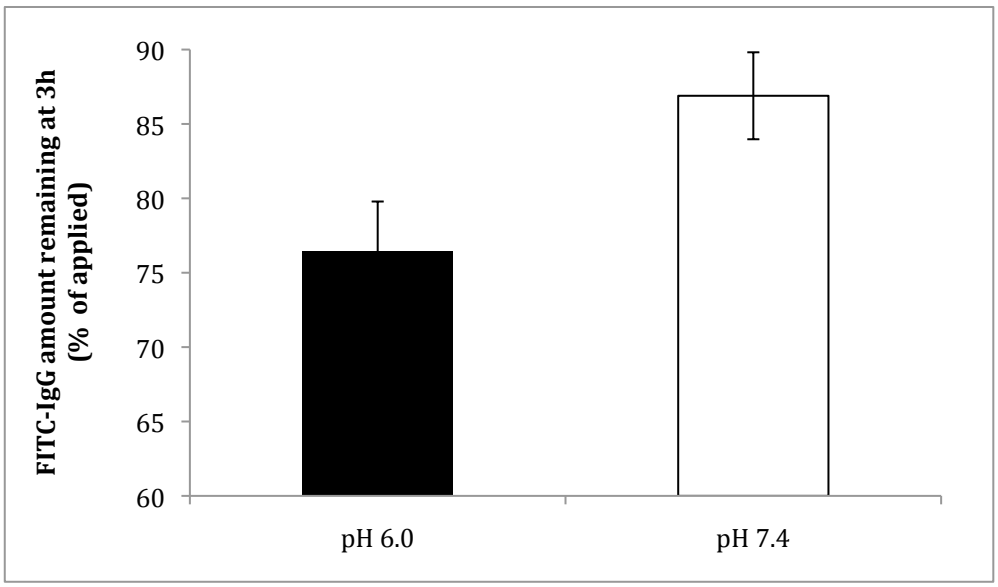


***Figure 7.3. Effect of pH on association of FITC-IgG with Calu-3 layers. Cell association presented as amount of FITC-IgG in the apical solution following its incubation with the cells at pH 6.0 or 7.4 for 3 hours. Results expressed as % of the amount applied initially (5 µg/ml, equating to 2.5 µg). Data presented as the mean ± SD (n=3).***

*7.3.3.2 Association of FITC-IgG with cells: competition with unlabelled IgG*

Incubation of FITC-IgG with the cells in the presence of unlabelled IgG (at pH 6.0) resulted in significantly higher (p=0.015) levels of FITC-IgG (93% of the applied amount) being detected in the removed apical solution at the end of incubation period

compared to application of FITC-IgG on its own (76% of the added amount, shown in the previous section), as illustrated in Figure 7.4.

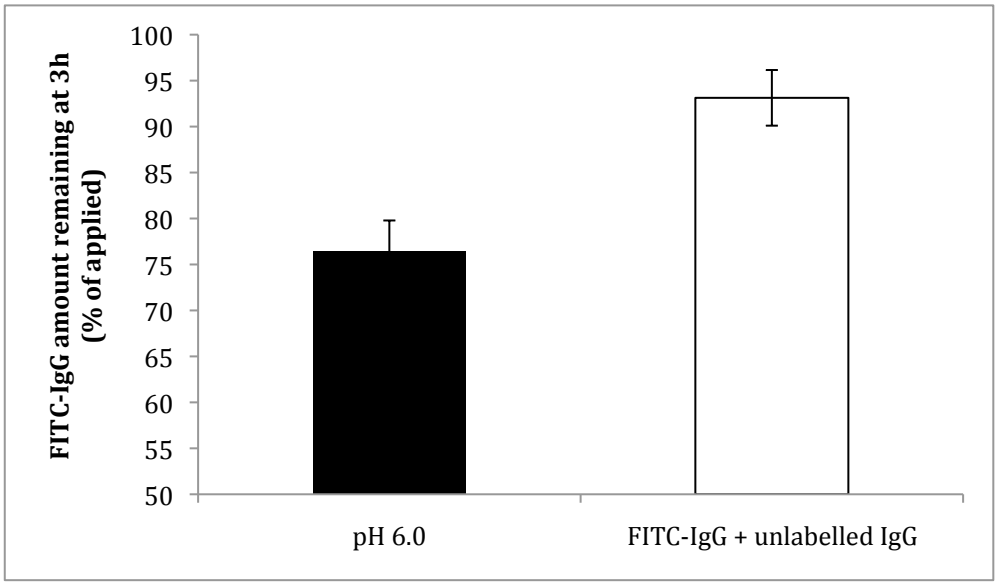


***Figure 7.4. Effect of unlabelled IgG on association of FITC-IgG with Calu-3 layers. Cell association presented as amount of FITC-IgG in the apical solution following its incubation with the cells (at pH 6.0) on its own (5 µg/ml, equating to 2.5 µg) or in the presence of unlabelled IgG (20 µg/ml or 10 µg) for 3 hours. Results shown as % of the amount applied initially. Data presented as the mean ± SD (n=3).***

*7.3.2.3 Cell uptake of FITC-IgG: effect of pH and competition with unlabelled IgG*

Figure 7.5 shows the uptake of FITC-IgG by Calu-3 cells in different experimental situations. Although it is apparent from the figure that cell uptake was lower following the application of IgG to cells at pH 7.4 compared to pH 6.0, this difference was not statistically significant (p=0.09). On the other hand, application of unlabelled IgG (4x higher amount compared to FITC-IgG; pH 6.0) resulted in suppression of cellular uptake of FITC-IgG by approximately 19%; the difference was statistically significant compared to the uptake of FITC-IgG at pH 6.0 (p=0.007) and pH 7.4 (p=0.004).

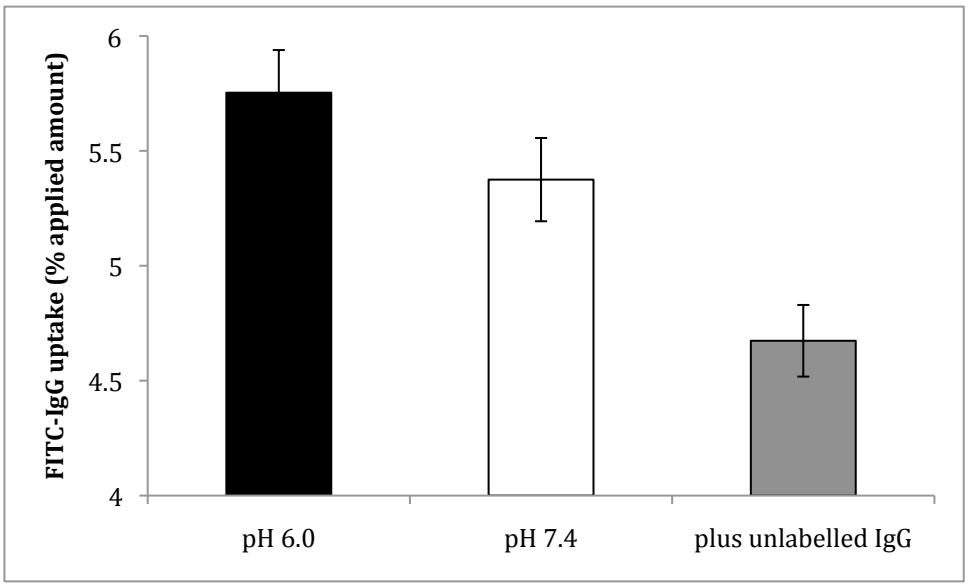


***Figure 7.5. Effect of pH and unlabelled IgG on cell uptake of FITC-IgG. Cells were incubated with samples for 3 hours. The amount of unlabelled IgG applied to the cells (at pH 6.0) was 4x higher than FITC-IgG (10 µg and 2.5 µg, respectively). Uptake expressed as % of the amount applied apically. Data presented as the mean ± SD (n=3).***

### 7.3.3 IgG transport experiments

*7.3.3.1 IgG transport across Calu-3 layers*

Figure 7.6 shows the amount of IgG present in the basolateral solution at different times following its addition on the apical surface of the layers. There was an increase in basolateral IgG levels from approximately 4 ng (at time 0 min, prior apical addition of IgG) to 51 ng (at time 60 min). Thereafter, a plateau was observed, with the basolateral IgG amount remaining somewhat stable (51-52 ng) from 60 min to 120 min.

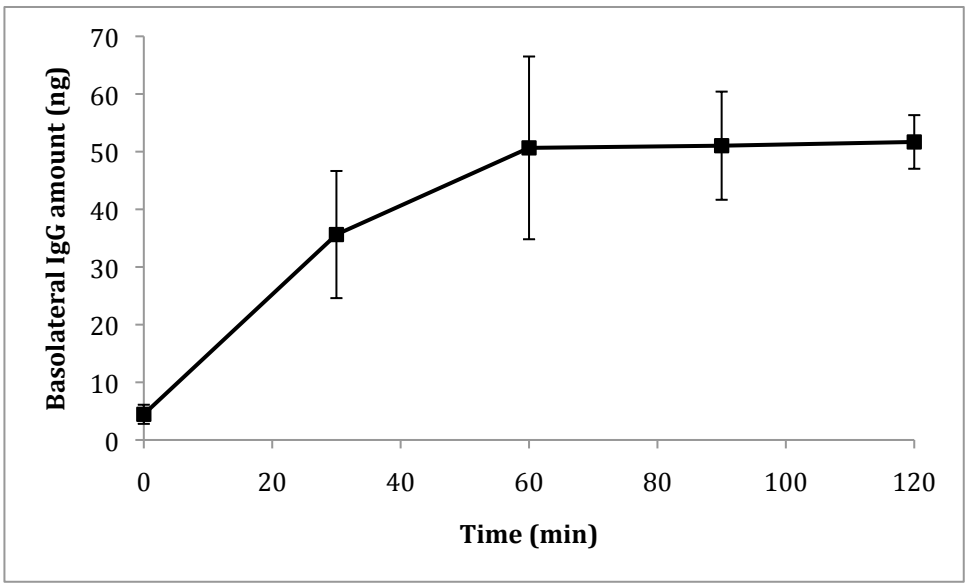


***Figure 7.6. Apical-to-basolateral transport of IgG across Calu-3 layers. Transport presented as IgG amount (ng) in the basolateral solution at different time intervals following addition of 1 µg/ml (500 ng) of IgG to the apical surface of the cells at pH 6.0. Data presented as the mean ± SD (n=4).***

*7.3.3.2 Transport saturation*

Cumulative amounts of IgG present in the basolateral solution following its addition at varying concentrations (50 ng/ml, 500 ng/ml and 5 μg/ml) on the apical side of the cell layers are shown in Figure 7.7. It is worth pointing out here that in the current experiment, the basolateral solution was replaced completely at each IgG sampling point (every 30 min), as opposed to sampling 100 μl volumes, performed in the previous experiment. Another important point to highlight is that the experiments described here and in the next section (7.3.3.3) were conducted on Calu-3 cells of a different batch and higher passage numbers (passage 43-44) than cells used in work described in other sections of this chapter (passage 21-27). Cumulative basolateral IgG amount in Figure 7.7 followed a similar pattern at all added concentrations, but basolateral IgG levels were lower (at all time intervals) for application of 50 ng/ml IgG as compared to application at higher concentrations of 500 ng/ml and 5 μg/ml (the difference in basolateral IgG amount between 50 ng/ml and 500 ng/ml application, measured at 180 min, was statistically significant; $p=0.025$). It is interesting to note that basolateral IgG levels measured following the apical addition at 5 μg/ml were similar to those obtained with 500 ng/ml, indicating no further increase in IgG transport with increasing apical concentration.

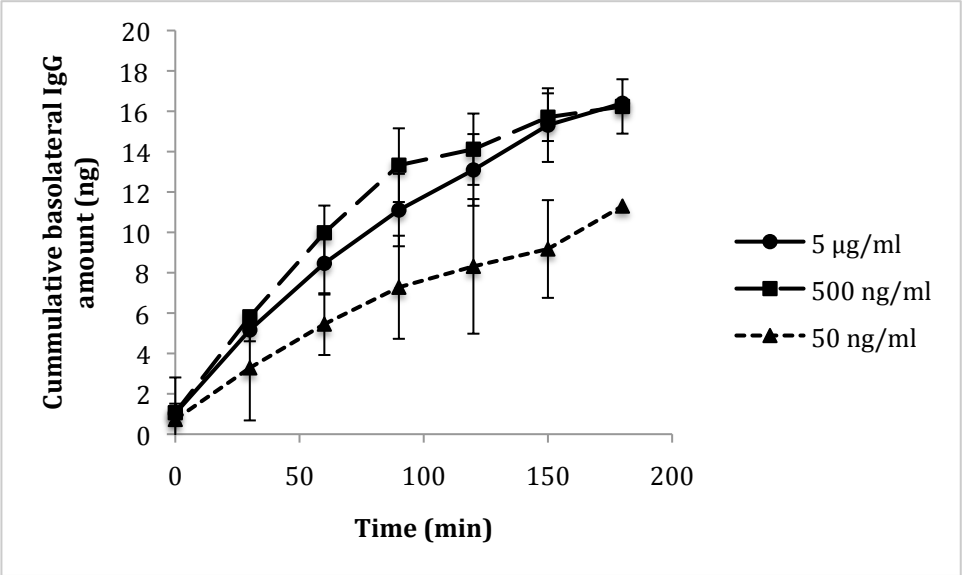


***Figure 7.7. Apical-to-basolateral transport of IgG across Calu-3 layers: transport saturation. Transport presented as IgG amount (ng) present in the basolateral solution at different time intervals following its application (on the apical side of Calu-3 layers) at 50 ng/ml, 500 ng/ml and 5 µg/ml. Basolateral solution was replaced completely every 30 min (at each IgG sampling interval). Results are shown as the mean ± SE (n=3).***

*7.3.3.3 Receptor competition*

Figure 7.8 shows the pattern in basolateral IgG amount following its application to the cell layers on its own or in conjunction with rabbit IgG (rIgG; applied at 50x higher concentration than IgG). Basolateral IgG levels increased with time (from approximately 3 ng to 11 ng) after its application on its own. Co-addition of rIgG resulted in a considerably lower increase in the basolateral levels of IgG (from approximately 1.2 ng to 2.6 ng), with similar levels seen at all time intervals.

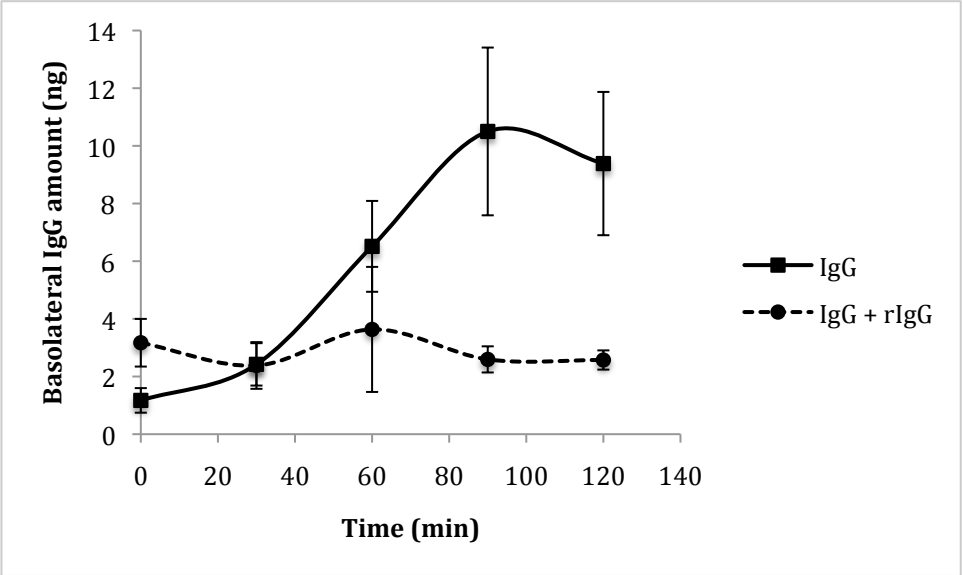


***Figure 7.8. Apical-to-basolateral transport of IgG across Calu-3 layers: receptor competition. Transport presented as IgG amount (ng) present in the basolateral solution at different time intervals following its application (on the apical side of confluent Calu-3 layers) in the presence or absence of rabbit IgG (rIgG). IgG was applied apically at 1 µg/ml, whereas rIgG was applied at 50 µg/ml (both in HBSS, pH 6.0). Results are shown as the mean ±SE (n=3).***

### *7.3.3.4 IgG transport across Caco-2 monolayers*

The application of IgG to Caco-2 monolayers resulted in a small increase in basolateral IgG levels with time from approximately 0.7 ng to 2.7 ng (Figure 7.9).

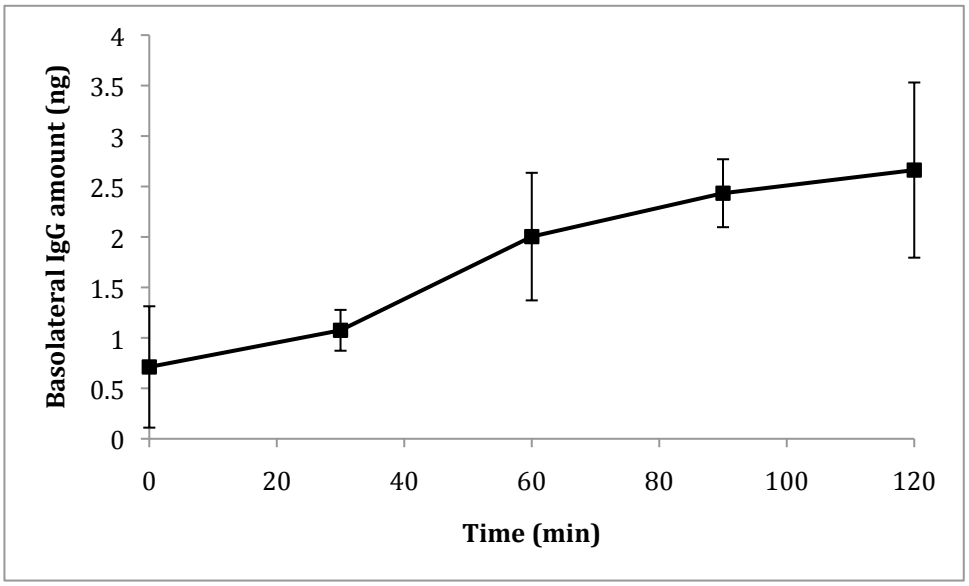


***Figure 7.9. Apical-to-basolateral transport of IgG across Caco-2 monolayers. Transport presented as IgG amount (ng) present in the basolateral solution following its addition to the apical side of Caco-2 cell monolayers. IgG was applied at 1 µg/ml in HBSS (pH 6.0). Data presented as the mean ± SD (n=4).***

### 7.3.4 Adsorption of IgG or Fc to NPs

*7.3.4.1 Nanoparticle size characterisation*

Figure 7.10 shows DLS size characterisation of NPs (red, sulfate-modified NPs of 30 nm nominal diameter) before their incubation with IgG or Fc (i.e. unmodified) and following adsorption of IgG or Fc. For uncoated NPs (7.10a), the most abundant (approximately 90%) particle population had average hydrodynamic radii of approximately 21 nm (i.e. average diameters of 42 nm). Larger particulates in the micron range (suggesting aggregation and/or presence of other particulate material in the analysed sample) were also observed. With IgG-adsorbed NPs (7.10b), about 88% of particle populations had average radii of 220 nm (equivalent to 440 nm diameter), with NP populations of other sizes, namely those with mean radii of about 26 nm and larger micron-sized particles, also observed to a lesser extent. Finally, DLS analysis

of Fc-adsorbed NPs revealed that particle populations of two sizes were present in the samples; 2.4% of these had average radii of approximately 19 nm (diameter 38 nm), while the majority (around 98%) were NPs with mean radii of approximately 60 nm (diameter 120 nm).

**a)**

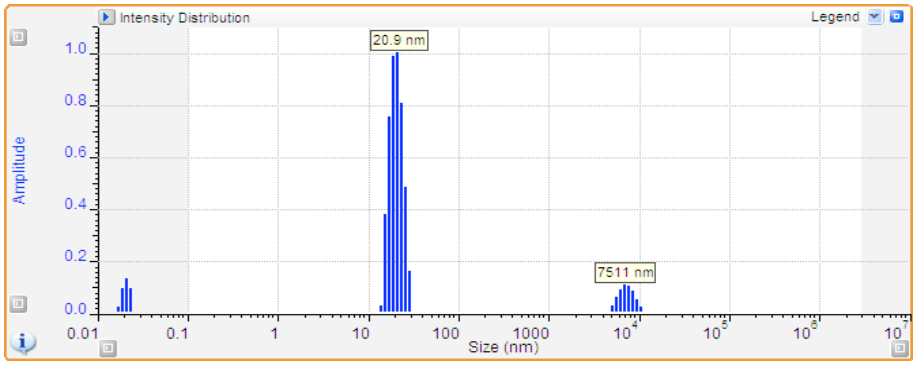


| Pk | % Area | Rh (nm) | Position | Std Dev | % RSD | MW (kD) |
|---|---|---|---|---|---|---|
| 1 | 90.1 | 20.95 | 21.38 | 3.45 | 16.5 | --- |
| 2 | 9.9 | 7510.65 | 7079.46 | 1346.18 | 17.9 | --- |

**b)**

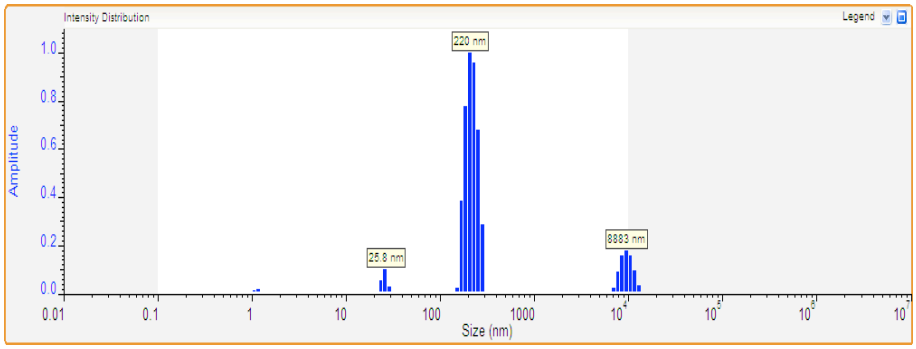


| | % Area | Rh (nm) | Position | Std Dev | % RSD |
|---|---|---|---|---|---|
| 1 | 3.2 | 25.83 | 26.30 | 1.63 | 6.3 |
| 2 | 87.9 | 219.74 | 208.93 | 31.86 | 14.5 |
| 3 | 8.9 | 8882.71 | 9660.51 | 757.98 | 8.5 |

**c)**

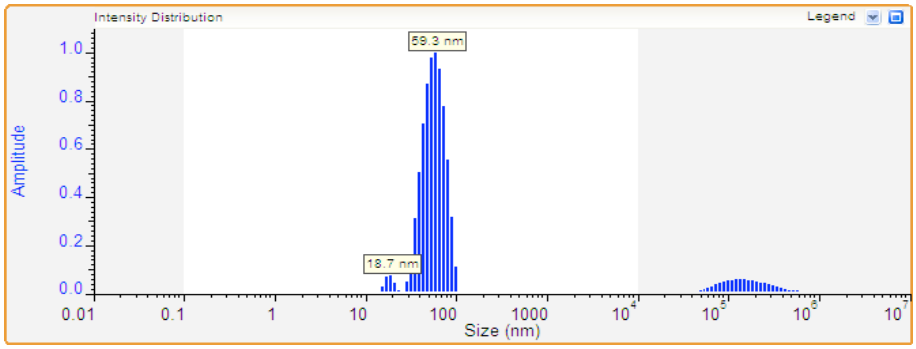


| | % Area | Rh (nm) | Position | Std Dev | % RSD |
|---|---|---|---|---|---|
| 1 | 2.4 | 18.75 | 19.28 | 1.83 | 9.8 |
| 2 | 97.6 | 59.28 | 60.26 | 15.72 | 26.5 |

***Figure 7.10. Size characterisation of unmodified (a), IgG-adsorbed (b) and Fc-adsorbed NPs (c) by Dynamic Light Scattering (DLS). Tables show information on mean sizes (radii) and size distributions of detected NP populations. The result represents the mean of ten measurements, performed in HBSS (pH 6.0) at 25°C.***

### 7.3.5 Confocal microscopy analysis of cellular uptake of IgG- or Fc-NPs

*7.3.5.Cell uptake of IgG-adsorbed NPs*

Figure 7.11 shows confocal micrographs of Calu-3 cells (as confluent filter-cultured layers) incubated with IgG-adsorbed NPs. The micrographs reveal the presence of green fluorescence (green channel) resulting from FITC-IgG and red fluorescence (red channel) from fluorescent latex NPs. Furthermore, green and red fluorescence was observed to occur at the same locations - i.e. to co-localise.

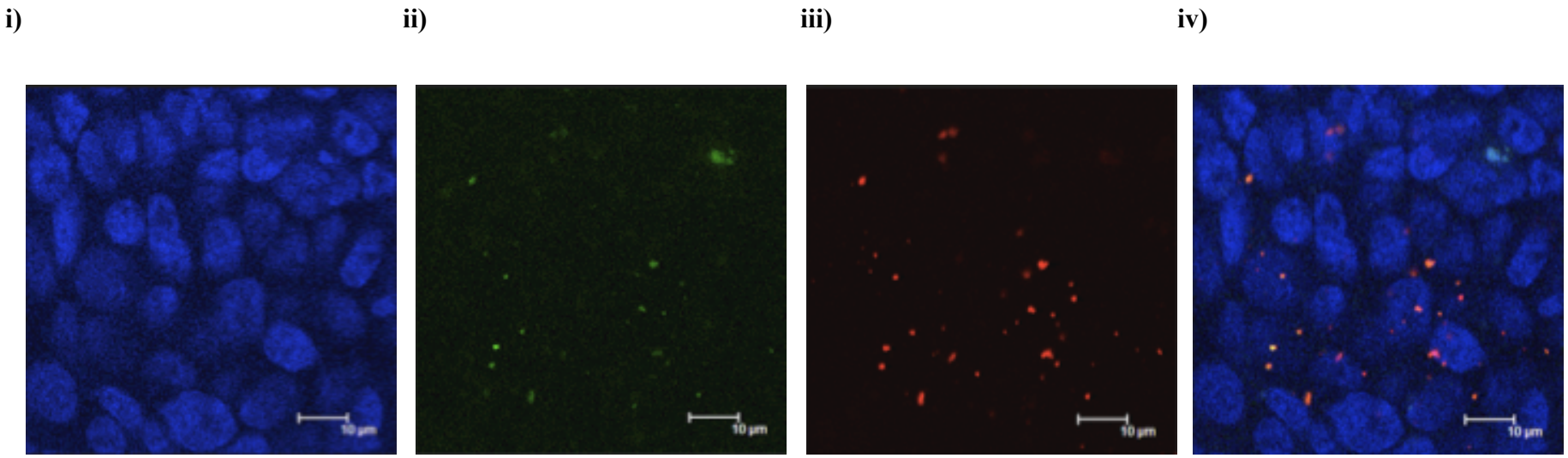


*Figure 7.11. Uptake of FITC-IgG-adsorbed NPs by Calu-3 cells. i) Blue channel: DAPI-labelled cell nuclei, ii) Green channel: FITC-IgG, iii) Red channel: fluorescently labelled (red) polystyrene NPs, and iv) Overlay image (all channels).*

*7.3.5.2 Cell uptake of Fc-adsorbed NPs*

Confocal microscopy analysis of cellular internalization of Fc-adsorbed NPs is shown in Figure 7.12. Red, FITC-Fc-immobilised NPs can clearly be seen associated with the cells (7.12a). Similarly to IgG-adsorbed NPs, it is clear from the micrographs that green and red fluorescence (due to FITC-Fc and red NPs, respectively) was observed at the same areas, indicating Fc-association with the NPs. Furthermore, Fc-adsorbed NPs (non-fluorescent Fc) were seen in the interior of the cells (7.12b), with distribution of NPs throughout the vertical z-axis of the cells (7.12b ii) and some even seen at the level of the filter (seen as continuous blue fluorescence on the bottom/right hand side of the micrograph). Figure 7.12c shows the uptake of YG Fc-NPs (non-fluorescent Fc) in cells that were subsequently stained for the TJ protein, ZO-1. Again, punctate fluorescence from the NPs was clearly apparent within the cells, at the level above and below the TJs (c iii). Note that both red and YG NPs were sulfate modified and Fc-adsorption was performed in the same way. It is apparent from Figure 7.12 that with Fc-NPs, punctate fluorescence of smaller dimensions was observed compared to IgG-NPs (Figure 7.11).

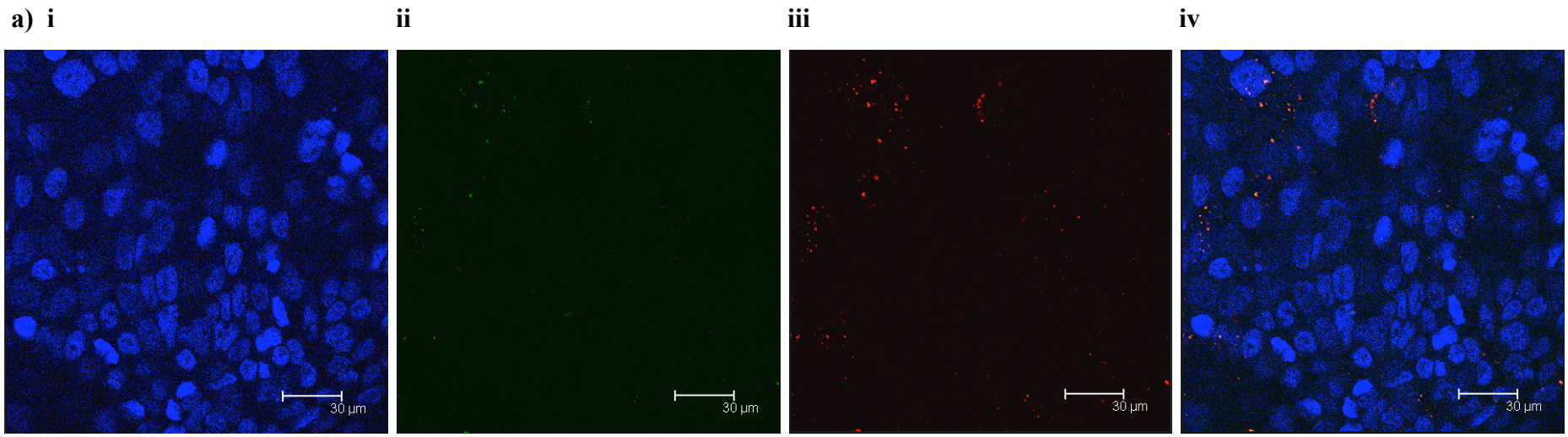
a) i
ii
iii
iv
30 µm
30 µm
30 µm
30 µm

**b)** **i** **ii**

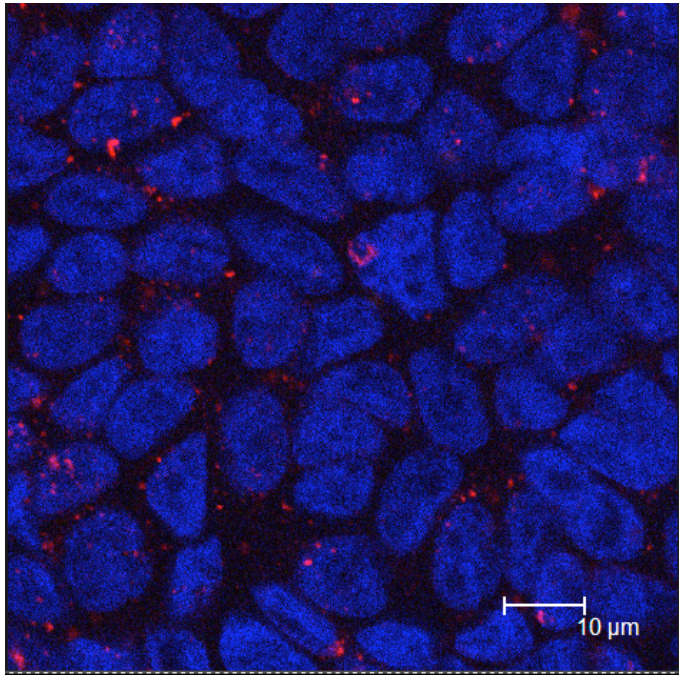


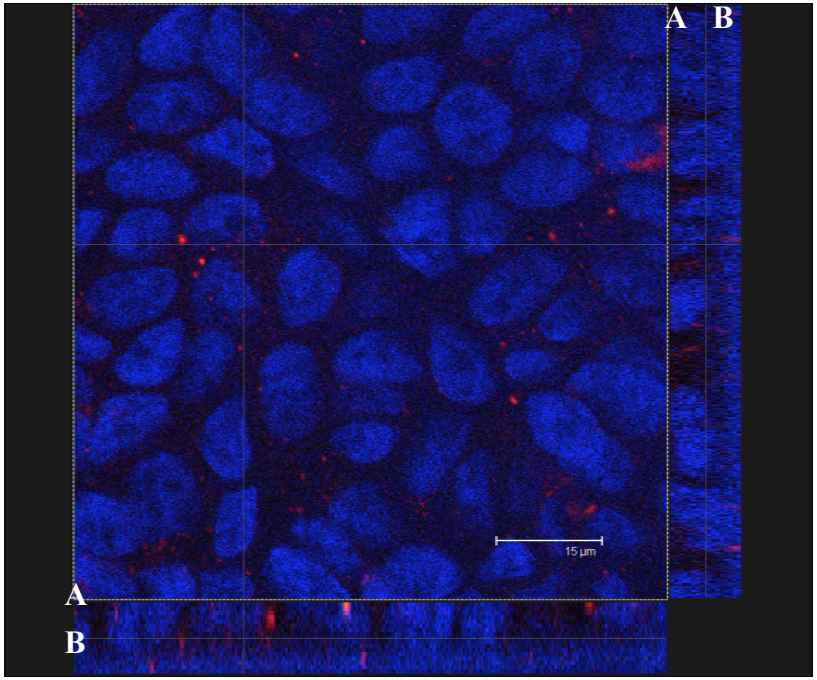

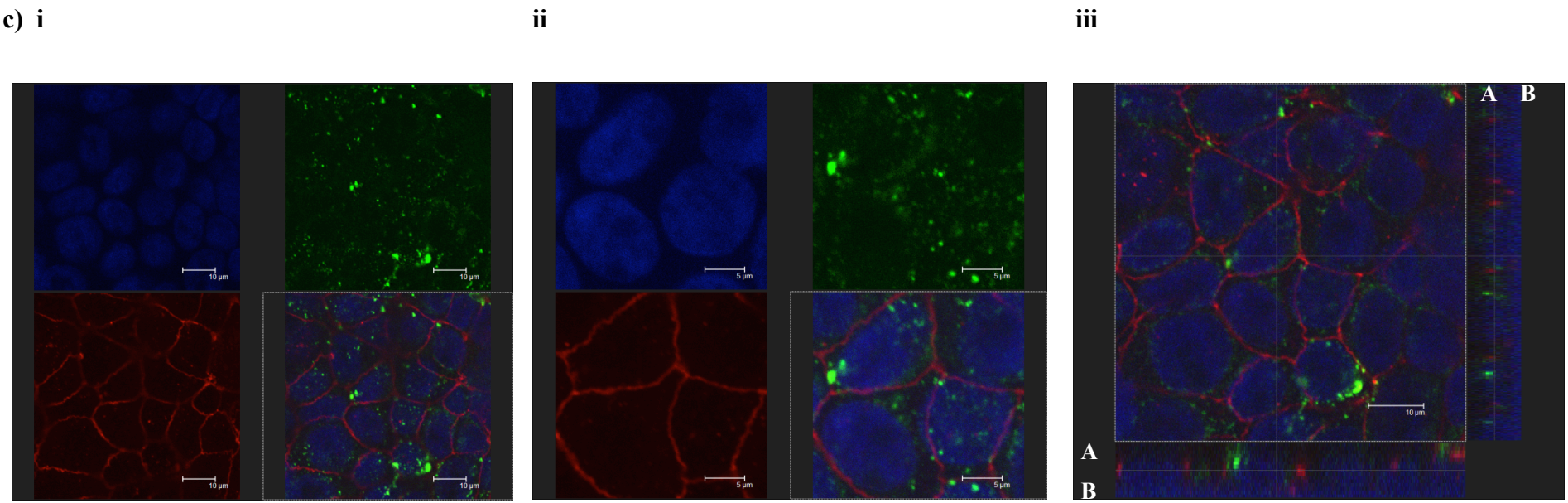


*Figure 7.12. Uptake of Fc-adsorbed NPs by Calu-3 cells. a) Uptake of red (sulfate-modified) NPs coated with FITC-Fc; i) Blue channel: DAPI-labelled cell nuclei, ii) Green channel: FITC-Fc, iii) Red channel: red polystyrene NPs, and iv) Overlay image (all channels). b) Uptake of red Fc-NPs. i: Single section (approximately midway between apical surface and the filter plastic), and ii: Three dimensional image showing vertical axis where A is the apical side and B is the basolateral side of the cells. c) Uptake of Yellow-Green Fc-NPs. i: Single section showing blue channel (DAPI-stained cell nuclei), green channel (YG NPs), red channel (secondary, TRITC-labelled antibody directed towards primary, anti ZO-1 antibody) and overlay image, ii: same as i, but higher magnification, and iii: three dimensional image showing vertical axis (right hand side and bottom of the micrograph), where A is apical side and B is basolateral side of the cells.*

### *7.3.5.3 LysoTracker® staining*

Cellular localisation of Fc-NPs following their incubation with filter-cultured Calu-3 cells in the form of a confluent layer in the presence of the lysosomal marker, Lysotracker® Red, is shown in Figure 7.13. Again, Fc-NPs were observed in the interior of the cells, as suggested by the presence of green fluorescence across the vertical cross-sections, with a somewhat more prominent distribution of fluorescence on the apical side. The presence of red staining due to the Lysotracker® probe was relatively weak, despite its use at higher than recommended concentrations (see section 7.2.5.3) and observation of this phenomenon was repeatable. Although very low staining level is apparent, with the exception of one area (marked by the white box), red fluorescence did not co-localise with green fluorescence due to Fc-NPs.

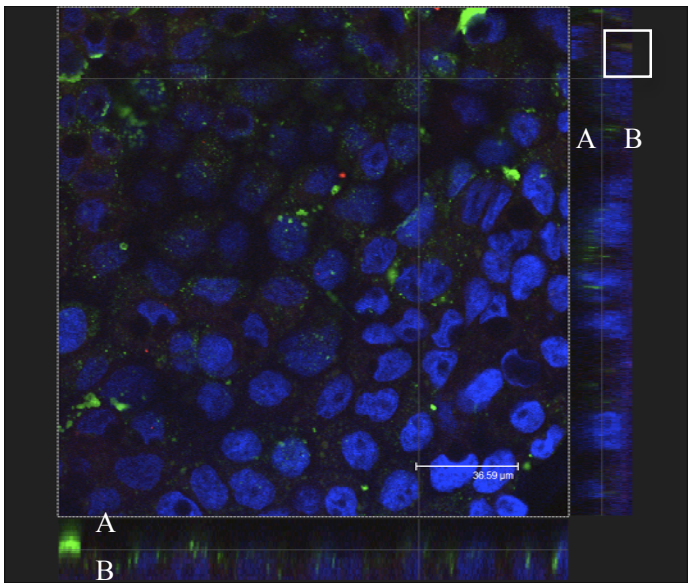


***Figure 7.13. Confocal microscopy micrograph showing cellular distribution of Fc-NPs and lysosomal probe, Lysotracker®. NPs and Lysotracker® (100 nM) were incubated with confluent Calu-3 layers for 2 hours. Green fluorescence is due to YG NPs (Fc-adsorbed) and Red fluorescence is due to the Lysotracker® red probe. White box shows a region where green and red fluorescence co-localised. A is the apical side and B is the basolateral side of the cells.***

### 7.3.6 Cell uptake of Fc-NPs: measurement of NP fluorescence

*7.3.6.1 Cell uptake of Fc-NPs, comparison with unmodified NPs, and effect of IgG*

The extent of Fc-NP internalization by Calu-3 cells following an incubation period of three hours is shown in Figure 7.14. A comparison is made with the uptake of NPs in the presence of 'free' IgG. Furthermore, the level of unmodified NP uptake is also depicted in the figure. Approximately 12% of the applied Fc-NPs were taken up by the cells. In contrast, when Fc-NPs were added in combination with IgG, there was a decrease in uptake of Fc-coated NPs to approximately 8% of the applied amount (though this decrease lies just outside of the 95% significance, with $p=0.06$). Finally, the internalization of unmodified NPs by cells was the lowest, with approximately 5% of the applied NPs observed in the supernatants of lysed cells. This value was statistically lower than those obtained with Fc-NPs when applied both on their own and with IgG ($p=0.042$ and 0.02, respectively).

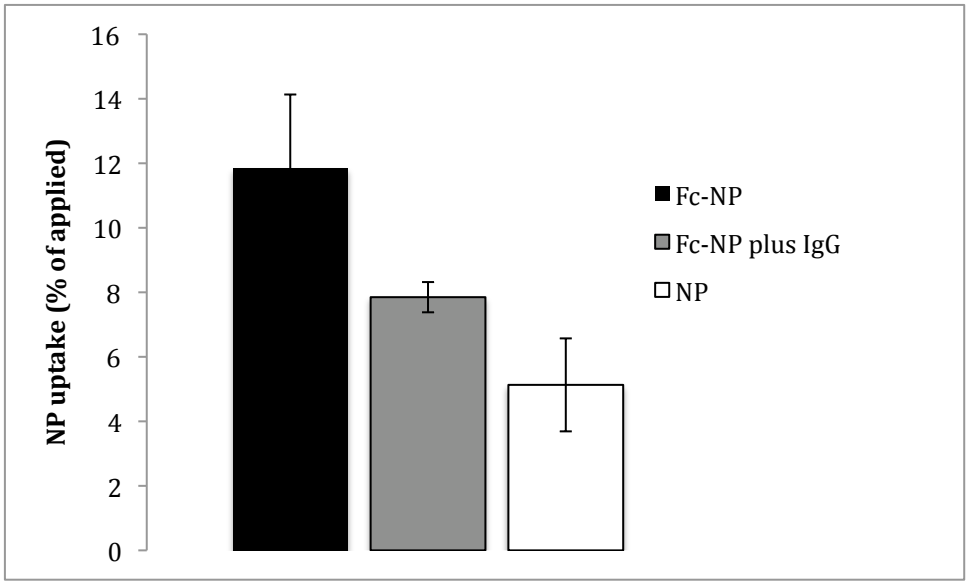


***Figure 7.14. Cell uptake of Fc-NPs, Fc-NPs in the presence of IgG (5 µg/ml) and unmodified NPs (all in HBSS, pH 6.0). 50 nm carboxy-modified (YG) NPs (coated or non-coated with IgG) were used, which were incubated with Calu-3 layers for 3 hours. NP uptake is expressed as % relative to the applied amount. Data presented as the mean ± SD (n=4).***

*7.3.6.2 Effect of non-fluorescent Fc-NPs on cell uptake of fluorescent Fc-NPs*

Application of non-fluorescently labelled Fc-NPs in combination with the labelled Fc-NPs was associated with a reduction in cellular uptake of fluorescent Fc-NPs (Figure 7.15). Approximately 18% of the applied Fc-NPs were taken up by cells following their application on the apical side of the cell layers. In contrast, when fluorescent Fc-NPs were added in conjunction with non-labelled NPs (Fc-adsorbed), their uptake was significantly ($p=0.02$) lower (approximately halved to about 9% of the applied amount).

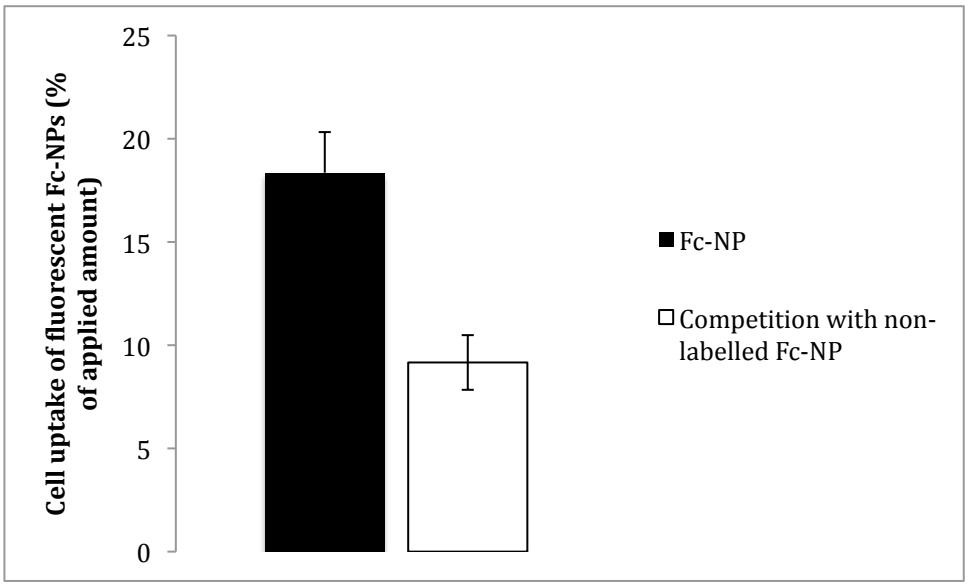


***Figure 7.15. Effect of non-fluorescently labelled Fc-NPs on cellular uptake of labelled (fluorescent) Fc-NPs. Non-labelled NPs were used at a 5-fold higher concentration compared to labelled NPs. Labelled and non-labelled NPs were carboxy-modified and of an identical nominal diameter (50 nm). Adsorption of Fc was conducted in the manner described in section 7.2.4 for both types of NPs. NPs were incubated with Calu-3 layers for 3 hours. NP uptake is expressed as % relative to the applied amount. Data presented as the mean ± SD (n=3).***

### 7.3.7 Fc-coated NP transport across cell layers

*7.3.7.1 Transport of Fc-NPs and unmodified NPs*

Figure 7.16 illustrates the apical-to-basolateral translocation of Fc-immobilised NPs (Fc-NPs) and unmodified NPs. A dramatic difference in the extent of NP transport between Fc-NPs and unmodified NPs can be noted from the figure. While there was a gradual build up of NPs in the basolateral solution in both cases, this increase was considerably steeper in the case of Fc-NPs compared to unmodified NPs, with basolateral NP levels reaching final values (at 180 min) of approximately 1.1% and 0.3%, respectively (which were significantly different; p=0.0004).

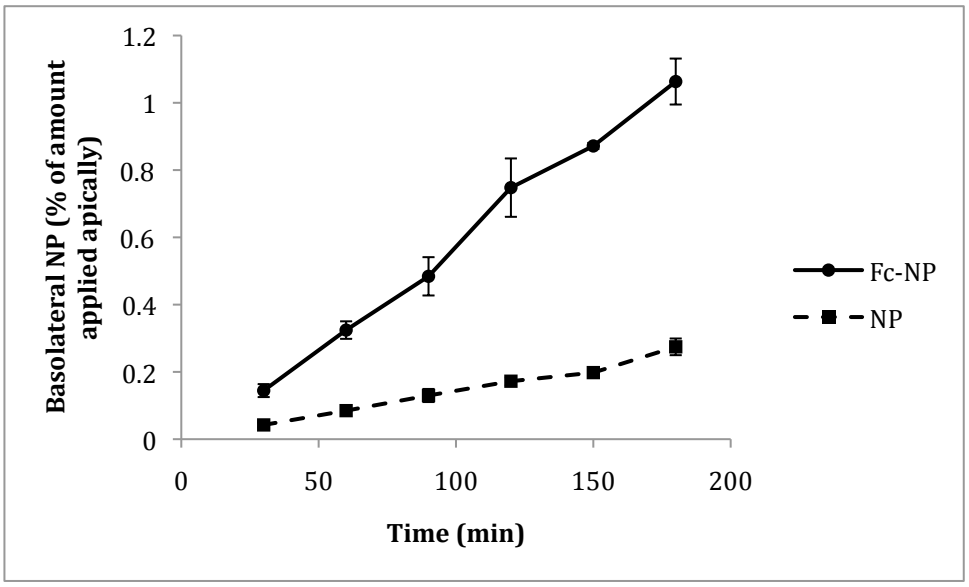


***Figure 7.16. Apical-to-basolateral transport of Fc-adsorbed (Fc-NP) and unmodified NPs ('NP') across Calu-3 layers. Carboxy-modified NPs were used and NPs were applied to cells at an identical concentration in both cases. The presence of NPs in the basolateral solution was measured every 30 min for 180 min. NP transport is expressed as % relative to the applied amount. Data presented as the mean ± SD (n=3).***

### *7.3.7.2 Effect of IgG on Fc-NP transport*

The influence of IgG presence on the extent of apical-to-basolateral transport of Fc-NPs is shown in Figure 7.17. Rather than measuring the transport over time as in the preceding experiment (section 7.2.7.1), in this instance the basolateral solution was only sampled once following a 3-hour incubation of cells with the NPs. In this experiment, approximately 3.6% of the apically added Fc-NPs were found in the basolateral solution at the end of the incubation period. The extent of Fc-NP transport that occurred in the presence of free IgG was significantly lower (approximately 1.5%; p=0.04).

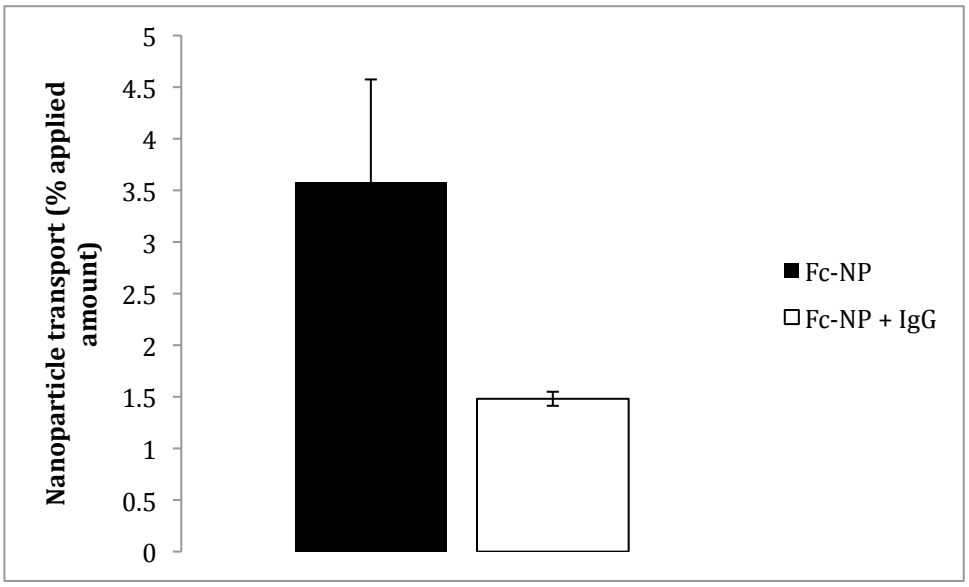


***Figure 7.17. Effect of IgG on apical-to-basolateral transport of Fc-NPs across the Calu-3 layers. IgG applied at 5 µg/ml. The presence of NPs (YG, sulfate modified) in the basolateral solution was measured at time 180 min. NP transport is expressed as % relative to the applied amount. Data presented as the mean ± SD (n=3).***

*7.3.7.3 Effect of non-fluorescent Fc-NPs on transport of fluorescent Fc-NPs*

Similarly to the uptake experiment, co-application of non-fluorescent Fc-NPs with fluorescent Fc-NPs led to a reduction of apical-to-basolateral movement of the latter (Figure 7.18). While there was an increase in relative amount of NPs found basolaterally over time in both cases, higher fluorescence values (and therefore NP amounts) over time were observed when Fc-NPs were applied *per se* compared to co-application. For example, this difference at time 180 min was statistically significant ($p=0.024$).

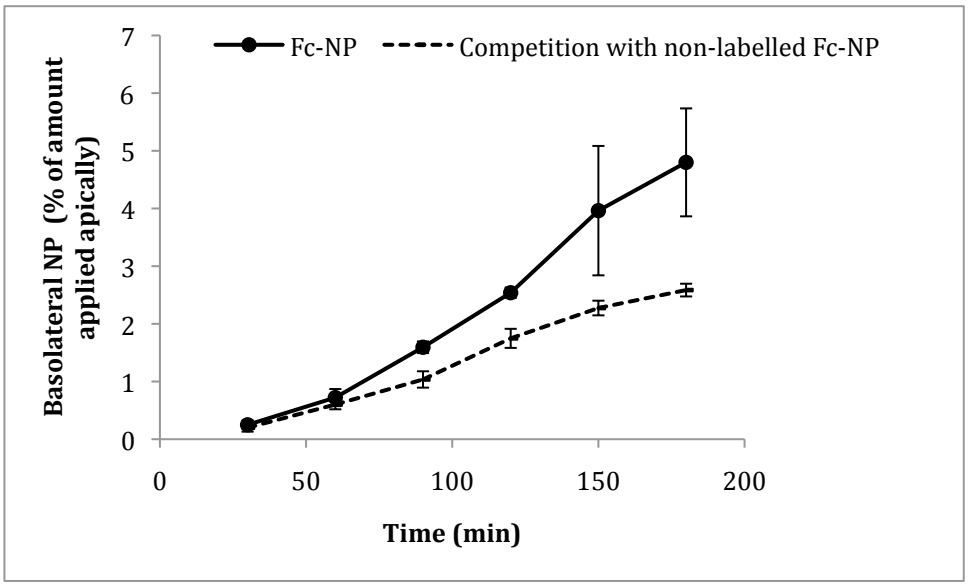


***Figure 7.18. Apical-to-basolateral transport of Fc-NPs (fluorescent) across Calu-3 layers in the absence and presence of unlabelled Fc-NPs. Non-labelled NPs were used at a 5-fold higher concentration compared to labelled NPs. Labelled and non-labelled NPs were carboxy-modified and of an identical nominal diameter (50 nm). Adsorption of Fc was conducted in the manner described in section 7.2.4 for both types of NPs. Fluorescent NPs in the basolateral solution were quantified every 30 min for 180 min (3 hours). NP transport is expressed as % relative to the applied amount. Data presented as the mean ± SD (n=3).***

*7.3.7.4 Co-adsorption of Fc and an investigational therapeutic protein on the NPs and transport across the cell layers*

Figure 7.19 displays the data on transport of 'coated' and uncoated NPs across the Calu-3 layers; NPs were either coated with Fc, or with Fc and an investigational therapeutic antibody fragment (Fab, 'CTM01'). Both systems were seen to traverse the cell layers to a similar extent, with 7.4% and 7.8% of the applied NPs being detected in the basolateral solution at 180 min for Fc-NPs and CTM01-Fc-NPs, respectively. In contrast, the transport of NPs coated with the therapeutic antibody fragment only

(CTM01-NP) was significantly lower, with approximately 3.6% of the apically applied NPs translocating across the cell layers.

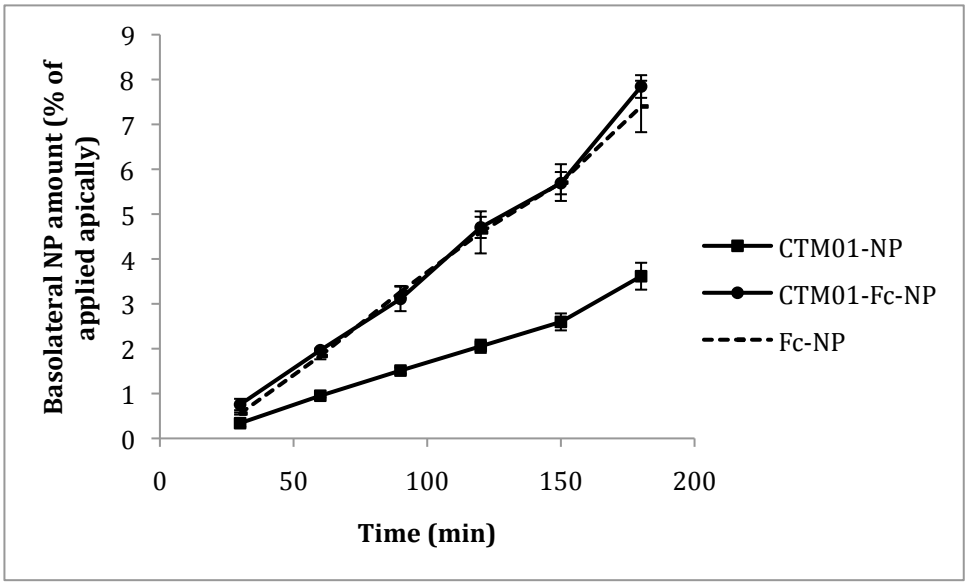


***Figure 7.19. Transport of differently coated NPs (carboxy-modified) across the Calu-3 layers. NPs were coated with a therapeutic antibody fragment (Fab), CTM01, with Fc, or with both, CTM01 and Fc. The basolateral solution was tested for fluorescence (NP presence) at different time intervals (every 30 min) for 180 min. NP transport is expressed as % relative to the applied amount. Data presented as the mean ± SD (n=3).***

*7.3.7.5 Association of NPs with filter (Transwell®) plastic*

Association of NPs with the filters, following their apical-to-basolateral transport across the cell layers, for the systems investigated in the experiment above (section 7.3.7.4) is illustrated in Figure 7.20. It is apparent from the figure that approximately 7% of apically applied NPs coated with the therapeutic Fab (CTM01) were associated with the filters. For NPs co-adsorbed with CTM01 and Fc and those with Fc only, the values were similar at 11 and 12%, respectively. While the difference in relative NP amount that was associated with the filters lies just outside statistical significance for CTM01-NPs and CTM01-Fc-NPs ($p=0.051$) the difference in values for CTM01-NPs and Fc-NPs is statistically significant ($p=0.023$).

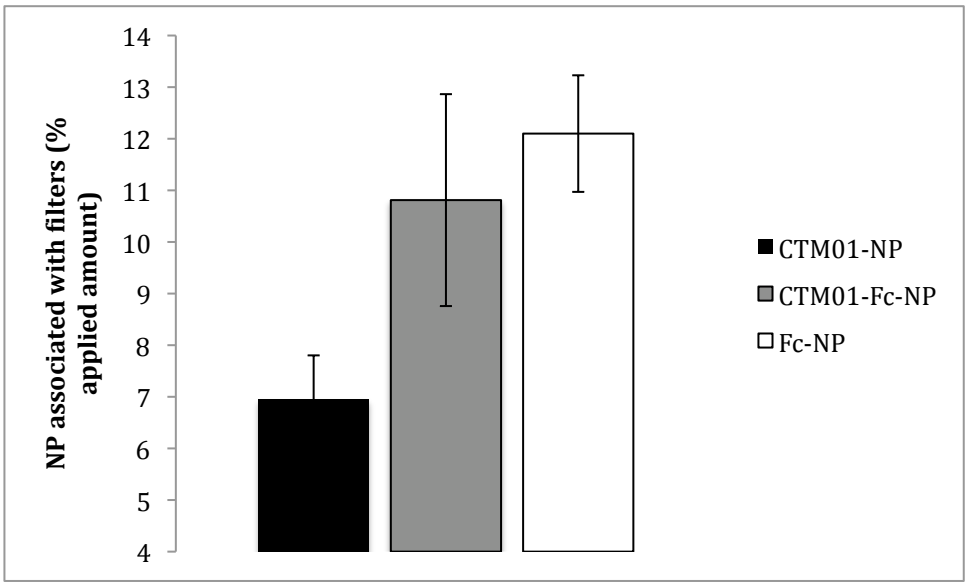


***Figure 7.20. Association of differently coated NPs with filter plastic (of the Transwell® system) following their transport across the Calu-3 layers. NPs were coated with the therapeutic antibody fragment (Fab), CTM01, with Fc, or with both, CTM01 and Fc. Coated NPs were applied to cells at an identical concentration in all cases. Filters were excised and NPs lysed with 50% acetone to release the entrapped fluorochrome. The extent of NP association with the filters is expressed as % relative to the applied amount. Data presented as the mean ± SD (n=3).***

## 7.4 Discussion

The enhancement of mucosal absorption through reversible opening of epithelial TJs is more efficacious with relatively small therapeutic proteins such as peptides. Indeed, it is apparent from the literature discussed in Chapter 1 (sections 1.5.1.3 and 1.5.1.4) that most studies attempting to improve mucosal absorption through TJ modulation incorported peptides having a relatively low $M_W$, including octreotide (1 kDa), buserelin (1.3 kDa) and salmon calcitonin (approximately 3.4 kDa). With larger proteins such as antibodies, the use of this strategy becomes rather inefficient. Miyamoto and co-workers (1) studied the effect of poly-$_L$-arginine (TJ-opening absorption enhancer), on nasal absorption of FITC-dextrans (FDs) with average $M_W$s ranging from 4.3 to 167 kDa in rats and showed that the extent of absorption enhancement was dependent upon the $M_W$. Consequently, the bioavailability was seen to decrease exponentially with the increasing $M_W$ of FDs. Based on the relationship between the achieved bioavailability and the $M_W$ of FDs, the authors of this study propose that the maximal $M_W$ of protein drugs exhibiting efficient absorption with the paracellular permeability enhancer, poly-$_L$-arginine, is about 20 kDa, assuming a 10% lower limit of bioavailability for developing a potent nasal delivery system. However, it must be noted that there are very few reported studies in the literature addressing the capacity of the paracellular route as a function of the $M_W$ of the therapeutic, following opening of the cellular TJs. Our work utilising chitosan in an attempt to improve the permeability of antibodies across Calu-3 layers (Chapter 6) found that chitosan exhibited a limited effect on antibody permeability. As argued previously (section 7.1), an alternative to paracellular transport would be to deliver large $M_W$ protein therapeutics through the transcellular route.

Work detailed in this chapter hence investigated the potential of the IgG/FcRn transcytotic pathway for mucosal delivery of large macromolecules (antibodies) and NPs, as a potential drug carrier system. This pathway has been investigated in some detail by other groups, as will be discussed later, and its potential for use in the field of mucosal delivery of macromolecules has, to some extent, been proven. Indeed, the IgG/FcRn transcytotic transmucosal pathway has been exploited commercially; the drug delivery technology of Syntonix Pharmaceuticals relied on construction of therapeutic proteins conjugated to the Fc domain of IgG ('Fc-fusion proteins') (33), the potential of which was demonstrated in phase I clinical studies (as will be discussed later).

As for any transport route, the usefulness of the IgG/FcRn transcytotic pathway for delivery of therapeutic biologicals is highly dependent on its capacity and therefore the amount of the therapeutic that it can transport. To this end, while some researches are demonstratrating the potential of the FcRn/IgG pathway for mucosal delivery of macromolecules (as will be disussed later) others have argued that this route is associated with a limited capacity (34). Furthermore, to the best of our knowledge, there are no studies reported in the literature that investigated potential of the IgG/FcRn transport pathway for cellular uptake and transport of NPs across epithelial cells or mucosal surfaces. This work attempted to address these points.

As mentioned earlier, endogenous FcRn expression in Calu-3 cells has been shown previously by applying Western blotting analysis (11). It should be however noted that this is the sole published work showing this information. In the present work, FcRn expression in Calu-3, as well as in Caco-2 cells, was demonstrated by

immunofluorescence. Confocal micrographs of the cells cultured as polarised layers imaged following the FcRn staining procedure revealed abundant distribution of fluorescence throughout the cell cytoplasm. Interestingly, considerably lower flourescence was clearly apparent in cells cultured under LCC conditions, demonstrating the importance of appropriate culture conditions. The absence of fluorescence in the control (cells treated with the secondary antibody only) is strongly suggestive that the fluorescence seen following the applied imunofluorescence procedure, is is due to FcRn and is a clear indication of receptor expression.

FcRn immunostaining in filter-cultured Caco-2 cells was performed for corroboration, as, unlike Calu-3 cells, FcRn expression in the Caco-2 cell line has been demonstrated previously in a number of studies (14, 35, 36). The pattern of fluorescence, indicating FcRn presence, in Caco-2 cells appeared similar to that seen in Calu-3 cells. However, the comparison of the level of FcRn expression in the two cell lines was not possible due to the qualitative nature of the immunostaining/confocal technique.

In primates, FcRn is expressed predominantly in the upper airway epithelium as demonstrated by Spiekermann *et al* (11). In this study the lungs of adult humans and non-human primates (cynomologus macaque) were examined for expression of FcRn and found that total cell lysates obtained from lungs of both species contained a 45-kDa glycosylated protein consistent with human FcRn, as assessed by SDS-PAGE and Western blotting. When lung tissue samples were visualized by immunohistochemistry, FcRn was found localized predominantly at the apical region of bronchial epithelial cells lining the large and small airways. Furthermore, cell lysates prepared from the Calu-3 cell line (used in this thesis) and BEAS-2B (another

human bronchial epithelial cell line) also contained FcRn.

To assess the pH-dependence of IgG binding to FcRn, FITC-IgG was incubated with confluent cell layers at a slightly acidic or physiological environment (pH 6.0 and 7.4, respectively). Determination of the levels of FITC-IgG in the apical solution at the end of the incubation interval revealed a difference in apical FITC-IgG amount, relative to that applied, depending on the pH (76% versus 87% at pH 6.0 and 7.4, respectively). Such a disappearance of FITC-IgG from the apical solution following its incubation with the cells could have been a result of its transcellular transport, cell uptake, its binding to FcRn (present at both the cell interior and cell surface), and/or a combination of all these processes. Although this experiment did not provide information with regards to the fate of FITC-IgG following its application, data suggests that one or more of the above-mentioned possible processes causing IgG removal are likely to be significantly more efficient at pH 6.0. While IgG binding to FcRn present within the acidic compartments (following its internalisation) is unlikely to be affected by the pH of the apical solution, IgG binding to FcRn present at the cell surface is facilitated at pH 6.0, possibly accounting for the observed difference discussed above. Detection of higher levels of FITC-IgG in the apical solution following its incubation with the cells in the presence of unlabelled IgG compared to levels observed after FITC-IgG application on its own, suggests that the uptake, transport and/or receptor binding (processes discussed above) occur through mechanisms specific to IgG.

Although the disappearance of IgG from the apical solution was seen to be pH-dependent, as discussed above, its cell uptake was not affected by pH (the difference

in uptake between pH 7.4 and 6.0 was not statistically significant). On the other hand, suppression of cellular uptake of FITC-IgG by unlabelled IgG (Figure 7.5) again indicated that FITC-IgG internalised through an IgG-specific pathway.

Findings similar to ours have also been published by Sato *et al.* (36). Their work demonstrated that the binding of FITC-labelled human IgG to the membrane surface of Caco-2 cells increased as the pH of incubation buffer decreased. Recently the work by Stirling *et al*. (37), which used the porcine kidney cell line, IB-RS2 (expressing FcRn with a high homology to human FcRn), also demonstrated that there was little binding of porcine IgG at pH 7.8, but binding was clearly evident at pH 6.0.

Periodic measurement of IgG levels in the basolateral solution following its application on the apical surface of the cell layers revealed that IgG traversed the Calu-3 layers. A pattern of an initial increase in basolateral IgG level, followed by a plateau was typically observed in experiments where the basolateral solution was sampled at regular intervals. Observation of this phenomenon can possibly be attributed to transport saturation with time and/or the property of IgG to traverse the epithelial cell layers in a bidirectional manner, as documented previously (14).

An important point to note is the presence of bovine IgG (bIgG) in the cell culture serum, which could have potentially interferred with IgG uptake/transport studies in our work. However, extensive cell washing and serum starving prior to IgG uptake and transport experiments was undertaken to ensure its maximal removal. Furthermore, human FcRn does not bind significantly to bIgG (38). Therefore, taking both factors into account, one would assume that the potential for its interference in

IgG transport and uptake experiments in the present study was very low. Also, the quantification method used in the present experiments was specific to (human) IgG, therefore permitting the experimental setup used in this work.

Apical-to-basolateral IgG transport data demonstrate that the process is saturable, as following IgG application on the apical surface of the cell layers at varying concentrations the increases in the apical IgG concentration beyond a certain level did not produce an increase in basolateral IgG amount (Figure 7.7). Such transport saturation with an increasing concentration of the ligand indicates a receptor-mediated process; this phenomenon would not be exhibited by a non-specific mode of transport, such as passive paracellular movement.

To further confirm that IgG transport in Calu-3 layers is receptor-mediated, rabbit IgG (rIgG) was used in the transport experiment. rIgG has previously been shown to possess an ability to bind to human FcRn (38). However the analytical method used to quantify IgG in the transport experiment was specific to human IgG only and could not detect rIgG. Therefore, the rIgG in effect acted as a competitive inhibitor. Importantly, data from this experiment showed that co-application of excess rIgG with (human) IgG suppressed the apical-to-basolateral transport of the latter, suggesting again that the transport of (human) IgG across the Calu-3 cell layers is indeed mediated by FcRn.

The difference in the amount of IgG transported across the Calu-3 cell layers between different experiments (namely the experiment detailed in section 7.3.3.1 with those in sections 7.3.3.2 and 7.3.3.3) must be noticed. The reasons for the observed

discrepancy (approximately 4.8-fold) are not clear at the present moment. What can be highlighted as a potential cause is that the cells used in the experiments described in the former section were of a considerably lower passage number (passage 23) and of a different batch compared to those in the latter sections (passages 43-44).

An interesting finding was encountered following the comparison of IgG transport in Calu-3 and Caco-2 cells. In the monolayers of the Caco-2 cell line, the maximal level of IgG found in the basolateral solution following its addition on the apical side was markedly lower compared to those measured in Calu-3 layers. This is particularly interesting considering that Calu-3 cells used in the studies were grown under AIC conditions where the presence of mucus may have potentially presented a barrier to IgG transport, compared to non-mucus producing Caco-2 cells. It may be possible that the observed inter-cell line difference in IgG transport is a result of variations in the extent of FcRn expression in the two cell lines.

At this point it is worth mentioning that experiments comparing the transport of FITC-dextrans across Calu-3 and Caco-2 cell layers (section 3.3.3.5) found that the extent of permeability of these compounds was notably lower across the Calu-3 as compared to Caco-2 cells, hence demonstrating a less restrictive paracellular barrier in Caco-2 monolayers (compared to Calu-3 cells). With the receptor-mediated transcellular transport of IgG on the other hand, the opposite appears to be the case (i.e. higher rate of IgG transport across Calu-3 than Caco-2 monolayers), which is further evidence that IgG translocation across the cell layers could not have arisen from its movement through the paracellular pathway.

While the mechanism of IgG transcytosis in epithelial cells (which was briefly discussed in Chapter 1) was not the focus of our work, it is worth highlighting that recent studies have attempted to elucidate the intracellular mechanisms involved in IgG trafficking in epithelial cells. For example, Sato *et al.* (36) investigated the effects of endocytosis inhibitors on internalization of human IgG by Caco-2 cells and showed that IgG uptake was significantly inhibited by a mixture of metabolic inhibitors (sodium azide and 2-deoxyglucose). However, the uptake of FITC-IgG at pH 6.0 was not inhibited by clathrin-dependent endocytosis inhibitors (phenylarsine oxide and chlorpromazine) and caveolin-dependent endocytosis inhibitors (nystatin and indomethacin). In contrast, macropinocytosis inhibitors such as cytochalasin B and 5-(N-ethyl-N-isopropyl) amiloride significantly decreased its uptake. This study therefore showed that FcRn-mediated internalization of IgG in human intestine most likely occurs by a process other than clathrin- and caveolin-dependent mechanisms. In another recently-published study, Tzaban *et al.* (39) showed that in polarized cells FcRn is sorted by the recycling endosomes (RE) into distinct recycling and transcytotic pathways in a strongly polarized manner. The authors observed that FcRn localizes to the RE, and that MyoVb and Rab25 regulate a sorting step that specifies transcytosis for FcRn in both directions without affecting their recycling.

Perhaps the most clinically relevant study investigating the prospect of delivering protein therapeutics *via* the IgG/FcRn pathway is that by Dumont *et al.* (17) In this study, the authors investigated whether FcRn can mediate the absorption of Fc-fusion proteins through the lung by administering erythropoietin fused to Fc (EpoFc, $M_W$ 112 kDa) to 22 healthy male volunteers. EpoFc was deposited into the central lung at doses of 3, 10 or 30 μg/kg. A dose-dependent absorption through the lungs was seen,

wich achieved maximal serum concentrations of 0.2, 1.2 and 7.1 ng/ml, respectively. Furthermore, Low *et al*. (16) tested the absorption of FSH–Fc fusion proteins ($M_W$ 94.5-128 kDa) following the pulmonary delivery in four cynomolgus monkeys. The authors demonstrated maximum serum concentrations of FSH–Fc fusion proteins between 69 and 131 ng/ml.

FcRn-mediated delivery of protein therapeutics has however been criticised in the literature for its low delivery capacity, with Sakagami and co-workers arguing that this strategy is promising for pulmonary delivery of highly potent proteins only (34). Indeed when one considers the above-mentioned studies in humans and non-human primates, it can be noticed that maximal serum concentrations achieved were approximately 7 ng/ml and approximately 130 ng/ml for Epo and FSH (Fc constructs), respectively. However, most biologics in the market, including the immunoglobulin-based therapeutic molecules, require plasma concentrations in mg range, as exemplified by the following tumor necrosis factor (TNF) antagonists. Infliximab [Remicade, a chimeric (human-murine) monoclonal IgG1], which is used in the treatment of Crohn's disease and rheumatoid arthritis requires plasma trough concentrations above 1 μg/ml for a clinical response (40). The pharmacokinetic data of Adalimumab (Humira™, a recombinant human monoclonal IgG1 used in rheumatoid arthritis and psoriasis) and Etanercept (Enbrel®, a dimeric fusion protein consisting of the extracellular ligand-binding portion of the human TNF receptor, linked to the Fc portion of human IgG1) indicated average steady state therapeutic plasma concentrations of 5.5±2.5 mg/L and 1.78-1.88 mg/L, respectively (41). Therefore, if the use of the IgG/FcRn pathway is to be considered for pulmonary delivery of currently marketed biologics, and those requiring similar plasma

concentrations for clinical response, there is indeed a necessity for an improvement in absorption capacity.

Assessment of IgG transport across the Calu-3 layers in this work indicated a transport capacity ranging from 9-45 ng per $cm^2$ per hour [estimated by dividing the amount of IgG transported in 1 hour by the cell layer area (1.1 $cm^2$)]. Assuming that IgG absorption across the bronchial mucosa *in vivo* occurs to a similar extent (in terms of amount per surface area per time) and with a surface area of human bronchi of 1300 $cm^2$ (42) one could extrapolate that an absorption capacity of approximately 12 µg-59 µg per hour is potentially achievable through the FcRn pathway *in vivo*. However, one must exercise caution with this hypothetical projection. Drug transport across the pulmonary mucosal surfaces *in vivo*, where factors not present in the epithelial cell layer model (e.g. mucociliary clearance, extracellular tissue, etc.) will undoubtedly play a role in the transport process, is more than likely to be different to that across the epithelial cell culture models. Furthermore, it is not clear whether FcRn expression *in vivo* in cells lining the bronchial tubes is similar in extent to Calu-3 cells and whether regions of the lung other than bronchi also contribute towards FcRn-mediated transepithelial transport. Finally, in the *in vitro* experiments presented in this thesis, IgG was in contact with the cell layers and therefore available for transport for a relatively long period of time (2-3 hours). However, this scenario is unlikely to occur *in vivo*, where a functional mucociliary mechanism (43) may potentially clear a proportion of the administered FcRn-targeted therapeutic molecule (if the administered formulation is entrapped within the mucus layer and less so if the therapeutic traverses the mucus layer in a short period of time). Nevertheless, as pointed out previously, in addition to the bronchial epithelium, other segments of the

lung may participate in FcRn-mediated transport (including alveolar epithelium with its huge surface area), contributing to the overall absorption.

The present work investigated whether it would be potentially possible to improve the absorption capacity of a receptor-mediated pathway by employing nanoparticulate carriers. In the case of IgG/FcRn pathway, such a nanocarrier would be surface-decorated with IgG or Fc, exploiting transport *via* FcRn, while the therapeutic macromolecules will be encapsulated (and protected) within the interior of these carriers. Surface adsorption of the therapeutic biologic to the nanocarrier (alongside IgG or Fc), providing that it does not hinder the binding of surface-adsorbed IgG (or Fc) to FcRn, is another possibility. The therapeutic-incorporated/adsorbed carrier would then be transported transmucosally through the FcRn transcytotic pathway, not as individual molecules, but as a number of therapeutic molecules in the NP carrier system.

To the best of our knowledge there are no published studies investigating the potential of FcRn pathway for mucosal transport of NPs. Furthermore, it was not clear at the beginning of the study whether the association of NPs with IgG, or Fc, affects the transcytotic process by which FcRn normally transports free IgG. It must be highlighted that polystyrene NPs were used as nanocarrier models, due to the convenience of their availability in different sizes, different surface modifications and fluorophores (allowing imaging and quantification). IgG or Fc was not chemically conjugated to the NPs; these molecules were instead physically adsorbed on the NP surface, taking advantage of their ability to adsorb non-covalently and almost irreversibly onto the surface of polystyrene NPs (44, 45) through hydrophobic

interactions. Hydrophobic sorption of IgG to the NPs was assumed to occur randomly, as shown in previous studies for polystyrene NPs (46, 47) with immobilised IgG adopting random geometries, including those that potentially permit binding of the immobilised protein to the receptor.

Characterisation of NPs for their size by dynamic light scattering (DLS) revealed that IgG-adsorbed NPs had mean radii of 220 nm, as compared to mean radii of approximately 21 nm observed for unmodified ('naked') NPs. It must be noted that the observed size for IgG-NPs was considerably larger than expected from the protein adsorption process if one would make the following assumption with regards to adsorption of IgG to NPs. Small angle X-ray scattering data show that the leg of the T-shaped IgG has a length of 58 Å (5.8 nm) (48). Therefore, a maximal increase in the diameter of NPs by 11.6 nm would be expected to occur following the immobilisation of IgG molecules on the surface of NPs as a single layer. Following the adsorption of IgG to gold nanoparticles, Khlebtsov *et al.* (49) found that the thickness of adsorbed layer of IgG was equal to 5–6 nm. However, in our work, the larger than expected change in NP diameter following the adsorption of IgG on their surface is, perhaps, not surprising given the tendency of IgG to aggregate in solution (50), which could occur before its immobilisation on the NPs, resulting in adsorption of large aggregated complexes, and/or after its binding to the NPs. Furthermore, adsorption of the weakly charged IgG on the surface of negatively charged polystyrene NPs may have resulted in diminished colloidal stabilisation of the NPs due to a reduction in surface charge repulsion.

Nevertheless, adsorption of Fc fragment of IgG onto NPs instead of whole IgG

produced smaller NPs having mean radii of approximately 60 nm (i.e. 120 nm diameter) (Figure 7.10). Such a nanoparticulate system is also expected to potentially bind to the FcRn receptor and undergo transcytosis, as it is the Fc portion of IgG that bings to FcRn and is subsequently transcytosed (27). Furthermore, with a mean diameter of 120 nm, Fc-adsorbed NPs are probably still ameanable to cell endocytotic processes (51).

Determination of cellular uptake of NPs by visualization through confocal microscopy revealed that IgG-immobilised NPs were found in the interior of the cells, suggesting their uptake by the cells. Furthermore, and highly important for this study, co-localisation of fluorescence from FITC-IgG with that of red NPs was observed, suggesting that IgG remains associated with the NPs following their uptake by the cells. The confocal images further showed that IgG-NPs were largely found inside the cells as micron-sized structures/aggregates, in addition to smaller, nano-sized particles.

In the case of Fc-adsorbed NPs, observed punctate fluorescence resulting following their application to the cells suggested that NPs in this case were smaller than IgG-NPs (Figure 7.11), though some large complexes were also observed for Fc-NPs (Figure 7.12). This is in agreement with the DLS data. Fc-adsorbed polystyrene NPs localised within the interior of Calu-3 cells following their incubation with the cell layers. Importantly, and similarly to FITC-IgG-NPs, fluorescence from Fc (FITC-Fc) was seen to co-localise with that of the NPs (Figure 7.12a), indicating that Fc remained associated with the NPs within the interior of the cells. It must be pointed out at this stage that the fluorescence intensity of FITC-IgG or FITC-Fc would be

expected to decrease when present in an acidic environment (due to pH sensitivity of FITC), such as that within endosomes. This may be a possible explanation for the somewhat lower observed fluorescence in the green confocal channel (FITC-Fc) compared to the red channel (NPs) in the case of FITC-Fc-NPs (Figure 7.12a).

Also cruically, NPs were in some cases observed uniformly throughout the vertical axis of the cells, including below the level of the TJs (Figure 7.12a) and at the level of the Transwell® filter (Figure 7.12b), suggesting their translocation across the cells. Furthermore, staining of the cells for lysosomes revealed that Fc-coated NPs generally did not co-localise with the lysosomes, though the result of this experiment must be interpreted with caution due to low observed staining.

In addition to qualitative data obtained from confocal imaging, cellular uptake and transport of Fc-NPs across the cell layers was also quantified by measurement of NP fluorescence. Cellular uptake of Fc-NPs was significantly higher than that of unmodified NPs, suggesting that adsorption of Fc on the NP surface promotes their cellular uptake. Furthermore, Calu-3 uptake of Fc-NPs was inhibited by soluble ('free') IgG, implying the likelihood that Fc-NPs were internalized by cells through an IgG-specific pathway. This was further confirmed by the experiment where the effect of non-fluorescently labelled Fc-NP on cell uptake of fluorescently labelled Fc-NPs was tested. This experiment was conducted to induce competitive receptor inhibition by presenting the competing ligand to the cells in the same manner as the tested ligand. Data obtained clearly showed that non-labelled Fc-NPs significantly reduced the uptake of traceable (fluorescently-labelled) Fc-NPs, suggesting that Fc-NP internalisation is a saturable process.

In agreement with the uptake data, Fc-immobilised NPs were seen to traverse the cell layers in a larger extent than unmodified NPs, suggesting that, in addition to promoting their cellular uptake, coating of NPs with Fc facilitates their transport across the cell layers. Inhibition of Fc-NP transport across the cell layer barriers by soluble IgG and by non-labelled Fc-NPs indicates the involvement of the IgG transport pathway in the transepithelial movement of Fc-NPs and that this transport is saturable.

Final experiments tested the effect of NP coating with an investigational therapeutic antibody fragment (Fab, CTM01), with or without Fc, on their transport across the cell layers. This was done to determine whether coating of NPs with a protein other than Fc facilitates their transport across the cells and also to test the potential of the Fc-NP carrier system to transport therapeutic macromolecules across the epithelial barriers. It was found that co-adsorbing the therapeutic Fab with Fc on the surface of NPs significantly improved their transport across the cell layers to levels very similar to those observed with Fc-NPs. In contrast, NPs coated with the Fab only were seen to traverse the cell layer barriers in a considerably less efficient fashion. Furthermore, testing the filter plastic for the presence of NPs (after the transport study) revealed that Fc-adsorbed NPs associated with the filters to a significantly larger extent than Fab-adsorbed NPs, indicating a greater apical-to-basolateral translocation of NPs with surface-adsorbed Fc.

## 7.5 Conclusion

Using the Calu-3 epithelial cell model, which is shown to express FcRn, this work investigated IgG transport across the cells and the potential of this route for transepithelial delivery of NPs. IgG was found to traverse the Calu-3 layers in a fashion that strongly suggested FcRn involvement. Furthermore, adsorption of Fc on the surface of NPs was seen to promote their cellular uptake and transport across the cell layers. Experiments investigating the cellular uptake and transport of Fc-NPs revealed data suggestive of FcRn involvement in this process. This work therefore shows that the IgG/FcRn transcytotic pathway offers potential for mucosal delivery of protein and NP-based therapeutics.

## 7.6 References


1. M. Miyamoto, H. Natsume, I. Satoh, K. Ohtake, M. Yamaguchi, D. Kobayashi, K. Sugibayashi, and Y. Morimoto. Effect of poly-L-arginine on the nasal absorption of FITC-dextran of different molecular weights and recombinant human granulocyte colony-stimulating factor (rhG-CSF) in rats. Int J Pharm. 226:127-138 (2001).
2. T. Jung, W. Kamm, A. Breitenbach, E. Kaiserling, J.X. Xiao, and T. Kissel. Biodegradable nanoparticles for oral delivery of peptides: is there a role for polymers to affect mucosal uptake? Eur J Pharm Biopharm. 50:147-160 (2000).
3. R.J. Mrsny. Lessons from nature: "Pathogen-Mimetic" systems for mucosal nano-medicines. Adv Drug Deliv Rev. 61:172-192 (2009).
4. A.F. Kotze, H.L. Luessen, B.J. de Leeuw, A.G. de Boer, J.C. Verhoef, and H.E. Junginger. Comparison of the effect of different chitosan salts and N-trimethyl chitosan chloride on the permeability of intestinal epithelial cells (Caco-2). J Control Release. 51:35-46 (1998).
5. J. Blanchette, N. Kavimandan, and N.A. Peppas. Principles of transmucosal delivery of therapeutic agents. Biomed Pharmacother. 58:142-151 (2004).
6. L.G. Morphisand D. Gitlin. Maturation of the maternofoetal transport system for human gamma-globulin in the mouse. Nature. 228:573 (1970).
7. F.W. Brambell. The transmission of immunity from mother to young and the catabolism of immunoglobulins. Lancet. 2:1087-1093 (1966).
8. N.E. Simisterand A.R. Rees. Isolation and characterization of an Fc receptor from neonatal rat small intestine. Eur J Immunol. 15:733-738 (1985).
9. N.E. Simisterand K.E. Mostov. An Fc receptor structurally related to MHC class I antigens. Nature. 337:184-187 (1989).
10. C.M. Story, J.E. Mikulska, and N.E. Simister. A major histocompatibility complex class I-like Fc receptor cloned from human placenta: possible role in transfer of immunoglobulin G from mother to fetus. J Exp Med. 180:2377-2381 (1994).
11. G.M. Spiekermann, P.W. Finn, E.S. Ward, J. Dumont, B.L. Dickinson, R.S. Blumberg, and W.I. Lencer. Receptor-mediated immunoglobulin G transport across mucosal barriers in adult life: functional expression of FcRn in the mammalian lung. J Exp Med. 196:303-310 (2002).
12. J.P. Haymann, J.P. Levraud, S. Bouet, V. Kappes, J. Hagege, G. Nguyen, Y. Xu, E. Rondeau, and J.D. Sraer. Characterization and localization of the neonatal Fc receptor in adult human kidney. J Am Soc Nephrol. 11:632-639 (2000).
13. E.J. Israel, S. Taylor, Z. Wu, E. Mizoguchi, R.S. Blumberg, A. Bhan, and N.E. Simister. Expression of the neonatal Fc receptor, FcRn, on human intestinal epithelial cells. Immunology. 92:69-74 (1997).
14. B.L. Dickinson, K. Badizadegan, Z. Wu, J.C. Ahouse, X. Zhu, N.E. Simister, R.S. Blumberg, and W.I. Lencer. Bidirectional FcRn-dependent IgG transport in a polarized human intestinal epithelial cell line. J Clin Invest. 104:903-911 (1999).
15. A.J. Bitonti, J.A. Dumont, S.C. Low, R.T. Peters, K.E. Kropp, V.J. Palombella, J.M. Stattel, Y. Lu, C.A. Tan, J.J. Song, A.M. Garcia, N.E. Simister, G.M. Spiekermann, W.I. Lencer, and R.S. Blumberg. Pulmonary delivery of an erythropoietin Fc fusion protein in non-human primates through

an immunoglobulin transport pathway. Proc Natl Acad Sci U S A. 101:9763-9768 (2004).
16. S.C. Low, S.L. Nunes, A.J. Bitonti, and J.A. Dumont. Oral and pulmonary delivery of FSH-Fc fusion proteins via neonatal Fc receptor-mediated transcytosis. Hum Reprod. 20:1805-1813 (2005).
17. J.A. Dumont, A.J. Bitonti, D. Clark, S. Evans, M. Pickford, and S.P. Newman. Delivery of an erythropoietin-Fc fusion protein by inhalation in humans through an immunoglobulin transport pathway. J Aerosol Med. 18:294-303 (2005).
18. A.J. Bitontiand J.A. Dumont. Pulmonary administration of therapeutic proteins using an immunoglobulin transport pathway. Adv Drug Deliv Rev. 58:1106-1118 (2006).
19. J.A. Dumont, S.C. Low, R.T. Peters, and A.J. Bitonti. Monomeric Fc fusions: impact on pharmacokinetic and biological activity of protein therapeutics. BioDrugs. 20:151-160 (2006).
20. K.J. Kim, T.E. Fandy, V.H. Lee, D.K. Ann, Z. Borok, and E.D. Crandall. Net absorption of IgG via FcRn-mediated transcytosis across rat alveolar epithelial cell monolayers. Am J Physiol Lung Cell Mol Physiol. 287:L616-622 (2004).
21. D.C. Roopenianand S. Akilesh. FcRn: the neonatal Fc receptor comes of age. Nat Rev Immunol. 7:715-725 (2007).
22. R. Rodewald. Selective antibody transport in the proximal small intestine of the neonatal rat. J Cell Biol. 45:635-640 (1970).
23. R. Rodewald. Intestinal transport of antibodies in the newborn rat. J Cell Biol. 58:189-211 (1973).
24. D.R. Abrahamsonand R. Rodewald. Evidence for the sorting of endocytic vesicle contents during the receptor-mediated transport of IgG across the newborn rat intestine. J Cell Biol. 91:270-280 (1981).
25. T.A. Waldmannand E.A. Jones. The role of cell-surface receptors in the transport and catabolism of immunoglobulins. Ciba Found Symp. 9:5-23 (1972).
26. V. Ghetieand E.S. Ward. Multiple roles for the major histocompatibility complex class I- related receptor FcRn. Annu Rev Immunol. 18:739-766 (2000).
27. A.P. West, Jr.and P.J. Bjorkman. Crystal structure and immunoglobulin G binding properties of the human major histocompatibility complex-related Fc receptor(,). Biochemistry. 39:9698-9708 (2000).
28. E.A. Jonesand T.A. Waldmann. The mechanism of intestinal uptake and transcellular transport of IgG in the neonatal rat. J Clin Invest. 51:2916-2927 (1972).
29. R. Rodewald. pH-dependent binding of immunoglobulins to intestinal cells of the neonatal rat. J Cell Biol. 71:666-669 (1976).
30. R. Siekmeierand G. Scheuch. Systemic treatment by inhalation of macromolecules--principles, problems, and examples. J Physiol Pharmacol. 59 Suppl 6:53-79 (2008).
31. A. Kamyshny, O. Toledano, and S. Magdassi. Adsorption of hydrophobized IgG and gelatin onto phosphatidyl choline-coated silica. Colloids and Surfaces. 13:187-194 (1999).
32. G.J. Russell-Jones, L. Arthur, and H. Walker. Vitamin B12-mediated transport of nanoparticles across Caco-2 cells. Int J Pharm. 179:247-255 (1999).

33. R.S. Blumberg, W. Lencer, N.E. Simister, and A.J. Bitonti. Central Airway Administration for Systemic Delivery of Therapeutics, The Brigham and Women's Hospital Inc. Children's Medical Center Corporation Brandeis University Syntonix Pharmaceuticals, Inc., United States, 2004.
34. M. Sakagami, Y. Omidi, L. Campbell, L.E. Kandalaft, C.J. Morris, J. Barar, and M. Gumbleton. Expression and transport functionality of FcRn within rat alveolar epithelium: a study in primary cell culture and in the isolated perfused lung. Pharm Res. 23:270-279 (2006).
35. S.M. Claypool, B.L. Dickinson, J.S. Wagner, F.E. Johansen, N. Venu, J.A. Borawski, W.I. Lencer, and R.S. Blumberg. Bidirectional transepithelial IgG transport by a strongly polarized basolateral membrane Fcgamma-receptor. Mol Biol Cell. 15:1746-1759 (2004).
36. K. Sato, J. Nagai, N. Mitsui, R. Yumoto, and M. Takano. Effects of endocytosis inhibitors on internalization of human IgG by Caco-2 human intestinal epithelial cells. Life Sciences. 85:800-807 (2009).
37. C.M. Stirling, B. Charleston, H. Takamatsu, S. Claypool, W. Lencer, R.S. Blumberg, and T.E. Wileman. Characterization of the porcine neonatal Fc receptor--potential use for trans-epithelial protein delivery. Immunology. 114:542-553 (2005).
38. R.J. Ober, C.G. Radu, V. Ghetie, and E.S. Ward. Differences in promiscuity for antibody-FcRn interactions across species: implications for therapeutic antibodies. Int Immunol. 13:1551-1559 (2001).
39. S. Tzaban, R.H. Massol, E. Yen, W. Hamman, S.R. Frank, L.A. Lapierre, S.H. Hansen, J.R. Goldenring, R.S. Blumberg, and W.I. Lencer. The recycling and transcytotic pathways for IgG transport by FcRn are distinct and display an inherent polarity. J Cell Biol. 185:673-684 (2009).
40. U. Klotz, A. Teml, and M. Schwab. Clinical pharmacokinetics and use of infliximab. Clin Pharmacokinet. 46:645-660 (2007).
41. I. Nestorov. Clinical pharmacokinetics of TNF antagonists: how do they differ? Semin Arthritis Rheum. 34:12-18 (2005).
42. R.R. Mercer. Morphometry for alpha particle hits of critical targets in the lungs. In W. USDOE Office of Energy Research, DC (United States) (ed.), 1998.
43. S. Edsbacker, P. Wollmer, O. Selroos, L. Borgstrom, B. Olsson, and J. Ingelf. Do airway clearance mechanisms influence the local and systemic effects of inhaled corticosteroids? Pulm Pharmacol Ther. 21:247-258 (2008).
44. J. Serra, J. Puig, A. Martin, F. Galisteo, M.J. Galvez, and R. Hidalgo-Alvarez. On the adsorption of IgG onto polystyrene particles: electrophoretic mobility and critical coagulation concentration. Colloid & Polymer Science. 270:574-583 (1992).
45. F. Galisteo-Gonzalez, A. Martin-Rodriguez, and R. Hidalgo-Alvarez. Adsorption of monoclonal IgG on polystyrene microspheres. Colloid & Polymer Science. 272:352-358 (1994).
46. E. Imbert-Laurenceau, M. Berger, G. Pavon-Djavid, A. Jouan, and V. Migonney. Surface modification of polystyrene particles for specific antibody adsorption. Polymer. 46:1277-1285 (2005).
47. V.V. Shmanai, T.A. Nikolayeva, L.G. Vinokurova, and A.A. Litoshka. Oriented antibody immobilization to polystyrene macrocarriers for immunoassay modified with hydrazide derivatives of poly(meth)acrylic acid. BMC Biotechnol. 1:4 (2001).

48. I. Pilz, O. Kratky, and F. Karush. Changes of the conformation of rabbit IgG antibody caused by the specific binding of a hapten. X-ray small-angle studies. Eur J Biochem. 41:91-96 (1974).
49. N.G. Khlebtsov, V.A. Bogatyrev, B.N. Khlebtsov, L.A. Dykman, and P. Englebienne. A Multilayer Model for Gold Nanoparticle Bioconjugates: Application to Study of Gelatin and Human IgG Adsorption Using Extinction and Light Scattering Spectra and the Dynamic Light Scattering Method. Colloid Journal. 65: 622-635 (2003).
50. R.D. Soltisand D. Hasz. Dissociation of IgG aggregates at low pH. Immunology. 46:411-414 (1982).
51. J. Rejman, V. Oberle, I.S. Zuhorn, and D. Hoekstra. Size-dependent internalization of particles via the pathways of clathrin- and caveolae-mediated endocytosis. Biochem J. 377:159-169 (2004).

# Chapter 8

# Summary and Future Directions

## 8.1 Overall Summary

Mucosal surfaces offer a potential for non-invasive delivery of biotherapeutics, including peptides, proteins and antibodies. However, these surfaces are naturally designed to limit the movement of material from the external environment (mucosal lumen) into the systemic circulation. A mucosally administered protein therapeutic has to overcome many barriers, physical and biochemical, if it is to reach the systemic circulation. These barriers were discussed in Chapter 1 and include mucus and the mucociliary clearance mechanism, protease enzymes, the inter-epithelial tight junctions (TJs) and the cellular membranes.

Investigating mucosal drug absorption *in vitro* requires models of the mucosal surface(s) of interest. In this respect, several options exist and each system is associated with its advantages and drawbacks. Mucosal models based on epithelial cell layers minimise animal usage and are extensively used (in academia and the pharmaceutical industry), with a demonstrated record of *in vitro-in vivo* correlation (as discussed in Chapter 3).

The Calu-3 cell line was selected in this work as a model of the airway epithelium. One of the advantages of using the Calu-3 cell line as an *in vitro* mucosal model is its capacity to produce mucus when cultured under appropriate conditions. In this thesis, initial work focused on establishing and characterising the Calu-3 cell layer model. Data shown in Chapter 3 demonstrated that, following their growth on filters under air-interfaced culture (AIC) conditions, Calu-3 cells form polarised layers of closely packed cells exhibiting a TEER >500 $\Omega cm^2$. Cells exhibited structural features that resemble the native epithelium, including the TJs, the microvilli and the secretory granules. Cell layers presented a barrier to the permeability of FITC-dextrans (FDs, paracellular markers), with the magnitude of the barrier being proportional to the $M_W$ of the marker and larger than that observed with Caco-2 monolayers. Furthermore, Calu-3 layers presented a significant barrier to the movement of nanoparticles (NPs).

Following characterisation of the Calu-3 layer model, several strategies were investigated in an attempt to improve the transport of macromolecules (FDs were used as macromolecular drug models) across the cell layers. The first class of compounds to be tested were alkylglycoside (AG) surfactants. Data obtained with three representative AGs, illustrated that these compounds exhibited severe toxicity (shown by three different toxicity assays) towards Calu-3 cells (and also HT29 cells), even after their use at considerably lower concentrations than those reported in the literature (Chapter 4). Furthermore, data indicated that the cellular toxicity of AGs is possibly a result of a disruptive effect on membranes. Although the use of AGs as absorption enhancers has been commercialised (the drug delivery platform of Aegis Therapeutics is based on these compounds), it must be noted that literature information on their mucosal toxicity *in vivo* or epithelial cell lines *in vitro* is

surprisingly limited. Considering their adverse toxic effects on cells, further studies evaluating the absorption enhancing potential of AGs were deemed inappropriate.

The experiments detailed in Chapter 5 investigated the effect of extracellular calcium depletion on TJ modulation. More specifically, the aim of the work presented in this part of the thesis was to investigate the conditions under which exhaustion of extracellular calcium produces the greatest effect on TJ opening. Calcium depletion has long been known to induce opening of the TJs, resulting in increased transport of macromolecules through the paracellular route. However it is unclear from the literature whether this strategy can be used to improve the absorption of macromolecular therapeutics in the *in vivo* settings, where removal of extracellular calcium (through the mucosally administered absorption enhancer) is likely to occur predominantly on the luminal side. The data presented in this chapter suggested that depletion of calcium on the apical side produced limited TJ modulation, although with a more sustainable depletion the effect was somewhat more pronounced. On the other hand, apical and basolateral calcium removal produced large effects on TJs, but this scenario is probably irrelevant in an *in vivo* situation, making calcium depletion an ineffective strategy for mucosal delivery of therapeutic macromolecules.

Thereafter, two formulations of chitosan, namely solution and chitosan in the form of NPs, were investigated for their effect on epithelial TJs and therefore their potential use as mucosal absorption enhancers. Observations noted in Chapter 6 demonstrated that chitosan NPs formulated by the ionic gelation method, at a concentration exhibiting low toxicity, displayed a similar TJ-opening effect to chitosan solution. This was shown by a similar reduction in TEER, FD4 permeability and an effect on

the TJ protein, ZO-1. This work therefore indicated that chitosan NPs could potentially be used to carry and protect fragile therapeutic macromolecules to the mucosal surface of interest and at the same time promote their absorption through TJ-opening. These results are of significance as, although a large number of published studies on chitosan (as a mucosal absorption-promoter) exist, only a few of these studies have reported TJ opening by chitosan NPs.

Significant progress has been made recently in understanding the function of epithelial TJs at the molecular level. This has enabled targeting of specific TJ components in an attempt to improve mucosal absorption of macromolecules. Examples include the study by Dutzar *et al.* (1), in which siRNA knock down of different TJ proteins was used to test the effect on permeability. However, it must be noted that while TJ opening appears to be an attractive strategy to facilitate mucosal absorption of macromolecules, caution must be advocated, as the long-term physiological consequences of repeated TJ-opening are unknown (2).

Furthermore, while it is potentially feasible to achieve mucosal absorption of smaller peptides and proteins by opening the epithelial TJs (provided this does not have any adverse long term consequences), this strategy becomes inefficient for larger macromolecules such as antibodies, or for nano-sized drug carriers. Moving away from TJ modulation, work presented in Chapter 7 investigated the potential of a transcytotic pathway for mucosal delivery of macromolecules. Very few transcytotic pathways are known to exist in epithelial cells and endocytotic activity at the apical plasma membrane of epithelial cells is low, which is logical considering the crucial physiological role of epithelia in filtering and repelling foreign substances in order to

protect cells and organs (3). Of these, the IgG/FcRn pathway has been studied and shown potential for use in transmucosal delivery of protein therapeutics.

Investigation of FcRn expression by immunofluorescence showed that Calu-3 cells express FcRn. IgG was shown to traverse the Calu-3 layers and studies characterizing this transport strongly indicated FcRn involvement in the process. In order to establish whether the IgG/FcRn pathway could potentially be hijacked to deliver nano-sized drug carriers, IgG or Fc was immobilised on the surface of model NPs and their cellular uptake investigated by confocal microscopy. This work revealed that IgG- or Fc-coated NPs were taken up by Calu-3 cells, with NPs clearly observed within the interior of the cells and, in some cases, at the level of the Transwell® filters. Adsorption of Fc on the surface of NPs was seen to promote their cellular uptake and transport across the cells, as measured by fluorescence. Characterisation of cell uptake and transport of Fc-NPs revealed data suggestive of FcRn involvement in this process. This work therefore showed that the IgG/FcRn transcytotic pathway offers potential for mucosal delivery of macromolecules and nanoparticulate-based therapeutics.

## 8.2 Future directions

The problem of overcoming the barrier presented by the mucosal surfaces in delivering protein therapeutics through this route is being extensively researched. The increase in number of macromolecular biotherapeutics on the market, will undoubtedly be followed by research into their mucosal delivery. Research that is producing a rapid expansion in biologics, is likely to increase the number of highly potent protein drugs, which would make good candidates for mucosal administration. Furthermore, research is likely to lead to reductions in the cost of pharmaceutical

ingredients based on biologics making routes of administration that achieve modest bioavailabilities (such as mucosal administration) more acceptable. Yet another point to make is that, in addition to the obvious advantages of improved patient acceptability (and therefore compliance), and reduced administration cost and risk to the patient, the development of drug delivery technologies for mucosal administration can also potentially extend the patent lifetime of drug products, providing an incentive to the pharmaceutical industry.

In terms of early-stage research in the area of mucosal delivery of protein drugs, new research tools have become available which may accelerate progress within this field. Examples include molecular biology techniques used by some groups (mentioned previously) to identify TJ proteins essential in maintaining the barrier property of the epithelium. Another particularly exciting research strategy in the area is the use of phage display libraries to identify specific molecules (normally peptides) with inherent epithelial translocating properties.

To conclude, non-invasive administration of protein therapeutics is currently far from being a widely available option for the patient. However, the ever-increasing number and use of biologics is likely to increase research into their non-invasive delivery, which in turn is expected to produce progress within this field.

## 8.3 References

1. B. Dutzar, L. Chen, and S.C. Chen. siRNA knockdown of claudin expression inhibits tight junction formation and induces loss of differentiation in respiratory epithelia, *The 2004 AAPS National Biotechnology Conference*, Boston, 2003.
2. R.J. Mrsny. Lessons from nature: "Pathogen-Mimetic" systems for mucosal nano-medicines. Adv Drug Deliv Rev. 61:172-192 (2009).
3. O. Harush-Frenkel, E. Rozentur, S. Benita, and Y. Altschuler. Surface charge of nanoparticles determines their endocytic and transcytotic pathway in polarized MDCK cells. Biomacromolecules. 9:435-443 (2008).